Fakultät für Medizin
Institut für Virologie

Generation and functional characterization of bi- and trispecific antibodies for treatment of chronic hepatitis B

Oliver Quitt

Vollständiger Abdruck der von der Fakultät für Medizin der Technischen Universität München zur Erlangung des akademischen Grades eines

Doktors der Naturwissenschaften (Dr. rer. nat.)

genehmigten Dissertation.

Vorsitzender: Prof. Dr. Dirk Busch

Prüfende der Dissertation:

1. Prof. Dr. Ulrike Protzer
2. Prof. Dr. Dietmar Zehn

Die Dissertation wurde am 20.02.2020 bei der Technischen Universität München eingereicht und durch die Fakultät für Medizin am 16.02.2021 angenommen.

Table of contents

Abstract

Despite the availability of an effective prophylactic vaccine, approximately 257 million people are worldwide chronically infected with the hepatitis B virus (HBV) and therefore harbor a high risk to develop liver cirrhosis and hepatocellular carcinoma (HCC). In 2015, HBV-related liver diseases resulted in approximately 887,000 deaths, yet a curative therapy for chronic hepatitis B (CHB) is still not available. Current treatment options efficiently suppress HBV-replication, but rarely achieve viral clearance, since the viral covalently closed circular DNA (cccDNA) in the nucleus is not targeted. Although viral suppression improves the outcome of CHB, patients require life-long treatment and still carry the risk of developing HBV-driven HCC. Consequently, further efforts that intent a curative therapy for HBV infection are still in need. This thesis describes the immunotherapeutic retargeting of endogenous T cells employing bi- and trispecific antibodies (bsAbs, tsAbs), which aims at achieving viral clearance through the elimination of the HBV-infected hepatocytes and cytokine-mediated degradation of the viral cccDNA. Through simultaneous binding of the HBV envelope protein (HBVenv) on hepatocytes and cluster of differentiation 3 (CD3) or CD28 on immune effector cells, they can activate T cells to establish and maintain a cytotoxic immune response toward the HBV-infected target cells.

The first part of the thesis focused on the construction, expression and *in vitro* characterization of the bispecific antibodies FabMAbαCD3 and FabMAbαCD28. These bivalent constructs are composed of the HBVenv-specific chimeric fragment antigen binding (Fab)-fragment 5F9 that is connected to a CD3- or CD28-specific single chain fragment variable (scFv) by a glycine-serine linker. The data showed that the constructs are successfully expressed and that they bind both of their antigens successfully. Moreover, purification via immobilized metal affinity chromatography (IMAC) yielded in functional preparations that induced T-cell activation and cytotoxic elimination of HBVenv-transgenic target cells. However, efficient T-cell redirection required the combined administration of both constructs.

To study the impact of size and binding valency, the constructs BiMAbαCD3 and BiMAbαCD28 were developed in cooperation with the German cancer research center (DKFZ) in Heidelberg. BiMAbs consist of two HBVenv-specific scFv C8 connected to the n-termini of the immunoglobulin G 1 (IgG1) fragment crystallizable (Fc) domain and two CD3- or CD28 targeting scFv that are fused to the respective c-termini resulting in tetravalent constructs with two binding sites for each antigen. Comparative analysis of the different formats displayed similar potency for the bi- and tetravalent constructs, regarding binding characteristics, T-cell activation and target cell elimination *in vitro*, yet BiMAbs displayed a substantially longer half-life in mice.

In the next step, the bsAb approach was applied to an HBV infection system with the human hepatoma cell line HepG2 NTCP as model. Hereby, the bsAb-mediated T-cell redirection induced specific elimination of the infected target cells and efficient

degradation of the viral cccDNA. Furthermore, a strong correlation between the multiplicity of infection (MOI) and the magnitude of the retargeted T-cell response was observed. FabMAbs inhibited HBV replication with an IC_{50} value of 0.719 nM.

Since the combination of CD3- and CD28-specific bsAbs was required for efficient T-cell redirection and in consideration of a therapeutic approach, the last part of the thesis aimed at the generation of trispecific constructs that combine both immune stimulatory scFvs. Two different trispecific antibodies, TriMAb and OKTriMAb, were constructed using the Fab fragment 5F9 as heterodimerization domain. The pentavalent TriMAb consists of two scFv C8 that are fused to the n-termini of the Fab fragment 5F9 as well as a CD3- and CD28 targeting scFv that is connected to c-terminus of heavy chain and light chain, respectively. To further increase binding valency, two TriMAbs were dimerized by n-terminal elongation of the CH1 domain by the amino acids DKTHTCPPCP, resulting in a F(Ab)2-like molecule. The scFvC8 were directly fused to the n-termini of HC and LC constant domains. This gave rise to an oktavalent construct with four binding sites for HBVenv as well as two for CD3 and CD28, which was termed OKTriMAb. Both constructs were successfully expressed and activated T cells in the presence of recombinant HBVenv. Moreover, TriMAb administration induced efficient target cell elimination and displayed a clear anti-viral effect, without the requirement of further co-stimulation.

Taken together, the administration of HBVenv-targeting bsAbs facilitated a robust T-cell redirection towards HBVenv-expressing target cells and might provide a feasible and promising approach for the treatment of CHB and HBV-associated HCC.

Zusammenfassung

Trotz der Verfügbarkeit eines wirksamen prophylaktischen Impfstoffes sind weltweit ungefähr 257 Millionen Menschen chronisch mit dem Hepatitis-B-Virus (HBV) infiziert und tragen daher ein erhöhtes Risiko, an einer Leberzirrhose und dem hepatozellulären Karzinom (HCC) zu erkranken. Im Jahr 2015 starben rund 887.000 Menschen an HBV-assoziierten Lebererkrankungen, da keine kurative Therapie der chronischen Hepatitis B (CHB) verfügbar ist. Die derzeitige Behandlung ermöglicht eine effektive Suppression der viralen Replikation, erreicht aber selten die vollständige Eliminierung des Virus, da die virale kovalent geschlossene zirkuläre DNA (cccDNA) im Zellkern nicht angegriffen wird. Obwohl die virale Suppression die Symptomatik der chronischen Erkrankung verbessert, benötigen Patienten eine lebenslange Behandlung. Darüber hinaus bleibt ein erhöhtes Risiko bestehen, an HCC zu erkranken. Daher sind weitere Anstrengungen erforderlich, eine kurative Therapie für CHB zu entwickeln. Diese Arbeit beschreibt die immuntherapeutische Aktivierung von endogenen T-Zellen unter Verwendung von bi- und trispezifischen Antikörpern (bsAbs, tsAbs), was zur viralen Eliminierung durch das Abtöten der HBV-infizierten Hepatozyten und den Zytokin-vermittelten Abbau der viralen cccDNA führen soll. Durch die simultane Bindung des HBV-Hüllproteins (HBVenv) auf der Hepatozytenmembran und CD3 (englisch: cluster of differentiation 3) oder CD28 können diese Konstrukte T-Zellen aktivieren, um eine zytotoxische Immunantwort gegenüber den HBV-infizierten Zielzellen zu induzieren.

Der erste Teil der Arbeit konzentrierte sich auf die Konstruktion, Expression und *in vitro* Charakterisierung der beiden bispezifischen Antikörper FabMAbαCD3 und FabMAbαCD28. Diese bivalenten Konstrukte bestehen aus dem HBVenv-spezifischen chimären Fab (englisch: fragment antigen binding) Fragment 5F9 welches mittels eines Glycin-Serin-Linkers mit einem CD3-spezifischen beziehungsweise einem CD28-spezifischen scFv (englisch: single chain fragment variable) Fragment verbunden sind. Es wurde herausgefunden, dass beide Konstrukte erfolgreich exprimiert werden können und dass sie ihre Antigene erfolgreich binden. Darüber hinaus führte die Reinigung mittels immobilisierter Metallionen-Affinitätschromatographie (IMAC) zur Gewinnung von funktionellen Konstrukten, deren Anwendung zu einer T-Zell-Aktivierung und zur Eliminierung von HBVenv-transgenen Zielzellen *in vitro* führte. Eine effiziente Aktivierung der T-Zellen erforderte jedoch die kombinierte Applikation beider Antikörper.

Um die Auswirkungen von Größe und Valenz zu untersuchen, wurden die tetravalenten Konstrukte BiMAbαCD3 und BiMAbαCD28 in Zusammenarbeit mit dem deutschen Krebsforschungszentrum (DKFZ) in Heidelberg entwickelt und anschließend eine vergleichende Analyse der verschiedenen Formate durchgeführt. Diese BiMAbs bestehen aus zwei HBVenv-spezifischen scFv Fragmenten C8, welche mittels der Fc (englisch: fragment crystallizable) Domäne des humanen Immunglobulin G 1 mit zwei CD3-spezifischen beziehungsweise CD28-spezifischen scFv Fragmenten verbunden sind. Die Ergebnisse zeigten eine vergleichbare Wirksamkeit für die bi- und tetravalenten Konstrukte in Bezug auf ihre Bindungseigenschaften, die T-Zell-Aktivierung und die

Eliminierung der Zielzellen *in vitro*, jedoch demonstrierten BiMAbs eine wesentlich längere Halbwertszeit in einem Mausmodel.

Im nächsten Schritt wurde der immuntherapeutische Ansatz auf ein HBV-Infektionssystem übertragen, wobei HepG2 NTCP-Zellen als Modellzelllinie dienten. Dabei führte die bsAb-vermittelte T-Zell-Aktivierung zu einer spezifischen Eliminierung der infizierten Zielzellen und darüber hinaus zu einem effizienten Abbau der viralen cccDNA. Zusätzlich wurde eine starke Korrelation zwischen der Multiplizität der Infektion (MOI) und der induzierten T-Zell-Antwort beobachtet. FabMAbs inhibierten die HBV-Replikation mit einem IC_{50}-Wert von 0,719 nM.

Da die Kombination von CD3- und CD28-spezifischen bsAbs für die Induktion einer effiziente T-Zell-Aktivierung erforderlich war, zielte der letzte Teil der Arbeit auf die Generierung von trispezifischen Antikörpern ab, welche beide immunstimulierenden Domänen in einem Konstrukt vereinen. Zwei verschiedene Formate, TriMAb und OKTriMAb, wurden erfolgreich konstruiert, wobei das Fab-Fragment 5F9 als Heterodimerisierungsdomäne diente. Der pentavalente TriMAb besteht aus zwei scFv Fragmenten C8, welche mit den n-Termini des Fab Fragments verbunden sind, sowie einem CD3-spezifischen scFv-Fragment, welches mit der schweren Kette des Fab Fragments verknüpft ist und einem CD28-spezifischen scFv Fragment, welches mit der leichten Kette des Fab-Fragments verbunden ist. Um die Anzahl der Bindungen weiter zu erhöhen wurden zwei TriMAbs durch die Verlängerung der CH1 Domäne um die Aminosäuren DKTHTCPPCP verknüpft, was zur Entstehung eines F(Ab)2-ähnlichen Moleküls führte. Die beiden scFv-Fragmenten C8 wurden direkt mit den konstanten Domänen der schweren und leichten kette verknüpft, wodurch ein oktavalentes Konstrukt mit vier Bindestellen für HBVenv und jeweils zwei Bindestellen für CD3 und CD28 entstand, welches OKTriMAb genannt wurde. Beide Konstrukte konnten erfolgreich exprimiert werden und induzierten eine spezifische T-Zell-Aktivierung in Gegenwart von rekombinantem HBVenv. Darüber hinaus führte die Anwendung von TriMAb zu einer effizienten Eliminierung von Zielzellen *in vitro* und zeigte einen deutlichen antiviralen Effekt, ohne dass eine weitere Co-Stimulation erforderlich war.

Zusammengenommen induzierte die Verabreichung von HBVenv-spezifischen bsAbs eine robuste T-Zell-Aktivierung und die effektive Eliminierung von HBVenv-exprimierenden Zielzellen und könnte einen praktikablen und vielversprechenden Ansatz für die Behandlung von chronischer Hepatitis B und dem HBV-assoziierten HCC bieten.

Abbreviations

µl	microliter
µM	micromolar
AA	amino acid
AAV	adeno-associated virus
Ab	antibody
ADCC	antibody-depended cell-mediated cytotoxicity
ALL	acute lymphoblastic leukemia
ALT	alanine amino transferase
anti-HBs	HBsAg-specific antibodies
AP-1	activator protein 1
APC	antigen presenting cell
APOBEC	apolipoprotein B mRNA editing enzyme, catalytic polypeptide-like
BCL-2	B-cell lymphoma 2
BCR	B-cell receptor
Bim	BCL-2 interacting mediator of cell death
BiMAbs	Refers the constructs BiMAbαCD3 and BiMAbαCD28
BiTE	bispecific T-cell engager
bsAb	bispecific antibody; Refers the four constructs BiMAbαCD3, BiMAbαCD28, FabMAbαCD3 and FabMAbαCD28
cccDNA	covalently closed circular DNA
CD	cluster of differentiation
CD40L	CD40 ligand
CDC	complement-mediated cytotoxicity
C_H1	first constant domain of the heavy chain
CHB	chronic hepatitis B
C_L	constant domain of the light chain
CRS	cytokine release syndrome
CTL	cytotoxic T lymphocyte
CTLA-4	cytotoxic T-lymphocyte-associated protein 4
CTV	CellTrace Violet
DC	dendritic cell
DKFZ	German cancer research center

DNA	deoxyribonucleic acid
E:T ratio	effector to target ratio
EC_{50}	half maximal effective concentration
EGFR	epithelial growth factor receptor
ELISA	enzyme-linked immunosorbent assay
EMA	European medicines agency
EpCAM	epithelial cell adhesion molecule
ER	endoplasmic reticulum
ETV	entecavir
Fab	fragment antigen binding
FabMAbs	Refers to the constructs FabMAbαCD3 and FabMAbαCD28
FasL	first apoptosis signal ligand
Fc	fragment crystallizable
FCS	fetal calf serum
FcγR	Fc γ receptor
FDA	US food and drug administration
G_4S	glycine-serine
grzB	granzyme B
GSG	glycosaminoglycan
GαH	goat anti human antibody
HBc	HBV core protein
HBeAg	hepatitis B virus e antigen
HBVenv	HBV envelope protein
HBsAg	hepatitis B virus surface antigen
HBV	hepatitis B virus
HBx	hepatitis B virus x protein
HC	heavy chain
HCC	hepatocellular carcinoma
HRP	horse radish peroxidase
HSPG	heparan sulfate proteoglycan
i.p.	intraperitoneally
i.v.	intravenously
IC_{50}	half maximal inhibitory concentration
ICS	intracellular cytokine staining

IFNγ	interferon γ
Ig	immunoglobulin
IL-2	interleukin 2
ITAM	immunoreceptor tyrosine-based activation motifs
kb	kilo base
kD	kilodalton
LAM	lamivudine
LAMP	lysosomal membrane glycoprotein
LAT	linker for activation of T cells
LC	light chain
Lck	lymphocyte-specific protein tyrosine kinase
mAb	monoclonal antibody
MFI	mean fluorescence intensity
mg	milligram
MHC	major histocompatibility complex
ml	milliliter
MOI	multiplicity of infection
MVB	multivesicular bodies
n.d.	not detectable
NA	nucleos(t)ide analogue
NF-AT	nuclear factor of activated T-cells
NF-κB	nuclear factor kappa-light-chain-enhancer of activated B cells
NHL	non-Hodgkin’s lymphoma
nM	nanomolar
NTCP	sodium taurocholate co-transporting polypeptide
O/N	over night
OD	optical density
ORF	open reading frame
P	hepatitis B virus polymerase
P2A	self-cleaving A2 peptide
PBMC	peripheral blood mononuclear cell
PBS	phosphate-buffered saline
PD-1	programmed cell death protein 1
Peg-IFNα	pegylated interferon-α

pg	picogram
pgRNA	pregenomic RNA
PLC-γ	phospholipase C-γ
pMHC	peptide-MHC complex
preC-C	preCore-Core
preS-S	preSurface-Surface
qPCR	quantitative polymerase chain reaction
rcDNA	relaxed circular DNA
rpm	rounds per minute
RNA	ribonucleic acid
s.c.	subcutaneously
scFv	single chain fragment variable
SCID	severe combined immune deficient
scIL-12	single chain IL-12
SLP-76	SH2 domain containing leukocyte protein of 76 kD
$t_{1/2}$	half-life
TAP	transporter associated with antigen processing 1
TCR	T-cell receptor
TDF	tenofovir disoproxil fumarate
T_{FH}	follicular helper T cell
TGFβ1	transforming growth factor beta 1
T_H	T helper cell
TIL	tumor-infiltrating lymphocyte
TIM3	mucin-domain containing-3
TNFα	tumor necrosis factor α
tsAb	trispecific antibody; refers to the constructs TriMAb and OKTriMAb
uPA	urokinase type plasmogen activator
V_H	variable domain of the heavy chain
V_L	variable domain of the light chain
w/o	without
WB	western blot
WGA	wheat germ agglutinin
WHO	world health organization
ZAP-70	ζ-chain associated protein

1 Introduction

1.1 The hepatitis B virus

The following chapter will introduce the biology of the hepatitis B virus. It will cover the virus structure and replication cycle, viral pathogenesis, the limitations of current therapies as well as the prerequisites for specific targeting of HBV-infected hepatocytes with bispecific antibodies.

1.1.1 Molecular biology and replication cycle of HBV

1.1.1.1 Structure of viral particles

The hepatitis B virus is a small enveloped DNA virus that belongs to the family *Hepadnaviridea* (Schaefer, 2007). Like all members of this family, HBV shows a narrow host specificity and a strong tropism for infecting hepatocytes (Ganem and Prince, 2004). The infectious HBV virion with a size of 42 nm in diameter was first described by Dane et al. in 1970 (Dane et al., 1970) and is thus referred to as “Dane particle” (Fig. 1a). The partially double stranded DNA genome, termed relaxed circular DNA (rcDNA), is associated with the viral polymerase and embedded in an icosahedral capsid that is assembled by the hepatitis core protein (HBc). The capsid is engulfed by a lipoprotein membrane that is composed of host lipids and the hepatitis B envelope protein, which exists in the three isoforms small (S), middle (M) and large (L) (Nassal, 2015). Moreover, infected cells produce spherical and filamentous particles with a size of 22 nm that do not contain viral DNA and are therefore not infectious (Hu and Liu, 2017). These subviral particles can exceed the number of infectious virions ~10^5-fold (Ganem and Prince, 2004).

HBV is phylogenetically divided into 10 different genotypes (A-J) (Peeridogaheh et al., 2018), and can be grouped in four major serological subtypes (*ayw*, *ayr*, *adw* and *adr*), according to epitopes in the immunogenic loop of the envelope protein (Kramvis, 2014). The individual geno- and subtypes show a distinct geographical distribution and can further influence disease severity, treatment response, and the risk of HCC development (Peeridogaheh et al., 2018).

1.1.1.2 Genome organization

Due to its limited coding capacity of only 3.2 kilo bases (kb), the HBV genome is highly organized. It has four partially overlapping open reading frames (ORF), which are termed precore-core (preC-C), presurface-surface (preS-S), P, and X (Fig. 1b) (Ganem and Prince, 2004). The preC-C region encodes the HBc and the hepatitis B e antigen (HBeAg) by differential initiation of translation. Expression of the C region, employing the internal start codon, results in the production of the 22 kilo Dalton (kD) HBc, which forms the viral capsid and is localized in the cytoplasm.

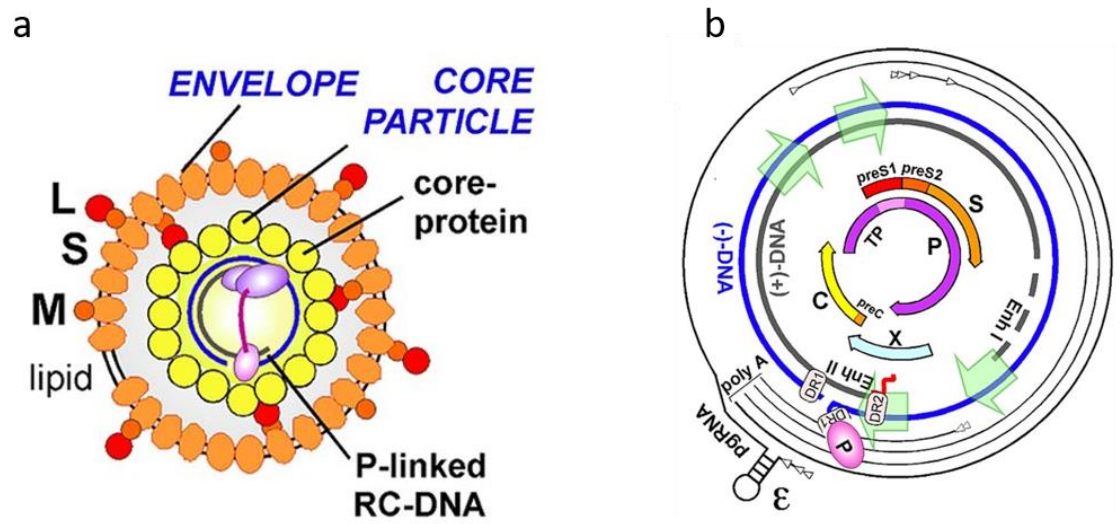

Figure 1: Structure of infectious HBV particles and genome organization. **(a)** The partially double-stranded rcDNA is associated with the viral polymerase and embedded in an icosahedral capsid that is assembled by the HBc. The capsid is engulfed by a lipoprotein membrane that is composed of host lipids and the hepatitis B envelope proteins, which exists in the three isoforms S, M and L (Nassal, 2015). **(b)** The HBV genome is highly organized with four open reading frames: preC-C, preS-S, P, and X. Outer lines depict viral transcripts. Transcription starts are marked with white arrowheads, ε symbolizes the encapsidation signal on pregenomic RNA (pgRNA). Green arrows stand for promotors, Enh I / Enh II transcriptional enhancers, DR1 / DR2 direct repeats, TP the terminal protein domain of P protein (Nassal, 2015).

In contrast, translation of the complete ORF leads to the expression of a 24 kD pre-Core protein that carries a signal sequence driving its co-translational translocation into the endoplasmic reticulum (ER) (Ganem and Prince, 2004). Cleavage by cellular proteases in the Golgi complex results in the generation of a 16 kD peptide that is secreted into the bloodstream, the HBeAg (Takahashi et al., 1983). It is supposed to regulate the immune response by eliciting tolerance in HBe/HBc specific T cells (Chen et al., 2004) and is further used as a marker for HBV infection. The viral envelope proteins S, M and L are encoded by the preS-S region and are also generated by differential initiation of transcription. Translation of the S region alone will result in expression of the S-protein. Addition of the preS2 region leads to the production of the M-protein and further extension with preS1 results in the expression of the L-protein. Consequently, all three isoforms share the same carboxy-terminal domain, and S-specific antibodies will also bind M and L. The P region encodes the viral polymerase, a 90 kD multifunctional enzyme with reverse transcriptase and RNaseH activity, which elicits DNA synthesis and RNA encapsidation during viral replication (Seeger and Mason, 2015). The non-structural HBV X protein (HBx) is encoded by the X region and has been shown to play a crucial role during initiation and maintenance of viral replication after HBV infection (Lucifora et al., 2011).

1.1.1.3 Replication cycle

The replication cycle starts with attachment to the host cell, mediated by reversible interaction between the myristoylated preS1 domain and glycosaminoglycan (GSG) side chains of heparan sulfate proteoglycans (HSPG) (Schulze et al., 2007), followed by specific binding to the sodium taurocholate co-transporting polypeptide (NTCP). NTCP is a multiple transmembrane transporter for bile acids and was identified as the functional receptor of HBV (Yan et al., 2012). It is predominantly expressed on primary hepatocytes and consequently causes the liver tropism of HBV. Transgenic expression of NTCP renders human hepatoma cell lines susceptible to HBV infection (Yan et al., 2012) and was also employed in our facility to generate the clonal cell line HepG2 NTCP K7 (Ko et al., 2018), which is used in infection experiments in this thesis. Endocytosis of viral particles has been shown to be clathrin-dependent and is mediated by interaction of the L-protein with the clathrin heavy chain and clathrin adaptor protein 2 (Huang et al., 2012). However, the requirement of caveolin-1 function for productive infection of HepaRG cells gives evidence for a second uptake route via caveolin-mediated endocytosis (Macovei et al., 2010). After fusion of the viral envelope with the host cell membrane, the viral capsid is released into the cytoplasm and amino-terminal nuclear localization sequences in the HBc polypeptide drive its transport to the nucleus (Eckhardt et al., 1991), followed by translocation via the cellular transport receptors importin α and β (Rabe et al., 2003). At the nuclear basket, the viral capsid is arrested through interaction with nucleoporin 153 and disassembles, thereby delivering the HBV genome into the karyoplasm (Schmitz et al., 2010). Inside the nucleus the partially single-stranded rcDNA is completed by the host cell DNA repair machinery (Ji and Hu, 2017), and is converted into the cccDNA. This episomal mini-chromosome further associates with histone proteins, forming nucleosomes (Bock et al., 1994) and a superhelical structure (Miller and Robinson, 1984), which persists in the nucleus of infected cells. The cccDNA serves as template for the cellular RNA-polymerase II, leading to the generation of pregenomic and subgenomic transcripts (Will et al., 1987), and expression of viral proteins. During spontaneous self-assembly of HBc (Birnbaum and Nassal, 1990), pregenomic RNA is packaged into the capsid, followed by reverse transcription, which is both mediated by the viral polymerase (Pollack and Ganem, 1994). Expression of the precore protein results in the secretion of HBeAg, as described in 1.1.1.1. The synthesis of envelope proteins takes place at the ER, where the polypeptide chains are co-translationally integrated into the lipid bilayer. Matured capsids bud into intracellular membranes bearing HBVenv and are subsequently exported from the cell via multivesicular bodies (MVB) (Watanabe et al., 2007). Alternatively, capsids are re-imported into the nucleus, resulting in the establishment and maintenance of a stable cccDNA pool (Tuttleman et al., 1986).

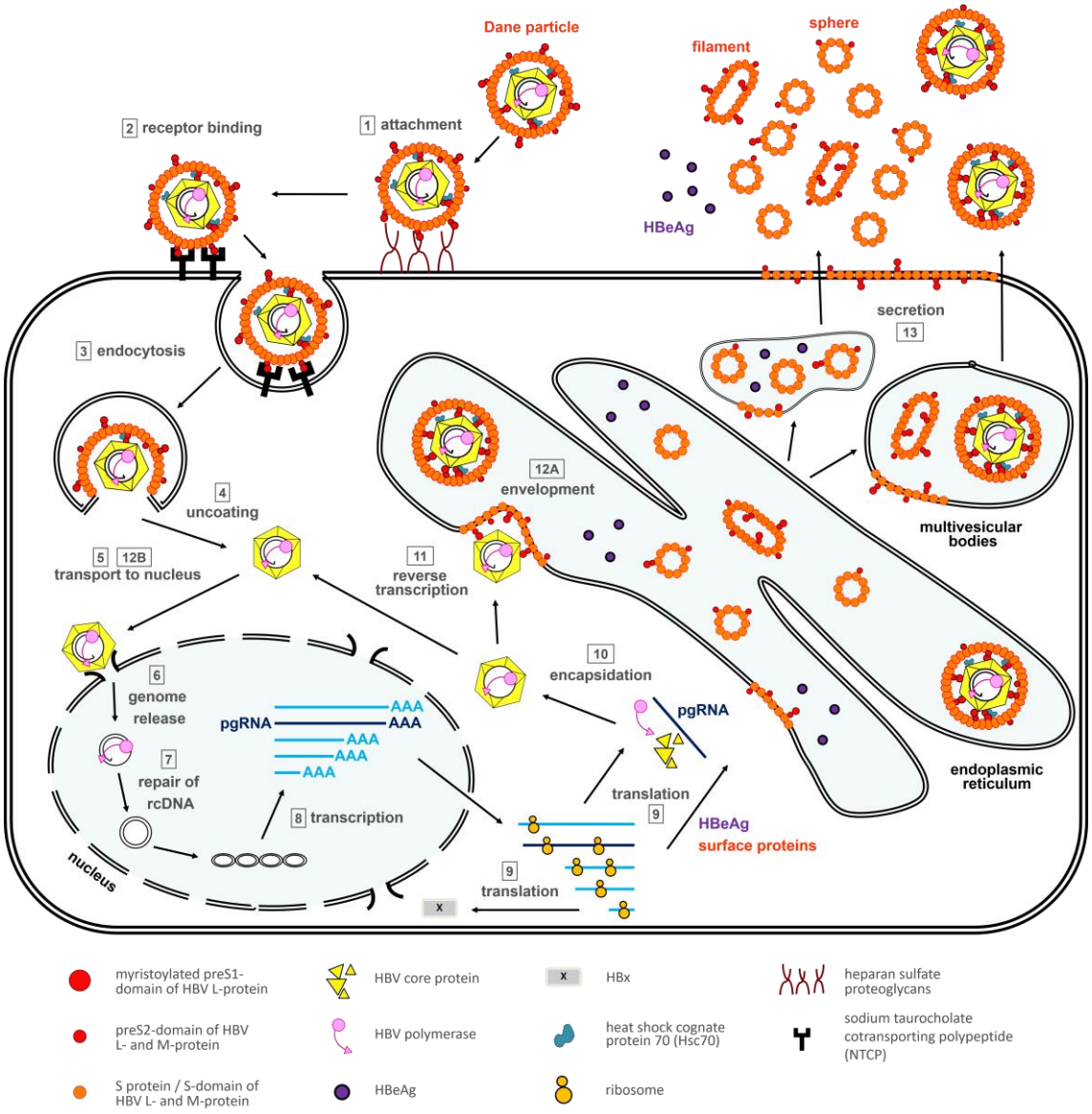

Figure 2: Replication cycle of HBV. (1) After interaction with heparan sulfate proteoglycans, (2) the HBV virion binds to NTCP and (3) is endocytosed. Following (4) uncoating, (5) the capsid is transported to the nucleus and (6) the viral genome is released into the karyoplasm, (7) where the rcDNA is converted into cccDNA and (8) transcription of viral RNAs is initiated. (9) Viral proteins are translated and (10) the pgRNA is encapsidated by self-assembling core protein followed by (11) reverse transcription into rcDNA. The capsid (12A) buds into HBVenv-bearing intracellular membranes or is (12B) re-imported into the nucleus. (13) The enveloped capsid leaves the cell via multivesicular bodies. Moreover, HBeAg, empty virions, spheres and filaments are secreted. During these processes, HBVenv is translocated to cell surface and exposed on the infected hepatocyte (Ko et al., 2017).

Subviral particles have been shown to self-assemble in a pre-Golgi compartment (Huovila et al., 1992) and leave the cell either via multivesicular bodies (filaments) (Jiang et al., 2015) or the Golgi apparatus (spheres) (Patient et al., 2007) and are referred to as hepatitis B surface antigen (HBsAg). Through dynamic lipid bilayer exchange between the ER, Golgi apparatus and the cell membrane, HBVenv is translocated to cell surface and exposed on the infected hepatocyte (Fig. 2). This is an essential prerequisite for the

specific targeting of HBV-infected cells with the bi- and trispecific antibodies that were generated and studied in this thesis.

1.1.2 Course of infection and HBV-associated liver diseases

The course of HBV-infection can vary between patients and is associated with the age and the HBV-specific immune response in the infected individual. Infection of adults mostly results in an acute self-limiting course and leads to viral clearance. In contrast, infants and young children often fail to control the virus and thus, are at high risk to develop chronic hepatitis B. Moreover, experiments in the chimpanzee model demonstrated that the outcome of infection is modulated by the size of the viral inoculum. It was observed that infection with a high dose (10^4-10^{10}) leads to viral clearance, whereas a low dose (10^1) favors persistent infection (Asabe et al., 2009).

1.1.2.1 Acute infection

An acute infection occurs in more than 95% of immunocompetent adults and will eventually lead to viral elimination. In Europe and North America, where the HBV prevalence is low, infections are mainly acute and the virus is transmitted through unprotected sexual contact and unsterile injections (Peeridogaheh et al., 2018). Since HBV infection itself shows no cytopathic effect, pathogenesis and disease develop when infected cells are engaged by the host immune system, resulting in liver inflammation and destruction of infected hepatocytes (Chisari et al., 2010). The disease can proceed without symptoms, cause self-limiting cholestatic hepatitis with jaundice, or in rare cases lead to fulminant hepatitis (Peeridogaheh et al., 2018). Infection with HBV is characterized by a poor induction of the innate immune response (Wieland et al., 2004a) and thus, viral clearance is predominately mediated by T cells that accumulate in the infected liver (Thimme et al., 2003). Along this line, a vigorous and multispecific T-cell response can be detected in patients with acute hepatitis that finally achieve viral clearance (Chisari et al., 2010). Acute infections are associated with a low mortality rate of 0.5-1%, which can be assigned to fulminant hepatitis (Peeridogaheh et al., 2018).

1.1.2.2 Chronic infection

Chronic HBV infection is defined by viral persistence for more than six months and is determined by presence of the serological biomarker HBsAg in the blood or serum of patients. Only 2.6% of immunocompetent adults, but 30-90% of children below the age of five will develop chronic HBV infection. In areas with high HBV prevalence, such as Southeast Asia and sub-Saharan Africa, infections are predominantly chronic and the virus is transmitted maternally during pregnancy or in the perinatal period. The primary infection is generally asymptomatic without profound signs of liver damage. However, chronically infected individuals have a severely increased risk to develop HBV-related liver diseases like fibrosis, cirrhosis and HCC, which can still manifest years after the primary infection. Progression of liver disease can be accelerated by certain risk factors, such as co-infection with the hepatitis D or C virus as well as alcohol abuse (Peeridogaheh et al., 2018). In contrast to individuals with acute hepatitis, in chronically infected patients only oligoclonal and dysfunctional T-cell responses can be detected,

which fail to eliminate the infection (Chisari et al., 2010). Thus, restoration of an efficient HBV-specific T-cell response employing bispecific antibodies is an interesting approach for a potential therapy. Follow up studies of CHB patients infected at young age indicated that approximately 15–25% of chronic HBV carriers die of cirrhosis or HCC (Rizzetto and Ciancio, 2008, Peeridogaheh et al., 2018). According to the World Health Organization (WHO), approximately 257 million people are worldwide chronically infected with HBV and the related liver diseases resulted in around 887.000 deaths in the year 2015 (WHO, 2019).

1.1.2.3 HBV-associated hepatocellular carcinoma

Hepatocellular carcinoma is a leading cause of cancer related death worldwide (Balogh et al., 2016) and associated with HBV infection in 45-50% of patients (Peeridogaheh et al., 2018, Tantiwetrueangdet et al., 2018). The previous establishment of cirrhosis is considered to be a major risk factor for cancer development, as it occurs in 80-90% of HCC cases (Llovet et al., 2003). However, CHB patients have been reported to develop HCC also in the absence of cirrhosis (Chayanupatkul et al., 2017). Cancer development is thought to occur through three molecular mechanisms, which are introduced in the following. First, expression of the viral X protein has been shown to modulate cellular processes on various levels including expression and activity of several proteins as well as epigenetic mechanisms (Liu et al., 2016a). Among others, carcinogenic effects of the X protein are driven by impairment of DNA repair mechanisms (Qadri et al., 2011) or upregulation of apoptosis inhibition genes such as B-cell lymphoma 2 (BCL-2) and myeloid cell leukemia-1 (Shen et al., 2013). Second, the viral DNA has been shown to integrate into the host genome, which is observed in 85-90% of HBV-related HCC cases (Peeridogaheh et al., 2018). Integration sites demonstrated a preference for functional genomic regions (Zhao et al., 2016), which in turn can induce genomic instability and hepatocarcinogenesis through mutations in tumor suppressor or oncogenes. Third, persistent inflammation and necrosis, accompanied by compensatory proliferation of hepatocytes will lead to accumulation of genetic damage, which is a key factor in HCC development (Peeridogaheh et al., 2018). Hereby, the viral load has been shown to determine the severity of inflammation-induced liver damage (Biazar et al., 2015) and consequently the risk of HCC development (Pazgan-Simon et al., 2018).

HCC patients have a poor prognosis with a median survival period of about 11 months (Greten et al., 2005). Liver resection and transplantation are the treatment options of choice for patients with early stage disease (Balogh et al., 2016) and have the highest curative rates with a 5-year survival of up to 74% (Allemann et al., 2013). Systemic therapy with the serine/threonine kinase inhibitor sorafinib is the standard of care for patients with advanced HCC and end stage disease that are no candidates for surgical therapy (Balogh et al., 2016). However, medication with sorafinib has major side effects (Iavarone et al., 2011) and can increase patient survival by only a few months (Balogh et al., 2016). Interestingly, HCC has been reported to maintain HBVenv expression in some cases (Han et al., 1993, Wang et al., 2002), which renders bispecific antibodies a potential novel treatment option for these patients.

1.1.3 Prophylaxis and treatment

1.1.3.1 Prophylactic vaccination

An effective recombinant HBV vaccine was introduced in 1986 and has been very successful in reducing the rate of infection as well as HBV-related morbidity and mortality (Peeridogaheh et al., 2018). The vaccine contains HBsAg and leads to the production of HBVenv-specific antibodies that can neutralize the virus and thereby provide protection in 95% of vaccinated individuals (WHO, 2017). Since newborns from infected mothers are at particular risk to get infected, a combination of active immunization with the recombinant vaccine and passive immunization with HBV-specific antibodies within the first 24 hours after birth is recommended. This vaccination strategy successfully prevents HBV infection in 80-95% of children and significantly reduces mother to child transmission (Peeridogaheh et al., 2018). Although vaccination provides a feasible and effective approach to prevent HBV infection, it cannot be used as treatment for CHB patients.

1.1.3.2 Treatment options

Current therapies include pegylated interferon-α (Peg-IFNα) and nucleos(t)ide analogues (NAs), however, both medications fail to cure the disease effectively. Thus, the goal of antiviral therapy is to reduce CHB-related morbidity and mortality.

Treatment with Peg-IFNα can lead to sustained viral control, yet displays low response rates and elicits viral elimination in only 10% of patients (Zoulim et al., 2016). The exact mechanism of the Peg-IFNα-mediated antiviral effect is still not completely understood, but it is has been shown to decrease viral transcripts through epigenetic regulation of cccDNA (Belloni et al., 2012), degrade cccDNA by induction of apolipoprotein B mRNA-editing enzyme, catalytic polypeptide-like (APOBEC) expression (Lucifora et al., 2014) and raise the antiviral potential of natural killer cells (NK cells) (Micco et al., 2013).

NA therapy specifically suppresses viral replication by inhibition of the reverse transcriptase, yet the covalently closed circular DNA (cccDNA) is not targeted and remains in the nucleus of the infected hepatocytes. This allows for reactivation of HBV after cessation of antiviral therapy (Zoulim et al., 2016). Consequently, NA therapy requires life-long treatment and carries the risk of long-term toxicity (Gill et al., 2015), as well as spontaneous HBV-driven HCC development in absence of liver cirrhosis (Chayanupatkul et al., 2017, Bruix et al., 2017). Moreover, continuous medication with NAs increases the risk of drug resistance and consequently failure of treatment (Peeridogaheh et al., 2018). Nucleos(t)ide analogs include lamivudine (LAM), telbivudine, adefovir dipivoxil, entecavir (ETV), and tenofovir disoproxil fumarate (TDF). Among these, ETV and TDF are especially effective and show the lowest rates of emerging resistant mutants during long-term treatment (Lin et al., 2016). While continues medication with LAM resulted in 76.3% of treatment-resistant HBV mutants within an 8-year study (Yuen et al., 2007), numbers for ETV (Ono et al., 2012), and TDF (Buti et al., 2015) were below 1% within 4 and 7 years, respectively. Long-term treatment with ETV and TDF leads to effective viral suppression in more than 90% of patients and is

generally well tolerated (Terrault et al., 2016). Importantly, treatment with NAs can furthermore delay the development of cirrhosis as well as the progression to HCC in cirrhotic patients (Lin et al., 2016). Extending antiviral therapy after hepatectomy and liver transplantation has also been shown to improve patient survival (Pazgan-Simon et al., 2018). However, although ETV-treatment can decrease the risk of HCC-development in cirrhotic patients by 60%, a significantly elevated risk remains (Su et al., 2016). Taken together, current therapies efficiently interfere with the viral replication cycle, but rarely achieve viral elimination or “functional cure” (Block et al., 2013), a clinical situation defined by undetectable levels of HBV-DNA in the serum, normalized levels of alanine amino transferase (ALT), as well as seroconversion from HBsAg to HBsAg-specific antibodies (anti-HBs) (Bertoletti and Bert, 2018). Consequently, further efforts that intent a curative therapy for HBV infection are still needed.

1.2 The adaptive immune system

The next chapter will introduce T lymphocytes and their role in the adaptive immune system. It will cover fundamental mechanisms of T-cell mediated immunity, elaborate on the characteristics of T-cell responses in acute and chronic HBV infection, and describe the composition and signaling pathways of the T-cell receptor (TCR). This knowledge is essential to understand the concept of bsAb-mediated T-cell redirection.

1.2.1 T-cell mediated immunity

1.2.1.1 The role of T cells in the clearance of pathogens

Matured T cells leave the thymus and recirculate between the blood and secondary lymphoid organs until they encounter their specific antigen (Gowans and Knight, 1964, Marchesi and Gowans, 1964). Each naïve T cell is equipped with a unique T-cell receptor (Meuer et al., 1983a, Meuer et al., 1983b) that is generated through rearrangement of genomic DNA (Royer et al., 1984). In contrast to antibodies, the TCR is unable to recognize native antigen, but binds proteosomally processed peptides presented by the major histocompatibility complex (MHC) on antigen presenting cells (Zinkernagel and Doherty, 1974). APCs, including monocytes, macrophages, dendritic cells (DCs) and B lymphocytes, ingest antigen from the site of infection or tumor, and migrate to secondary lymphoid organs, where they present it to T cells in the context of MHC. After contact with the matching peptide-MHC complex (pMHC) that is exposed on the APC, the naïve T cell is activated or “primed”, which in turn leads to proliferation and differentiation into effector T cells that share clonal identity (Murphy and Weaver, 2016). Based on the expression of the co-receptors CD8 and CD4, the T-cell population can be divided into two subsets, which exert different effector functions upon activation (Cantor and Boyse, 1975, Reinherz et al., 1979).

$CD8^+$ T cells recognize peptides with a length of 8-10 amino acids (AA) that are presented on MHC class I molecules (Bouvier and Wiley, 1994). Upon priming through APCs, their main task is the elimination of infected or carcinogenic target cells, which is why they are referred to as cytotoxic T lymphocytes (CTL). The interaction of the TCR on primed T cells and pMHC on target cells results in the release of cytotoxic granules containing granzymes and perforin and thereby induces the lysis of the target cell (Peters et al., 1991). The lysosomal membrane glycoproteins lamp-1 (CD 107 a), lamp-2, and CD63, are incorporated in membranes of granules and become translocated to the CTL plasma membrane during degranulation (Peters et al., 1991). Thus, their membranous localization can be used as degranulation marker, implicating cytotoxic T-cell function. Activated $CD8^+$ T lymphocytes can furthermore induce a non-cytotoxic immune responses by the release of cytokines, such as interferon γ (IFNγ), interleukin 2 (IL-2), or tumor necrosis factor α (TNFα) (Murphy and Weaver, 2016).

$CD4^+$ T cells recognize peptides presented on MHC class II molecules. Peptide length is not constrained and can vary between 12 and 25 AAs (Rammensee et al., 1995). Although $CD4^+$ T cells can become cytotoxically active, their main function is the

assistance of immune cells by the secretion of modulatory cytokines and therefore they are referred to as T helper cells (T_H). Upon activation, naive $CD4^+$ T cells can differentiate into activating T_H1 and T_H2 cells (Mosmann et al., 1986, Killar et al., 1987) or inhibiting regulatory T cells (Gershon and Kondo, 1970). T_H1 cells further activate T cells and macrophages through the release of IL-2 and IFNγ, while T_H2 cells secrete IL-4, 5, 6 and 10 (Del Prete et al., 1991), resulting in the stimulation of pre-B cells that in turn differentiate into antibody-producing plasma cells (Murphy and Weaver, 2016).

The origin and processing of immunogenic peptides differs between MHC classes. Cytosolic proteins are proteosomally degraded and translocated into the ER by the transporter associated with antigen processing 1 (TAP) (Shepherd et al., 1993). In the ER they bind and stabilize MHC I and are subsequently shuttled to the cellular membrane. In contrast, extracellular antigen that is taken up by APCs is degraded in acidified vesicles, followed by loading on MHC II and presentation on the cell surface (Bikoff and Birshtein, 1986, Eisenlohr and Hackett, 1989). Importantly, antigen from the extracellular space can also be presented on MHC I (Bevan, 1976a, Bevan, 1976b). This process is known as cross presentation and allows the priming of $CD8^+$ T cells in settings where viruses do not infect the APCs (Jung et al., 2002). This mechanism has been shown to play an important role in the induction of HBV-specific T-cell responses (Murata et al., 2018).

1.2.1.2 T-cell mediated immunity in CHB

As already briefly mentioned in 1.1.2 the course of HBV infection largely depends on the virus specific T-cell response. The importance of a vigorous and multi-specific $CD8^+$ and $CD4^+$ T-cell response that controls viral infection via cytolytic (Rehermann and Nascimbeni, 2005) and cytokine-mediated (Guidotti and Chisari, 2001) mechanisms has been demonstrated in several studies. In contrast, viral persistence and the development of CHB are characterized by depletion and/or exhaustion of HBV-specific T cells (Protzer et al., 2012). The mechanisms of viral persistence are still not completely understood, but there is evidence that it can be partially attributed to the expression of immunomodulatory viral proteins as well as tolerance-mediating mechanisms in the liver (Protzer et al., 2012). The secretion of HBeAg into the bloodstream has been shown to elicit tolerance in HBc/HBeAg-specific T cells (Chen et al., 2004). A similar function is believed to be exerted by HBsAg (Chisari et al., 2010), since high serum titers are often associated with chronic infection and HBVenv-specific T-cell responses can hardly be detected in CHB patients (Webster et al., 2004). Moreover, overexpression of HBx has been shown to inhibit proteasome activity (Hu et al., 1999), which in turn will impair antigen processing and presentation.

Independently, the liver is described as an organ with unique immune features that promote tolerance rather than immunity (Thomson and Knolle, 2010, Knolle, 2012), and thus offers a niche for persistent viral infections (Protzer et al., 2012). Tolerizing mechanisms in the liver include hepatocyte-mediated T-cell elimination (suicidal emperipolesis) (Benseler et al., 2011), hepatic priming of naïve T cells that results in the

upregulation of BCL-2 interacting mediator of cell death (Bim) and increased apoptosis (Lopes et al., 2008, Holz et al., 2008, Holz et al., 2012). Furthermore, excess of co-inhibitory signals mediated by programmed cell death protein 1 (PD-1) (Iwai et al., 2003), cytotoxic T-lymphocyte-associated protein 4 (CTLA-4) (Schurich et al., 2011), T-cell immunoglobulin and mucin-domain containing-3 (TIM3) (Liu et al., 2016b) and transforming growth factor beta 1 (TGFβ1) (Tinoco et al., 2009) contribute to a tolerogenic environment.

However, the T-cell exhaustion in CHB patients is restricted to HBV-specific T cells, which only make up around 0.01-2% of the total population (Chang et al., 2009). Even though a recent study highlighted that CHB might be associated with systemic immune regulatory mechanisms extending beyond HBV (Park et al., 2016), the majority of T cells in CHB patients remains functional and is vacant for immunotherapeutic approaches, including adoptive T-cell therapy or treatment with bispecific antibodies.

1.2.1.3 TCR composition and signaling

The interaction between the T-cell receptor and pMHC is a fundamental event during the initiation of T-cell activation. However, the TCR itself is not capable of transmitting the activation signal to intracellular components. Therefore, it is non-covalently associated with the CD3 protein complex (Reinherz et al., 1982) that comprises the four subunits γ-, δ-, ε and ζ-chain (Borst et al., 1983), which carry intracellular immunoreceptor tyrosine-based activation motifs (ITAM) that contain two YXXL/I-motifs (Reth, 1989). Upon TCR engagement, the tyrosines within ITAMs are phosphorylated by the lymphocyte-specific protein tyrosine kinase (Lck) (van Oers et al., 1996), which is associated with the cytoplasmic domains of the co-receptors CD4 (Rudd et al., 1988) and CD8 (Veillette et al., 1988). Phosphorylation of both YXXL/I-motifs enables specific binding of the ζ-chain associated protein (ZAP-70) (Chan et al., 1991). Recruitment of ZAP-70 to ITAMs results in its activation by Lck, followed by the phosphorylation of its downstream substrates linker for activation of T cells (LAT) (Zhang et al., 1998) and SH2 domain containing leukocyte protein of 76 kD (SLP-76) (Jackman et al., 1995). This initiates a signaling cascade mediated by phospholipase C-γ (PLC-γ) and Ca^{2+} influx (Delon et al., 1998), resulting in the activation of the transcription factors nuclear factor kappa-light-chain-enhancer of activated B cells (NF-κB) (Li et al., 2005), nuclear factor of activated T-cells (NF-AT) (Shaw et al., 1988) and activator protein 1 (AP-1) (Rincón and Flavell, 1994). Eventually, this induces an alteration of gene expression and in turn leads to T-cell activation, proliferation and differentiation (Murphy and Weaver, 2016).

The phosphorylation of ITAMs by Lck is the first detectable biochemical signal upon TCR-pMHC interaction. However, the process that translates MHC binding into ITAM phosphorylation remains an area of investigation. In the inactive conformation, electrostatic interactions between the cytoplasmic tails of CD3 and the plasma membrane result in a close association of the two, which sterically inhibits the phosphorylation of ITMAs by Lck (Xu et al., 2008). Thus, dissociation of intracellular CD3 domains from the membrane is required for intracellular signal transduction. The

mechanism of ITMA release is still unknown, but is proposed to involve TCR clustering (Minguet et al., 2007) and mechanical forces exerted by highly dynamic interaction and relative motion between T cell and APC upon TCR engagement (Ma et al., 2012). This external force can be sensed by the TCR (Kim et al., 2009) and has been shown to induce T-cell signaling (Feng et al., 2017) and potentiate T-cell effector function (Basu et al., 2016). It is likely that binding of CD3-targeting bispecific antibodies might be able to induce CD3 clustering as well as mechanical stimulation, which is the basis of bsAb-mediated T-cell redirection.

However, the signaling induced by the TCR complex is not sufficient to achieve full activation of naive T cells without further co-stimulation. This is mediated by additional receptors exposed on the T-cell membrane, which specifically interact with ligands presented on the surface of APCs (Murphy and Weaver, 2016), establishing a so-called immunological synapse (Huppa and Davis, 2003). The best understood co-stimulatory receptor is CD28 (Aruffo and Seed, 1987) and its ligands B7.1 (CD80) (Freedman et al., 1987) and B7.2 (CD86), which are especially presented by specialized APC, as for example dendritic cells (Lim et al., 2012). Activation of CD28 amplifies TCR signaling and is required for maximal activation of PLC-γ, thereby stimulating the survival (Boise et al., 1995) and proliferation (June et al., 1987) of T cells , as well as the production of cytokines (Jenkins et al., 1991). In the absence of co-stimulatory signals, T cells can become insusceptible to further stimulation (T-cell anergy) (Harding et al., 1992) or undergo apoptosis (Beyersdorf et al., 2015).

1.2.2 B-cell mediated immunity

1.2.2.1 The role of B cells in the clearance of pathogens

Naïve B cells encounter their antigen in primary lymphoid follicles. In contrast to the TCR, the B cell receptor (BCR) recognizes complement bearing native protein that is presented by follicular dendritic cells or macrophages via complement receptors (LeBien and Tedder, 2008). Upon BCR engagement the antigen is internalized and presented to follicular helper T cells (T_{FH}) via MHC class II molecules (Victora and Nussenzweig, 2012). T_{FH} cells that are specific for the presented peptide are activated and in turn stimulate the B cell via CD40-CD40L interaction and the secretion of cytokines, such as IL-21 (Grewal and Flavell, 1998). B-cell activation results in proliferation and differentiation into memory B cells or antibody-producing plasma cells. The secreted antibodies (Abs) inhibit the spread of pathogens and toxins by specific binding of their target antigen, which can prevent cell entry (neutralization) and facilitates the ingestion by macrophages via binding to fragment crystallizable (Fc) receptors (opsonization). Moreover, interaction between antibody and target antigen on cell surfaces results in the elimination of pathogens through complement-mediated cytotoxicity (CDC) and elimination of infected host cells by NK cells via antibody-depended cell-mediated cytotoxicity (ADCC) (Murphy and Weaver, 2016).

1.2.2.2 Structure of antibodies

Antibodies consist of a variable domain and a constant domain. The constant region exists in the 5 different isotypes immunoglobulin M (IgM), IgD, IgG, IgA and IgE and determines the function of the antibody (Murphy and Weaver, 2016). The predominant isotype in the human body is IgG (Schroeder and Cavacini, 2010), which is made up of two heavy (HC) and two light chains (LC), which are linked via disulfide bonds (Fig. 3). Based on differences in functionality, IgG molecules can be further divided in the Fc domain and two antigen-binding fragments (Fab). The Fab fragments bind the antigen and determine the specificity of the antibody, while the Fc domain interacts with Fc receptors on various immune cells, leading to the exertion of antibody-mediated effector function, as for example ADCC.

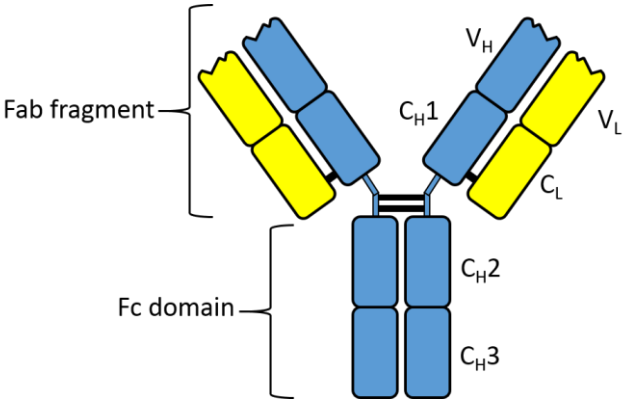

Figure 3: Schematic representation of an IgG1. IgG1 is made up of two heavy chains (blue) and two light chains (yellow). Each HC is divided in a variable domain (V_H) and a constant domain, which consists of C_H1, C_H2 and C_H3. The LC is also made up of a variable domain (V_L) and a constant domain (C_L). The heterodimeric protein is stabilized by cysteine bonds between C_H1 and C_L, as well as between the two HCs in the hinge region (black lines). Adapted from Janeway`s Immunobiology p.:141.

1.2.2.3 B-cell immunity in CHB

Since T cells are widely accepted as key players in the establishment of functional cure, the importance of the B-cell mediated immunity in the setting of HBV infection has been neglected over decades (Zhang et al., 2018). It is clear now that HBVenv-specific neutralizing antibodies can bind to infectious virions and thereby inhibit viral infection (Golsaz Shirazi et al., 2014) as well as contribute to viral elimination by antibody-mediated effector function, including CDC and ADCC (Gao et al., 2017). Moreover, they confer protection against re-infection, which is also the basis of the prophylactic vaccination (WHO, 2017). Viral elimination is associated with seroconversion from HBsAg to anti-HBs (Bertoletti and Bert, 2018) and also anti-HBe antibodies seem to be involved in the HBV-specific immune response, as they can be detected in patients who cleared infection, but are absent in chronically infected individuals (Chisari et al., 2010). Recent studies further highlighted the significance of the humoral immunity, showing HBV reactivation after B-cell depletion in lymphoma patients (Loomba and Liang, 2017) and spontaneous viral clearance after bone marrow transplantation from vaccinated donors to CHB patients (Lindemann et al., 2016).

The neutralizing antibodies have also been investigated as treatment option in pre-clinical models (Eren et al., 2000) and CHB patients (Galun et al., 2002). The administration induced a significant but transient reduction of HBsAg and HBV-DNA in the serum, yet did not achieve sustained viral control. This argues that treatment with conventional antibodies can efficiently clear HBV from the circulation, yet Fc receptor-mediated immunity fails to induce an adequate cytotoxic immune response against the infected hepatocytes. This limitation might be overcome by combination of HBVenv-specific antibodies with stronger immunostimulatory moieties, such as CD3- or CD28 specific antibodies. The combination of two distinct specificities within one molecule results in the generation of a so-called bispecific antibody.

1.3 Bispecific antibodies as immunotherapeutic tools

1.3.1 Principles of bispecific antibodies

Bispecific antibodies were developed as an alternative immunotherapeutic approach for treatment of cancer. Simultaneous binding of a native tumor-associated antigen and the CD3 complex on the T-cell membrane induces the establishment of a transient cytolytic synapse, which can result in the lysis of the tumor cell. Consequently, the mode of action is independent of the T-cell specificity and MHC-dependent antigen presentation (Baeuerle and Reinhardt, 2009). Theoretically, this approach allows the redirection of any CD3-positive effector cell towards a therapeutic target of choice, including the HBV envelope protein that is exposed on the surface of infected hepatocytes (Fig. 4).

In most cases, an antibody can be reduced to its variable region, without losing antigen-binding specificity and affinity. The connection of the light chain and heavy chain variable domains through a linker sequence allows the construction of single-chain binding moieties, which are termed single chain fragment variable (scFv). The combination of two scFvs in one polypeptide results in the generation of a bispecific T-cell engager (BiTE) (Baeuerle and Reinhardt, 2009, van Spriel et al., 2000), which has been established as a common format in the field of bsAb research. Most constructs developed up to date are directed against the CD3 complex and such bsAbs have been shown to induce efficient tumor cell lysis without the requirement of further co-stimulation (Liu et al., 2017, Loffler et al., 2000, Riesenberg et al., 2001).

1.3.2 Clinical application of bispecific antibodies

At the moment, more than 43 different bispecific antibodies are in various stages of clinical development (Labrijn et al., 2019). Most of them are targeting cancer-associated antigens such as CD19, CD20, CD30, the epithelial cell adhesion molecule (EpCAM) or the epithelial growth factor receptor (EGFR) and facilitate T-cell redirection through CD3 engagement. A second major application is the treatment of inflammatory and autoimmune diseases through combinatory neutralization of cytokines, including IL-1α, IL-1β, IL-13, IL-17 and TNFα. Up to date, three bispecific antibodies have successfully entered the market. They are briefly described in the following.

1.3.2.1 Catumaxomab

Catumaxomab was the first bispecific antibody to receive market approval by the European medicines agency (EMA) in 2009 (Linke et al., 2010). It is a hybrid IgG antibody, which is produced through the quadroma technology (Milstein and Cuello, 1983) and consists of a murine IgG2a and rat IgG2b. It targets EpCAM, recruits T cells via interaction with CD3, and moreover, activates macrophages, DCs and NK cells via Fc receptor-mediated effector function. Thus, it is referred to as trifunctional antibody. Catumaxomab is indicated for the treatment of malignant ascites, but was employed in further clinical trials for ovarian cancer, gastric cancer and epithelial cancer (Kontermann

and Brinkmann, 2015). The dosing schedule comprises four intraperitoneal infusions of 10, 20, 50 and 150 µg on day 0, 3, 7 and 10, respectively (Heiss et al., 2010).

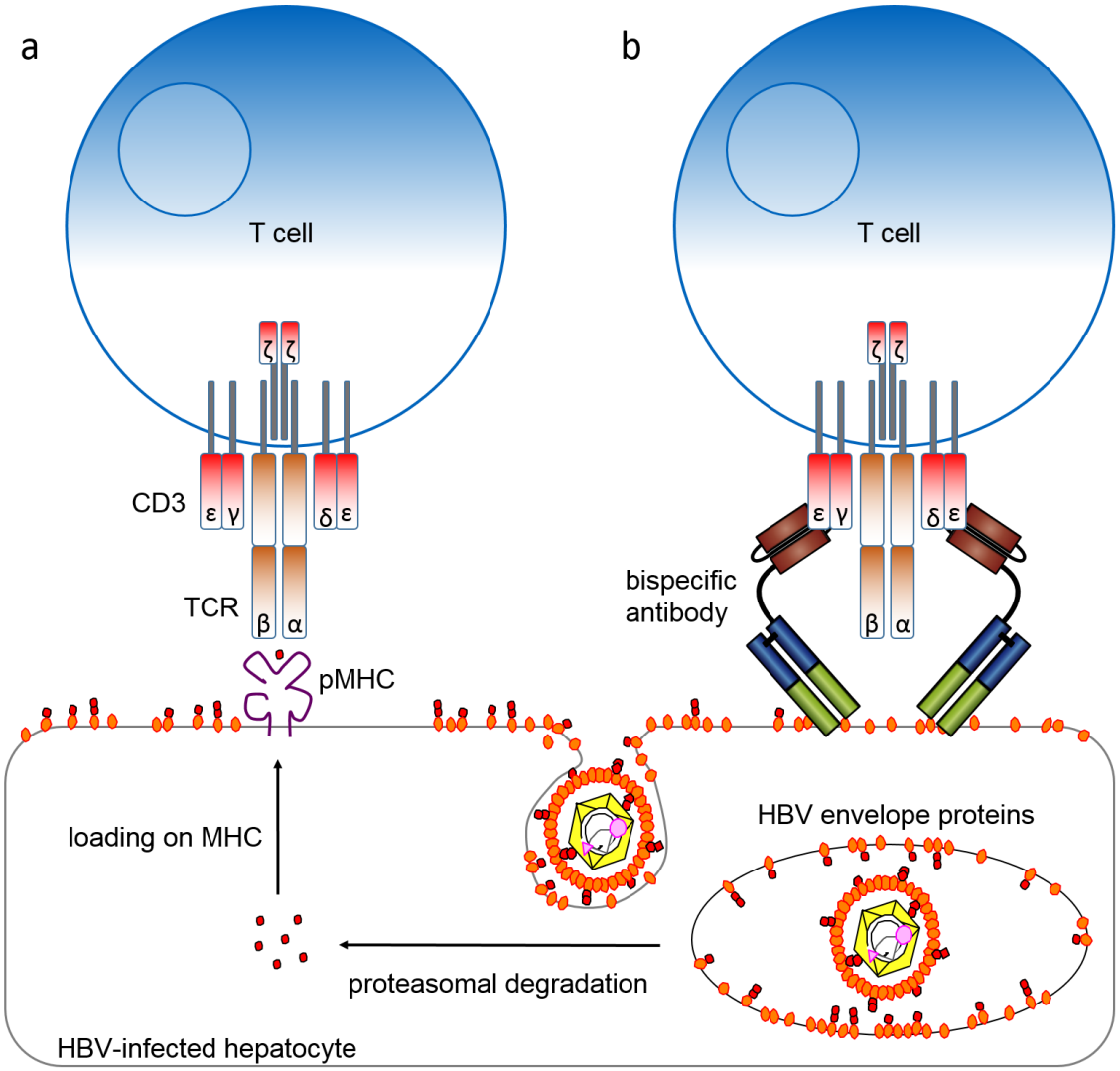

Figure 4: Schematic comparison of endogenous and bsAb-mediated T-cell activation in the context of HBV infection. (a) The TCR complex, consisting of T-cell receptor and CD3, specifically recognizes proteolytically processed peptide derived from the HBV envelope protein, which is presented on MHC class I. **(b)** Through simultaneous binding of CD3 on the T cell and native HBV envelope protein exposed on the surface of the infected hepatocyte, the bispecific antibody induces a transient immunological synapse. This process is independent of the endogenous T-cell specificity and MHC-dependent antigen presentation.

Since the origin of the molecule is non-human, mouse- and rat-specific antibodies were detected in around 70% of patients after the four consecutive administrations. The immunogenicity of catumaxomab did not result in adverse side-effects and was rather associated with an improved clinical outcome. However, this is thought to be associated with a good physical condition of the respective patients and is not mediated by antibody treatment (Linke et al., 2010). The immunogenicity of non-human domains in bispecific antibodies still needs to be considered, as long-term treatment with such constructs will probably result in drug neutralization and thereby limit the therapeutic effect. Although,

catumaxomab-treatment showed promising results (Linke et al., 2010) and acceptable tolerability (Heiss et al., 2010) in various trials, it was withdrawn from the market in 2017 after its manufacturer went insolvent and its production was not lucrative anymore (GmbH, 2017). This highlights that the manufacture of bispecific antibodies can be labor- and cost-intensive, which needs to be considered independently of their efficacy.

1.3.2.2 Blinatumomab

Blinatumomab is a bispecific antibody of the BiTE format that has been developed as treatment option for acute lymphoblastic leukemia (ALL) and non-Hodgkin's lymphoma (NHL). It combines specificities for CD3 as well as CD19, a cell differentiation antigen solely present on B cells during nearly all states of development. In 2014, it was approved by the US food and drug administration (FDA) for the treatment of refractory/relapsed ALL. Due to a mean half-life of 2.10 hours (Blincyto (Blinatumomab) [package insert] Thousand Oaks), blinatumomab is applied via continuous intravenous infusion, which is required to reach therapeutic drug concentrations in the circulation. The drug is applied with doses of 5 or 15 µg/ml^2/day resulting in a steady state concentration of 211 and 621 pg/ml, respectively (Lee et al., 2016). Despite its small size, renal excretion of the construct has been shown to be negligible and elimination of blinatumomab is believed to occur via catabolic pathways (Lee et al., 2016). A recent meta-analysis described complete remission rates of 45% in ALL and 20% in NHL patients upon medication with blinatumomab (Yu et al., 2019), and thus clearly underlines the potency of bispecific antibodies as novel immunotherapeutic agents.

1.3.2.3 Emicizumab

Emicizumab is a recombinant bispecific full-length antibody designed for the treatment of hemophilia A (Labrijn et al., 2019). This genetic disease manifests in a bleeding disorder caused by mutations in the factor 8 gene that result in a dysfunction of clotting factor VIII (FVIII) (Konkle et al., 1993). Manufacturing of emicizumab is achieved through the "knobs-into-holes" technology that facilitates the heterodimerization of heavy chains with different specificities resulting in the generation of bispecific IgG (Merchant et al., 1998). By simultaneous binding of the serine protease factor IXa and the factor X (FX), emicizumab mimics the function of FVIII and thereby promotes phosphorylation-mediated activation of FX, which in turn regulates hemostasis (Kitazawa et al., 2012). In August 2017, a phase 3 clinical trial demonstrated significantly lower bleeding rates in hemophilia A patients upon prophylactic treatment with emicizumab (Oldenburg et al., 2017) paving the path for its approval by the FDA in November the same year (Labrijn et al., 2019). Emicizumab exemplifies the broad application spectrum of bispecific antibodies, which extends beyond their potential in immunotherapy.

1.3.2.4 Risks and side effects of bsAb-treatment

The administration of bispecific antibodies is associated with certain risks and potential side effects. One concern is unspecific T-cell activation and cytokine release in the absence of target antigen. Bispecific antibodies that engage CD3 or CD28 could potentially trigger TCR signaling, similar to commercial monoclonal antibodies that are

used for *in vitro* T-cell stimulation. However, monoclonal CD3 or CD28 antibodies fail to provide T-cell stimulation in a soluble state. To mimic clustering of TCRs by recruiting CD3 and CD28 to an artificial immunological synapse and to exert mechanical forces induced by the relative motion between T cell and APC upon TCR engagement, monoclonal antibodies need to be immobilized by adsorption to a surface or interaction via Fc receptors (Geppert and Lipsky, 1988, Hussain et al., 2015) (see also 1.2.1.3). Consequently, the presence of target antigen should be required to induce bsAb-mediated T-cell redirection, as binding to the target antigen enables local clustering of CD3 and CD28 molecules, as well as the exertion of mechanical forces, when provided either adsorbed to a surface or membrane-bound on the surface of target cells. To minimize Fc-receptor binding, the mutations C220S, E233P, L234A, L235A, G236del, N297Q, K322A, A327G, P329A, A330S and P331S are commonly introduced into the Fc domains of bispecific constructs (Saunders, 2019). These mutations are also employed in the BiMAb constructs that were characterized in this thesis (see also 2.2.1).

The most common side effect upon treatment with T-cell stimulating therapies is the excessive release of proinflammatory cytokines, also known as cytokine release syndrome (CRS) (Shimabukuro-Vornhagen et al., 2018). The clinical manifestation of CRS can range from mild flu-like symptoms to a severe life-threatening cytokine storm; however, the pathophysiology of CRS remains incompletely understood. It is believed to be induced by IFNγ-mediated activation of bystander cells, in particular macrophages, which in turn respond with a massive release of cytokines, including TNFα, IL-10, and especially IL-6 (Teachey et al., 2013). IL-6 has been shown to contribute to several symptoms that are associated with severe CRS, such as vascular leakage (Wei et al., 2013), intravascular coagulation (Levi and Ten Cate, 1999), and myocardial dysfunction (Pathan et al., 2004). In 2017, the IL-6-receptor specific antibody tocilizumab was FDA-approved for treatment of the cytokine release syndrome and its administration has been shown to reduce blinatumomab-induced CRS in refractory ALL patients (Teachey et al., 2013).

In the setting of HBV immunotherapy, a further concern is the systemic activation of T cells by soluble HBsAg in the circulation of infected patients, which can on the one hand increase the risk of CRS-development and on the other hand lead to immunopathology in non-hepatic uninfected tissue. However, bsAb-engagement of soluble HBsAg should neither result in efficient clustering of T-cell antigens, nor exert a mechanical stimulation of CD3 and CD28 and therefore, T-cell activation should be limited. Nevertheless, undirected T-cell activation by soluble HBsAg needs to excluded by *in vivo* experiments with murine HBV-infection models.

Another potential risk in the setting of HBV-immunotherapy is an overwhelming T-cell response against the infected hepatocytes, which can induce severe liver inflammation, hepatotoxicity, and ultimately acute liver failure (Tillmann and Patel, 2014). The percentage of infected hepatocytes in CHB patients will clearly influence the bsAb-meditated hepatotoxicity and is known to vary between 1 and 70% (Wursthorn et al.,

2006). Thus, dosing regiments for such constructs need to be carefully evaluated in the pre-clinical and clinical setting.

1.3.3 Rational for the development of trispecific antibodies

The advances in recombinant antibody technology and limited efficacy of CD3-engaging bispecific constructs in the treatment of solid tumors inspired scientists to add further functionality to T-cell engaging molecules. Providing directed co-stimulation through CD28-engaging bispecific antibodies is a promising approach to increase the efficacy of CD3-targting bispecific molecules and has been shown to increase T-cell stimulation *in vitro* (Hornig et al., 2012) and enhance the anti-tumor effect *in vivo* in an xenogeneic ovarian tumor model (Skokos et al., 2020). Moreover, a combination therapy with CD3- and CD28-engaging bispecific antibodies will be tested as treatment option for ovarian cancer in the near future (Mullard, 2020). This clearly underlines the potency of co-stimulation through CD28-targeting molecules in overcoming current limitations of bsAb-mediated immunotherapy. However, the use of antibody cocktails is associated with several practical hurdles during pre-clinical and clinical development. Assessment of toxicology as well as pharmacokinetics need to be performed for each construct individually as well as in combination resulting in increased pre-clinical work-load and high expenses during clinical trials (Mullard, 2020).

One option to circumvent this hurdle is the development of multi-specific antibodies that combine binding moieties for multiple therapeutic targets in one single construct. The design of such molecules has been successfully achieved by several groups displaying promising redirection capacity through engagement of CD16 and NKp46 on NK cells (Gauthier et al., 2019) or CD3 and CD28 on T cells (Wu et al., 2020). The trispecific antibody SAR442257 by Sanofi, which displays monovalent binding to CD38 and CD3 and CD28, is currently tested in a phase 1 clinical trial for treatment of patients with relapsed and refractory multiple myeloma and non-Hodgkin’s lymphoma (NCT04401020). (Mullard, 2020).

Early on during this project, it became evident that co-stimulation with CD28-specific antibodies is also required to induce a potent immune response in the setting of bsAb-mediated HBV immunotherapy. The combination of CD3- and CD28-specific constructs did not only enhance T-cell redirection synergistically, but was also needed for efficient target cell elimination. Additionally, the development of trispecific constructs was clearly recommended during an advisory board meeting with the Paul-Ehrlich-Institut (PEI), as a single molecule will have reduced regulatory requirements during further pre-clinical and clinical development of a potential product.

1.4 Aims of the work

Current HBV therapies efficiently interfere with the viral replication cycle, but rarely achieve viral eradication, since the viral cccDNA in the nucleus of the infected host cell is not targeted. Although viral suppression improves the outcome of CHB, patients require life-long treatment and still carry an increased risk for HCC development, which is associated with a poor prognosis. This thesis is based on the hypothesis that bispecific antibodies that bind the HBV envelope protein, as well as CD3 or CD28, can redirect endogenous T cells toward HBV-infected hepatocytes and achieve viral clearance through specific elimination of infected cells. The aim of this study was the generation and functional characterization of diverse bi- and trispecific antibody constructs. It should be investigated if the construction of such antibodies is feasible, and moreover, if they can redirect T cells toward HBV-infected hepatocytes to achieve viral clearance by the elimination of the cccDNA. The term FabMAbs refers to the constructs FabMAbαCD3 and FabMAbαCD28 and the term BiMAbs refers to the constructs BiMAbαCD3 and BiMAbαCD28. The abbreviation bsAbs includes all four bispecific constructs.

The first part of the thesis comprised the generation and functional characterization of the two bispecific antibodies FabMAbαCD3 and FabMAbαCD28. This included the cloning and recombinant expression of the constructs, as well as studies on antigen binding and the redirection potential towards recombinant HBVenv and HBVenv-expressing target cells. Moreover, the producibility as well as long-term storage were investigated.

To study the impact of size and binding valency, the constructs BiMAbαCD3 and BiMAbαCD28 were developed in cooperation with the DKFZ in Heidelberg. In the second part of the thesis, the two different bsAb formats were intensively compared regarding their affinity, redirection efficiency, activation and target cell elimination, as well as their half-life in mice.

In the next step, the bsAb approach was applied to an HBV infection system with HepG2 NTCP cells as model cell line. It was analyzed, if FabMAb-mediated T-cell redirection induces specific elimination of infected target cells and if this cytotoxicity is accompanied by specific reduction of the viral parameters, including cccDNA. Furthermore, the correlation between the multiplicity of infection and the magnitude of the retargeted T-cell response was studied.

Since the combination of CD3- and CD28-specific bsAbs was found to be required for efficient T-cell redirection in all previous experiments and in consideration of a therapeutic approach, the last part of the thesis aimed at the generation of trispecific constructs that combine both immune stimulatory scFvs. This comprised the construction and expression of two trispecific antibodies, TriMAb and OKTriMAb, and experiments that analyzed the redirection potential and antiviral effect of these antibodies. Finally, the expression and purification of the lead candidate TriMAb was investigated in more detail and experiments on the functionality of the purified construct were perform

2 Results

2.1 Development and functional analysis of bispecific antibodies

2.1.1 FabMAbαCD3

2.1.1.1 Structural and biochemical properties of FabMAbαCD3

FabMAbαCD3 is composed of an HBVenv-specific chimeric Fab-fragment that is connected to a CD3-specific scFv by a glycine-serine (G_4S) linker (Fig. 5a, b, Fig. 6a). The chimeric Fab-fragment consists of HBVenv-specific murine heavy and kappa chains that are derived from the antibody 5F9 (Golsaz Shirazi et al., 2014, Golsaz-Shirazi et al., 2016) and the human IgG1 C_H1. The C_H1 domain is c-terminally elongated by 5 amino acids (EPKSC) of the hinge domain, to allow disulfide bond formation between Cys218 of HC and Cys214 of the LC. The AA numbers refer to the protein sequence in figure 5 (Fig. 5a, b). The scFvCD3 was generated by fusing the variable domains of the murine antibody OKT3 (Kung et al., 1979) with a G_4S linker (Fig. 6a). The FabMAbαCD3 construct has a molecular weight of 77.5 kD and facilitates monovalent binding to both antigens. To enable efficient purification under neutral pH conditions, FabMAbαCD3 was equipped with a C-terminal 10x His-tag. The molecular construction of this molecule was performed by myself. Further information about the procedure is provided in the methods section.

2.1.1.2 FabMAbαCD3 is successfully produced by HEK 293T cells

The heterodimeric protein was expressed as a single ORF with the two chains being separated by the self-cleaving A2 peptide (P2A). Usage of a P2A site allows equimolar expression of the two chains, but prolongs the HC-scFvOKT3 polypeptide by 21 c-terminal AA, which remain even after successful self-cleavage (Fig. 5a). Thus, potential influences on protein size, structure, and functionality need to be considered. As producer cell line, human embryonic kidney (HEK) 293T cells were used. To increase production efficiency, stable producer cell lines were generated by combination of antibiotic selection and single cell dilution. FabMAbαCD3-containing supernatant was harvested every 3 to 4 days, sterile-filtered, and used for functional assays to determine the binding and redirection capacity.

2.1.1.3 FabMAbαCD3 binds the HBV envelope protein

To ensure successful cloning of the 5F9 variable domains as well as correct heterodimer formation, binding of FabMAbαCD3 to HBVenv was analyzed by Enzyme-Linked Immunosorbent Assay (ELISA). HBsAg from human serum was coated on 96-well polystyrene plates as bait, and binding of the construct to HBsAg was detected with a polyclonal HRP goat-anti human antibody (HBsAg ELISA), followed by the assessment of horse radish peroxidase (HRP) activity. Functional HBVenv-binding Abs were detected in the supernatant of producer cell lines resulting in a strong ELISA signal, while

phosphate-buffered saline (PBS) controls did not. The ELISA signal was always specifically depending on the presence of HBsAg (Fig. 6b). These data indicated that the 5F9 variable domains were successfully inserted into the construct resulting in the generation of an HBVenv-specific Fab-fragment. It further demonstrated expression and functional heterodimerization in HEK 293T cells, as well as secretion into the supernatant.

a

FabMAbαCD3 HC-scFvOKT3 peptide: MW = 54.01 kD; total MW with LC = 77.52 kD

```
0   EVQLVESGGGLVHPGRSLKVSCAASGFTFNNYAMSWVRQTPDRRLELVAVINSDGRSTFYPDTVMGRFTISRDNAKNTLY
80  LQMSSLKSEDTAIYYCARTFYADYWGQGTTLTVSSASTKGPSVFPLAPSSKSTSGGTAALGCLVKDYFPEPVTVSWNSGA
160 LTSGVHTFPAVLQSSGLYSLSSVVTVPSSSLGTQTYICNVNHKPSNTKVDKKVEPKSCGGGGSGGGGSGGGGSTSQVQLQ
240 QSGAELARPGASVKMSCKASGYTFTRYTMHWVKQRPGQGLEWIGYINPSRGYTNYNQKFKDKATLTTDKSSSTAYMQLSS
320 LTSEDSAVYYCARYYDDHYCLDYWGQGTTLTVSSGGGGSGGGGSGGGGSQIVLTQSPAIMSASPGEKVTMTCSASSSVSY
400 MNWYQQKSGTSPKRWIYDTSKLASGVPAHFRGSGSGTSYSLTISGMEAEDAATYYCQQWSSNPFTFGSGTKLEINHHHHH
480 HHHHHLEGSGATNFSLLKQAGDVEENPG
```

```
HC variable 5F9                          : [1 : 120]
HC constant hu IgG1                      : [121 : 212]
hinge domain fragment: Cys218 for        : [213 : 218]
disulfide bond with LC
3x(G4S) Linker                           : [219 : 233]
TS: adaptor sequence SpeI                : [234 : 235]
HC scFv OKT3                             : [236 : 352]
SS: adaptor sequence XbaI^SpeI           : [353 : 354]
3x(G4S) Linker                           : [355 : 369]
LC scFv OKT3                             : [370 : 475]
10x His Tag                              : [476 : 485]
LE: adaptor sequence XhoI                : [486 : 487]
P2A residual Aa                          : [488 : 508]
```

b

FabMAbαCD3/28 LC: MW = 23.51 kD

```
0   DIVMTQSHKFMSASVGDRVSISCKASQNVDTTVAWFQQKPGQSPKLLIYWASTRHSGVPDRFTGSGSRSGFTLTISNVQS
80  EDLAVYFCQQYSIFPYTFGGGTKLEIKRTVAAPSVFIFPPSDEQLKSGTASVVCLLNNFYPREAKVQWKVDNALQSGNSQ
160 ESVTEQDSKDSTYSLSSTLTLSKADYEKHKVYACEVTHQGLSSPVTKSFNRGEC
```

```
LC variable 5F9                          : [1   : 107]
LC kappa constant                        : [108 : 214]
Cys214: disulfide bond with HC           : [214]
```

Figure 5: Amino acid sequences of FabMAbαCD3.(a) Amino acid sequence of the FabMAbαCD3 HC5F9-scFvOKT3 peptide. Adaptor sequences are traces of the cloning procedure. TS: restriction recognition site of SpeI; SS: ligation site of XbaI- and SpeI-digested DNA fragments; LE: restriction recognition site of XhoI. **(b)** Amino acid sequence of the FabMAbCD3/28 LC peptide.

2.1.1.4 FabMAbαCD3 activates T cells in the presence of immobilized HBsAg

In the next step, activation of T cells through FabMAbαCD3 was assessed. Therefore, freshly isolated peripheral blood mononuclear cells (PBMC) were cultured on HBsAg-coated plates in the presence of FabMAbαCD3-containing supernatant for 72 hours. Supernatant of non-transfected HEK 293T cells (w/o Ab) and wells without HBsAg (-HBsAg) served as controls. As readout for T-cell activation, changes in cell morphology

and IFNγ release were evaluated. Microscopic analysis showed distinct cluster formation of PBMC within the first 12 hours in FabMAbαCD3 treated HBsAg coated wells, while cells in control samples showed no changes in morphology (Fig. 6c). ELISA-based determination of IFNγ levels after 72 hours revealed T-cell activation with values around 5000 pg/ml. In control samples, no IFNγ secretion was observed (Fig. 6d). These findings suggest that FabMAbαCD3 can interact with CD3 and thereby activate T cells in the presence of TCR clustering on HBsAg-coated plates, resulting in IFNγ secretion. It is hereby clearly stated that the cloning procedure of FabMAbαCD3 as well as results mentioned in 2.1.2-2.1.4 were already included in the Master's Thesis "Generation and functional analysis of bispecific antibodies for immunotherapy of chronic hepatitis B virus infection" by Oliver Quitt (Quitt, 2013).

2.1.1.5 FabMAbαCD3 fails to activate T cells in the presence of HBVenv-expressing target cells without co-stimulation through mAbαCD28

To study, if FabMAbαCD3 is able to redirect and activate T cells to establish a cytotoxic immune response against HBVenv-expressing hepatocytes, human hepatocellular carcinoma (Huh7) cells were stably transfected with the small HBV envelope protein (Huh7S) and employed in co-cultures. Huh7S cells and PBMC were cultivated in the presence of FabMAbαCD3-containing supernatant for 64 hours and target cell viability was measured in real-time employing an xCELLigence RTCA. Parental Huh7 cells and supernatant of non-transfected HEK 293T cells (w/o Ab) served as controls. Target cell viability did not change in the presence of FabMAbαCD3, and IFNγ secretion, serving as marker for T-cell activation, was not observed. To examine, if the induction of a cytotoxic immune response requires co-stimulation of the TCR signaling in this setting, cultures were supplied with a commercial monoclonal αCD28 antibody (mαCD28). Treatment with FabMAbαCD3 and mαCD28 led to a strong decrease in cell viability of HBVenv-expressing Huh7S cells, while parental Huh7 cells stayed viable over the course of the experiment. Control treatment with mαCD28 alone did not show any effect on target cell viability. Target cell elimination was accompanied by specific IFNγ secretion (Fig. 6e, f). These data led to the conclusion that single treatment with FabMAbαCD3 fails to activate T cells on HBVenv-expressing target cells, yet this limitation can be overcome by co-stimulation with a monoclonal αCD28 antibody.

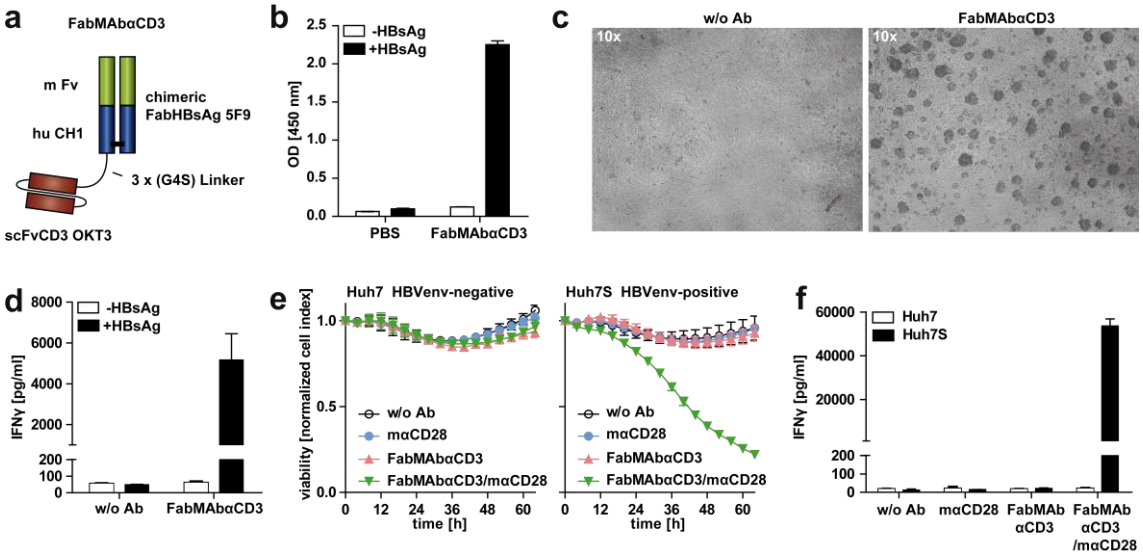

Figure 6: FabMAbαCD3 binds HBVenv and redirects T cells towards HBVenv-expressing target cells. **(a)** Schematic representation of FabMAbαCD3. **(b)** Binding of FabMAbαCD3 to HBsAg determined by ELISA. FabMAbαCD3 in the supernatant of producer cell lines (HEK 293T) interacting with human serum derived HBsAg was detected using polyclonal goat anti-human IgG HRP antibodies. Wells supplied with PBS or without HBsAg served as controls. **(c)** Microscopic analysis of cell morphology after 12-hour culture of PBMC on HBsAg-coated plates treated with supernatant of FabMAbαCD3 producer cell lines (HEK 293T) (right) or with supernatant of non-transfected HEK 293T cells (w/o Ab). **(d)** IFNγ concentration in the supernatant of co-cultures determined by ELISA. PBMC were cultured on HBsAg-coated plates and treated with supernatant of FabMAbαCD3 producer cell lines (HEK 293T) for 72 hours. Supernatant of non-transfected HEK 293T cells (w/o Ab), or wells without HBsAg served as controls. **(e)** Target cell viability was determined over 64 hours in real-time employing an xCELLigence RTCA. HBVenv-postivie Huh7S (right) or HBVenv-negative Huh7 cells (left) were co-cultured with PBMC and treated with supernatant of FabMAbαCD3 producer cell lines (HEK 293T) and a commercial monoclonal αCD28 antibody (1 µg/ml), singly or in combination. Cells treated with supernatant of non-transfected HEK 293T cells (w/o Ab) served as controls. **(f)** IFNγ concentration in the supernatant of the co-cultures described in (e) after 64 hours quantified by ELISA. Data are presented as mean values ± SD of (b) triplicate analysis or (d-f) triplicate co-cultures (*n* = 3).

2.1.2 Co-stimulation with FabMAbαCD28

2.1.2.1 Structural and biochemical properties of FabMAbαCD28

To increase the specificity of the co-stimulatory signal, a second bispecific molecule was generated by replacement of the scFvCD3 with a CD28-specific scFv. The variable domains of scFvCD28 are derived from the antibody 9.3 (Baroja et al., 1989) (Fig. 7a, b, Fig. 8a). Consequently, FabMAbαCD28 is very similar in structure and size with a molecular weight of 78.2 kD. The molecular construction of this molecule was performed by myself. Further information about the procedure is provided in the methods section.

a

FabMAbαCD28 HC-scFv9.3 peptide: MW = 54.69 kD; total MW with LC = 78.20 kD

```
0   EVQLVESGGGLVHPGRSLKVSCAASGFTFNNYAMSWVRQTPDRRLELVAVINSDGRSTFYPDTVMGRFTISRDNAKNTLY
80  LQMSSLKSEDTAIYYCARTFYADYWGQGTTLTVSSASTKGPSVFPLAPSSKSTSGGTAALGCLVKDYFPEPVTVSWNSGA
160 LTSGVHTFPAVLQSSGLYSLSSVVTVPSSSLGTQTYICNVNHKPSNTKVDKKVEPKSCGGGGSGGGGSGGGGSTSQVQLQ
240 QSGPGLVTPSQSLSITCTVSGFSLSDYGVHWVRQSPGQGLEWLGVIWAGGGTNYNSALMSRKSISKDNSKSQVFLKMNSL
320 QADDTAVYYCARDKGYSYYYSMDYWGQGTTVTVSSRGGGGSGGGGSGGGGSDIELTQSPASLAVSLGQRATISCRASESV
400 EYYVTSLMQWYQQKPGQPPKLLIFAASNVESGVPARFSGSGSGTNFSLNIHPVDEDDVAMYFCQQSRKVPYTFGGGTKLE
480 IKRNHHHHHHHHHHLEGSGATNFSLLKQAGDVEENPG
```

HC variable 5F9	: [1 : 120]
HC constant hu IgG1	: [121 : 212]
hinge domain fragment: Cys218 for disulfide bond with LC	: [213 : 218]
3x(G4S) Linker	: [219 : 233]
TS: adaptor sequence SpeI	: [234 : 235]
HC scFv 9.3	: [236 : 352]
SR: adaptor sequence XbaI	: [353 : 354]
3x(G4S) Linker	: [355 : 371]
LC scFv 9.3	: [372 : 484]
10x His Tag	: [485 : 494]
LE: adaptor sequence XhoI	: [495 : 496]
P2A residual Aa	: [497 : 517]

b

FabMAbαCD3/28 LC: MW = 23.51 kD

```
0   DIVMTQSHKFMSASVGDRVSISCKASQNVDTTVAWFQQKPGQSPKLLIYWASTRHSGVPDRFTGSGSRSGFTLTISNVQS
80  EDLAVYFCQQYSIFPYTFGGGTKLEIKRTVAAPSVFIFPPSDEQLKSGTASVVCLLNNFYPREAKVQWKVDNALQSGNSQ
160 ESVTEQDSKDSTYSLSSTLTLSKADYEKHKVYACEVTHQGLSSPVTKSFNRGEC
```

LC variable 5F9	: [1 : 107]
LC kappa constant	: [108 : 214]
Cys214: disulfide bond with HC	: [214]

Figure 7: Amino acid sequences of FabMAbαCD28.(a) Amino acid sequence of the FabMAbαCD28 HC5F9-scFv9.3 peptide. Adaptor sequences are traces of the cloning procedure. TS: restriction recognition site of SpeI; SS: ligation site of XbaI- and SpeI-digested DNA fragments; LE: restriction recognition site of XhoI. **(b)** Amino acid sequence of the FabMAbCD3/28 LC peptide.

2.1.2.2 FabMAbαCD28 has lower expression efficiency than FabMAbαCD3

A stable FabMAbαCD28 producer cell line was generated by antibiotic selection and single cell dilution and the supernatant was tested in HBsAg ELISAs. Supernatant of producer cell lines resulted in a strong OD 450 signal, while PBS controls did not (Fig. 8b). Comparison of supernatants of the FabMAbαCD3-producing cell lines showed a lower signal for FabMAbαCD28. To investigate, if this effect was cell line dependent, new producer cell lines were generated based on Chinese hamster ovary (CHO) K1 cells. Comparison of the cell lines revealed a better expression in CHO K1 cells for both constructs, yet antibody amounts from FabMAbαCD28 producer lines were still about 50% lower than those from FabMAbαCD3 cell lines (Fig. 8c). To provide the highest antibody concentration possible, further experiments were performed with supernatants from CHO K1 producer cell lines.

2.1.2.3 Co-application of FabMAbαCD28 enhances T-cell activation specifically in the presence of immobilized HBsAg

Next, the effect of FabMAbαCD28 in co-cultures of PBMC on HBsAg-coated plates was studied. Co-cultures were supplied with supernatant containing FabMAbαCD3, FabMAbαCD28, or the combination in a 1:1 ratio. Supernatant of non-transfected CHO K1 cells (w/o Ab) and wells without HBsAg (-HBsAg) served as controls. PBMC were cultured for 72 hours and the concentration of IFNγ in the supernatant was determined by ELISA. In FabMAbαCD3-treated wells, cytokine levels around 5000 pg/ml were measured, while IFNγ was undetectable in FabMAbαCD28-treated samples. However, the combination of both constructs resulted in a synergistic effect, reaching IFNγ concentrations of around 10000 pg/ml. IFNγ secretion was always completely dependent on the presence of HBsAg (Fig. 8d).

2.1.2.4 Combination of the bispecific constructs induces a cytotoxic immune response against HBVenv-expressing target cells

To investigate, if the combination of FabMAbαCD3 and FabMAbαCD28 allows redirection and cytotoxic T-cell activation towards HBVenv-expressing cells, Huh7S cells and PBMC were co-cultured in the presence of the bsAbs, singly or in combination. Target cell viability was measured in real-time for 160 hours employing an xCELLigence RTCA. Parental Huh7 cells and supernatant of non-transfected CHO K1 cells (w/o Ab) served as control. In accordance with lacking IFNγ secretion, target cell viability did not change in the presence of FabMAbαCD28. Treatment with FabMAbαCD3-containing supernatant of CHO K1 cells induced about 50% elimination of Huh7S cells in the co-cultures at relatively late time points, although IFNγ was not detectable (Fig. 8e, f). The combination of both constructs led to distinct and specific elimination of HBVenv-expressing Huh7S cells, accompanied by IFNγ release. T-cell activation, namely elimination of target cells and secretion of IFNγ, was always dependent on the expression of the HBV envelope protein (Fig. 8e, f). These data indicated that co-application of FabMAbαCD28 is able to specifically enhance FabMAbαCD3-mediated T-cell activation resulting in efficient target cell elimination. Single treatment with FabMAbαCD28 failed to induce T-cell activation in the presence of immobilized HBsAg or Huh7S cells. It is important to emphasize that all studies mentioned were conducted with supernatant of producer cell lines and quantitative comparisons are therefore to be taken with caution. To study the FabMAb-depended T-cell redirection in more detail, experiments needed to be performed with purified constructs.

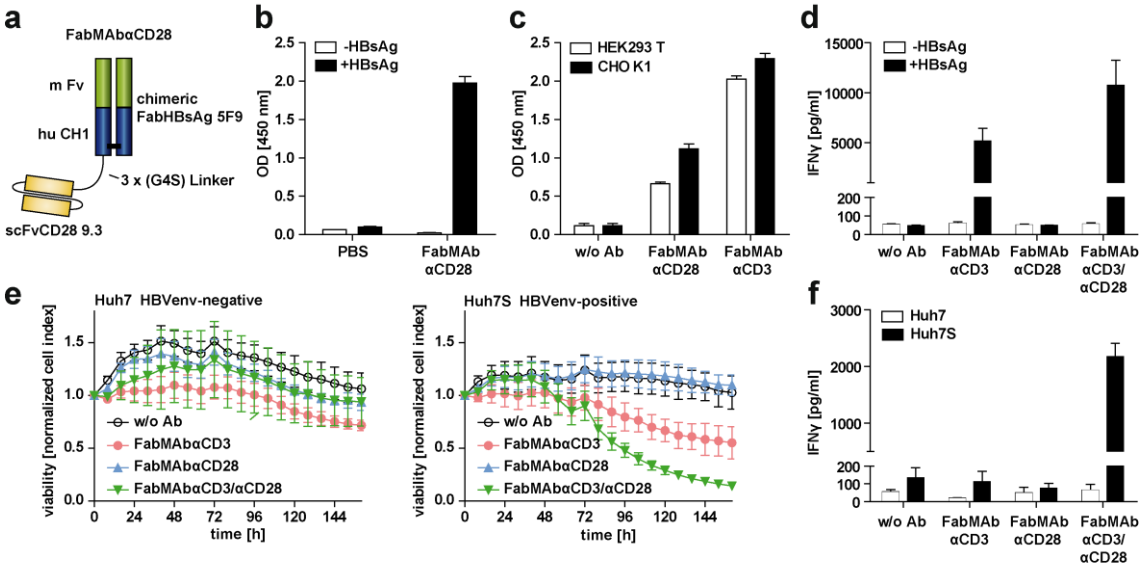

Figure 8: FabMAbαCD28 enhances FabMAbαCD3-mediated T-cell activation synergistically and promotes specific target-cell elimination. Schematic representation of FabMAbαCD28. **(b)** Binding of FabMAbαCD28 to HBsAg determined by ELISA. FabMAbαCD28 in the supernatant of producer cell lines (HEK 293T) interacting with human serum derived HBsAg was detected using polyclonal goat anti-human IgG HRP antibodies. Wells supplied with PBS or without HBsAg served as controls. **(c)** Comparative ELISA analysis of antibody-containing supernatants of HEK293T and CHO K1 producer cell lines. FabMAbs interacting with human serum derived HBsAg were detected using polyclonal goat anti-human IgG HRP antibodies. Supernatant of the respective non-transfected producer cells (w/o Ab) served as controls. **(d)** IFNγ concentration in the supernatant of PBMC cultured on HBsAg-coated plates and treated with supernatant of FabMAbαCD3 producer cell lines (CHO K1), FabMAbαCD28 producer cell lines (CHO K1), or the combination (ratio 1:1) after 72 hours. The cytokine concentration in the supernatant was determined by ELISA. Supernatant of the non-transfected CHO K1 cells (w/o Ab) served as controls. **(e)** Cell viability of Huh7S (right) and Huh7 control cells (left) in co-culture with PBMC treated with supernatant of FabMAbαCD3 producer cell lines (CHO K1), FabMAbαCD28 producer cell lines (CHO K1), or the combination (ratio 1:1). Cells treated with supernatant of non-transfected CHO K1 cells (w/o Ab) served as controls. Target cell viability was determined over 160 hours in real-time employing an xCELLigence RTCA. **(f)** IFNγ concentration in the supernatant of co-cultures described in (e) after 160 hours quantified by ELISA. Data are presented as mean values ± SD of **(b, c)** triplicate analysis or **(d-f)** triplicate co-cultures (*n* = 3).

2.1.3 Purification of FabMAbs

2.1.3.1 Production at InVivo Biotech Services

Purification of FabMAbs was outsourced to InVivo Biotech Services, to allow large scale production of the constructs. FabMAbs were expressed in a 5-liter culture of HEK 293 suspension cells and purified with a combination of IMAC and size exclusion chromatography (SEC). It is important to mention that the constructs were expressed using a two-vector system, preventing the need for a P2A site. Thus, purified constructs do not contain the P2A residues and are smaller by 2.4 kD, which might influence their structure and functionality. The production yielded in 15 mg (FabMAbαCD3) and 30 mg (FabMAbαCD28). Purity was determined in house by polyacrylamide gel electrophoresis (PAGE) following Coomassie staining (Fig. 9a). PAGE was performed under reducing and non-reducing conditions to assess the integrity of the monomeric as well as the dimeric state of the constructs. Under reducing conditions FabMAbs migrated with an apparent molecular weight of ~55 and ~23 kD, which correspond to the heavy chain-scFv polypeptide and the light chain, respectively. Under non-reducing conditions, the constructs migrated with a molecular weight of ~100 kD, that can be assigned to the respective FabMAb heterodimer. Purity of the constructs was over 95% under reducing conditions, yet FabMAbαCD3 samples showed additional bands with high molecular weight (>130 kD) under non-reducing conditions. Since these impurities were absent under reducing conditions, they can be assigned to aggregation of FabMAbαCD3.

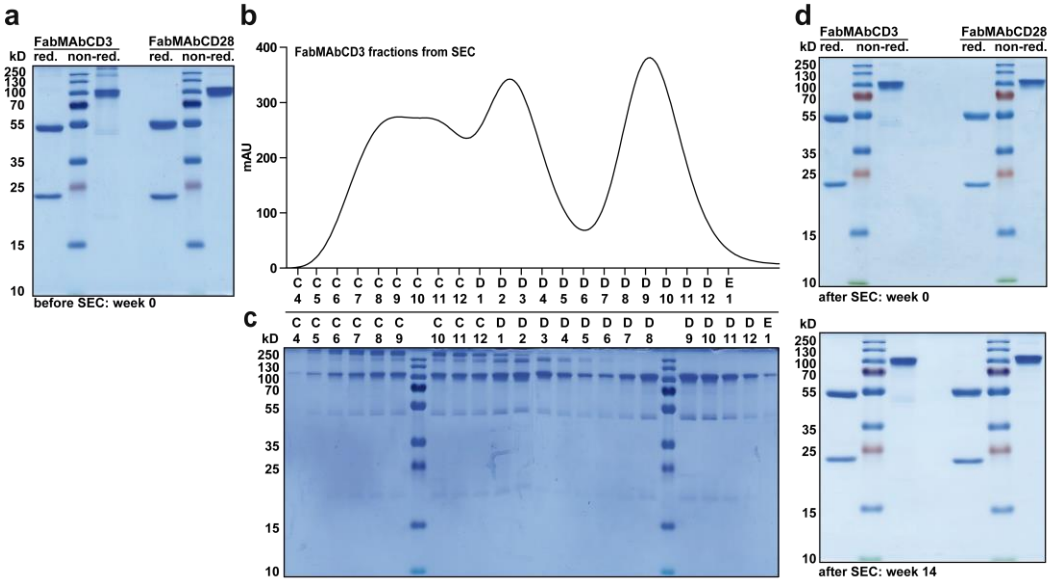

Figure 9: Size exclusion chromatography allows efficient aggregate elimination in FabMAbαCD3 samples. (a) 2.5 µg of the indicated purified construct were separated by PAGE (12.5%)under reducing and non-reducing conditions, and total protein in the preparation was stained with Coomassie. **(b)** Size exclusion chromatography **(**SEC) chromatogram of FabMAbαCD3 sample using a HiPrep Sephacryl S-200 column. The milli absorption units (mAu) are based on the absorption at 280 nm. **(c)** 15 µl of the indicated fraction were separated by PAGE (12.5%) under non-reducing conditions, and total protein in the preparation was stained with Coomassie. **(d)** 2.5 µg of the indicated purified construct were separated by PAGE (12.5%) under reducing and non-reducing conditions, and total protein in the preparation was stained with Coomassie. Samples were analyzed directly after SEC and 14 weeks later (bottom).

2.1.3.2 Size exclusion chromatography of FabMAbαCD3

To remove the FabMAbαCD3 aggregates, a second SEC was performed at the protein expression and purification facility of the German Research Center for Environmental Health under the direction of Dr. Arie Geerlof using a HiPrep Sephacryl S-200 column. The chromatogram and Coomassie staining of the collected fractions demonstrated a clear separation of aggregates from heterodimers (Fig. 9b, c), thereby increasing the purity to above 95%. Fractions D7 till E1 were pooled, stored at 4 °C, and monitored for 14 weeks. Since no re-aggregation of the constructs was observed (Fig. 9d), constructs were stored long-term at 4 °C. Thus, both bsAbs were available at high purity and were used in further experiments.

2.1.4 Purified FabMAbs are functional and induce a cytotoxic immune response against HBVenv-expressing target cells

The highly purified bsAbs were employed in co-cultures with Huh7S cells and PBMC to determine their functionality. 1, 10, and 100 nM of the constructs, singly or in combination, were applied and target cell viability was assessed in real-time for 96 hours employing an xCELLigence RTCA. As marker for T-cell activation, the IFNγ concentration in the culture was determined by ELISA. Single treatment with FabMAbαCD3 did neither result in loss of cell viability, nor in the secretion of IFNγ at any concentration analyzed (Fig. 10a-c). In contrast, treatment with FabMAbαCD28 induced specific and dose-depended elimination of Huh7S cells at 1 nM and 10 nM. At 1 nM, the elimination resulted in about 50% target cell elimination and IFNγ secretion was not observed. At 10 nM, the cell viability was reduced by almost 100% and this effect was accompanied by specific secretion of IFNγ (Fig. 10a-c). When both antibodies were used in combination, 100% of target cells were eliminated and IFNγ secretion was already observed at a concentration of 1 nM. Increasing the dosage to 10 nM could neither enhance the kinetics of target cell elimination nor IFNγ release, yet a minor loss of cell viability was observed for HBVenv-negative Huh7 control cells at around 72 hours. This effect was not accompanied by IFNγ release. At 100 nM, treatment with FabMAbαCD28 and the combination showed a distinct negative effect on the viability of Huh7 control cells, while specific elimination of Huh7S cells was not further enhanced. The adverse effect was accompanied by a very mild elevation of IFNγ levels in the culture (Fig. 10a-c). These data indicated that the purification with IMAC and SEC leads to a preparation of functional bsAbs, which can induce a cytotoxic immune response against HBVenv-expressing target cells. Even though FabMAbαCD28 induced T-cell activation upon single administration, the combination of both constructs was substantially more effective at lower concentrations (1 nM). High concentrations of FabMAbαCD28 and the combination (100 nM) led to unspecific elimination of Huh7 control cells. This antigen-independent T-cell activation was accompanied by comparatively low secretion of IFNγ and was also observed in the absence of CD3 engagement. The increased sensitivity upon co-administration of FabMAbαCD3 and FabMAbαCD28 provides a

therapeutic window between 1 and 10 nM, in which efficient elimination of target cells is achieved, while control cells are not affected.

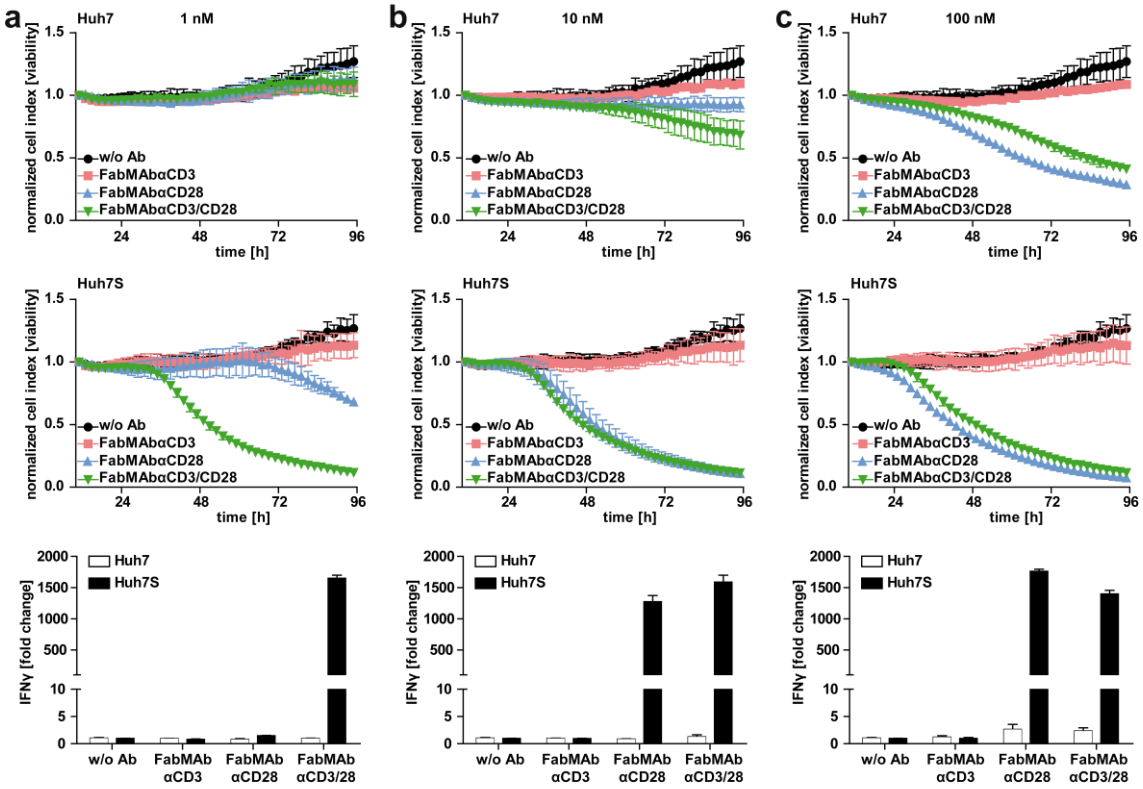

Figure 10: Purified FabMAbs induce a cytotoxic immune response against HBVenv-expressing target cells. (a-c) Cell viability of Huh7 (top) and Huh7S cells (middle) in co-culture with PBMC and FabMAbαCD3, FabMAbαCD28, or the combination (1:1 ratio) using a total antibody concentration of **(a)** 1 nM, **(b)** 10 nM or **(c)** 100 nM. Co-cultures in the absence of bsAbs (w/o Ab) served as controls. Cell viability was determined over 96 hours in real-time employing an xCELLigence RTCA. The IFNγ concentration in the supernatant of co-cultures (bottom) was determined by ELISA after 96 hours. The optical density (OD) at 450 nm was normalized to the respective w/o Ab control (Huh7 cells) and is depicted as fold change. Data are presented as mean values ± SD of triplicate co-cultures (*n* = 3).

2.2 Comparison of bi- and tetravalent bispecific antibodies

2.2.1 Development and production of tetravalent bispecific antibodies

2.2.1.1 Structural and biochemical properties of BiMAbs

To study the impact of size and binding valency on the functionality and efficacy of cytotoxic T-cell redirectors in the setting of HBV infection, a second set of bsAbs was developed in cooperation with Dr. Frank Momburg (DKFZ, Heidelberg). BiMAbs consist of two HBs-specific scFv C8 (Bohne et al., 2008) connected to the n-termini of IgG1 Fc domains via a G_4S linker. For recruitment of effector cells two CD3- or CD28 specific scFv were fused to the Fc c-termini, resulting in tetravalent constructs with two binding sites for each antigen and a molecular weight of 165 kD (Fig. 11a, b, Fig. 12a). To avoid aberrant disulfide formation in the absence of Ig light chains Cys220 was mutated to Ser. Effector function mediated by Fc γ receptor (FcγR) binding, namely antibody depended cytotoxicity (ADCC) and complement dependent cytotoxicity (CDC), were reduced by introduction of the mutations C220S, E233P, L234A, L235A, G236del, N297Q, K322A, A327G, P329A, A330S and P331S into the Fc domain. These AA changes refer to the nomenclature of “recommendations for the description of protein sequence variants” by the human genome variation society (Human genome variation society), since they are well established in the field of antibody protein biochemistry. To enable efficient purification, BiMAbs were equipped with a Strep-tag II between the Fc domain and the c-terminal scFvs (Fig. 11a, b). The molecular construction of these molecules was performed by Frank Momburg.

2.2.1.2 Production at Proteros Biostructures GmbH

BiMAbs were produced by Proteros Biostructures GmbH. The constructs were expressed in HEK 293 suspension cells and purified with a combination of ion-exchange chromatography and SEC. Purity was determined by PAGE following Coomassie staining. Gels were furthermore loaded with FabMAb samples to allow a direct comparison of the formats. Migration patterns of FabMAbs were already described in 2.1.3.1. The homodimeric BiMAbs migrated with a molecular weight of ~85 kD under reducing and ~170 kD under non-reducing conditions (Fig. 12b). Western blot (WB) analysis with polyclonal goat anti human IgG antibodies visualized bands with the same migration pattern (Fig. 12c). At the time point of comparative analysis, all constructs had been stored at 4 °C for over 10 months. BsAb preparations, especially BiMAbαCD3 showed signs of aggregation and fragmentation, but purity under non-reducing conditions was still above 90% in case of all four constructs. The high quality of the preparations allowed the comparative analysis of antigen binding and redirection capacity.

a

BiMAbαCD3 peptide: MW monomer = 82.3 kD; MW dimer = 165 kD

```
0   MAEVQLVESGGGLLQPGGSLRLSCAASGFTFSGYAMSWVRQAPGKGLEWVSSISGSGGSTYYADSVKGRFTISRDNSKNT
80  LYLQMNSLRAEDTALYYCAKPPGRQEYYGSSIYYFPLGNWGQGTLVTVSSASTKGPKLEEGEFSEARVQSALTQPASVSV
160 APGQTARITCGGNNIGSKSVHWYQQKPGQAPVLVVYDDSDRPSGIPERFSGSNSGNTATLTISRVEAGDEADYYCQVWDS
240 SSDLVVFGGGTKLTVLGNSGGGGSGGGGSGGGGSASEPKSSDKTHTCPPCPAPPAAGPSVFLFPPKPKDTLMISRTPEVT
320 CVVVDVSHEDPEVKFNWYVDGVEVHNAKTKPREEQYNSTYRVVSVLTVLHQDWLNGKEYKCAVSNKGLASSIEKTISKAK
400 GQPREPQVYTLPPSRDELTKNQVSLTCLVKGFYPSDIAVEWESNGQPENNYKTTPPVLDSDGSFFLYSKLTVDKSRWQQG
480 NVFSCSVMHEALHNHYTQKSLSLSPGKDPGWSHPQFEKSRGGGGQVQLQQSGAELARPGASVKMSCKASGYTFTRYTMHW
560 VKQRPGQGLEWIGYINPSRGYTNYNQKFKDKATLTTDKSSSTAYMQLSSLTSEDSAVYYCARYYDDHYCLDYWGQGTTLT
640 VSSGNSGGGGSGGGGSGGGGSASQIVLTQSPAIMSASPGEKVTMTCSASSSVSYMNWYQQKSGTSPKRWIYDTSKLASGV
720 PAHFRGSGSGTSYSLTISGMEAEDAATYYCQQWSSNPFTFGSGTKLEIN
```

HC scFv C8	: [1 : 138]
Yol-linker	: [139 : 147]
LC scFv C8	: [148 : 256]
GNS: adaptor sequence EcoRI	: [257 : 259]
3x(G4S) Linker	: [260 : 274]
AS: adaptor sequence NheI	: [275 : 276]
Fc domain	: [277 : 507]
DPG: adaptor sequence BamHI/SmaI	: [508 : 510]
Strep tag II	: [511 : 518]
SR: adaptor sequence XbaI	: [519 : 520]
4x(G) Linker	: [521 : 524]
HC scFv OKT3	: [525 : 643]
GNS: adaptor sequence EcoRI	: [644 : 646]
3x(G4S) Linker	: [647 : 661]
AS: adaptor sequence NheI	: [662 : 663]
LC scFv OKT3	: [664 : 769]

b

BiMAbαCD28 peptide: MW monomer = 82.3 kD; MW dimer = 165 kD

```
0   MAEVQLVESGGGLLQPGGSLRLSCAASGFTFSGYAMSWVRQAPGKGLEWVSSISGSGGSTYYADSVKGRFTISRDNSKNT
80  LYLQMNSLRAEDTALYYCAKPPGRQEYYGSSIYYFPLGNWGQGTLVTVSSASTKGPKLEEGEFSEARVQSALTQPASVSV
160 APGQTARITCGGNNIGSKSVHWYQQKPGQAPVLVVYDDSDRPSGIPERFSGSNSGNTATLTISRVEAGDEADYYCQVWDS
240 SSDLVVFGGGTKLTVLGNSGGGGSGGGGSGGGGSASEPKSSDKTHTCPPCPAPPAAGPSVFLFPPKPKDTLMISRTPEVT
320 CVVVDVSHEDPEVKFNWYVDGVEVHNAKTKPREEQYNSTYRVVSVLTVLHQDWLNGKEYKCAVSNKGLASSIEKTISKAK
400 GQPREPQVYTLPPSRDELTKNQVSLTCLVKGFYPSDIAVEWESNGQPENNYKTTPPVLDSDGSFFLYSKLTVDKSRWQQG
480 NVFSCSVMHEALHNHYTQKSLSLSPGKDPGWSHPQFEKSSGGGGQVQLQESGPGLVTPSQSLSITCTVSGFSLSDYGVHW
560 VRQSPGQGLEWLGVIWAGGGTNYNSALMSRKSISKDNSKSQVFLKMNSLQADDTAVYYCARDKGYSYYYSMDYWGQGTTV
640 TVSSRGGGSGGGGSGGGGSDIELTQSPASLAVSLGQRATISCRASESVEYYVTSLMQWYQQKPGQPPKLLIFAASNVESG
720 VPARFSGSGSGTNFSLNIHPVDEDDVAMYFCQQSRKVPYTFGGGTKLEIKR
```

HC scFv C8	: [1 : 138]
Yol-linker	: [139 : 147]
LC scFv C8	: [148 : 256]
GNS: adaptor sequence EcoRI	: [257 : 259]
3x(G4S) Linker	: [260 : 274]
AS: adaptor sequence NheI	: [275 : 276]
Fc domain	: [277 : 507]
DPG: adaptor sequence BamHI/SmaI	: [508 : 510]
Strep tag II	: [511 : 518]
SS: adaptor sequence XbaI^SpeI	: [519 : 520]
4x(G) Linker	: [521 : 524]
HC scFv 9.3	: [525 : 643]
SR: adaptor sequence XbaI	: [644 : 645]
3x(G4S) Linker	: [646 : 660]
LC scFv 9.3	: [661 : 771]

Figure 11: Amino acid sequences of BiMAbs. Amino acid sequence of the **(a)** BiMAbαCD3 monomer and **(b)** BiMAbαCD28 monomer. Adaptor sequences are traces of the cloning procedure. GNS: restriction recognition site of EcoRI; AS: restriction recognition site of NheI; DPG: restriction recognition site of BamHI and SmaI; SR: restriction recognition site of XbaI; SS: ligation site of XbaI- and SpeI-digested DNA fragments.

2.2.2 FabMAbs and BiMAbs bind their target proteins

2.2.2.1 BsAbs bind CD3 and CD28 on human T cells

Binding to the targets CD3 and CD28 on T cells was determined by flow cytometry. Human PBMC were incubated with 1 µM of bsAbs and subsequently stained for CD4, CD8 and human IgG. Flow cytometry analysis detected IgG-positive $CD4^+$ and $CD8^+$ T cells in case of all four bsAbs (Fig. 12d, e). It is hereby clearly stated that staining and analysis of BiMAb samples in this figure were performed by Shanshan Luo. To further compare the binding to CD3 and CD28 on $CD8^+$ and $CD4^+$ T cells, PBMC were incubated with a half-logarithmic dilution series of FabMAbs at concentrations ranging from 0.03-1000 nM. Calculation of the half maximal effective concentration (EC_{50}) values with non-linear regression resulted in 29.6 nM (FabMAbαCD3) and 392.6 nM (FabMAbαCD28) for $CD8^+$ T cells and 20.04 nM and 210.5 nM when $CD4^+$ T cells were analyzed (Fig. 12f).

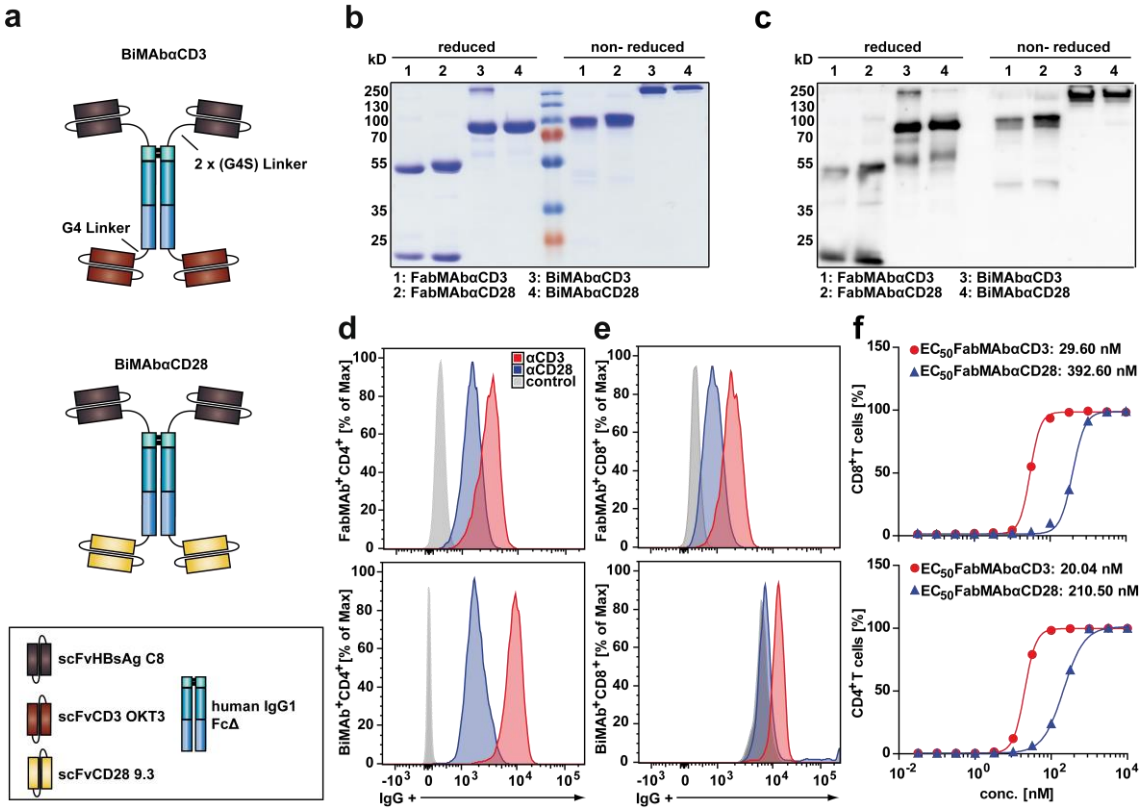

Figure 12: Purified bsAbs bind CD3 and CD28 on human T cells. (a) Schematic representation of BiMAbs. **(b)** 2.5 µg of the indicated bispecific antibody were separated by PAGE (12.5%) under reducing and non-reducing conditions, and total protein in the preparation was stained with Coomassie. **(c)** WB of bsAbs under reducing and non-reducing conditions. 100 ng of the respective antibody were separated by a 12.5% polyacrylamide SDS-gel and transferred to a polyvinylidene fluoride membrane. BsAbs were detected with polyclonal goat anti human IgG antibodies. **(d, e)** FACS analysis of human IgG on **(d)** $CD4^+$ T cells or **(e)** $CD8^+$ T cells after incubation with 1 µM FabMAbs (top panel) or BiMAbs (bottom panel). BsAbs interacting with CD3 and CD28 on T cells were detected with anti-human IgG PE antibodies. Controls were incubated with anti-human IgG PE antibodies, only. **(f)** Non-linear regression of the percentage of IgG positive $CD8^+$ (top) and $CD4^+$ (bottom) T cells after incubation with a half-logarithmic dilution series of FabMAbs ranging from 1000-0.03162 nM. Binding to T cells was determined by flow cytometry as described in (d, e). EC_{50} was calculated using non-linear regression log(agonist) vs. response variable slope with a robust fit (Prism). Data are presented as single values of a representative experiment.

2.2.2.2 BiMAbs and FabMAbs bind the HBV envelope protein with different characteristics

To compare the binding characteristics of FabMAbs and BiMAbs to HBVenv, an HBsAg ELISA was performed using a half-logarithmic dilution series of bsAbs at concentrations ranging from 0.03-1000 nM. Calculation of EC_{50} values with non-linear regression resulted in 1.6 nM for FabMAbαCD3, 2.1 nM for FabMAbαCD28 and 0.7 nM for the BiMAbs (Fig. 13a). To demonstrate a broad applicability of the constructs, the binding capacity to several HBVenv geno- and subtypes was analyzed by ELISA. Since goat anti human IgG antibodies led to a high background signal in this setting, alternative detection antibodies were employed. An anti-6x His Tag antibody allowed specific detection of FabMAbs, while BiMAbs were detected with a Strep Tag II specific antibody (Fig. 13b). HBsAg in serum from a genotype panel (Paul-Ehrlich-Institut) was captured with HBVenv-specific antibodies (Murex HBsAg Version 3 from DiaSorin) and detected with a combination of bsAbs and tag-specific HRP-labeled antibodies. The binders C8 and 5F9 recognized all analyzed HBVenv genotypes with a distinct binding characteristics. 5F9 showed reduced signals for the genotypes E, F2 and H. C8 showed reduced binding to D1_ayw2 and D2_ayw2, while D2_awy3 was recognized well (Fig. 13c). To investigate, if the bsAbs can interact with HBVenv on the membrane of target cells, Huh7 hepatoma cells were transiently transfected with an mCherry-HBVenv fusion protein and incubated with 50 nM of bsAbs. Cell membranes and bsAbs were stained with wheat germ agglutinin (WGA) and a goat anti-human IgG antibody, respectively, and co-localization was visualized by confocal microscopy (Fig. 13d). Positive IgG-staining was exclusively found on mCherry-HBVenv transfected cells. This data led to the conclusion, that all four constructs bind the HBV envelope protein successfully and that they should be analyzed for their capacity to redirect T cells towards HBV-infected cells. It is hereby clearly stated that immunofluorescence staining and analysis of BiMAb samples in this figure were performed by Lili Zhao and Shanshan Luo.

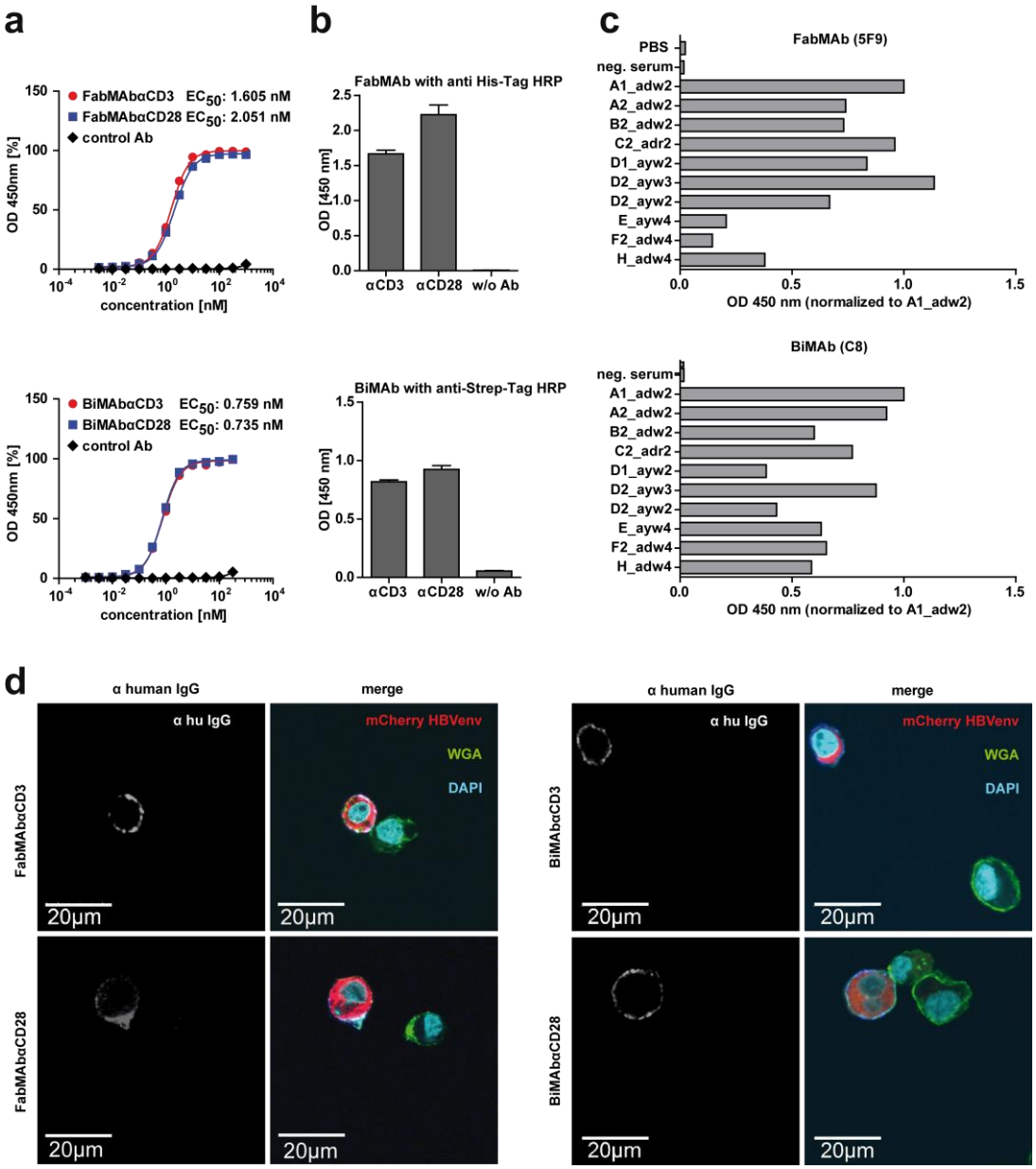

Figure 13: BsAbs bind the HBV envelope protein on hepatoma cell membranes. (a) ELISA analysis of the interaction of FabMAbs (top panel) or BiMAbs (bottom panel) with patient derived HBsAg. BsAbs were applied employing a half-logarithmic dilution series ranging from 1000-0.03162 nM and were detected using polyclonal goat anti-human IgG HRP antibodies. As control antibody served Erbitux®. EC_{50} was calculated using non-linear regression log(agonist) vs. response variable slope with a robust fit (Prism). **(b)** HBsAg-coated plates were incubated with 10 nM FabMAb (top) or BiMAb (bottom) and bsAbs interacting with patient derived HBsAg were detected by StrepMAb classic-HRP (BiMAb) or anti-6x His-Tag antibody HRP-conjugate (FabMAb). PBS-coated plates (w/o Ab) treated with the respective secondary antibody served as control. **(c)** The binding characteristics of FabMAbs (top) and BiMAbs (bottom) to several HBVenv geno- and subtypes were determined by ELISA. HBsAg derived from different HBV genotypes was captured with HBVenv-specific antibodies (Murex HBsAg Version 3 from DiaSorin) and incubated with 50 nM FabMAbαCD28 (top) or BiMAbαCD28 (bottom). BsAbs were detected by StrepMAb classic-HRP (BiMAb) or anti-6x His-Tag antibody HRP-conjugate (FabMAb). The OD at 450 nm was normalized to the respective A1_adw2 value. **(d)** Immunofluorescence staining to study binding of bsAbs to mCherry-HBVenv expressing Huh7 cells. Cells were incubation with 50 nM of BiMAbs (top) or FabMAbs (bottom) and bsAbs were detected with anti human IgG Alexa Flour 647 antibodies. Membranes are stained with WGA and nuclei with DAPI. Data are presented as mean value ± SD of **(a)** three independent triplicate analyses (*n* = 9), **(b)** triplicate analyses (*n* = 3) or **(c)** single values.

2.2.3 Bi- and tetravalent constructs activate T cells with comparable potency

2.2.3.1 BsAbs titration in the presence of HBsAg demonstrates the benefit of co-stimulation

For comparison of the redirection potential of the different antibodies, PBMC were cultured on HBsAg-coated plates for 72 hours in the presence of bsAbs. Since results in 2.1.4 demonstrated that bsAb concentrations above 10 nM can lead to loss of cell viability on parental Huh7 cells, without enhancing the rate or kinetics of cytotoxic target cell elimination, redirection potential at low concentration was investigated. Therefore, 0.1, 0.316, 1, 3.162, and 10 nM of each antibody as well as a mixture of the respective formats in a 1:1 ratio was used. As readout for T-cell activation the release of IFNγ, IL-2, and TNFα was determined by ELISA. Single application of the CD3- or CD28-specific constructs induced cytokine levels below 500 pg/ml, yet the combination of both constructs led to a profound and synergistic increase, reaching values above 5000 pg/ml. Single treatment with FabMAbαCD28 resulted in cytokine levels around 1000 pg/ml. Nevertheless, co-application of FabMAbαCD3 enhanced cytokine levels synergistically (Fig. 14a-c).

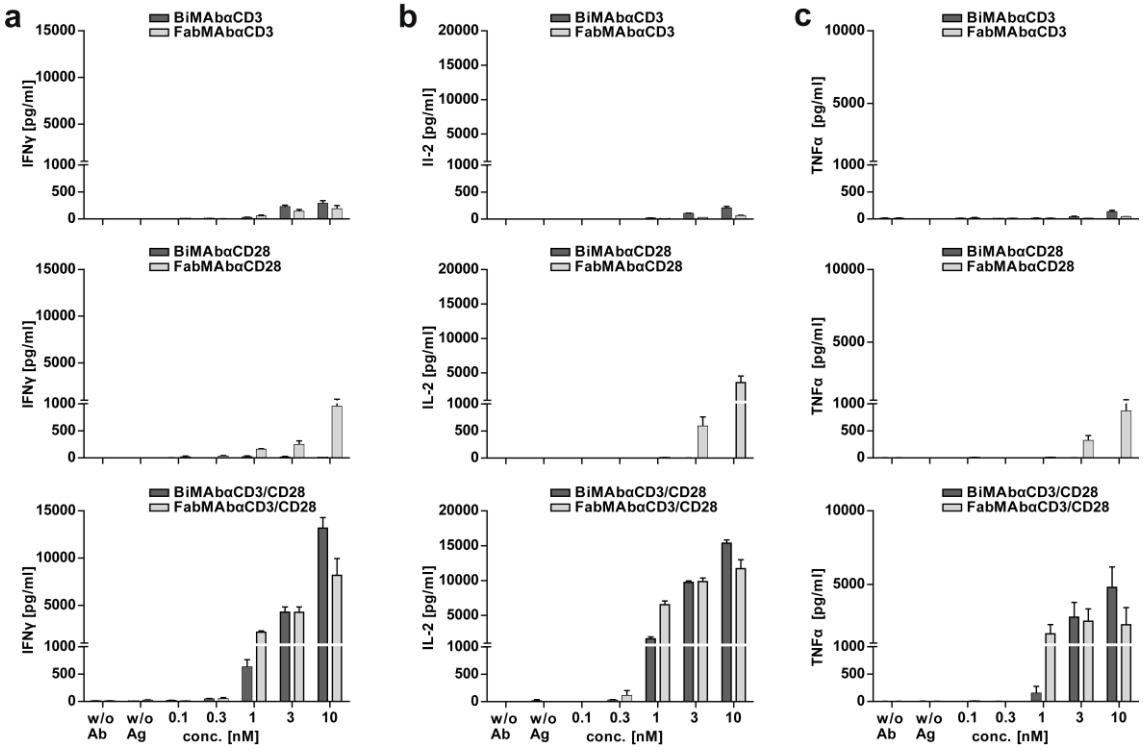

Figure 14: Combination of CD3- and CD28-specific constructs enhances cytokine secretion synergistically. (a) IFNγ**, (b)** IL-2**,** and **(c)** TNFα concentration in the supernatant of PBMC cultured on HBsAg-coated plates in the presence of the indicated bsAb-concentration after 72 hours quantified by ELISA. Samples without HBsAg in the presence of 10 nM antibody (w/o Ag) and in the absence of bsAbs (w/o Ab) served as controls. Data are presented as mean values ± SD of triplicate co-cultures (*n* = 3).

The benefit of co-stimulation was further demonstrated by evaluation of CD25 expression and lysosomal associated membrane protein 1 (LAMP-1) translocation via flow cytometry. Dot plot analysis showed an increase in size and granularity of the PBMC after 72-hour co-culture, when they were cultured on HBsAg-coated plates in the presence of bsAbs (Fig. 15a). According to live/dead staining analysis, the viability of PBMC was above 95% (Fig. 15a). The ratio of CD4/CD8 T cells was ~3:1 for bsAb-treated PBMC in HBsAg-coated plates and ~4.3:1 for PBMC in control wells. The experiments in this thesis were performed with PBMC of various healthy donors with different CD4/CD8 ratios. A ratio of ~4:1 was observed for at least 2 donors and might be a donor-intrinsic characteristic.

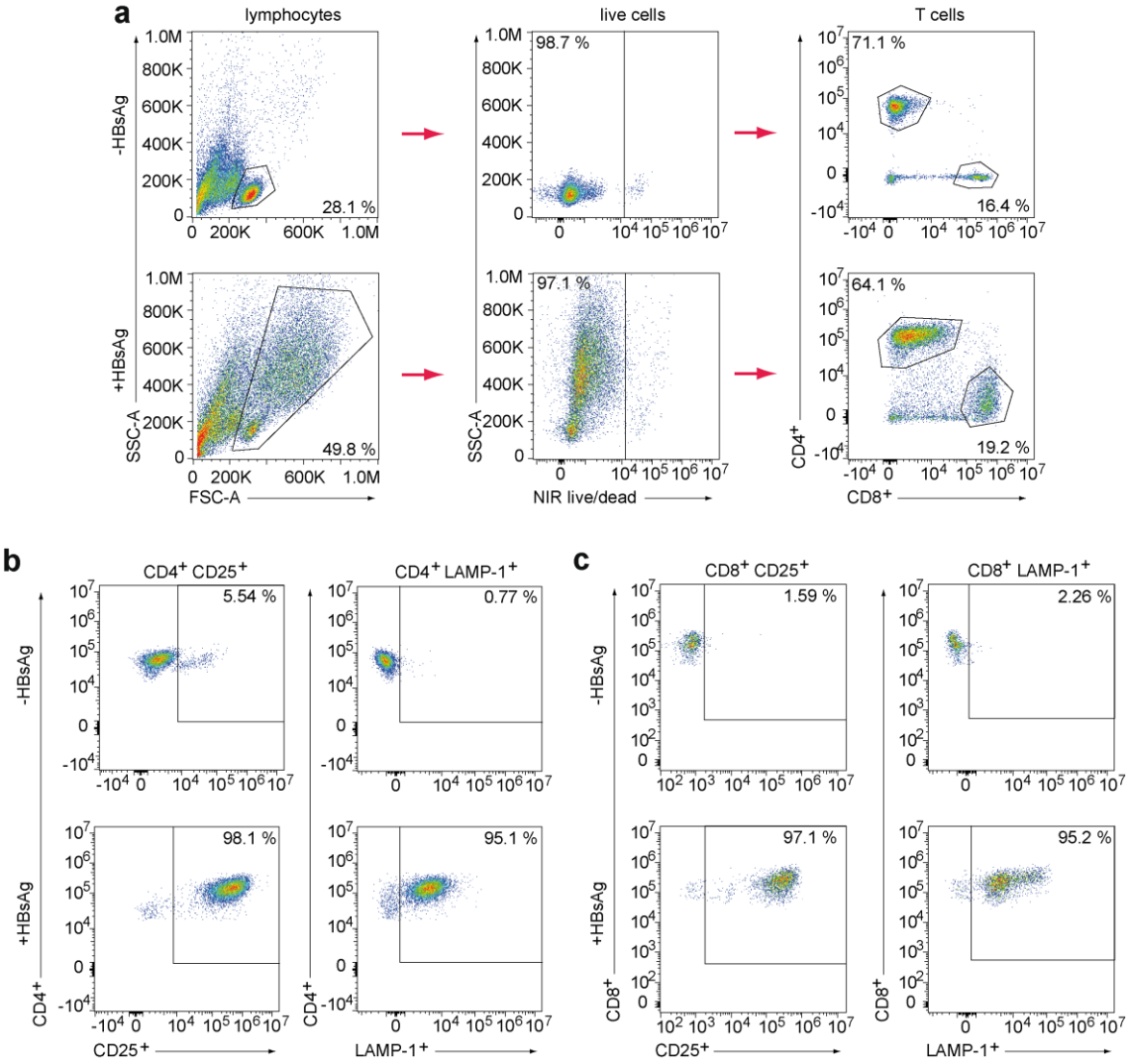

Figure 15: Gating strategy for detection of CD25 and LAMP-1 positive T cells. PBMC were cultured on control plates (top) or HBsAg-coated plates (bottom) in the presence of 3 nM FabMAbαCD3 and FabMAbαCD28 in combination (1:1 ratio). **(a)** PBMC were gated for lymphocytes, which were further gated on living cells and CD4- as well as CD8-expression to distinguish T cells **(b)** Dot blots of $CD4^+$ T cells that are gated for the expression of CD25 (left) or LAMP-1 (right). **(c)** Dot blots of $CD8^+$ T cells that are gated for the expression of CD25 (left) or LAMP-1 (right).

Similar to the cytokine profile, single treatment with CD3-specififc antibodies and FabMAbαCD28 induced upregulation of CD25 and LAMP-1 translocation, but the combination of the respective formats further increased the percentage of positive $CD4^+$ and $CD8^+$ T cells. Analysis of the mean fluorescence intensity (MFI) even indicated a synergistic effect. While CD25 was equally upregulated on both T-cell types, LAMP-1 levels were higher on $CD8^+$ T cells, especially when the MFI was taken into account (Fig. 15b, c, Fig. 16a-d). Compared to the data presented in 2.1.1.4, single treatment with FabMAbαCD3 and BiMAbαCD3 induced activation and degranulation of T cells. However, T-cell activation upon single treatment with CD3-engaging bsAbs was only observed in co-cultures with recombinant HBVenv and not in co-cultures with HBVenv transgenic Huh7S cells or HBV-infected HepG2 NTCP K7 cells. A similar pattern was also observed in 2.1.2.3.

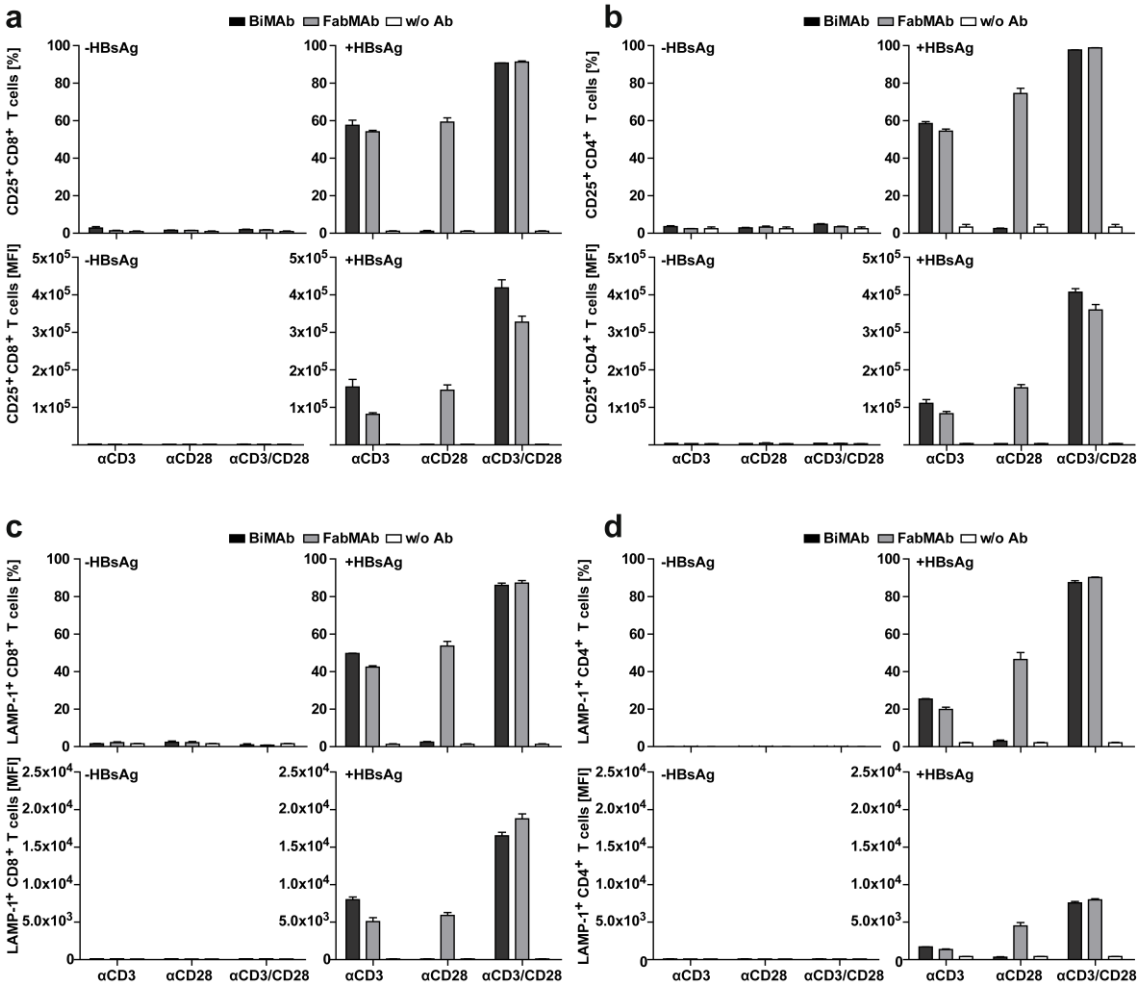

Figure 16: Combination of CD3- and CD28-specific constructs increases CD25 expression and LAMP-1 translocation. (a, b) CD25 expressing **(a)** $CD8^+$ or **(b)** $CD4^+$ T cells in the absence (left) or presence (right) of immobilized HBsAg after 72-hour co-culture treated with 3 nM of the indicated bsAbs, singly or in combination (1:1 ratio). The quantification is shown as percentage of positive cells (respective top panel) and MFI of the population (respective bottom panel). **(c, d)** LAMP-1 expressing **(c)** $CD8^+$ or **(d)** $CD4^+$ T cells in the absence (left) or presence (right) of immobilized HBsAg after 72-hour co-culture treated with 3 nM of the indicated bsAbs, singly or in combination (1:1 ratio). The quantification is shown as percentage of positive cells (respective top panel) and MFI of the population (respective bottom panel). Data are presented as mean values ± SD of triplicate co-cultures (n = 3).

To analyze the T-cell proliferation upon stimulation with the bsAbs, PBMC were stained with Cell Trace Violet (CTV) prior to start of co-culture. Even though proliferation was observed upon single treatment with the bsAbs, T cells proliferated substantially stronger, when the culture was supplied with the combination of the respective formats. $CD4^+$ and $CD8^+$ underwent 2-3 cell divisions within 72 hours of culture (Fig. 17a-c). These data demonstrated that providing a co-stimulation clearly increases the activation, proliferation and degranulation of the redirected T cells and consequently further characterization in this study was performed with a combination of the CD3- or CD28-specific constructs. Moreover, a total antibody concentration of 3 nM was defined as reasonable working concentration.

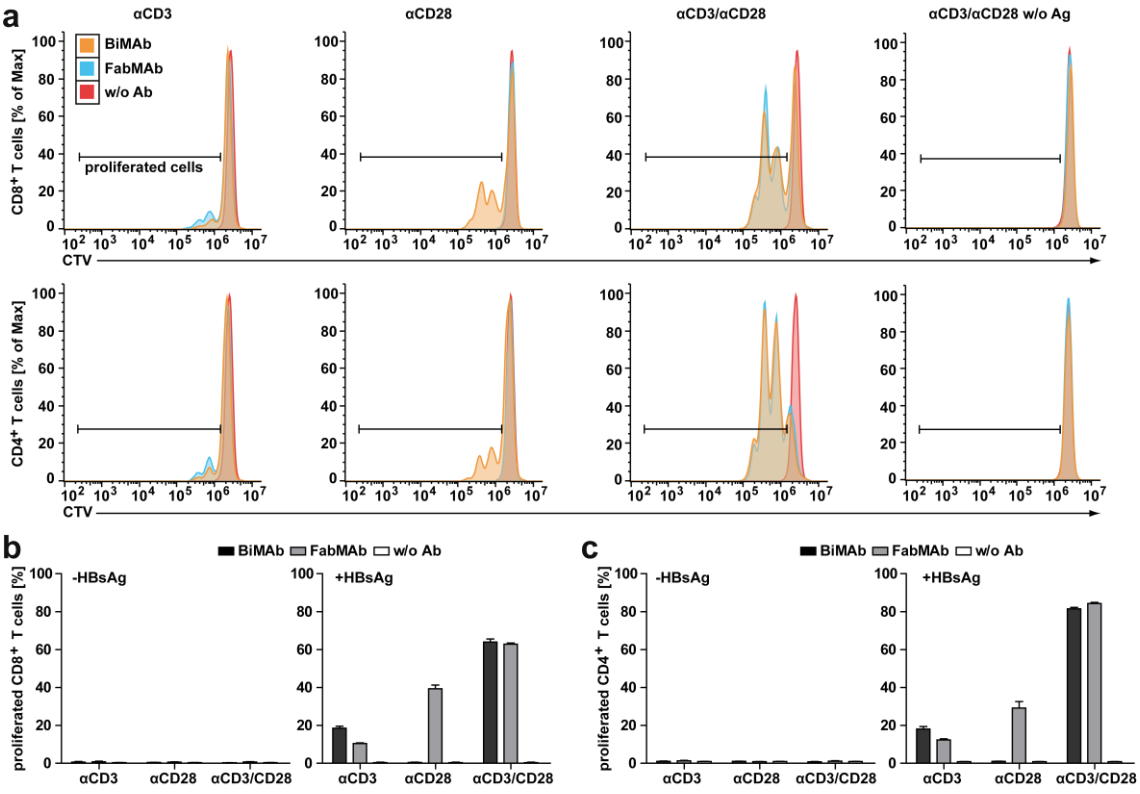

Figure 17: Combination of CD3- and CD28-targeting constructs stimulates T-cell proliferation. **(a)** Histograms of CTV-stained $CD8^+$ (top) and $CD4^+$ (bottom) T cells after 72-hour co-culture on immobilized HBsAg supplied with 3 nM of the indicated bsAbs, singly or in combination (1:1 ratio) **(b, c)** Quantification of proliferated **(b)** $CD8^+$ or **(c)** $CD4^+$ T cells in the absence (left) or presence (right) of immobilized HBsAg after 72-hour co-culture treated with 3 nM of the indicated bsAbs, singly or in combination (1:1 ratio). **(b, c)** Data are presented as mean values ± SD of triplicate co-cultures (*n* = 3).

2.2.3.2 BiMAbs and FabMAbs activate T cells with similar kinetics

Next, the kinetics of T-cell activation in cultures with Huh7S cells were investigated. Huh7S cells and PBMC were co-cultured with 3 nM of bsAbs in combination and supernatants were collected after 4, 8, 12, 24, 48, and 72 hours, followed by measurement of IFNγ, IL-2 and TNFα. Cytokines were first detectable after 12 hours and

continually increased over the course of the experiment. The strongest increase took place between 12 and 24 hours post start of co-culture (Fig. 18a).

To define the percentage of cytokine-secreting cells, intracellular cytokine staining (ICS) was performed. PBMC were harvested 4, 8, 12, 24, and 48 hours after the start of co-culture and stained for expression of IFNγ, IL-2 and TNFα. $CD4^+$ and $CD8^+$ T cells started to express cytokines already within the first 4 hours. After 48 hours, ~50% of $CD8^+$ and ~70% of $CD4^+$ T cells in the culture stained positive for at least one of the cytokines. While a substantial amount of T cells showed expression of two or more cytokines, around 50% of T cells stained positive for TNFα only (Fig. 18b). The percentage of polyfunctional T cells was determined by the use of Boolean combination gates (FlowJo).

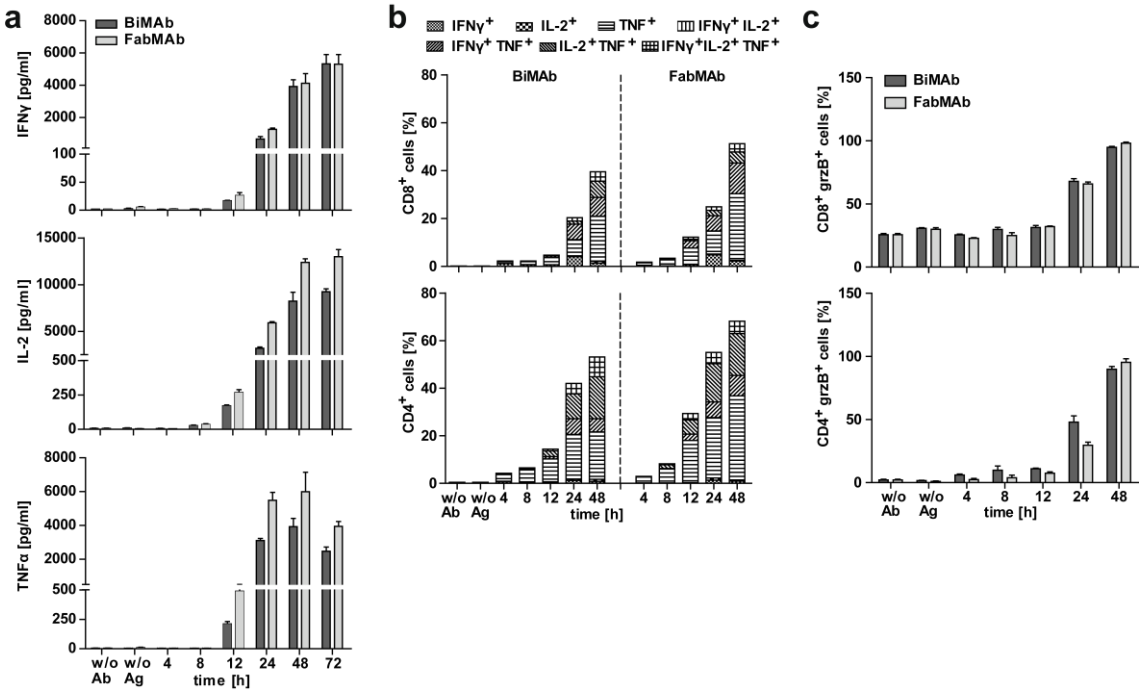

Figure 18: BiMAbs and FabMAbs activate T cells with similar kinetics. (a-c) PBMC were co-cultured with HBVenv-positive Huh7S cells and 3 nM of CD3- and CD28-targeting BiMAb or FabMAb in combination (1:1 ratio). **(a)** IFNγ (top) IL-2 (middle)**,** and TNFα (bottom) concentration in supernatants of co-cultures of PBMC and Huh7S cells at the indicated time points quantified by ELISA. Supernatants of Huh7 cells co-cultured with PBMC and 3 nM antibody after 72 hours (w/o Ag) and Huh7S cells co-cultured with PBMC in the absence of bsAbs after 72 hours (w/o Ab) served as controls. **(b)** Intracellular cytokine staining of IFNγ, IL-2, and TNFα for $CD8^+$ (top) and $CD4^+$ (bottom) T cells at indicated time points in co-culture with Huh7S cells. PBMC co-cultured with Huh7 cells and 3 nM antibody after 48 hours (w/o Ag) and PBMC co-cultured with Huh7S in the absence of bsAbs after 48 hours (w/o Ab) served as controls. The percentage of polyfunctional T cells was determined by the use of Boolean combination gates (FlowJo). **(c)** Intracellular staining of grzB for $CD8^+$ (top) and $CD4^+$ (bottom) T cells at indicated time points after co-culture with Huh7S. PBMC co-cultured with Huh7 cells and 3 nM antibody after 48 hours (w/o Ag) and PBMC co-cultured with Huh7S in the absence of bsAbs after 72 hours (w/o Ab) served as controls. Data are presented as mean values ± SD of triplicate co-cultures (*n* = 3).

The cytotoxic potential of the redirected T cells was determined by analysis of granzyme B (grzB) expression. PBMC were co-cultured with Huh7S cells in the presence of bsAbs

and harvested after 4, 8, 12, 24, and 48 hours. The major increase of grzB expression was detected between 12 and 24 hours. After 48 hours, flow cytometry analysis determined more than 90% of grzB-expressing T cells. $CD8^+$ T cells showed higher background expression than $CD4^+$ T cells (Fig. 18c).

2.2.3.3 BsAbs induce dose-depended elimination of HBVenv-positive target cells

To compare the efficacy of target cell elimination, Huh7S cells and PBMC were co-cultured with 0.1, 0.316, 1, 3.162, and 10 nM of bsAbs in combination for 96 hours and target cell viability was measured in real-time employing an xCELLigence RTCA. FabMAbs and BiMAbs induced target cell elimination when applied at a concentration of 0.3 nM or higher. Rate and kinetics were very comparable and correlated positively with the antibody concentration. The maximum was reached at 1 nM, with around 50% of eliminated target cells within the first 48 hours of co-culture (Fig. 19a, b). Minor loss of cell viability of HBVenv-negative Huh7 control cells was detected at high antibody concentration (>3 nM) and late time points. The rate of target cell elimination correlated with the concentration of IFNγ, IL-2, TNFα, and grzB detected in the co-cultures (Fig. 19c-d).

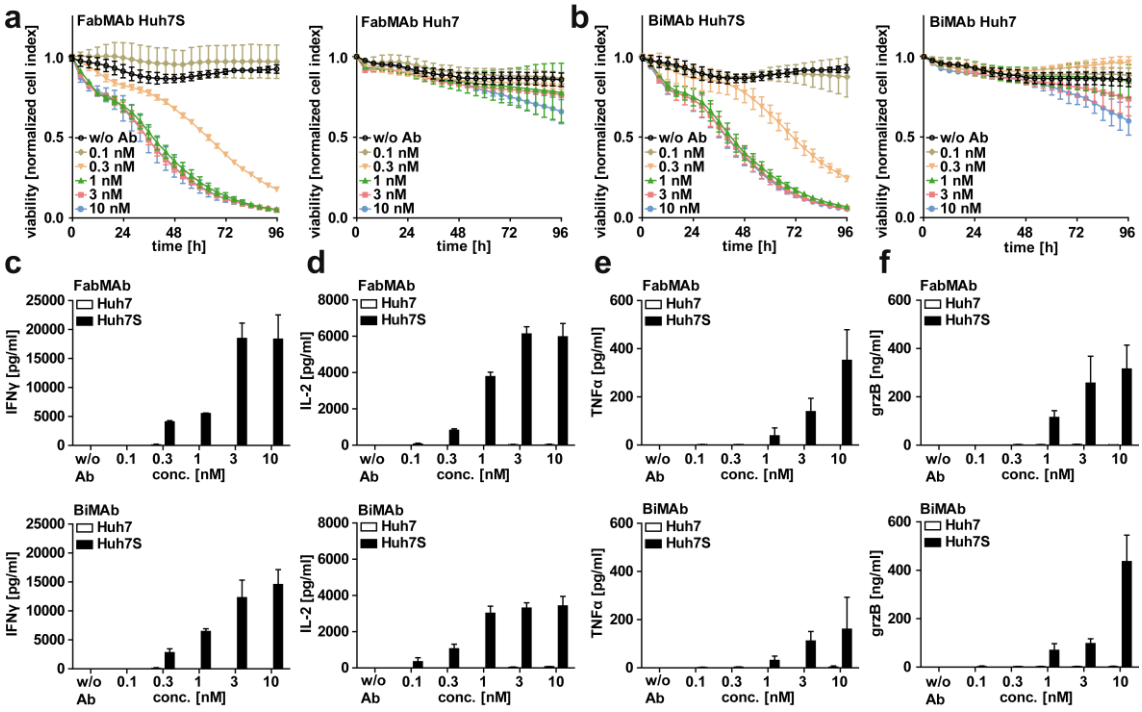

Figure 19: BiMAbs and FabMAbs activate T cells to eliminate HBVenv-expressing target cells with comparable kinetics. (a-f) PBMC were co-cultured with HBVenv-positive Huh7S cells or HBVenv-negative parental Huh7 cells and treated with CD3- and CD28-targeting BiMAb or FabMAb in combination (1:1 ratio) at indicated concetration. **(a, b)** Cell viability of HBVenv-positive Huh7S cells (left) or HBVenv-negative parental Huh7 cells (right) in co-culture with PBMC supplied with increasing doses of **(a)** FabMAbs or **(b)** BiMAbs. Samples without bsAbs (0 nM) served as controls. Target cell viability was determined over 96 hours in real-time employing an xCELLigence RTCA. **(c-f)** The concentration of **(c)** IFNγ, **(d)** IL-2, **(e)** TNFα and **(f)** grzB in the supernatant of co-cultures after 96 hours was determined by LEGENDplex analysis. Data are presented as mean values ± SD of triplicate co-cultures (*n* = 3).

Cytokine secretion was exclusively observed in cultures with Huh7S cells. These data indicate that BiMAbs and FabMAbs can redirect and activate T cells to eliminate HBVenv-expressing Huh7S cells in a comparable manner, when CD3- and CD28 specific constructs are applied in combination.

In consideration of a potential therapeutic approach, cytotoxic potential of PBMC of CHB patients in the setting of antibody-mediated T-cell redirection was assessed. PBMC were co-cultured with Huh7S cells in the presence of BiMAbs and target cell viability was measured in real time. The rate and kinetics of target cell elimination were comparable to experiments with PBMC of healthy donors (Fig. 20a).

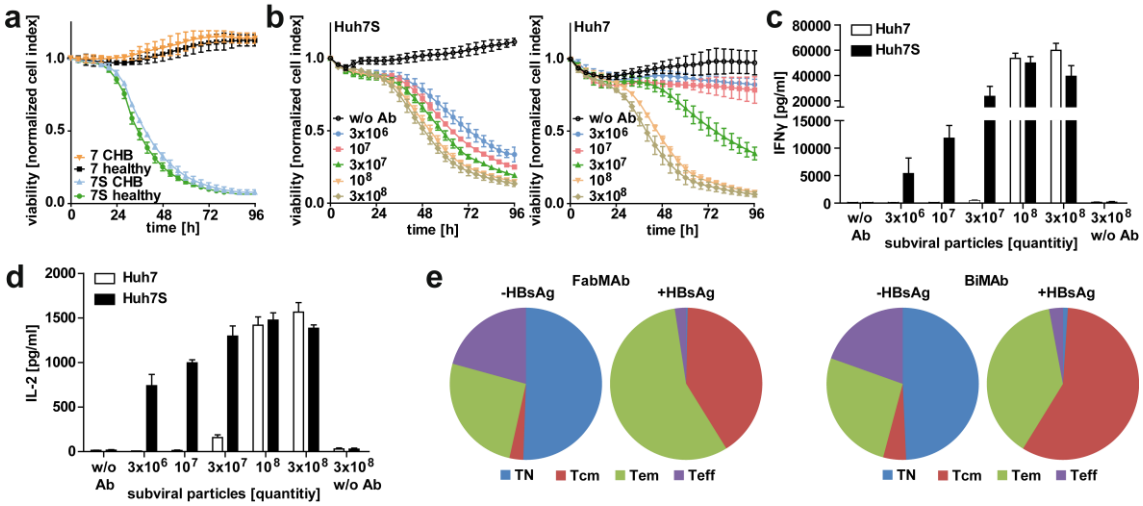

Figure 20: BsAbs activate T cells from CHB patients to eliminate HBVenv-expressing target cells. **(a-d)** PBMC were co-cultured with HBVenv-positive Huh7S cells or HBVenv-negative parental Huh7 cells and treated with 3 nM CD3- and CD28-targeting BiMAb or FabMAb in combination (1:1 ratio). **(a)** Cell viability of HBVenv-positive Huh7S cells and HBVenv-negative Huh7 cells in co-culture with PBMC of a CHB patient or healthy donor supplied with 3 nM BiMAbs in combination (1:1 ratio). Target cell viability was determined over 96 hours in real-time employing an xCELLigence RTCA. **(b)** Cell viability of HBVenv-positive Huh7S cells (left) or HBVenv-negative Huh7 cells (right) in co-culture with PBMC treated with 3 nM FabMAbs in combination (1:1 ratio). Co-cultures were supplied with the indicated doses of subviral particles. Samples without FabMAbs and subviral particles (w/o Ab) served as control. **(c, d)** Concentration of **(c)** IFNγ and **(d)** IL-2 in the supernatant of co-cultures described in (b) after 96 hours determined by ELISA. **(e)** PBMC were cultured on HBsAg-coated plates (+HBsAg) or control plates (-HBsAg) and treated with 3 nM FabMAbs in combination (1:1 ratio) (left) or BiMAbs in combination (1:1 ratio) (right). The percentage of (T_N), central memory (T_{CM}), effector memory (T_{EM}) and effector T cells (T_{EFF}) was subsequently determined via flow cytometry. The subsets of $CD8^+$ T cells were defined employing the markers CD45RO, CD45RA, CCR7 and CD62L according to Golubovskaya and Wu (Golubovskaya and Wu, 2016). Data are presented as **(a-d)** mean values ± SD of triplicate co-cultures (*n* = 3) or **(e)** mean values of triplicate co-cultures (*n* = 3).

Since CHB patients harbor high levels of soluble HBsAg in the blood circulation, it is important to consider a potential influence on the efficacy and safety of HBVenv-specific bsAbs. To study these effects, co-cultures were supplemented with increasing doses of subviral particles, ranging from $3x10^6$ to $3x10^8$ particles per ml. As readout, target cell elimination and cytokine release was measured. Kinetics of Huh7S cell elimination remained unchanged, but noticeable loss of Huh7 cell viability was detected when subviral particles in the culture reached values above $3x10^7$/ml (Fig. 20b). Elimination of

Huh7 cells was accompanied by IFNγ and IL-2 release at concentrations of 10^8 and $3x10^8$ subviral particles per ml (Fig. 20c, d).

To determine the influence of antibody treatment on the T-cell subset composition, PBMC were cultured on HBsAg-coated plates in the presence of 3 nM FabMAbs or BiMAbs in combination and the percentage of naïve (T_N), central memory (T_{CM}), effector memory (T_{EM}) and effector T cells (T_{EFF}) was determined by flow cytometry. In control samples (w/o Ab and w/o Ag) ~40% of T_N, ~20% of T_{EM} and T_{EFF}, and 5% of T_{CM} were detected. Treatment with bsAbs increased the percentage of T_{CM} and T_{EM} to ~40%, while T_{EFF} and T_N were hardly detectable anymore (Fig. 20e).

Taken together, these data led to the conclusion that the bsAbs can activate T cells of CHB patients to eliminate HBVenv-expressing target cells. Furthermore, the T-cell subset composition of bsAb-treated PBMC showed a memory-effector phenotype, while untreated PBMC contained a high proportion of naïve T cells. It is important to emphasize, that the potential elimination of uninfected hepatocytes in the presence of soluble HBsAg need to be considered and must be carefully evaluated in the *in vivo* setting.

2.2.3.4 The half-life of BiMAbs and FabMAbs differs substantially in mice

Finally, the impact of the antibody format on the serum availability in C57BL/6 mice was evaluated. To limit the number of animals for this experiment, Fab- and Fc-specific detection antibodies were used for ELISA. This allowed specific detection of FabMAbs (Fig. 21a) and BiMAbs (Fig. 21b), when the constructs were applied in a mixture. However, for convenience reasons BiMAb samples were quantified employing an Architect® (anti-HBs), whereas FabMAb concentration was determined by ELISA. Since quantification by Architect® measurement requires bivalent binding to HBVenv, FabMAbs cannot be detected in this assay. Animals were injected intravenously (i.v.), intraperitoneally (i.p.), or subcutaneously (s.c.) with 50 µg of BiMAbαCD28 and FabMAbαCD28, or vehicle (PBS). Mice were bled after 1, 6, 12, 24, 48 and 72 hours and the antibody levels in the serum were determined (Fig. 21c). It is hereby clearly stated that injection of antibodies and bleeding of mice was performed by Julia Festag and Eva Loffredo-Verde.

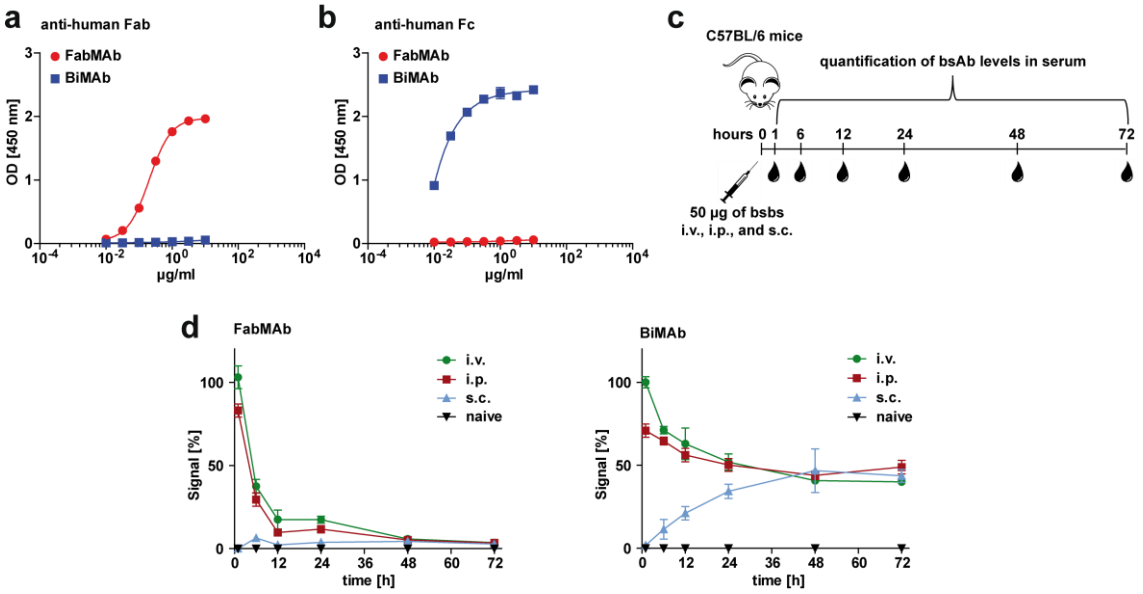

Figure 21: The half-life of BiMAbs and FabMAbs differs substantially in C57BL/6 mice. **(a, b)** HBsAg ELISA to demonstrate specific detection of FabMAbs and BiMAbs by goat anti-human Fab HRP antibodies and goat anti-human Fc HRP antibodies, respectively. HBsAg-coated plates were incubated with a half-logarithmic dilution series ranging from 10-0.01 nM of **(a)** FabMAbαCD28 and **(b)** BiMAbαCD28. BsAbs were detected with goat anti-human Fc HRP antibodies (BiMAb) or goat anti-human Fab HRP antibodies (FabMAb). **(c)** Schematic representation of the mouse experiment for the evaluation of half-life ($t_{1/2}$) with 3 mice per group. Blood drops indicate the time point of bleeding and collection of serum. **(d)** Half-life of BiMAbs (left) and FabMAbs (right) in mouse sera of C57BL/6 mice. 50 µg of BiMAbαCD28 and FabMAbαCD28 in 200 µl PBS were injected i.v., i.p., or s.c. Control mice (naïve) were injected with 200 µl PBS only. Mice were bled after 1, 6, 12, 24, 48 and 72 hours and the antibody concentration in the serum was determined by ELISA (FabMAbs) or Architect® (BiMAbs). The values were normalized to the 1-hour time point of the i.v. injected group. **(a, b)** Data are presented as mean value ± SD of triplicate parallel analyses (*n* = 3). **(d)** BiMAb data is given as mean ± SD of single analysis for each mouse (*n* = 3) and FabMAb data represent mean ± SD of technical duplicates for each mouse (*n* = 6).

FabMAb serum levels decreased rapidly with a short half-life ($t_{1/2}$) below 6 hours, while BiMAbs persisted substantially longer. Within the first 48 hours, BiMAb levels reached a plateau at around 50% of the initial input, which was maintained until the end of the experiment, leading to a $t_{1/2}$ of at least 72 hours. Both formats demonstrated very similar serum availability after the respective i.v. and i.p. administration, whereas the s.c. route showed different kinetics. Subcutaneously applied FabMAbs were hardly detectable at all, while BiMAb levels increased continuously within the first 48 hours, reaching the same plateau as the other application routes (Fig. 21d).

Overall, treatment with BiMAbs and FabMAbs, singly and in combination, showed a very comparable redirection potential *in vitro* that was demonstrated by proliferation, cytokine secretion, and the establishment of a cytotoxic immune response towards HBVenv-expressing target cells. However, BiMAbs showed a substantially longer $t_{1/2}$ in C57BL/6 mice, which makes them the lead candidate for potential *in vivo* studies.

2.3 Evaluation of the bsAb-mediated antiviral effect

2.3.1 HepG2 NTCP K7 cells are highly susceptible to HBV infection

In the next step, the bsAb approach was applied to an HBV infection system, where HepG2 NTCP K7 cells were used as model cell line (Ko et al., 2018). To study the correlation between the MOI and the grade of infection in this setting, cells were infected with increasing MOI and the number of infected cells, as well as, the viral markers HBeAg, intracellular HBV DNA and cccDNA were quantified 10 days post infection. The amount of infected cells in the culture was determined by intracellular HBc-staining and flow cytometry analysis. The percentage of HBc-positive cells correlated positively with the MOI, ranging from 22.8% at low MOI (25 HBV virions/cell) to 82.4% at high MOI (500 HBV virions/cell) (Fig. 22a-c).

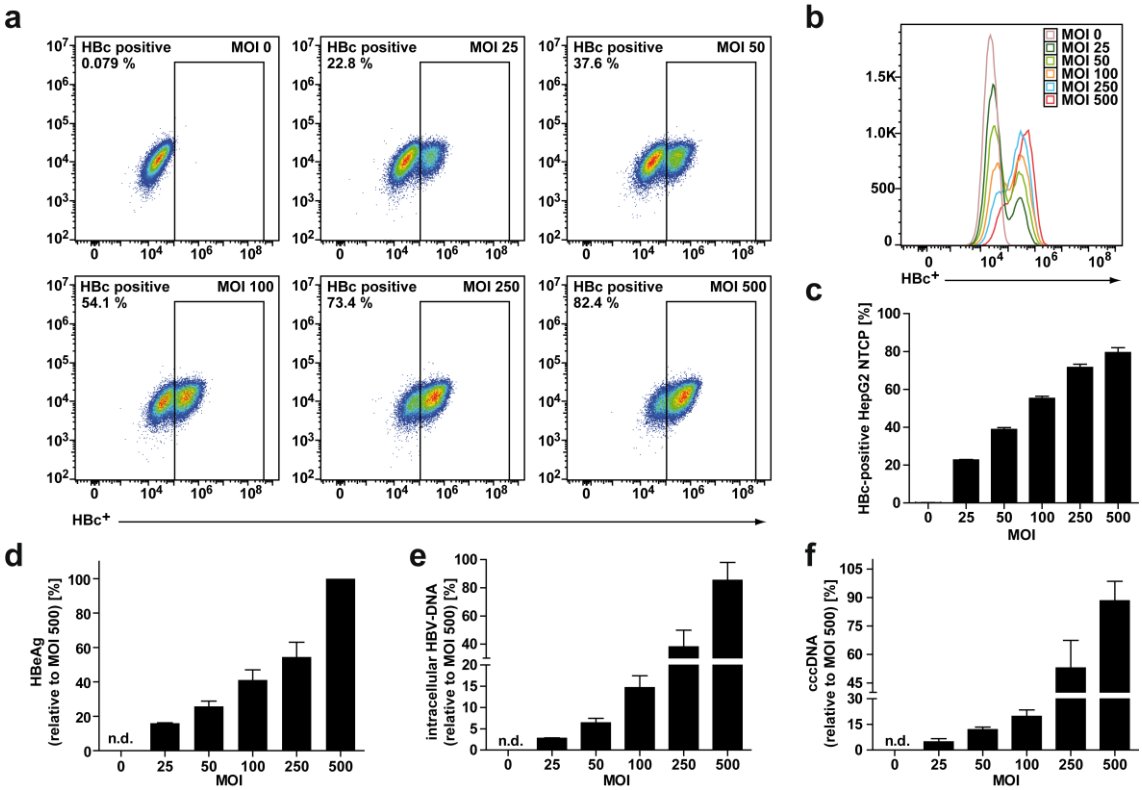

Figure 22: HepG2 NTCP K7 cells are highly susceptible to HBV infection. Cells were infected with the MOI 25, 50, 100, 250 and 500 HBV virions/cell and analysis was performed 10 days post infection. **(a)** Percentage of HBc-positive HepG2 NTCP cells after infection with the indicated MOI. Cells were stained for intracellular HBc expression with a combination of anti-HBc containing rabbit serum and anti-rabbit PE antibodies, and analyzed by flow cytometry. **(b)** Histogram of HBc-stained HepG2 NTCP cells infected with the indicated MOI. Sating was performed as described in (a). **(c)** Quantification of the percentage of HBc-HepG2 NTCP cells described in (a, b). **(d)** HBeAg in the supernatant of infected HepG2 NTCP cells secreted from day 8-10 quantified by AxSYM measurement. **(e)** Intracellular HBV-DNA and **(f)** cccDNA in infected HepG2 NTCP cultures. Cells were lysed 10 days post infection and viral DNAs were quantified by qPCR. **(c-f)** Data are presented as mean values ± SD of triplicate cultures (*n* = 3). n.d. = not detectable.

The viral parameters were quantified with an AxSYM (HBeAg) or qPCR (intracellular HBV-DNA, cccDNA) and showed similar patterns (Fig. 22d-f). However, HBeAg, intracellular HBV-DNA, and cccDNA levels increased by ~50%, when the MOI was raised from 250 to 500 HBV virions/cell, while the percentage of HBc^+ cell only showed a mild increase.

2.3.2 BsAbs activate T cells to eliminate infected HepG2 NTCP cells

The antibody-mediated cytotoxic immune response against HBV-infected target cells was evaluated in xCELLigence experiments as described in 2.2.3.3. HepG2 NTCP cells were infected at a MOI of 500 HBV virions/cell and co-cultured with PBMC in the presence of bsAbs at day 10 post infection (p.i.).

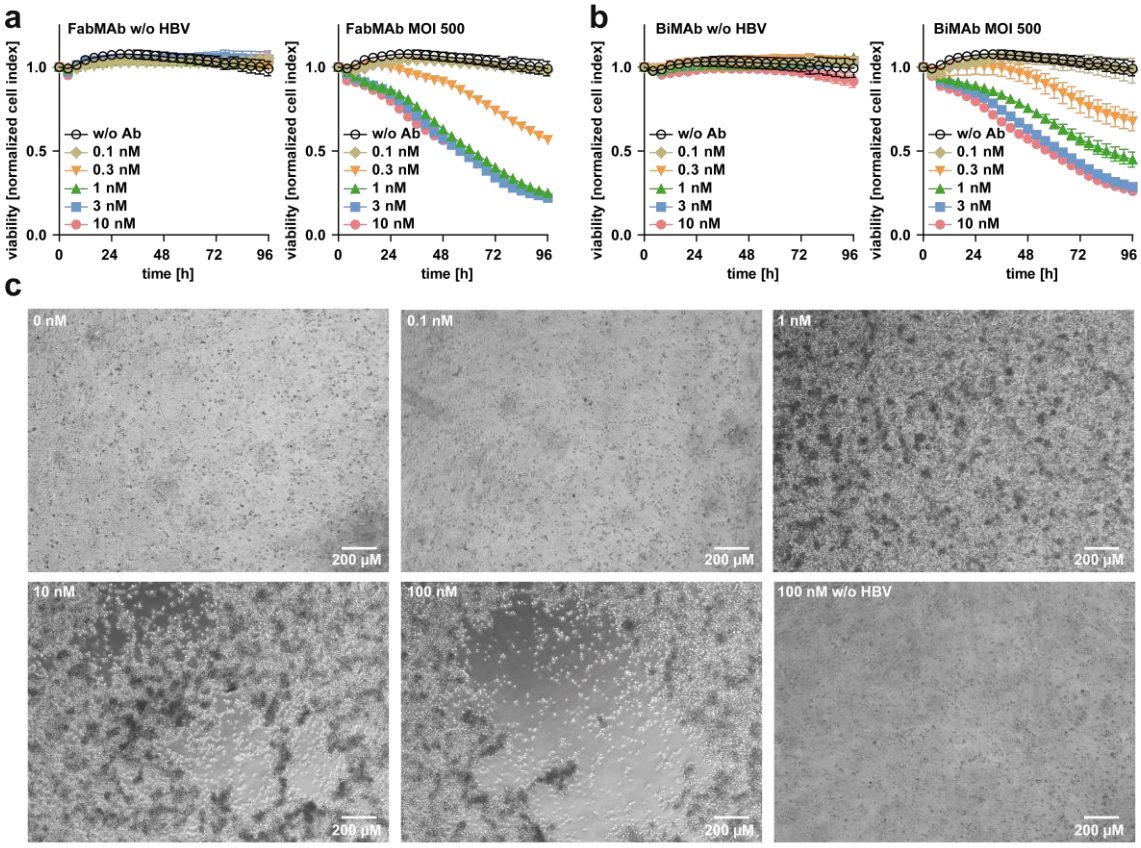

Figure 23: Treatment with bsAbs induces specific elimination of infected HepG2 NTCP cells. (a, b) Target cell viability was determined over 96 hours in real-time employing an xCELLigence RTCA. Cell viability of uninfected (left) or infected HepG2 NTCP cells (MOI 500 HBV virions/cell) (right) in co-culture with PBMC supplied with increasing dose of **(a)** FabMAbs or **(b)** BiMAbs in combination (1:1 ratio). Samples without bsAbs (w/o Ab) served as controls. **(c)** Microscopic analysis after 6 days of co-culture in the 24-well format. Infected HepG2 NTCP cells were treated with 0.1, 1, 10 and 100 nM of FabMAbs in combination (1:1 ratio). Uninfected HepG2 NTCP cells (w/o HBV) served as controls. **(a, b)** Data are presented as mean values ± SD of triplicate co-cultures (*n* = 3).

FabMAbs and BiMAbs induced target cell elimination, when applied at a concentration of 0.3 nM or higher. Rate and kinetics were comparable and correlated with the antibody concentration. However, the BiMAb-mediated target cell elimination was slower at 0.3 and 1 nM. In contrast to Huh7 controls, elimination of uninfected Hep2G NTCP cells was not detected. The reduction of cell viability was around 80% and correlated with the percentage of HBc-positive cells determined in 2.3.1 (Fig. 23a, b). A dose-depended T-cell activation and cytotoxic activity was further evaluated by microscopic analysis. Therefore, co-cultures were established in the 24-well format. Infected HepG2 NTCP cells were treated with 0.1, 1, 10 and 100 nM of FabMAbs in combination and co-cultures were maintained for 6 days. Fresh medium with bsAbs was supplied every two days. Treatment with 0.1 nM of the FabMAb combination did neither induce T-cell clustering, nor did it show a cytopathic effect. At a concentration of 1 nM, distinct clustering of PBMC was observed, while 10 nM resulted in notable rupture of the cell layer. This effect was not enhanced, when the bsAb concentration was increased to 100 nM. Uninfected HepG2 control cells showed no cytopathic effect, even at a concentration of 100 nM (Fig. 23c).

2.3.3 Treatment with bsAbs induces MOI-dependent T-cell activation and demonstrates an antiviral effect

To study the correlation between the level of infection and the efficacy of T-cell redirection, HepG2 NTCP cells were infected with different amount of HBV (MOI 0, 25, 50, 100, 250 and 500 HBV virions/cell) and employed in co-cultures with PBMC and 0, 0.1, 1 and 10 nM of FabMAbs in combination for 12 days (Fig. 24a). On day 3, the supernatant was analyzed for the presence of IFNγ, IL-2 and TNFα by ELISA. Cytokine levels correlated with the antibody concentration and the MOI. The secretion of cytokines was always completely depended on the presence of HBV and bsAbs (Fig. 24b). IFNγ levels increased until day 4 of co-culture and were undetectable from day 6 on (Fig. 24c). As readout for cytotoxicity, cell viability was determined by Cell Titer Blue assay (CTB) after 12 days. The loss of viability correlated with the MOI and showed about 90% reduction at a MOI of 500 HBV virions/cell and about 10% reduction at a MOI of 100 HBV virions/cell (Fig. 24d). To quantify the antiviral effect, HBeAg, intracellular HBV-DNA and cccDNA were measured 12 days after start of co-culture. At the highest viral load (MOI 500 HBV virions/cell) and at least 1 nM of bsAbs, a profound antiviral effect was detected, which led to 90% reduction of HBeAg and 99% reduction of intracellular HBV-DNA and cccDNA. Yet, the antiviral effect correlated with the MOI, leading to smaller efficacy at low MOIs (Fig. 24e). HBeAg levels in the culture showed a major reduction until day 6, which is consistent with the kinetics of IFNγ concentration determined earlier (Fig. 24f). To calculate half-maximal inhibitory concentration (IC50) values, a half-logarithmic dilution series ranging from 0.01 to 100 nM was employed. Non-linear regression of HBeAg values resulted in an IC50 value of 0.7194 nM (Fig. 24g). These data indicated that treatment with the bsAbs can activate T cells in the presence of HBV-

infected HepG2 NTCP cells, resulting in cytokine secretion, elimination of target cells, and profound reduction of viral parameters.

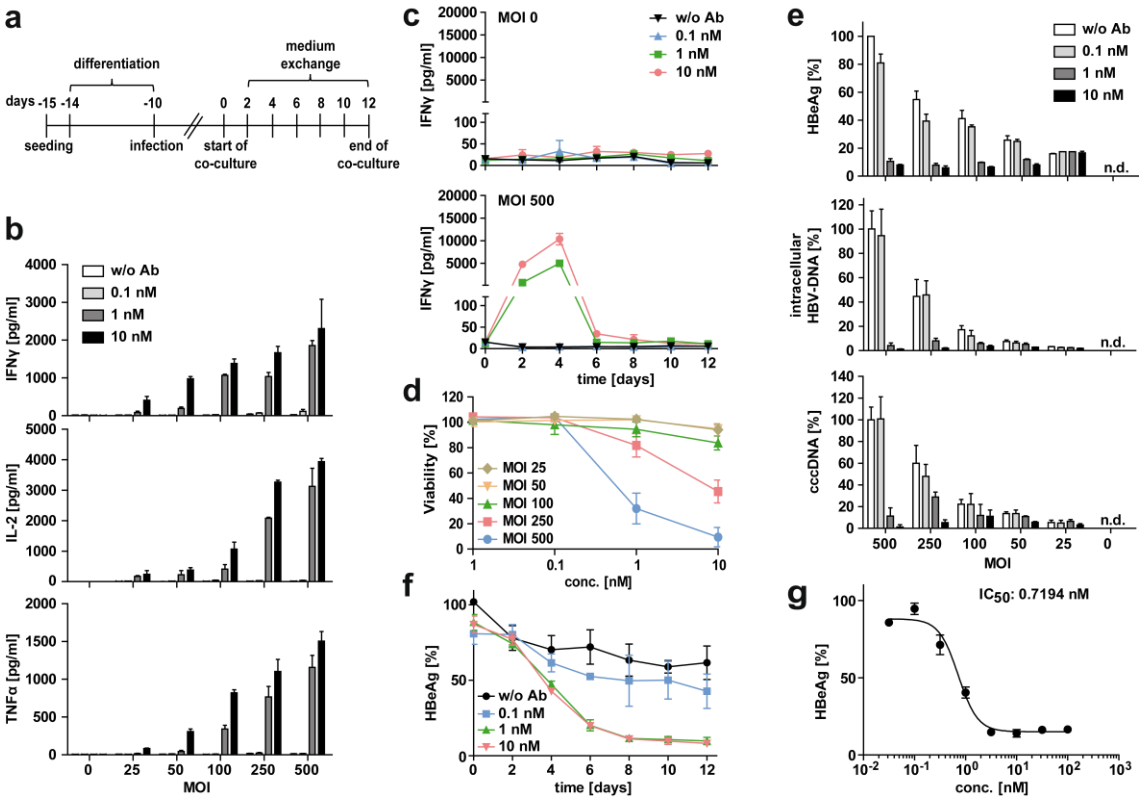

Figure 24: Treatment with bsAbs mediates a dose- and MOI-depended anti-viral effect. **(a)** Schematic representation of the co-culture setup employing infected HepG2 NTCP cells (MOI 500 HBV virions/cell) in the 24-well format. **(b)** Concentration of IFNγ (top), IL-2 (middle) and TNFα (bottom) in the supernatant of co-cultures of infected HepG2 NTCP cells (MOI 500 HBV virions/cell) and PBMC supplied with the indicated concentrations of FabMAbs in combination (1:1 ratio) after 3 days of co-culture. Cytokine concentrations in the supernatant were quantified by ELISA. **(c)** IFNγ concertation in the supernatant at indicated time points in co-cultures with uninfected (top) or infected HepG2 NTCP cells (MOI 500 HBV virions/cell) (bottom) and the indicated concentration of FabMAbs in combination (1:1 ratio). The IFNγ concertation in the supernatant was quantified by ELISA. **(d)** Viability of HepG2 NTCP cells infected with indicated MOI after a 12-day co-culture with PBMC and 10 nM FabMAbs in combination (1:1 ratio). The viability was determined with the Cell Titer Blue assay. **(e)** Levels of HBeAg (top), intracellular HBV-DNA (middle), and cccDNA (bottom) in co-cultures of infected HepG2 NTCP cells (infected with the indicated MOI) and PBMC after 12-day treatment with FabMAbs in combination (1:1 ratio) at indicated concentrations. Viral parameters were determined by Architect® (HBeAg) or qPCR (viral DNAs). Data are presented in percent relative to w/o Ab and MOI 500 HBV virions/cell. **(f)** HBeAg levels in supernatant of co-cultures of infected HepG2 NTCP cells (MOI 500 HBV virions/cell), PBMC and FabMAb in combination (1:1 ratio) at indicated time points. The HBeAg concentration was determined by AxSYM measurement. Data are presented in percent relative to w/o Ab and MOI 500 HBV virions/cell at day 0. **(g)** IC_{50} values of FabMAb treatment based on the HBeAg-level in the supernatant. Infected HepG2 NTCP cells (MOI 500 HBV virions/cell) were co-cultured with PBMC and a half-logarithmic dilution series of FabMAbs in combination (1:1 ratio) ranging from 100-0.01 nM for 12 days. EC_{50} was calculated using non-linear regression log(agonist) vs. response variable slope with a robust fit (Prism). Data are presented in percent relative to w/o Ab and MOI 500 HBV virions/cell. **(b-g)** Data are presented as mean values ± SD of triplicate co-cultures (*n* = 3). n.d. = not detectable.

2.4 Development and functional analysis of trispecific antibodies

2.4.1 Structural and biochemical properties of TriMAb and OKTriMAb

The combination of CD3- and CD28-specific bsAbs did not only synergistically enhance T-cell activation, but was also required to induce effective elimination of HBVenv-expressing Huh7S cell and HBV-infected HepG2 NTCP cells. In consideration of a therapeutic approach, both immune stimulatory scFv were combined in two trispecific antibody constructs (tsAbs), using the Fab5F9 as heterodimerization domain. The structure of the TriMAb is based on the construct FabMAbαCD3. To provide a co-stimulatory signal the scFvCD28 was fused to the c-terminus of the light chain. The affinity to HBVenv was further increased by addition of the scFvC8 to the n-termini of heavy and light chain, resulting in a pentavalent construct with a molecular weight of 162 kD, which contains three binding moieties for HBVenv and one for CD3 as well as CD28. (Fig. 25a, b, Fig. 27a).

To further increase binding valency, two TriMAbs were dimerized by n-terminal elongation of the C_H1 domain with the amino acids DKTHTCPPCP from the IgG1 hinge region. This allows disulfide bond formation between the respective Cys395 and Cys398 of the heavy chain, resulting in a $F(Ab)_2$-like molecule. To reduce protein size, the variable domains of Fab5F9 were removed and scFvC8 were directly fused to the n-termini of HC and LC constant domains. Hence, the Fab fragment lost its HBVenv-specificity and is used for heterodimerization only. This resulted in an oktavalent construct with four binding sites for HBVenv as well as two for CD3 and CD28, referred to as OKTriMAb (Fig. 26a, b, Fig. 27a). The molecular construction of this molecule was performed by myself. Further information about the procedure is provided in the methods section.

.

a

TriMAb C8-HC-scFvOKT3 peptide: MW = 80.9 kD; total MW with LC = 162 kD

```
0   MAEVQLVESGGGLLQPGGSLRLSCAASGFTFSGYAMSWVRQAPGKGLEWVSSISGSGGSTYYADSVKGRFTISRDNSKNT
80  LYLQMNSLRAEDTALYYCAKPPGRQEYYGSSIYYFPLGNWGQGTLVTVSSASTKGPKLEEGEFSEARVQSALTQPASVSV
160 APGQTARITCGGNNIGSKSVHWYQQKPGQAPVLVVYDDSDRPSGIPERFSGSNSGNTATLTISRVEAGDEADYYCQVWDS
240 SSDLVVFGGGTKLTVLGQPKAAPSVTLFPPSSAAAGGGGSGGGGSEVQLVESGGGLVHPGRSLKVSCAASGFTFNNYAM
320 SWVRQTPDRRLELVAVINSDGRSTFYPDTVMGRFTISRDNAKNTLYLQMSSLKSEDTAIYYCARTFYADYWGQGTTLTVS
400 SASTKGPSVFPLAPSSKSTSGGTAALGCLVKDYFPEPVTVSWNSGALTSGVHTFPAVLQSSGLYSLSSVVTVPSSSLGTQ
480 TYICNVNHKPSNTKVDKKVEPKSCGGGGSGGGGSTSQVQLQQSGAELARPGASVKMSCKASGYTFTRYTMHWVKQRPGQG
560 LEWIGYINPSRGYTNYNQKFKDKATLTTDKSSSTAYMQLSSLTSEDSAVYYCARYYDDHYCLDYWGQGTTLTVSSGGGGS
640 GGGGSGGGGSQIVLTQSPAIMSASPGEKVTMTCSASSSVSYMNWYQQKSGTSPKRWIYDTSKLASGVPAHFRGSGSGTSY
720 SLTISGMEAEDAATYYCQQWSSNPFTFGSGTKLEINHHHHHHHHHH
```

HC scFv C8	: [1 : 138]
Yol-linker	: [139 : 147]
LC scFv C8	: [148 : 276]
2x(G4S) Linker	: [277 : 286]
HC variable 5F9	: [287 : 403]
HC constant hu IgG1	: [404 : 499]
hinge domain fragment: Cys504 for disulfide bond with LC	: [500 : 504]
2x(G4S) Linker	: [505 : 514]
TS: adaptor sequence SpeI	: [515 : 516]
HC scFv OKT3	: [517 : 633]
SS: adaptor sequence XbaI^SpeI	: [634 : 635]
3x(G4S) Linker	: [636 : 650]
LC scFv OKT3	: [651 : 756]
10x His Tag	: [757 : 766]

b

TriMAb C8-LC-scFv9.3 peptide: MW = 81.7 kD; total MW with HC = 162 kD

```
0   MAEVQLVESGGGLLQPGGSLRLSCAASGFTFSGYAMSWVRQAPGKGLEWVSSISGSGGSTYYADSVKGRFTISRDNSKNT
80  LYLQMNSLRAEDTALYYCAKPPGRQEYYGSSIYYFPLGNWGQGTLVTVSSASTKGPKLEEGEFSEARVQSALTQPASVSV
160 APGQTARITCGGNNIGSKSVHWYQQKPGQAPVLVVYDDSDRPSGIPERFSGSNSGNTATLTISRVEAGDEADYYCQVWDS
240 SSDLVVFGGGTKLTVLGQPKAAPSVTLFPPSSAAAGGGGSGGGGSDIVMTQSHKFMSASVGDRVSISCKASQNVDTTVA
320 WFQQKPGQSPKLLIYWASTRHSGVPDRFTGSGSRSGFTLTISNVQSEDLAVYFCQQYSIFPYTFGGGTKLEIKRTVAAPS
400 VFIFPPSDEQLKSGTASVVCLLNNFYPREAKVQWKVDNALQSGNSQESVTEQDSKDSTYSLSSTLTLSKADYEKHKVYAC
480 EVTHQGLSSPVTKSFNRGECGGGGSGGGGSTSQVQLQQSGPGLVTPSQSLSITCTVSGFSLSDYGVHWVRQSPGQGLEWL
560 GVIWAGGGTNYNSALMSRKSISKDNSKSQVFLKMNSLQADDTAVYYCARDKGYSYYYSMDYWGQGTTVTVSSRGGGSGGG
640 GSGGGGSDIELTQSPASLAVSLGQRATISCRASESVEYYVTSLMQWYQQKPGQPPKLLIFAASNVESGVPARFSGSGSGT
720 NFSLNIHPVDEDDVAMYFCQQSRKVPYTFGGGTKLEIKRWSHPQFEK
```

HC scFv C8	: [1 : 138]
Yol-linker	: [139 : 147]
LC scFv C8	: [148 : 276]
2x(G4S) Linker	: [277 : 286]
LC variable 5F9	: [287 : 393]
LC kappa constant	: [394 : 500]
Cys500: disulfide bond with HC	: [500]
2x(G4S) Linker	: [501 : 510]
TS: adaptor sequence SpeI	: [511 : 512]
HC scFv 9.3	: [513 : 631]
SR: adaptor sequence XbaI	: [632 : 633]
3x(G4S) Linker	: [634 : 647]
LC scFv 9.3	: [648 : 759]
Strep tag II	: [760 : 767]

Figure 25: Amino acid sequences of TriMAb. Amino acid sequence of **(a)** the TriMAb C8-HC-scFvOKT3 peptide and **(b)** the TriMAb C8-LC-scFv9.3 peptide. Adaptor sequences are traces of the cloning procedure. TS: restriction recognition site of SpeI; SS: ligation site of XbaI- and SpeI-digested DNA fragments; SR: restriction recognition site of XbaI.

a

OKTriMAb C8-HC-scFv9.3 peptide: MW = 68.4 kD; total MW tetramer = 275 kD

```
0   MAEVQLVESGGGLLQPGGSLRLSCAASGFTFSGYAMSWVRQAPGKGLEWVSSISGSGGGSTYYADSVKGRFTISRDNSKNT
80  LYLQMNSLRAEDTALYYCAKPPGRQEYYGSSIYYFPLGNWGQGTLVTVSSASTKGPKLEEGEFSEARVQSALTQPASVSV
160 APGQTARITCGGNNIGSKSVHWYQQKPGQAPVLVVYDDSDRPSGIPERFSGSNSGNTATLTISRVEAGDEADYYCQVWDS
240 SSDLVVFGGGTKLTVLGQPKAAPSVTLFPPSSAAAGGGGGSGGGGSASTKGPSVFPLAPSSKSTSGGTAALGCLVKDYFP
320 EPVTVSWNSGALTSGVHTFPAVLQSSGLYSLSSVVTVPSSSLGTQTYICNVNHKPSNTKVDKKVEPKSCDKTHTCPPCPG
400 GGGSGGGGSTSQVQLQQSGPGLVTPSQSLSITCTVSGFSLSDYGVHWVRQSPGQGLEWLGVIWAGGGTNYNSALMSRKSI
480 SKDNSKSQVFLKMNSLQADDTAVYYCARDKGYSYYYSMDYWGQGTTVTVSSRGGGSGGGGSGGGGSDIELTQSPASLAVS
560 LGQRATISCRASESVEYYVTSLMQWYQQKPGQPPKLLIFAASNVESGVPARFSGSGSGTNFSLNIHPVDEDDVAMYFCQQ
640 SRKVPYTFGGGTKLEIKR
```

HC scFv C8	: [1 : 138]
Yol-linker	: [139 : 147]
LC scFv C8	: [148 : 276]
2x(G4S) Linker	: [277 : 286]
AS: adaptor sequence NheI	: [287 : 288]
HC constant hu IgG1	: [289 : 384]
Hinge domain fragment:Cys389 for ds bond with LC as well as Cys395 and Cys398 for ds bond with HC	: [385 : 399]
4x(G4S) Linker	: [400 : 409]
HC scFv 9.3	: [410 : 530]
SR: adaptor sequence XbaI	: [531 : 532]
3x(G4S) Linker	: [533 : 546]
LC scFv 9.3	: [547 : 658]

b

OKTriMAb C8-LC-scFvOKT3 peptide: MW = 68.9 kD; total MW tetramer = 275 kD

```
0   MAEVQLVESGGGLLQPGGSLRLSCAASGFTFSGYAMSWVRQAPGKGLEWVSSISGSGGGSTYYADSVKGRFTISRDNSKNT
80  LYLQMNSLRAEDTALYYCAKPPGRQEYYGSSIYYFPLGNWGQGTLVTVSSASTKGPKLEEGEFSEARVQSALTQPASVSV
160 APGQTARITCGGNNIGSKSVHWYQQKPGQAPVLVVYDDSDRPSGIPERFSGSNSGNTATLTISRVEAGDEADYYCQVWDS
240 SSDLVVFGGGTKLTVLGQPKAAPSVTLFPPSSAAAGGGGSGGGGSRTVAAPSVFIFPPSDEQLKSGTASVVCLLNNFYP
320 REAKVQWKVDNALQSGNSQESVTEQDSKDSTYSLSSTLTLSKADYEKHKVYACEVTHQGLSSPVTKSFNRGECGGGGSGG
400 GGSGGGGSGGGGSGGGGSTSQVQLQQSGAELARPGASVKMSCKASGYTFTRYTMHWVKQRPGQGLEWIGYINPSRGYTNY
480 NQKFKDKATLTTDKSSSTAYMQLSSLTSEDSAVYYCARYYDDHYCLDYWGQGTTLTVSSGGGGSGGGGSGGGGSQIVLTQ
560 SPAIMSASPGEKVTMTCSASSSVSYMNWYQQKSGTSPKRWIYDTSKLASGVPAHFRGSGSGTSYSLTISGMEAEDAATYY
640 CQQWSSNPFTFGSGTKLEIN
```

HC scFv C8	: [1 : 138]
Yol-linker	: [139 : 147]
LC scFv C8	: [148 : 276]
2x(G4S) Linker	: [277 : 286]
LC kappa constant	: [287 : 393]
Cys393: disulfide bond with HC	: [393]
4x(G4S) Linker	: [394 : 418]
TS: adaptor sequence SpeI	: [419 : 420]
HC scFv OKT3	: [421 : 537]
SS: adaptor sequence XbaI^SpeI	: [538 : 539]
3x(G4S) Linker	: [540 : 554]
LC scFv OKT3	: [555 : 660]

Figure 26: Amino acid sequences of OKTriMAb. Amino acid sequence of **(a)** the TriMAb C8-HC-scFvOKT3 peptide and **(b)** the TriMAb C8-LC-scFv9.3 peptide. Adaptor sequences are traces of the cloning procedure. AS: restriction recognition site of NheI; TS: restriction recognition site of SpeI; SR: restriction recognition site of XbaI; SS: ligation site of XbaI- and SpeI-digested DNA fragments.

2.4.2 Expression studies and purification of TriMAb

2.4.2.1 TsAbs are expressed successfully and bind HBVenv specifically

TsAbs were expressed using a two-vector system, with each chain being encoded on a separate ORF. As producer cell lines served HEK 293T and CHO K1 cells. To increase production efficiency, stable producer cell lines were generated by combination of antibiotic selection and single cell dilution. Supernatant was harvested every 3 to 4 days, sterile-filtered, and used for functional assays. Binding of tsAbs to HBVenv was analyzed by HBsAg ELISA. Here, supernatant of producer cell lines resulted in a strong ELISA signal (Fig. 27b). Comparison of the cell lines revealed a higher yield in HEK293T cells for both constructs (Fig. 27c). To provide the highest possible antibody concentration, further experiments were performed with supernatants of HEK 293T producer cell lines.

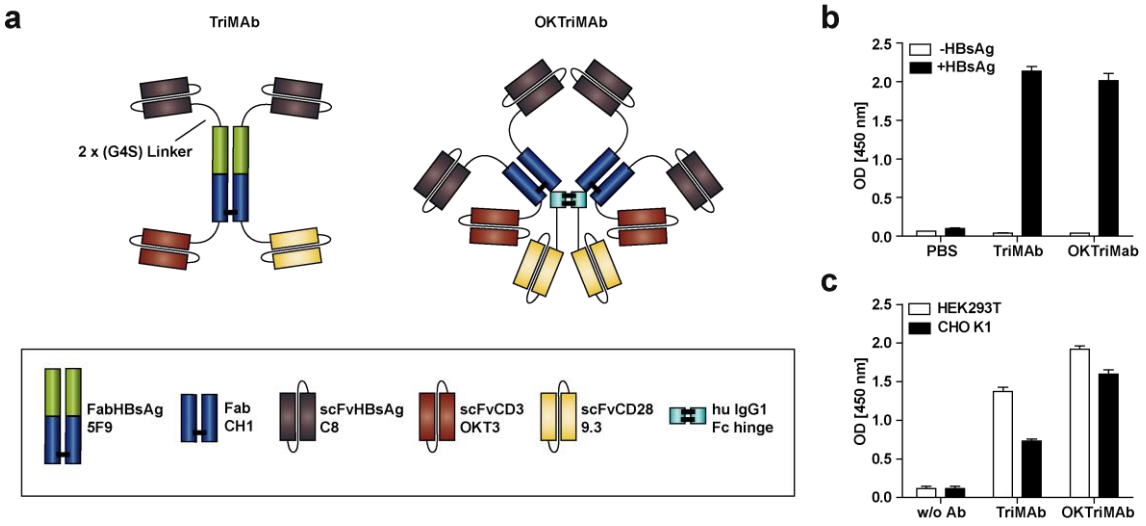

Figure 27: TriMAb and OKTriMAb are expressed and bind HBsAg. (a) Schematic representation of trispecific constructs. **(b)** Binding of TriMAb and OKTriMAb to HBsAg determined by ELISA. TriMAb and OKTriMAb in the supernatant of producer cell lines (HEK 293T) interacting with human serum derived HBsAg was detected using polyclonal goat anti-human IgG HRP antibodies. Wells supplied with PBS or without HBsAg served as controls. **(c)** Comparative ELISA analysis of antibody-containing supernatants of HEK293T and CHO K1 producer cell lines. TsAbs interacting with human serum derived HBsAg were detected using polyclonal goat anti-human IgG HRP antibodies. Supernatants of the respective non-transfected producer cells (w/o Ab) served as controls. Data are presented as mean value ± SD of triplicate analyses (*n* = 3).

2.4.2.2 The TriMAb-single chains are hardly secreted

Since TriMAb was selected as the lead candidate for further studies it was subjected to more detailed expression studies. The HBsAg ELISA with polyclonal goat anti human antibodies (GαH) gives no information about the integrity or paring of the TriMAb heterodimer and thus the construct was further modified. To allow specific detection of the separate chains, the HC was c-terminally equipped with a 10x His Tag and the LC with a Strep Tag II and the construct was codon-optimized for expression in CHO cells. The two separate chains where furthermore sub-cloned into a single ORF, with the two chains being separated by P2A site. Next, CHO cells were transfected with either the HC

only, the LC only, co-transfected with HC/LC, or transfected with the single ORF HC/LC construct, using a total of 5 µg plasmid DNA for all samples. After antibiotic selection for 4 weeks, supernatants were collected and employed in an HBsAg ELISA and detected with polyclonal goat anti human antibodies, or the tag-specific antibodies. Detection with GαH showed a 3-fold higher signal for the co-transfection sample, when compared to the single ORF construct. The signal for single transfection with the LC was ~20% lower than single ORF and the HC was hardly detected at all. Detection with the anti-His Tag antibody showed a 10-fold higher signal for the co-transfected samples. Here, single transfection with LC did not result in a signal and the HC was also not detectable. Detection with the Strep Tag II-specific antibody showed a similar pattern as GαH (Fig. 28a). This indicated that the individual chains are successfully detected by the tag-specific antibodies. Furthermore, TriMAb production is most efficient, when HC and LC are co-transfected on separate ORFs, while single chains are less secreted. Since the HC was undetectable upon single transfection, His Tag-pulled constructs should predominantly exist as dimers. Therefore, TriMAb purification was performed with IMAC.

2.4.2.3 Expression in serum-free medium increases the efficacy of IMAC

IMAC was performed with Protino Ni-NTA Agarose and gravity flow columns. A TriMAb CHO producer cell line, based on the co-transfection expression system, was cultured with or without 10% fetal calf serum (FCS) for 5 days and supernatants were employed in the purification procedure. The binding step was either performed for 4 hours or overnight (O/N). In total, 4 fractions were collected and analyzed by HBsAg ELISA. Samples without FCS had the highest antibody concentration in fraction 1, while samples with 10% FCS showed the peak in fraction 2 (Fig. 28b). The respective fractions were pooled, concentrated with centrifugal filters, and dialyzed against PBS, followed by Coomassie staining and WB analysis under reducing and non-reducing conditions. Under reducing conditions, samples without FCS showed a distinct band at 80 kD, referring to the TriMAb heavy and light chains, which are comparable in size (Fig. 28c). O/N incubation resulted in a higher yield than incubation for 4 hours. The purity in 0% FCS samples was above 90%. In contrast, preparations with 10% FCS contained various impurities and a strongly reduced signal at 80 kD. Under non-reducing conditions, TriMAb migrated with an apparent molecular size above 250 kD. WB analysis with polyclonal goat anti human IgG antibodies revealed bands with the same migration pattern (Fig. 28d). Proteins with incorrect size did not result in a positive signal. The sample without FCS and O/N incubation was further analyzed with His Tag- and Strep Tag II-specific antibodies. Both detection antibodies resulted in a specific signal with the same pattern as Coomassie staining and GαH analysis (Fig. 28e). These data indicated that cultivation in serum-free medium can enhance the purity in IMAC preparation. The yield can be further increased by a prolonged incubation time with Ni^{2+} sepharose resin. Moreover, both chains of TriMAb are expressed and migrate with the same molecular size under reducing and non-reducing conditions, respectively.

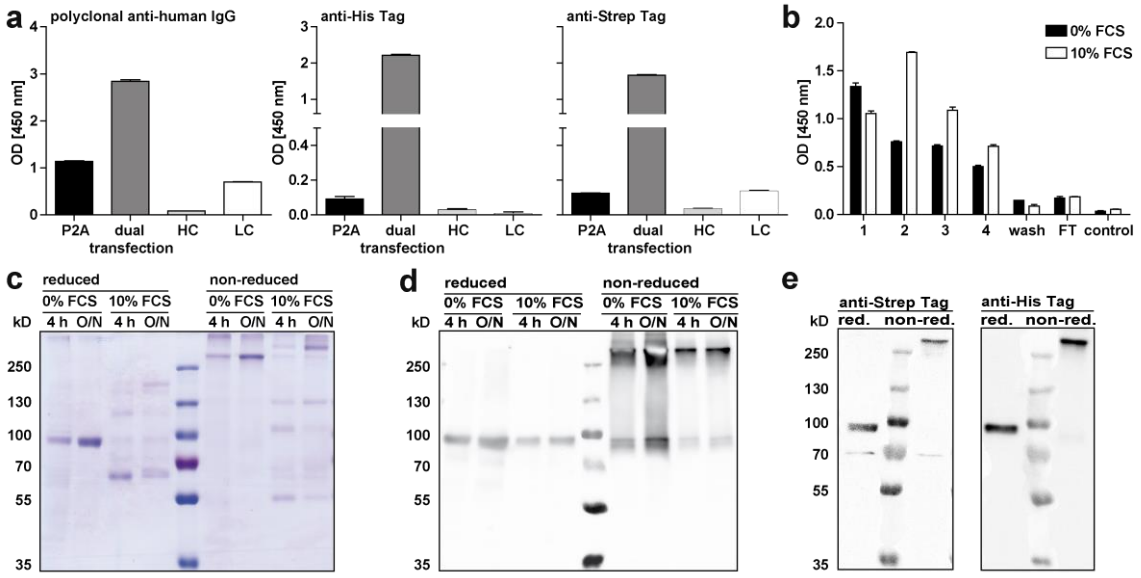

Figure 28: TriMAb is successfully purified with IMAC. (a) CHO cells that were either transfected with the HC only, the LC only, co-transfected with HC/LC, or transfected with the single ORF HC/LC construct and selected with antibiotics for 4 weeks. Superntants were analyzed by ELISA employing HBsAg-coated plates and constructs were detected with polyclonal anti-human IgG (left), anti-10x His Tag (middle), or anti-Strep Tag II (right) detection antibodies. (b) ELISA with HBsAg-coated plates to analyze the TriMAb concentration in IMAC fractions (diluted 1:100) after expression in cultures with 0 or 10% FCS. Detection was performed with polyclonal anti-human IgG antibodies. (c) Coomassie staining of pooled IMAC fractions (0 and 10% FCS) after incubation with Ni^{2+} sepharose resin for 4 hours or overnight. 15 µl of samples were loaded and separated by PAGE (8%) under reducing and non-reducing conditions. (d) WB analysis of samples described in (c). 15 µl of the respective sample were separated by an 8% polyacrylamide SDS-gel and transferred to a polyvinylidene fluoride membrane. Detection was performed with polyclonal goat anti human IgG antibodies. **(e)** WB of purified TriMAb samples (0% FCS, O/N). 100 ng of protein were separated by an 8% polyacrylamide SDS-gel and transferred to a polyvinylidene fluoride membrane. Detection was performed with anti-Strep Tag II (left) and with anti-10x His Tag detection antibodies. (a, b) Data are presented as mean values ± SD of triplicate analyses (*n* = 3).

2.4.3 Comparison of tri- and bispecific antibodies

2.4.3.1 Treatment with tsAbs activates T cells stronger than FabMAbs in combination

To compare the redirection of T cells through TriMAb and OKTriMAb and the FabMAbs in combination, experiments were first performed with cell culture supernatants, since purified antibodies were not yet available. PBMC were cultured on HBsAg-coated plates in the presence of antibody containing supernatant for 72 hours. Supernatant of non-transfected HEK 293T cells (w/o Ab) and wells without HBsAg (-HBsAg) served as controls. As readout for T-cell activation, IFNγ release, grzB expression, and LAMP-1 translocation were evaluated. Administration of tsAbs induced a two-fold (OKTriMAb) and three-fold (TriMAb) higher secretion of IFNγ than the combination of FabMAbs. In control samples, no IFNγ secretion was observed (Fig. 29a).

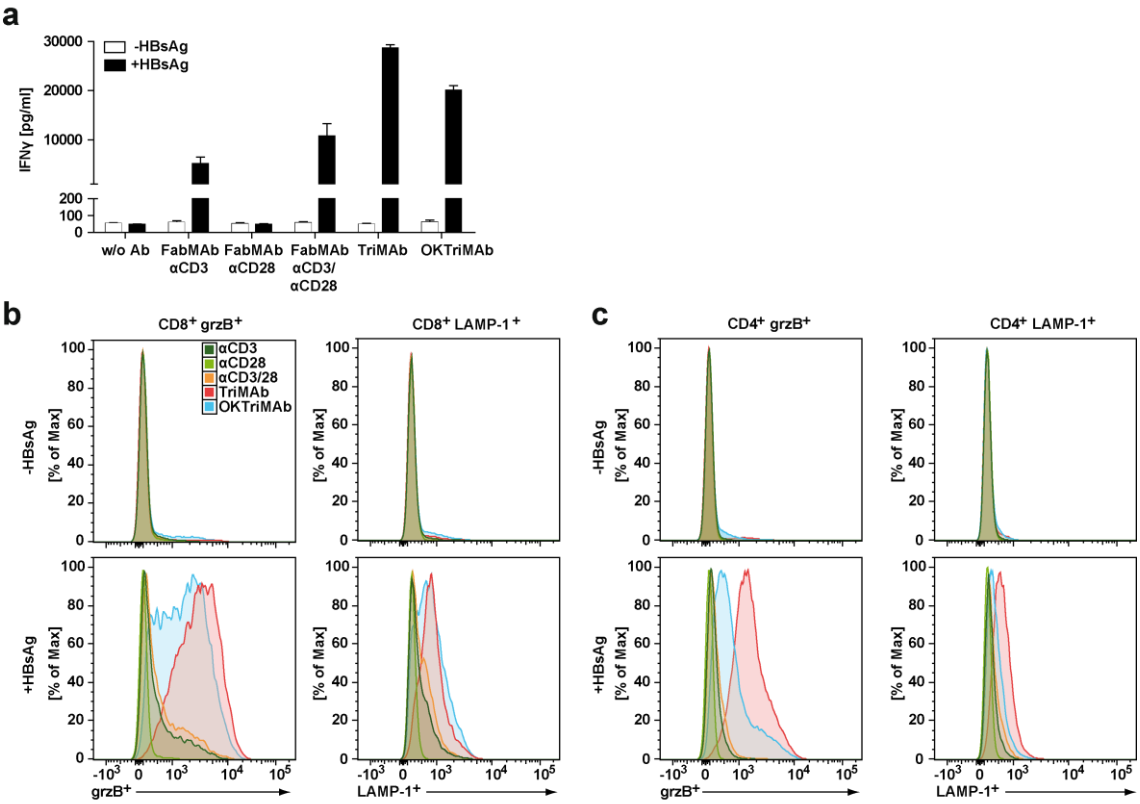

Figure 29: Treatment with tsAbs activates T cell to secrete IFNγ and induces grzB expression and LAMP-1 translocation. (a) IFNγ concentration in the supernatant of PBMC cultured on control plates (-HBsAg) or HBsAg-coated plates (+HBsAg) that were treated with supernatant of producer cell lines (HEK 293T) of indicated bi- and trispecific constructs after 72 hours. The cytokine concentration in the supernatant was determined by ELISA. Samples treated with supernatant from non-transfected HEK 293T cells (w/o Ab), served as controls. Supernatants of FabMAbs in combination were mixed in a 1:1 ratio. Data are presented as mean values ± SD of triplicate co-cultures (*n* = 3). **(b, c)** Histograms of **(b)** $CD8^+$ and **(b)** $CD4^+$ T cells stained for grzB-expression and LAMP-1 translocation after 72-hour co-culture with control plates (top) or with HBsAg-coated plates (bottom) in the presence of supernatant of producer cell lines of indicated bi- and trispecific constructs.

Analysis of grzB and LAMP-1 showed increased upregulation of both markers on $CD8^+$ and $CD4^+$ T cells in tsAbs treated samples (Fig. 29b, c). While the FabMAb combination led to ~50% of grzB and LAMP-1 positive $CD8^+$ T cells, both tsAbs induced nearly 100% (Fig. 30a). The percentage of $grzB^+$ $CD4^+$ T cells was comparable to $CD8^+$ T cells, while $LAMP\text{-}1^+$ cells were reduced by about 50% (Fig. 30b). These data was also published in the patent WO2016146702A1 (Protzer et al., 2016). MFI analysis showed a 2-fold (OKTriMAb) and 4-fold (TriMAb) higher grzB expression in tsAbs-treated $CD8^+$ T cells, compared to the combination of FabMAbs. The MFI pattern of LAMP-1 correlated with the percentage of positive cells (Fig. 30c). $CD4^+$ T cells showed lower MFI for LAMP-1 than $CD8^+$ T cells (Fig. 30d). This led to the conclusion that treatment with the trispecific antibodies can redirect and activate T cells in the presence of HBsAg-coated plates. Moreover, the redirection capacity of the trispecific constructs is comparable to the combination of FabMAbαCD3 and FabMAbαCD28. However, these results have to be taken with caution, since the antibody concentration in the supernatant was not quantified and antibodies were not adjusted to equimolar concentrations.

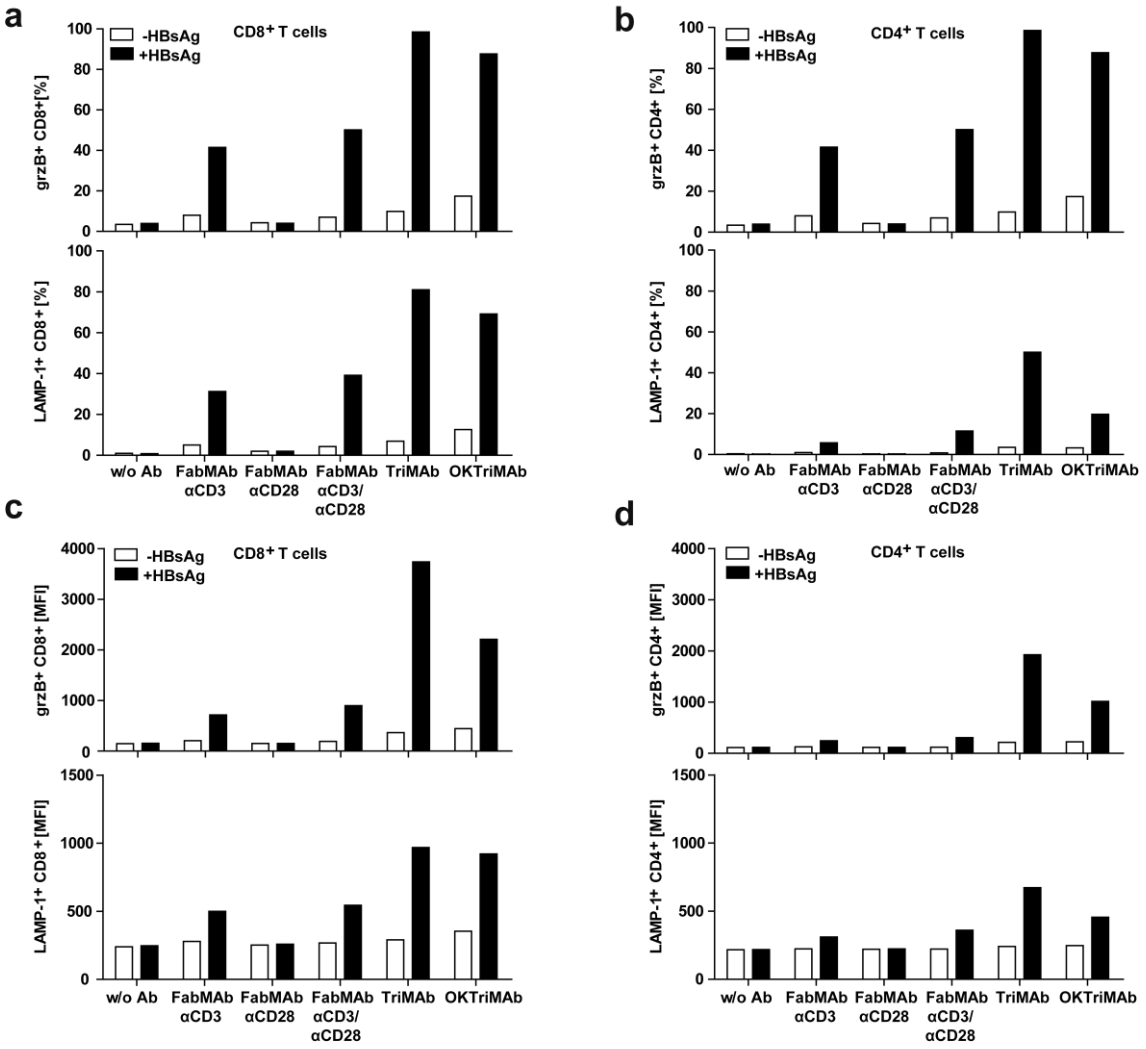

Figure 30: Redirection capacity of tsAbs is comparable to the combination of FabMAbs. **(a, b)** Percentage of grzB- (top) and LAMP-1-expressing (bottom) **(a)** $CD8^+$ or **(b)** $CD4^+$ T cells after 72-hour culture on control plates (-HBsAg) or HBsAg-coated plates (+HBsAg) treated with supernatant of producer cell lines (HEK 293T) of indicated bi- and trispecific constructs. Samples treated with supernatant from non-transfected HEK 293T cells (w/o Ab) served as controls. **(c, d)** MFI of grzB- (top) and LAMP-1 (bottom) expressing **(c)** $CD8^+$ or **(d)** $CD4^+$ T-cell populations after 72-hour co-culture on HBsAg-coated plates treated with supernatant of producer cell lines (HEK 293T) of indicated bi- and trispecific constructs. Samples treated with supernatant from non-transfected HEK 293T cells (w/o Ab) served as controls. Data are presented as mean values of triplicate co-cultures (n = 3).

2.4.3.2 Treatment with TriMAb induces target cell elimination without further co-stimulation

To study, if tsAbs can activate T cells to establish a cytotoxic immune response against HBVenv-expressing cells, Huh7S cells and PBMC were cultivated in the presence of TriMAb- and OKTriMAb-containing supernatant for 128 hours and target cell viability was measured in real-time employing an xCELLigence RTCA. As marker for T-cell activation, IFNγ levels in the culture were determined at the end of the experiment. Parental Huh7 cells and supernatant of non-transfected HEK 293 cells (w/o Ab) served as control. To increase the antibody availability in the culture, supernatants were concentrated using high recovery centrifugal filters and co-cultures were supplied with 0.5x, 1x, 5x and 10x

concentrated supernatant. Treatment with TriMAb induced elimination of Huh7S cells at the concentrations 5x and 10x (Fig. 31a) and the cytotoxic activity was accompanied by secretion of IFNγ (Fig. 31b). Huh7 control cells showed loss of cell viability at a concentration of 10x, yet in these cultures IFNγ release was not observed.

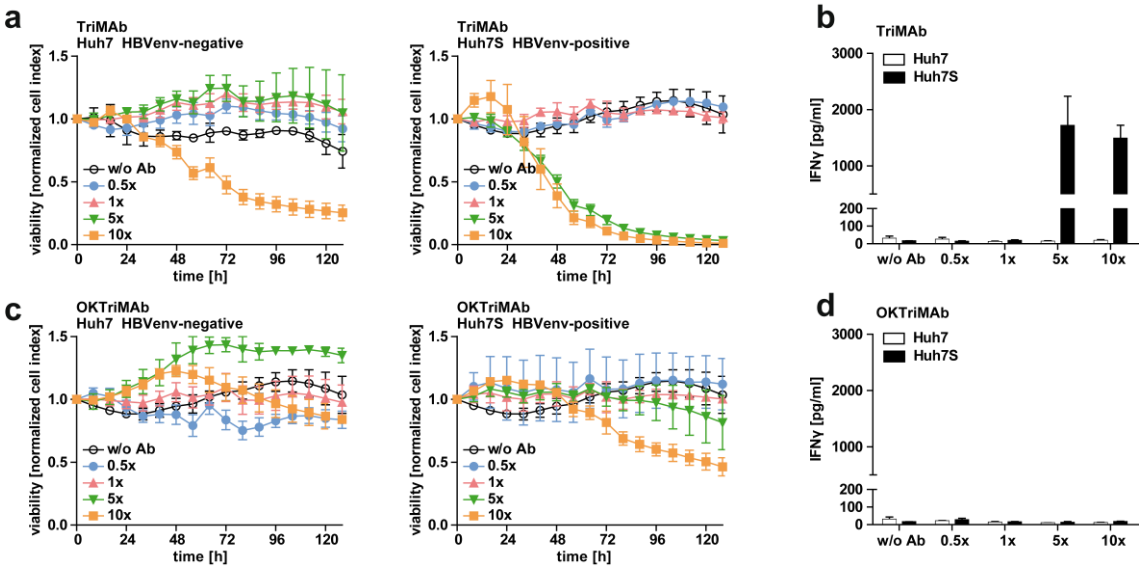

Figure 31: TriMAb induces elimination of HBVenv-expressing cells without further co-stimulation. Target cell viability was determined over 128 hours in real-time employing an xCELLigence RTCA. **(a)** Cell viability of HBVenv-negative Huh7 cells (left) and HBVenv-positive Huh7S cells (right) in co-cultures with PBMC and supernatant of TriMAb producer cell lines (HEK 293T) at indicated concentration. Samples treated with supernatant of non-transfected HEK 293T cells (w/o Ab) served as controls. **(b)** IFNγ concentration in the supernatant of co-cultures descripted in (a) after 128 hours determined by ELISA. **(c)** Cell viability of HBVenv-negative Huh7 cells (left) and HBVenv-positive Huh7S cells (right) in co-cultures with PBMC and supernatant of OKTriMAb producer cell lines (HEK 293T) at indicated concentration. Samples treated with supernatant of non-transfected HEK 293T cells (w/o Ab) served as controls. **(d)** IFNγ concentration in the supernatant of co-cultures described in (c) after 128 hours determined by ELISA. Data are presented as mean values ± SD of triplicate co-cultures (*n* = 3).

These data was also published in the patent WO2016146702A1 (Protzer et al., 2016). OKTriMAb treatment led to a loss of target cell viability at the concentration 10x (Fig. 31c). Kinetics were clearly reduced compared to TriMAb and IFNγ release was not observed (Fig. 31d). Huh7 control cells showed no reduction in viability upon OKTriMAb treatment. These data indicated that TriMAb can successfully redirect T cells towards HBVenv-expressing target cells with similar kinetics as the combination of bsAbs illustrated in 2.2.3.3, when the concentration “1x supernatant” is taken into account. These results have to be taken with caution, since the TriMAb concentration in the supernatant was not quantified. OKTriMAb failed to induce efficient target cell elimination in this setting, and thus, TriMAb was used as lead candidate for further investigation.

2.4.3.3 *Administration of IL-12 and hyper-IL6 fails to increase TriMAb-mediated target cell elimination*

In the next step, it was investigated, if TriMAb-mediated T-cell activation and target cell elimination can be further enhanced by co-application of immune-stimulatory cytokines. Therefore, co-cultures of Huh7S cells, PBMC and TriMAb-containing supernatant, were supplied with IL-12 or hyper-IL-6, followed by evaluation of cell viability. As marker for T-cell activation, IFNγ levels in the culture were evaluated at the end of the experiment. Parental Huh7 cells and supernatant of non-transfected HEK 293T cells (w/o Ab) served as control. Neither IL-12, nor hyper IL-6 had an influence on the kinetics of target cell elimination (Fig. 32a, c). However, IL-12 treatment led to a profound increase in IFNγ release, while hyper IL-6 did not (Fig. 32b, d).

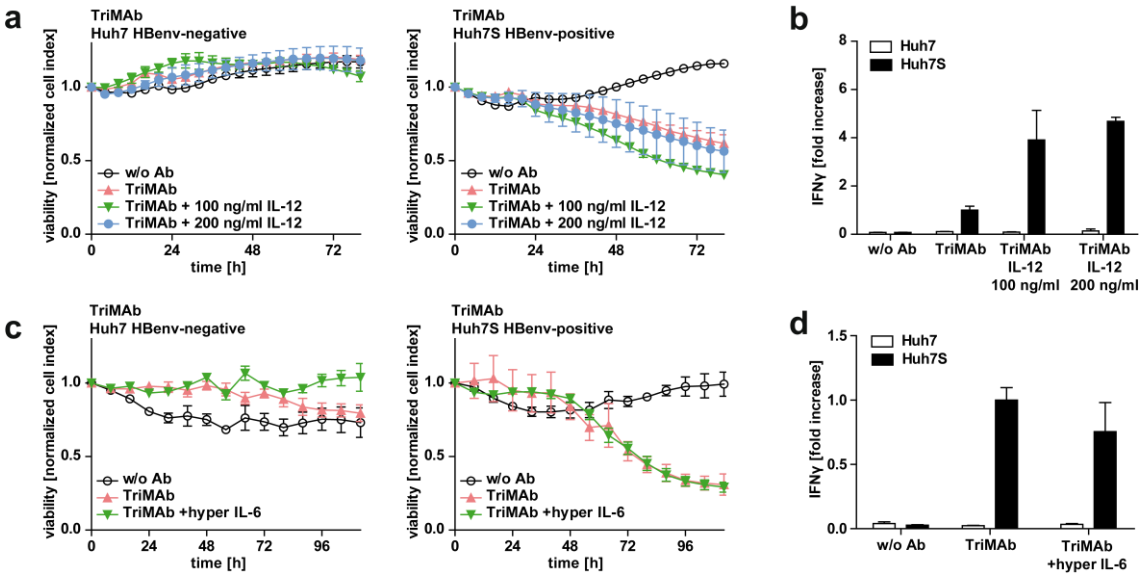

Figure 32: Administration of IL-12 and hyper-IL6 fails to increase TriMAb-mediated target cell elimination. (a) Cell viability of HBVenv-negative Huh7 cells (left) or HBVenv-positive Huh7S cells (right) in co-cultures with PBMC, supernatant of TriMAb producer cell lines (HEK 293T), and the indicated concentration of IL-12. Samples treated with supernatant of non-transfected HEK 293T cells (w/o Ab) served as controls. Target cell viability was determined over 80 hours in real-time employing an xCELLigence RTCA. **(b)** Fold-increase of IFNγ in the supernatant of IL-12 treated co-cultures described in (a). Values were normalized to the IFNγ concentration in TriMAb-treated cultures. **(c)** Cell viability of HBVenv-negative Huh7 cells (left) and HBVenv-positive Huh7S cells (right) in co-cultures with PBMC, supernatant of TriMAb producer cell lines (HEK 293T), and 20 ng/ml hyper-IL6. Samples treated with supernatant of non-transfected HEK 293T cells (w/o Ab) served as controls. Target cell viability was determined over 112 hours in real-time employing an xCELLigence RTCA. **(d)** Fold-increase of IFNγ in the supernatant of hyper IL-6 treated co-cultures described in (c). Values were normalized to the concentration in TriMAb-treated cultures. Data are presented as mean values ± SD of triplicate co-cultures (*n* = 3).

2.4.3.4 *Treatment with TriMAb induces trifunctional T cells*

To evaluate the sensitivity of TriMAb-mediated T-cell activation, co-cultures were performed with decreasing levels of immobilized HBsAg. PBMC were cultured on 5, 1, and 0.2 µg/ml of immobilized HBsAg for 72 hours and supplied with TriMAb or FabMAbs in combination. T-cell activation was determined by ICS for IFNγ, IL-2, and TNFα as well

as proliferation. Antibody-containing supernatants were applied undiluted, 1:10, and 1:100. Supernatant of non-transfected HEK 293 cells (w/o Ab) served as control.

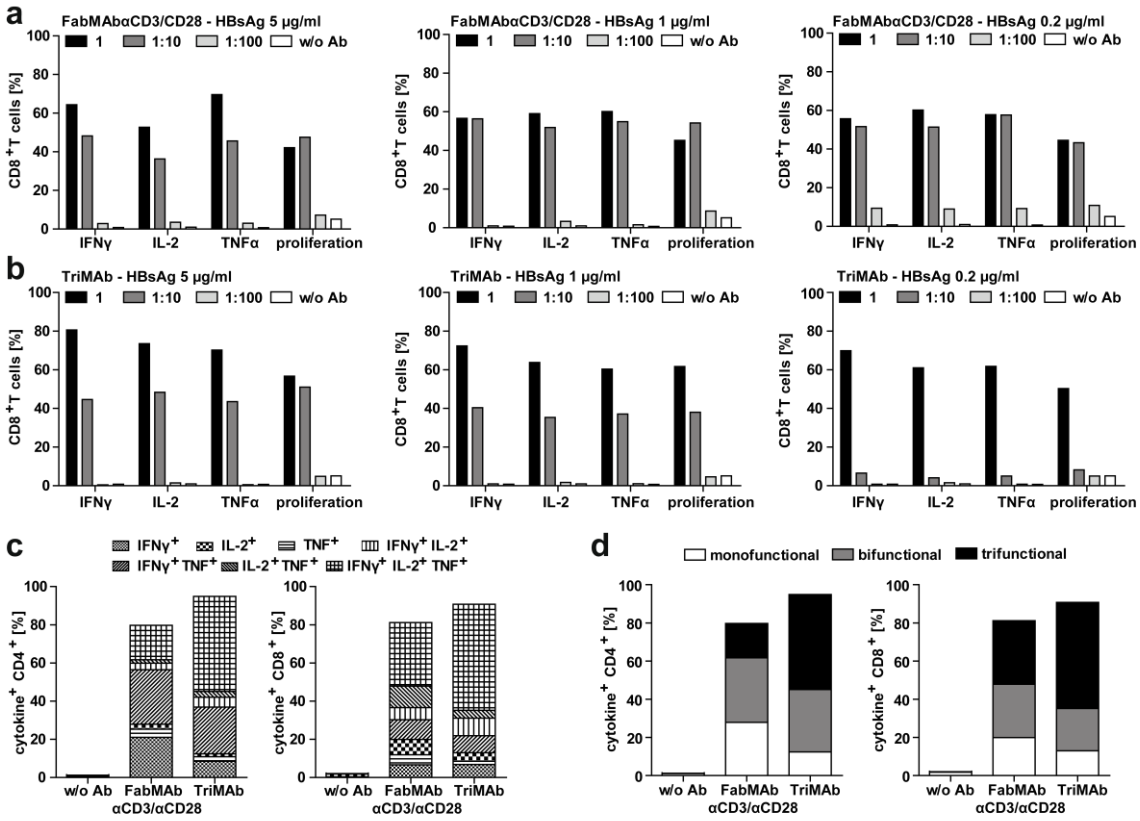

Figure 33: Treatment with TriMAb induces trifunctional T cells. (a, b) Percentage of IFNγ$^+$, IL-2$^+$, TNFα$^+$, or proliferating CD8$^+$ T cells after co-culture with 5 µg/ml (left), 1 µg/ml (middle), or 0.2 µg/ml of immobilized HBsAg in the treated with **(a)** supernatant of FabMAbαCD3 and FabMAbαCD28 producer cell lines (HEK 293T) in a 1:1 combination, and **(b)** supernatant of TriMAb producer cell lines (HEK 293T), after 72 hours of co-culture determined by ICS. Samples treated with supernatant of non-transfected HEK 293T cells (w/o Ab) served as controls. **(c, d)** Percentage of mono-, bi, and trifunctional CD8$^+$ T cells after co-culture with 5 µg/ml of immobilized HBsAg treated with supernatant of FabMAbαCD3 and FabMAbαCD28 producer cell lines (HEK 293T) in a 1:1 combination and **(b)** supernatant of TriMAb producer cell lines (HEK 293T) after 72 hours of co-culture determined by ICS. The percentage of polyfunctional T cells was determined by the use of Boolean combination gates (FlowJo). Data are presented as mean values of triplicate co-cultures (*n* = 3).

The percentage of activated T cells correlated with the antibody concentration and the quantity of HBsAg. When producer cell line derived supernatants were applied undiluted and with a 1:10 dilution, treatment with TriMAb or with the FabMAbs in combination showed a potent induction of cytokine expression, which was not observed when the 1:100 dilution was employed. At 5 µg/ml HBsAg and treatment with undiluted supernatant, FabMAbs in combination induced ~60% IFNγ$^+$, ~50% IL-2$^+$ and ~70% TNFα$^+$ CD8$^+$ T cells, while TriMAb-treated samples showed nearly 80% cytokine-positive T cells. The dilution had a stronger effect on TriMAb-mediated T-cell activation, with a reduction by ~50%, when the supernatant was diluted 1:10, while FabMAbs showed only a ~25% reduction. The titration of HBsAg had almost no effect on the redirection capacity

of FabMAbs, which performed almost equally well at all concentrations. In contrast, TriMAb failed to induce T-cell activation at 0.2 µg/ml HBsAg, when the supernatant was diluted 1:10 (Fig. 33a, b). To further characterize the state of activation, the amount of T cells that express a combination of IFNγ, IL-2 and TNFα was determined by use of Boolean combination gates in FlowJo. At 5 µg/ml HBsAg and treatment with undiluted supernatant, the FabMAb combination resulted in 20% mono-, 28% bi- and 33% trifunctional $CD8^+$ T cells, while TriMAb induced 13%, 22% and 56%, respectively. $CD4^+$ T cells showed similar patterns of polyfunctionality (Fig. 33c, d). These data suggest that TriMAb performs better at high antigen concentration, but is less sensitive when HBsAg levels are low. These results have to be taken with caution, since antibodies were not adjusted to equimolar concentrations.

2.4.3.5 Treatment with TriMAb elicits an antiviral effect

The TriMAb-mediated antiviral effect was evaluated in co-cultures with infected HepG2 NTCP cells, as described for bispecific antibodies in 2.3.3 (Fig. 34a). To study the correlation between the level of infection and the efficacy of T-cell redirection, HepG2 NTCP cells were infected at an MOI of 5, 50 and 500 HBV virions/cell. IFNγ release correlated positively with the MOI and was detectable at day 3, 6 and 10, when HepG2 NTCP cells were infected with an MOI of 50 HBV virions/cell or higher. IFNγ secretion was always dependent on the presence of HBV and TriMAb (Fig. 34b). To quantify the antiviral effect, HBeAg, intracellular HBV-DNA and cccDNA were measured 10 days after the start of co-culture. At an MOI of 500 HBV virions/cell, HBeAg, and intracellular HBV-DNA levels showed 60% reduction, while cccDNA levels where reduced by 20%. The antiviral effect correlated with the MOI, leading to smaller effects at lower MOIs (Fig. 34c, d). These data led to the conclusion that TriMAb can redirect T cells towards HBV-infected HepG2 NTCP cells, resulting in T-cell activation and reduction of viral parameters, without further co-stimulation.

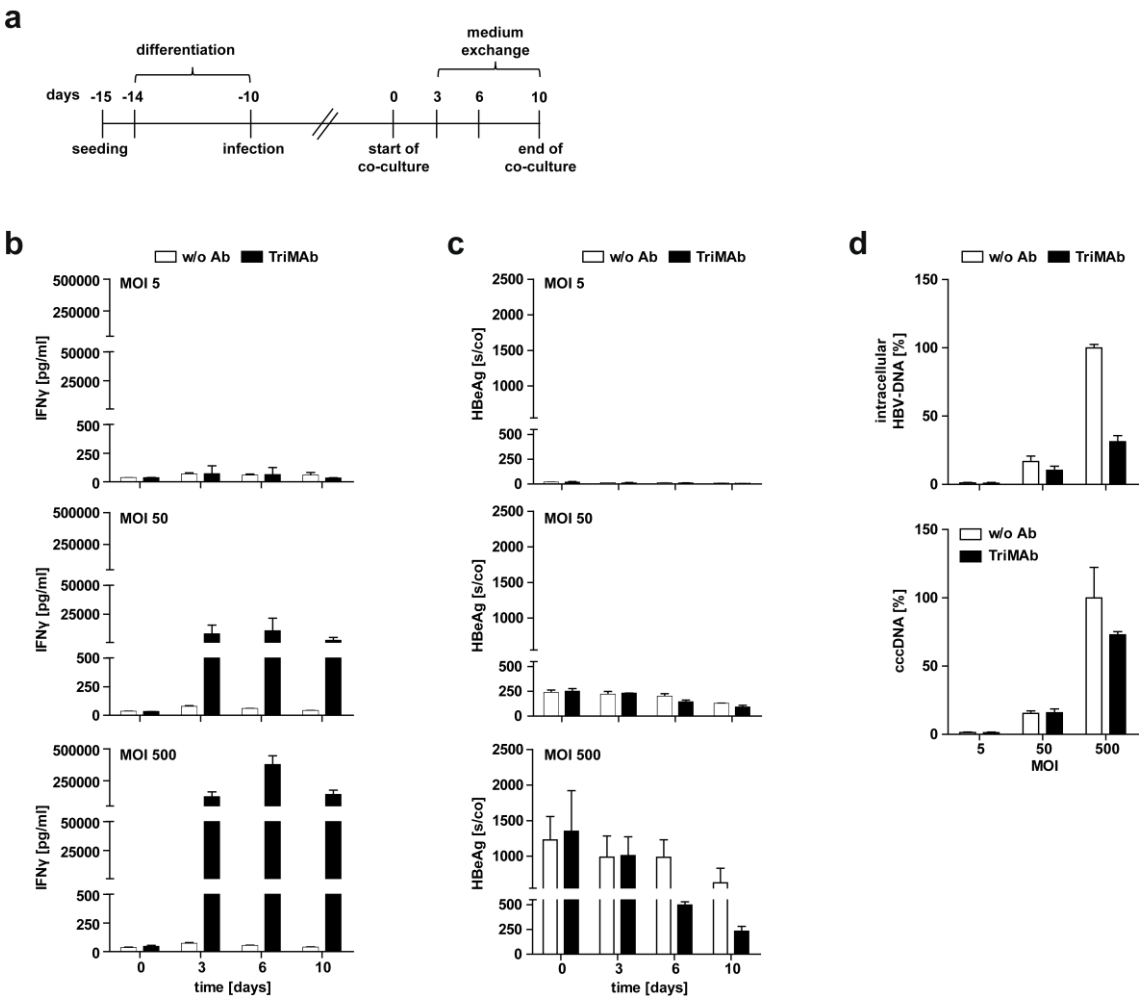

Figure 34: Treatment with TriMAb elicits an antiviral effect. (a) Schematic representation of the co-culture setup employing infected HepG2 NTCP cells (MOI of 5, 50 and 500 HBV virions/cell) and supernatant of TriMAb producer cell lines in the 24-well format. **(b)** Concentration of IFNγ in the supernatant of the co-culture of infected HepG2 NTCP cells and PBMC treated with supernatant of TriMAb producer cell lines (HEK 293T) at indicated time points after start of co-culture. The IFNγ concentration was determined by ELISA. **(c)** HBeAg levels in the supernatant of the co-culture of infected HepG2 NTCP cells and PBMC treated with supernatant of TriMAb producer cell lines (HEK 293T) at indicated time points after start of co-culture. HBeAg concentration was determined by AxSYM measurement. **(d)** Levels of intracellular HBV-DNA (top) and cccDNA (bottom) in co-cultures of infected HepG2 NTCP and PBMC after 10-day treatment with supernatant of TriMAb producer cell lines (HEK 293T) determined by qPCR. Data are presented in percent relative to w/o Ab and MOI 500 HBV virions/cell. **(b-c)** Data are presented as mean values ± SD of triplicate co-cultures (*n* = 3).

2.4.3.6 Purified TriMAb activates T cells to form clusters, secrete cytokines and eliminate HBVenv-expressing target cells

Finally, activation of T cells through purified TriMAb was assessed. Therefore, PBMC were cultured on HBsAg-coated plates for 72 hours supplied with 3 nM of TriMAb or FabMAbs, singly and in combination. Samples without antibodies (w/o Ab) and wells without HBsAg (-HBsAg) served as controls. As readout for T-cell activation, changes in cell morphology as well as IFNγ and IL-2 release were evaluated. Microscopic analysis showed distinct cluster formation of PBMC within the first 12 hours in TriMAb treated wells that were comparable to the combination of FabMAbs. Cells in control samples

showed no change in morphology (Fig. 35a). IFNγ and IL-2 levels in TriMAb treated cultures were also comparable to the combination of FabMAbs. In control samples, no cytokine secretion was observed (Fig. 35b, c).

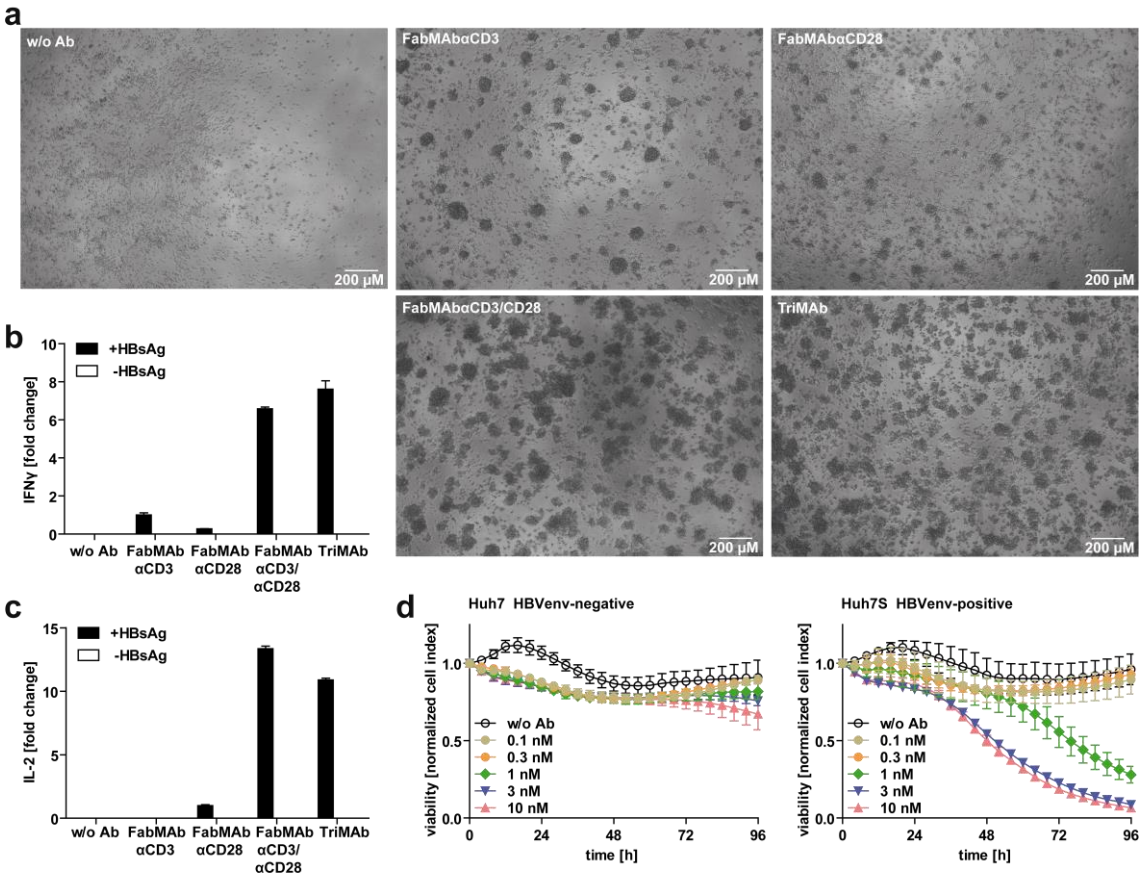

Figure 35: Purified TriMAb activates T cells to induce cluster formation, cytokine release and target cell elimination. (a) Microscopic analysis of cell morphology of PBMC cultured for 72 hours on HBsAg-coated plates supplied with 3 nM of TriMAb or FabMAb, singly or in combination (1:1 ratio). **(b, c)** Fold-increase of **(b)** IFNγ and **c)** IL-2 in the supernatant PBMC cultured on control plates (-HBsAg) or HBsAg-coated plates (+HBsAg) supplied with 3 nM of TriMAb or FabMAb, singly or in combination (1:1 ratio) after 72 hours. Values were normalized to FabMAbαCD3 (IFNγ) or FabMAbαCD28 (IL-2). **(d)** Target cell viability was determined over 96 hours in real-time employing an xCELLigence RTCA. Cell viability of HBVenv-negative Huh7 cells (left) or HBVenv-positive Huh7S cells (right) in co-culture with PBMC supplied with increasing doses of purified TriMAb. Samples without TriMAb (w/o Ab) served as controls. **(b-d)** Data are presented as mean values ± SD of triplicate co-cultures (*n* = 3).

To analyze the efficacy of target cell elimination, Huh7S cells and PBMC were co-cultured with 0.1, 0.316, 1, 3.162, and 10 nM of purified TriMAb for 96 hours and target cell viability was measured in real-time employing an xCELLigence RTCA. TriMAb induced target cell elimination when applied at a concentration of 1 nM or higher. Rate and kinetics of cell viability loss correlated positively with the antibody concentration. The maximum was reached at 3 nM, with around 50% of target cells being eliminated in the first 48 hours of co-culture (Fig. 35d). These data demonstrated that purified TriMAb is functional and induces T-cell activation with similar potency as the combination of FabMAbαCD3 and FabMAbαCD28.

3 Discussion

Current treatment options for chronic hepatitis B efficiently suppress viral replication, but rarely cure the disease. Consequently, further efforts that intent a curative therapy are in need. The underlying thesis demonstrates the immunotherapeutic retargeting of endogenous T cells employing bi- and trispecific antibodies. The application of these constructs facilitated a robust T-cell redirection towards HBVenv-expressing target cells and might provide a feasible and promising approach for the treatment of chronic hepatitis B and HBV-associated HCC, as discussed in the following.

3.1 Production and stability of bi- and trispecific antibodies

3.1.1 Bispecific antibodies

After successful design and cloning, the bispecific antibodies were expressed in HEK 293 T cells and bsAbs-containing supernatants were employed in functional assays to determine their binding and redirection capacity. Experiments with cell culture supernatants were useful for basic studies on expression and functionality as well as screening of producer cell lines, but did not allow further in depth analysis, since the antibody concentration could not be determined and furthermore varied between constructs, producer cell lines and even batches. Thus, the purification of the constructs was a crucial step within this study, as it firstly proved the producibility of the constructs and secondly allowed the accomplishment of reproducible experiments regarding dose-response correlation, activation kinetics and comparison of the bi- and tetravalent formats.

Since large-scale expression and purification of antibodies is not established in our institute, the production of bispecific antibodies was outsourced to InVivo Biotech services. In contrast to in-house studies, the expression was performed using a two-vector system, with the two chains being encoded on separate plasmids. Even though, usage of a P2A site allows convenient co-expression using a single ORF, it drastically reduces the expression efficiency and is therefore not recommended for large-scale production (Tim Welsink from InVivo Biotech Services, personal communication). We could confirm this during production of TriMAb, where the co-transfection of two plasmids yielded a 3-fold higher expression than usage of a P2A site (Fig. 28a).

Following successful production, the bsAbs were tested for their integrity and stability. In-house quality control of the FabMAb constructs revealed aggregates in the FabMAbαCD3 preparation, yet these could be successfully eliminated by further SEC (Fig. 9a-c). Since no re-aggregation was detected during storage at 4 °C for 12 months (Fig. 9d, Fig. 12b, c), the aggregation process presumably happened during expression or shipment of the preparation. Successful long-term storage at 4 °C demonstrated high stability and underlines the clinical feasibility of FabMAb-meditated HBV immunotherapy.

In contrast, WB analysis illustrated lower stability of BiMAbs, which was displayed by aggregation of BiMAbαCD3 and fragmentation of both constructs (Fig. 12c). Since the Fc domain is considered rather stable, the lower stability of tetravalent BiMAbs likely originated from the presence of the 4 scFv within the homodimer. Substantial differences in the stability of individual scFvs have been described in literature and can influence the quality and yield in the production of these molecules (Reiter et al., 1994, Willuda et al., 1999). Along this line, Fab-fragments have been shown to be more stable than the respective scFv derived from the same antibody, which resulted in an improved neutralization capacity *in vivo* (Quintero-Hernandez et al., 2007).

It is clear that the stability of bi- and trispecific constructs will go hand in hand with the clinical feasibility of this immunotherapeutic approach and therefore will play an important role in the further development of a potential therapy. Consequently, producibility and stability of the bispecific antibodies are as important as half-life and efficacy and need to be considered independently.

3.1.2 TriMAb

In contrast to the experiments with FabMAbs, the HBsAg ELISA and co-cultures with TriMAb-containing supernatants do not allow the assessment of the dimerization status. Successful redirection of effector cells could also be conferred by the individual chains applied in combination. To enable selective detection, the heavy and light chain were equipped with a His Tag or Strep Tag II, respectively. Expression studies showed that the single expression of the individual chains does not result in notable secretion into the supernatant, while co-expression of both chains increased the signal up to 10-fold. Singly expressed LC was detectable to some extent, yet the HC alone was not secreted at all (Fig. 28a). It is known that HC-dimers are retained in the cell as part of a quality control process until they dimerize with the cognate LC (Mains and Sibley, 1983). The retention is mediated by strong affinity to the intracellular chaperone HC-immunoglobulin binding protein (BiP), which interacts with the CH1 domain of the HC in the absence of the LC (Bole et al., 1986, Hendershot et al., 1987). The assembly of heavy and light chain reverses this interaction and thereby allows secretion of correctly folded and assembled Ig molecules from the cell (Hendershot, 1990, Feige et al., 2009). This mechanism has been shown to work also in CHO cells, which are widely used for large scale antibody production (Borth et al., 2005) and also for the TriMAb expression studies in 2.4.2. Along this line, efficient production of heavy-chain-only-antibodies in murine transgenic plasma cells requires deletion of the CH1 domain from the constant regions (Drabek et al., 2016). Even though a recent study demonstrated an LC-independent secretion of HC dimers from CHO-S cells (Stoyle et al., 2017), this was not observed during TriMAb expression in CHO K1 cells. These data indicated that purification based on the HC-associated tag, will result in an increased isolation of assembled dimers, and therefore, IMAC was chosen as the method of choice.

Yield and purity of TriMAb after IMAC was substantially affected by the presence of FCS in the supernatant. Samples with 10% FCS resulted in a notable contamination with

several proteins, while serum-free supernatants did not (Fig. 28c). During IMAC, proteins interact with the Ni^{2+} chelate residues according to the number of accessible histidine residues (Arnold, 1991). Although histidine makes up only 2% of the overall amino acid abundance, certain proteins contain naturally occurring contiguous histidines (Schmitt et al., 1993), which can lead to a co-purification with the His-tagged protein of interest, and thereby contaminate the preparation (Schmitt et al., 1993). Moreover, it is known that albumins, such as bovine serum albumin, contain several cysteines and therefore have a rather strong affinity to Ni^{2+} chelate residues during IMAC. Consequently, future production efforts should only be carried out with serum-free medium.

Another option is the exchange of the c-terminal tags followed by purification with Strep Tag II affinity chromatography, which should be less sensitive to the presence of serum proteins. WB-analyses of the purified sample showed clear expression of heavy and light chain, which migrated with an apparent molecular mass of 80 kD under reducing conditions (Fig. 28d, e) and therefore correspond with the expected size of the construct according to the peptide sequence (Fig. 25a, b). However, the result under non-reducing conditions, which showed a distinct band with a molecular mass greater than 250 kD, varied largely from the expected size of the heterodimer (~160 kD). Reasons for this observation may be a different migration pattern of the reduced protein marker compared to the non-reduced samples. TriMAb contains one intermolecular and eight intramolecular disulfide bonds, which persist under non-reducing conditions and may have substantial influence on the migration pattern in PAGE. Similar characteristics have been observed in FabMAb samples, where the apparent molecular mass of the dimer under non-reducing conditions is greater than expected (Fig. 9a, d). However, it cannot be excluded that the unexpected migration pattern originates in the formation of unspecific aggregates. Therefore, future TriMAb batches need to be analyzed additionally by high pressure liquid chromatography or dynamic light scattering to evaluate the size and integrity of the construct in more detail. After all, purified TriMAb demonstrated functionality by induction of T-cell cluster formation, cytokine secretion and target cell elimination (Fig. 35).

3.2 Successful redirection of T cells towards HBVenv-expressing cells requires co-stimulation with CD28-specific constructs

Unlike other bsAbs that are currently in clinical development (Trivedi et al., 2017), efficient T-cell activation in the setting of bsAb-meditated HBV immunotherapy was not achieved by single treatment with CD3-specific constructs, but required co-stimulation with CD28-specific antibodies. Possible factors that modulate the redirection efficiency are the epitopes recognized on CD3 and HBVenv, as well as antigen density on the target cell.

The CD3-specifific scFv that is used in all our constructs is derived from the well-studied murine antibody OKT3 and interacts exclusively with a conformational epitope on the

CD3ε subunit according to crystal structure analysis (Kjer-Nielsen et al., 2004). BsAbs equipped with scFv OKT3 have been shown to induce efficient target cell elimination without the requirement of further co-stimulation in the field of cancer immunotherapy (Rossi et al., 2014) and infectious diseases (Meng et al., 2018), yet it is not employed in clinical relevant constructs as blinatumomab or catumaxomab. However, also another CD3-binder that was tested in cooperation with Roche Diagnostics GmbH (Penzberg, Germany) required co-stimulation with CD28-specific constructs to induce T-cell activation in this setting (Eva Loffredo-Verde, unpublished). This finding indicates that the single targeting of CD3 will not be sufficient to redirect and activate T cells in the setting of HBV-targeting immunotherapy. Nevertheless, it cannot be excluded that other CD3 binders can improve the redirection efficiency of HBVenv-targeting bi- and trispecific antibodies and may circumvent the requirement of co-stimulation.

The targeting of HBVenv by BiMAbs and FabMAbs is mediated by the binders C8 and 5F9, respectively. TriMAb combines both HBVenv binders (Fig. 27a), however successful binding of the Fab-fragment to HBVenv has not been confirmed in this study. ELISA data and co-cultures with HBsAg clearly demonstrated binding of TriMAb to HBVenv (Fig. 27b, c, Fig. 28a), yet to which extent this binding is mediated by C8 or 5F9 remains to be investigated. Since studies have shown that membrane-proximal epitopes promote redirection efficiency of BiTEs (Bluemel et al., 2010, Li et al., 2017), different HBVenv binders can demonstrate individual activation capacity, independent of their mere affinity. Epitope mapping by alanine-substitution experiments indicated that C8 recognizes a conformational epitope in the “a” determinant of the small envelope protein (Lili Zhao, unpublished). This conformational structure is located in the major hydrophilic region of the S protein and consists of two loops, which are stabilized by disulfide bonds. It is exposed on the surface of viral particles and therefore is especially immunogenic (Roohi et al., 2005, Fields and Knipe, 1990). Studies with different HBsAg mutants indicated that also the antibody 5F9 recognizes an epitope in the “a” determinant (Golsaz-Shirazi et al., 2016). Since the antibody 5F9 can be used to stain denatured HBsAg in WB experiments, its epitope is most likely linear (Lili Zhao, unpublished). Thus, both binders recognize structures in the “a” determinant, but they do not share the same epitope.

To study the influence of different HBV genotypes on the binding characteristics of the bsAbs to HBVenv, an HBsAg genotype panel was screened. The data revealed distinct patterns for both binders, which differed about 5-fold between HBsAg variants with the strongest and weakest binding. 5F9 showed less binding to the genotypes E, F2 and H. The binding of C8 was reduced for D1_ayw2 and D2_ayw2, while D2_ayw3 was recognized well (Fig. 13c). Therefore, the HBV genotype can have an impact on the redirection capacity of bispecific antibodies, which needs to be considered. These findings argue that the isolation and evaluation of additional HBVenv-binders will be beneficial for further development of bsAb-mediated HBV immunotherapy, as they can modulate redirection capacity as well as broaden applicability through an increased HBV subtype coverage.

The level of HBVenv frequency and density on infected hepatocytes has not been documented in literature up to date and might furthermore vary strongly between patients and even single hepatocytes depending on their location within the liver, as well as, the level of infection. The frequency of CD19 that is successfully targeted in a variety of CD3-specific BiTEs against lymphoma has been described to be around $22x10^3$ molecules per cell (Ginaldi et al., 1998). Since the translocation of HBVenv to the cell membrane is believed to be a passive mechanism (see 1.1.1.3), it is expected to be exposed at comparatively low levels that may not be sufficient to induce a potent T-cell response upon single treatment with CD3-specific antibodies. In this study, the limitation was overcome by administration of a co-stimulatory signal through CD28 triggering. Providing co-stimulation through engagement of CD28 did also increase the sensitivity of targeted immunotherapy in other studies, illustrated by enhanced secretion of IFNγ and IL-2, as well as proliferation and expression of CD25 (Hornig et al., 2012).

Moreover, activation of CTLs with CD3ε-targeting BiTEs only, has been shown to induce apoptosis of the activated cells via CD95/first apoptosis signal ligand (FasL) interaction. This effect could be reduced by addition of CD28 co-stimulation, thereby increasing the live span of CTLs and the anti-tumoral effect *in vivo* (Daniel et al., 1998). The benefit of co-stimulation was further demonstrated in a recent study employing trispecific antibodies that target CD38 on myeloma as well as CD3 and CD28. Application of these constructs resulted in potent T-cell activation and suppressed myeloma growth in a humanized mouse model (Wu et al., 2020). These findings argue that co-stimulation via CD28 might be beneficial in the setting of antibody mediated T-cell redirection, as long as it does not increase the risk or severity of adverse side effects.

Since the life-threating cytokine-release syndrome suffered by six healthy volunteers following the administration of the superagonistic antibody TGN1412 in 2006 (Suntharalingam et al., 2006), the application of CD28-specific antibodies has been handled with caution in immunotherapeutic research. This superagonistic CD28 antibody is able to induce a full activation of primary resting T cells without pMHC/TCR interaction (Luhder et al., 2003), yet was shown to depend on FcγR interaction on monocytes (Hussain et al., 2015). The CD28-specific scFv in our constructs is derived from the hybridoma 9.3, and has been studied as full-length IgG format as well as scFv included in a bispecific construct. Stimulation with the cross-linked monoclonal antibody (mAb) 9.3 alone did neither induce the transcription factors NF-AT or NF-κB, nor the expression of cytokines like IFNγ, IL-2 or IL-4 (Siefken et al., 1998). However, use of scFv9.3 in a melanoma targeting BiTE, resulted in supra-agonistic CD28-triggering, which induced T-cell activation and melanoma cell elimination (Grosse-Hovest et al., 2003). Similar effects were also observed in the present study, where single treatment with FabMAbαCD28 resulted in efficient elimination of target cells and IFNγ release (Fig. 10a-c). Moreover, translocation of LAMP-1 upon single treatment with FabMAbαCD28 in the presence of HBsAg suggests that the lytic activity in these co-cultures is at least partially mediated by $CD8^+$ and $CD4^+$ T cells (Fig. 16c, d). This provides evidence that CD28-targeting bispecific antibodies may be able to activate T cells without additional stimulation.

However, simultaneous engagement of CD3 and CD28 increased T-cell activation synergistically and is clearly the method of choice in HBV-targeting immunotherapy. Additionally, the mutations in the Fc domain of BiMAbs should impair FcγR interaction, and thereby restrict T-cell redirection to the presence of HBVenv. FabMAbs that lack the Fc domain should always depend on HBVenv to allow crosslinking and synapse formation. This should localize the T-cell activation to HBV-infected hepatocytes in the liver or HBVenv-positive tumors and thereby reduce the risk of a systemic cytokine release syndrome. In this project, T-cell activation was clearly dependent on the presence of HBVenv and thus, we are convinced that co-stimulation with the CD28-specific constructs is a reasonable strategy to increase the sensitivity and efficacy of T-cell redirection in the setting of CHB. Nevertheless, dosing regiments for these constructs must be carefully evaluated in further pre-clinical models.

3.3 Comparison of FabMAbs and BiMAbs

3.3.1 Influence of the antibody format on the redirection capacity *in vitro*

The functional efficacy and pharmacokinetics of bsAbs strongly depend on their size, binding valency, and in particular the presence or absence of an Fc domain (Dahlen et al., 2018). To investigate the influence of these features on antibody-meditated T-cell redirection towards HBV-infected cells, two different bispecific antibody formats were developed and compared for their activation capacity. Manufacturing of both formats was equally feasible and long-term storage in PBS at 4 °C for one year did not result in notable aggregation or fragmentation of the constructs (Fig. 12).

Overall, the format had only a minor influence on the redirection capacity of the constructs *in vitro*. The mutations that were introduced in the Fc domain of BiMAbs should reduce ADCC and CDC (Armour et al., 1999, Xu et al., 2000, Idusogie et al., 2000), and thereby limit the T-cell stimulation to CD3 and CD28 triggering. An increased T-cell activation by BiMAbs was still expected, as they showed stronger binding to HBVenv (Fig. 13a), and furthermore, bivalent binding to the T-cell antigens. However, the use of equimolar concentrations throughout the study showed comparable potency of both formats in co-cultures with Huh7S cells (Fig. 18, Fig. 19), and even a slightly increased redirection capacity by FabMAbs in the presence of HBV-infected HepG2 NTCP cells (Fig. 23a, b). Differences between transgenic Huh7S cells and infected HepG2 NTCP cells can be explained by the underlying HBVenv genotype used in the different models. Huh7S cells express HBVenv of genotype A, which is recognized equally well by 5F9 and C8. In contrast, C8 displayed ~50% reduced binding to genotype D and serotype ayw, which was used in the experiments with infected HepG2 NTCP. This observation shows that the binding characteristic to HBVenv can affect the redirection efficiency and supports the benefit of additional HBVenv-binders for further development of bsAb-mediated HBV immunotherapy.

Other factors that potentially affect the redirection capacity are the size of the constructs and the presence of the rigid Fc domain, which may both have a steric influence on the formation of the immunological synapse. Current concepts of T-cell activation that are based on the kinetic segregation model for TCR triggering (Davis and van der Merwe, 2006) propose the exclusion of the CD45 phosphatase from the synapse as promotor for the phosphorylation of peptide-major histocompatibility complex (pMHC)-bound TCRs. This effect has been shown to be caused by the large extracellular domain of CD45 that is sterically excluded from regions with close cell-to-cell contact (James and Vale, 2012). Small constructs may drive this process more efficiently than larger ones, resulting in a stronger T-cell activation by FabMAbs. This may be a further explanation, why FabMAbs display comparable efficacy, even though they show reduced binding to HBVenv and only monovalent binding to the T-cell antigens. It may also be the reason for potent redirection activity of FabMAbαCD28, which was not observed upon single treatment with BiMAbαCD28 (Fig. 14a-c). This provides evidence that the size and rigidity of bsAbs can affect their redirection potential in the setting of HBV infection.

3.3.2 Influence of the antibody format on serum availability and half-life in mice

In contrast to the comparable redirection capacity, the format substantially influenced the half-life in C57BL/6 mice. The small size of FabMAbs, as well as the lack of the Fc domain suggests a short $t_{1/2}$ of about 2 hours in humans, comparable to antibodies of the BiTE® format (Portell et al., 2013). In mice, the measured $t_{1/2}$ was below 6 hours and is therefore in line with the half-life published for the BiTEs MT110 and muS110, which are similar in size (Amann et al., 2008). In case of BiMAbs, the molecular weight of 170 kD that limits renal elimination, as well as recycling through the neonatal Fc receptor (FcRn), suggests a prolonged $t_{1/2}$ comparable to full-length IgG1 that can be up to 30 days in humans (Mankarious et al., 1988). The murine FcRn has been described to bind human IgG1 Fc domains and facilitates antibody recycling in mice (Gurbaxani et al., 2006, Datta-Mannan et al., 2007). Yet, it is important to acknowledge that the mutations E233P, L234A, L235A, G236del, A327G, A330S and P331S, which are included in the BiMAb Fc domain, have been shown to impair the interaction with the FcRn (Stapleton et al., 2018) and therefore might negatively influence the pharmacokinetics of these constructs. In this study, the $t_{1/2}$ of BiMAbs was at least 72 hours. Serum level at later time points were not determined, but it can be assumed that the $t_{1/2}$ is comparable to human IgG1, which has been shown to be around 9.5 days in CD-1 ® mice (Unverdorben et al., 2016). The prolonged $t_{1/2}$ of BiMAbs was the major criterion to choose them as lead candidate for the tumor transplant model discussed in 3.7, considering FabMAbs would have required at least 2 injections daily in order to maintain a reasonable drug level in the circulation. In the patient setting however, a reduced $t_{1/2}$ might be beneficial in limiting the risk and severity of potential adverse side effects. It is to be expected that FabMAbs will be cleared from the circulation with similar kinetics as blinatumomab, namely 22.3 ± 5.0 L/d/m^2 (Klinger et al., 2012) and a mean half-life of 2.10 hours (Blincyto (Blinatumomab) [package insert] Thousand Oaks).

3.3.3 Kinetics of target cell elimination and cytokine-mediated antiviral effect

In co-cultures with HBsAg-coated plates or Huh7S cells, the redirection with the combination of CD3- and CD28-specififc constructs led to the induction of polyfunctional T cells, accompanied by cytokine secretion and target cell elimination. However, the kinetics of Huh7S cell and infected HepG2 NTCP cell elimination were slow compared to studies with CD19xCD3 (Loffler et al., 2000, Liu et al., 2017) or EpCAMxCD3 constructs (Riesenberg et al., 2001) that showed distinct target cell elimination within 24 hours of co-culture. This difference can be explained by generally low exposure of HBVenv on the target cells, as already discussed in 3.2. Moreover, HBVenv levels may be further reduced as result of a suboptimal experimental setup in the killing assays. Throughout all xCELLigence experiments Huh7S and infected HepG2 NTCP cells were trypsinized one day prior to the start of co-culture in order to be re-seeded in an E plate 96 that is compatible with the device. The trypsinization may on the one hand result in partial digestion of HBVenv on the surface and thereby reduce the amount of accessible target molecules. On the other hand, detachment of the cells will induce morphological changes and lead to a partial de-differentiation of the hepatoma cells, which is especially critical in case of infected HepG2 NTCP K7 cells that rely on differentiation to support efficient HBV replication (Ko et al., 2018). Recently it has been shown that seeding of Huh7S cells two weeks prior to co-culture increases the level of HBVenv in the culture and enhances S-CAR-meditated cytotoxicity drastically (Antje Malo, personal communication). This setting would be close to the in situ situation, where hepatocytes have a distinct polarization and are embedded in a fixed tissue context. This suggests that a longer incubation time between seeding of target cells and start of co-culture might enhance the strength and speed of bsAb-mediated T-cell redirection. How far the HBVenv levels in these cultures resemble the *in vivo* situation still needs to be determined.

Moreover, kinetics of target cell elimination can be strongly affected by the effector to target ratio (E:T ratio) in the co-culture. In our study, an E:T ratio of 1:1 (based on the assumptions that T cells make up 60% of the total PBMC and that every T cell in the population may become an effector cell) was used throughout all experiments. In contrast, the studies with the CD19xCD3 and EpCAMxCD3 constructs used E:T ratios of 10:1 (Liu et al., 2017), 20:1 (Loffler et al., 2000) or 25:1 (Riesenberg et al., 2001). Experiments with an E:T ratio of 1:1 employing a HIVenvxCD3 construct resulted in kinetics comparable to our data, namely around 50% of eliminated target cells within 48 hours of co-culture (Sung et al., 2015). This indicates that kinetics of target cell elimination can be strongly modulated by the effector to target ratio *in vitro*, yet it does not give information about the *in vivo* situation, where an adjustment of this ratio is not possible. Along this line, studies with enriched, pure or pre-activated T-cells have not been performed in this thesis, since the *in vivo* situation is closer resembled by an unstimulated PBMC population.

The kinetics can be furthermore influenced by the immune suppressive properties of hepatocyte-derived cell lines. Since it was shown that hepatocyte derived target cells display an intrinsic resistance to grzB-dependent apoptosis (Kafrouni et al., 2001) conferred by serine protease inhibitor-9 expression (Willberg et al., 2007), cytotoxic mechanisms most likely depend strongly on Fas/FasL interaction, which can influence the efficiency of target cell elimination.

The secreted levels of cytokines in the co-cultures were in the ng/ml range, which is in line with previously published studies (Liu et al., 2017). The profound secretion of IFNγ and TNFα needs to be emphasized, since it has been shown that these cytokines can induce cccDNA degradation without target cell lysis (Xia et al., 2016). The potency of a cytokine-mediated anti-viral effect through induction of APOBEC3 was recently also demonstrated in HBV-infected human hepatocytes in mice (Koh et al., 2018). The relevance of cytokine-induced effects in the setting of antibody-mediated T-cell redirection was further supported by transwell assays in our facility (Xia et al., 2016). PBMC, Huh7S cells and BiMAbs were cultured in the inlet that allowed cytokine diffusion to HBV-infected HepaRG cells, but prohibited direct contact between effector cells and the infected hepatoma cells. After 7 days of co-culture, a significant reduction in HBeAg, intracellular HBV-DNA and cccDNA was observed, which correlated with high levels of IFNγ, IL-2 and TNFα in the supernatant (Quitt, Luo et al., accepted at Journal of Hepatoloy). This gives evidence that the retargeted cytolytic T-cell response can be complemented by a local cytokine release that may further purge the viral cccDNA via non-cytolytic mechanisms, thereby limiting hepatotoxicity and preserving organ integrity.

3.4 Induction of cytotoxic CD4$^+$ T cells upon treatment with bi- and trispecific antibodies

The treatment with bsAbs in combination, as well as TriMAb, led to a strong induction of grzB-expression in CD4$^+$ T cells (Fig. 18c, Fig. 29c, Fig. 30b, d). Recent repetitions of binding studies with PBMC and bsAbs confirmed binding to T cells and showed particular strong engagement of CD4$^+$ T cells (Quitt, Luo et al., accepted at Journal of Hepatoloy). This is in line with literature that shows higher levels of CD3 (Valle et al., 2015) as well as CD28 (Lee et al., 1990) expression by CD4$^+$ T cells compared to their CD8$^+$ counterparts. This might lead to enhanced engagement and activation of CD4$^+$ T cells upon treatment with CD3- and CD28-targeting bispecific antibodies. Accordingly, increased proliferation (Fig. 17) and cytokine production (Fig. 18b) of CD4$^+$ T cells was observed. Moreover, experiments with isolated CD4$^+$ T cells and CD4$^+$-T-cell-depleted PBMC clearly demonstrated that CD4$^+$ T cells are able to efficiently eliminate HBVenv-expressing target cells upon treatment with bsAbs and are additionally essential for the production and secretion of proinflammatory cytokines, such as IFNγ (Quitt, Luo et al., accepted at Journal of Hepatoloy). Efficient target cell elimination by CD4$^+$ T cells has been reported in several studies (Wisskirchen et al., 2017, Appay et al., 2002, Brown, 2010, Quezada et al., 2010) and was in particular shown for BiTE-redirected T cells

(Haagen et al., 1994). Taken together, this data provides evidence that $CD4^+$ T cells are especially susceptible to redirection by CD3 and CD28-targeting molecules and can be regarded as key players in the bsAb-mediated T-cell therapy for CHB as they exhibit efficient target cell elimination as well as cytokine release. Even though, these findings have not been reproduced with TriMAb, a similar effect is to be expected, since TriMAb demonstrated comparable redirection capacity as the bsAbs in combination.

3.5 Effect of bsAb treatment on the T-cell subset composition

Treatment with bsAbs had a major influence on the composition of T-cell subsets in the PBMC population. In controls ~40% of T_N, ~20% of T_{EM} and T_{EFF}, and 5% of T_{CM} were detected, while the treatment with bsAbs increased the percentage of T_{CM} and T_{EM} to ~40%, while percentages of T_{EFF} and T_N were reduced to below 5% (Fig. 20e). These changes in the T-cell subset composition can originate from differentiation of naïve T cells into memory or effector cells, by unbalanced proliferation of the different subtypes, or activation-induced apoptosis upon bsAb-treatment. The underlying experimental setup does not provide clear evidence, which of these possibilities is the main driver behind this observation.

It has been shown in literature that stimulation of naïve human T cells with αCD3/αCD28-coated beads can induce differentiation into T cells with effector memory and central memory phenotype (Li and Kurlander, 2010, Shi et al., 2013). This provides evidence that artificial induction of CD3- and CD28-signaling by antibody engagement can result in memory formation *in vitro*. Activation with the bispecific antibodies in the presence of HBVenv will presumably lead to comparable CD3- and CD28-triggering and thereby can potentially induce the differentiation of naïve T cells in the co-culture into T_{CM} and T_{EM} (Fig. 20e). Induction of a memory phenotype has moreover been shown for bsAb-treated T cells *in vitro* (Hornig et al., 2012).

The proliferation capacity of the different T-cell subsets is known to differ with T_N and T_{CM} displaying a higher capacity than T_{EM} and terminally differentiated effector memory T cells that re-express CD45RA (T_{EMRA}) (Sallusto et al., 1999, Geginat et al., 2003). T_{EMRA} ($CCR7^-/CD45RA^+$) express the same markers as T_{EFF} that were analyzed in this thesis ($CD62L^-/CCR7^-/CD45RO^-/CD45RA^+$) (Golubovskaya and Wu, 2016) and thus, can be regarded as similar. This gives evidence that the percentage increase of T_{EM} upon treatment with the bsAbs can be rather assigned to differentiation from the naïve or central memory population than to relatively increased proliferation.

Additionally, it was shown that the *in vitro* TCR-stimulation of T_{EM} and T_{EMRA} was associated with increased rate of cell death in these populations (Geginat et al., 2003). This is in line with the general dogma of a short-lived effector memory cell population that exerts immediate effector function upon antigen re-encounter in non-lymphoid inflamed tissues (Sallusto et al., 2004). In the setting of bsAb-mediated T-cell activation,

efficient engagement of CD3 and CD28 on T_{EFF} or T_{EMRA} might lead to fast activation of these cells, followed by activation-induced apoptosis.

Taken together, literature provides evidence that treatment with bsAbs might be able to induce differentiation of T_N into T_{EM} and T_{CM} cells and we speculate that differentiation is the main driver behind the changes in the T-cell subset composition observed in figure 20e. To further elucidate the dynamics of differentiation and effector cell survival in the setting of bsAb-redirected T cells, further experiments with isolated subsets need to be performed.

3.6 Benefit evaluation of trispecific antibodies

Early studies using supernatants of producer cell lines showed stronger T-cell activation by the trispecific antibodies, indicated by increased cytokine secretion (Fig. 29a), grzB expression (Fig. 29b, d) and a greater percentage of trifunctional T-cells (Fig. 33c, d). Increased efficiency and sensitivity indicate a clear benefit for the use of trispecific antibodies. However, these results have to be taken with caution, since the antibody concentration in the supernatant was not quantified in these experiments and therefore antibodies could not be adjusted to equimolar concentrations.

Although OKTriMAb induced potent T-cell activation in the presence of immobilized HBsAg (Fig. 29a), efficient redirection towards HBVenv expressing target cells was not observed (Fig. 31c, d). This may be explained by the complex structure and the comparatively large size, which may sterically interfere with the formation of immunological synapses between T cells and HBVenv-expressing target cell. However, correct folding, dimerization and secretion of OKTriMAb have not been further investigated, since TriMAb showed a superior redirection capacity in early experiments (Fig. 29a, Fig. 31a, b) and was therefore selected as lead candidate for further studies. After all, OKTriMAb is a particularly complex molecule and the presence of eight scFvs will very likely have a strong impact on the producibility and stability of this construct, as described in 3.1.1. Taken together, further experiments are required to assess correct folding, dimerization and stability of OKTriMAb. This is a prerequisite to gain valid information about its redirection capacity.

In experiments with purified TriMAb the redirection capacity was comparable to the combination of FabMAbs. Production of TriMAb in our facility yielded pure preparations, yet the overall yield was low. Therefore, the impact of long-term storage on the integrity of the construct has not been evaluated so far. Even though the benefit of a highly potent single molecule was clearly stated by the PEI, large-scale producibility and stability of TriMAb during long-term storage is a major concern, which needs to be investigated in the future. TriMAb and OKTriMAb are both included in the Patent Cooperation Treaty application “Trispecific binding molecules for treating HBV infection and associated conditions” (Protzer et al., 2016), which has been filed by the Helmholtz Centre Munich and where I am a co-inventor.

3.7 TriMAb functionality depends on the presence of HBVenv

TriMAb- and OKTriMAb-mediated T-cell redirection was clearly dependent on the presence of HBVenv, which was either provided as recombinant protein adsorbed to the cell culture plate (Fig. 29, Fig. 33b, c, d), expressed by transgenic Huh7S cells (Fig. 31, Fig. 32), or expressed by HBV-infected HepG2 NTCP cells (Fig. 34). Activation of T cells in the absence of target antigen was not observed, even though these trispecific molecules exhibit simultaneous binding to CD3 and CD28.

As already briefly discussed in 1.2.1.3, the dissociation of ITAM-containing intracellular CD3 domains from the membrane is required for intracellular signal transduction and subsequent activation of the T cell. The release of ITAMs into the cytoplasm is proposed to require TCR clustering (Minguet et al., 2007) as well as mechanical forces exerted by highly dynamic interaction and relative motion between T cell and APC upon TCR engagement (Ma et al., 2012). Accordingly, monoclonal CD3 or CD28 antibodies only provide T-cell stimulation when they are immobilized by adsorption to a cell culture plate or bead, or by interaction with APCs via Fc receptors (Geppert and Lipsky, 1988, Hussain et al., 2015) and fail to do so in a soluble state. This interaction mimics the clustering of TCRs by recruiting CD3 and CD28 to an artificial immunological synapse, as well as the mechanical forces exerted by the relative motion between T cell and APC upon TCR engagement and is therefore required to induce T-cell activation in this artificial setting. To prevent this Fc-receptor-mediated cross-linking and provide dependence on HBVenv, the Fc domains in BiMAbαCD3 and BiMAbαCD28 were mutated (see 2.2.1.1).

Thus, mere binding of the T-cell antigens by soluble TriMAb or OKTriMAb will cross-link only few CD3 and CD28 molecules without inducing efficient clustering or exerting any mechanical force. Since TriMAb and OKTriMAb contain no Fc domain, potential interaction with APCs in the PBMC population can also be excluded. Only simultaneous engagement of immobilized HBVenv and the T-cell antigens will provide efficient clustering of CD3 and CD28 molecules, as well as the mechanical force that is required to induce potent T-cell activation.

3.8 Modulation of bsAb-mediated target cell elimination with IL-12 and hyper-IL6

The cytokine IL-12 has been described to regulate cell-mediated immunity by increasing the cytotoxic activity of $CD8^+$ T lymphocytes, thus was proposed to be a useful modulator in immunotherapeutic approaches (Mehrotra et al., 1993). Directed release of IL-12 has already been employed to enhance the sensitivity and efficacy of CAR T-cell-mediated anti-tumoral effects (Zhang et al., 2011) and was recently also investigated in the context of HBV immunotherapy in our facility (Meyer-Berg, 2016). We therefore decided to investigate the influence of recombinant IL-12 in setting of TriMAb-induced T-cell redirection. To enable recombinant expression of the heterodimeric cytokine, the two

subunits of IL-12 are fused by introduction of a G_6S linker, resulting in biological active single chain IL-12 (scIL-12) (Lieschke et al., 1997). Administration of scIL-12 in co-cultures of PBMC, Huh7S and TriMAb had no influence on the loss of cell viability, but led to a 5-fold increase in IFNγ release (Fig. 32a, b). A similar fold increase was observed in activated T cells, which constitutively expressed IL-12 upon retroviral transduction (Zhang et al., 2011). As already discussed in 3.3.3, the cytokine mediated antiviral effect can contribute to efficient cccDNA elimination and local release of IFNγ and TNFα in the liver may therefore be beneficial to the outcome of bsAb-based immunotherapy. However, systemic administration of tolerable doses of IL-12 alone or in combination with immunotherapeutic agents, like Rituximab or therapeutic vaccination, did not demonstrate a sustained antitumoral efficacy in clinical trials (Lasek et al., 2014). Since the clinical efficacy of IL-12 is limited by dose-dependent toxicity upon systemic administration, methods for targeted delivery and controlled expression have been developed. In the field of adoptive T-cell therapy this was achieved by scIL-12 expression under control of an NF-AT responsive promotor, which results in specific IL-12 production upon CAR-engagement in the presence of target antigen (Zhang et al., 2011). In the setting of bispecific molecules, targeted IL-12 delivery can be achieved by fusion of target-specific antibodies with scIL-12. Such constructs have been developed for cancer associated proteins like human epidermal growth factor receptor 2 (Peng et al., 1999), CD30 (Heuser et al., 2003) or the carcinoembryonic antigen (Makabe et al., 2005) and all of them displayed antitumoral activity. Targeted delivery of IL-12 in HBV immunotherapy could enhance cytotoxic activity specifically in the presence of HBVenv-expressing cells and thereby limit systemic adverse side effects. Co-administration of hypothetical Fab5F9-scIL12 or C8-scIL12 fusion proteins together with the bispecific antibodies might be an interesting approach to increase the cytokine-mediated antiviral effect, however, generation of such constructs has not been performed so far.

IL-6 trans-signaling has been described to be a mechanistically distinct and rapid process to induce the development of naïve into effector T cells within 18 hours. The differentiation has been shown to be dependent on the presence of cross-presenting liver sinusoidal endothelial cells and resulted in upregulation of grzB expression and a superior activation potential of the T cells (Bottcher et al., 2014). A comparable effect was conferred by administration of hyper-IL-6, a fusion protein of IL-6 and its receptor, in the presence of anti-CD3/CD28 coated microbeads (Bottcher et al., 2014). However, administration of hyper-IL-6 in co-cultures of PBMC, Huh7S and TriMAb had no influence on kinetics of target cell elimination or IFNγ release in our experiments (Fig. 32c, d). Since no increased cytokine release was observed by Bottcher and colleagues, it was also not expected in our setting. In contrast, substantial upregulation of grzB expression and rapid effector cell development might have a positive effect on the antibody-mediated cytotoxic T-cell response, yet was not observed in our system. Follow-up studies that compare the grzB-expression in the presence or absence of hyper-IL6 have not been performed so far. Thus, it is not possible to make a clear statement on the effect of hyper-IL-6 in bsAb-mediated HBV immunotherapy.

3.9 In vivo studies with BiMAbs in a tumor transplant model

In vivo studies on the functionality of HBVenv-targeting bispecific antibodies were performed by Shanshan Luo, and are included in the submitted manuscript (Quitt, Luo et al., accepted at Journal of Hepatoloy). Since the redirection potential of the constructs is restricted to human T cells, a tumor transplant model with human effector and target cells was established in Rag2/IL2Ryc$^{-/-}$ mice. Moreover, it was considered that patients with HBVenv-positive HCC at end stage would probably be the first patients to benefit from this novel therapeutic approach. 2x10^6 Huh7 and Huh7S cells were subcutaneously injected into the left and the right flank of each animal, respectively, and tumor growth was monitored for two weeks. Considering their substantially increased half-life (Fig. 21d), BiMAbs were chosen as lead candidate for this study. On day 14, when tumors were well established, mice were i.p. injected with 2x10^7 PBMC and i.v. injected with 100 µg of a BiMAbαCD3/CD28 combination (corresponding to ~2.5 mg/kg body weight), or PBS. The administration of bsAbs was repeated 4 times every 2 days. After 10 days of treatment, mice were sacrificed and tumors as well as sera were collected and analyzed. In BiMAb-treated animals, HBVenv-positive tumors were significantly smaller, while the size of HBVenv-negative tumors was unaffected. This correlated with the amount of tumor-infiltrating lymphocytes (TILs), determined by the presence of human CD8 transcripts via qPCR. To evaluate the activation status of TILs, the levels of human IFNγ, IL-2 and TNFα transcripts in the tissue of HBVenv-positive tumors were quantified by qPCR and the cytokines were increased in BiMAb-treated mice in comparison to control mice. As further readout for functionality, the HBsAg concentration in the serum was determined and showed significant reduction in BiMAb-treated animals. This tumor transplant model with HBVenv-expressing Huh7 cells demonstrates functionality of bsAbs *in vivo*. It showed that i.v. injected BiMAbs can engage i.p. administered T cells and further redirect them successfully towards HBVenv-positive tumors, resulting in T-cell activation, tumor infiltration and tumor cell elimination. However, the model lacks clinical relevant data on the antibody-mediated antiviral effect, which will clearly depend on efficient T-cell recruitment into the liver and the establishment of a cytotoxic immune response against HBV-infected hepatocytes. The evaluation of these subjects requires the use of murine HBV-infection models, which are described in the following.

3.10 Murine HBV-infection models

The establishment of murine infection models is particularly difficult, due to HBV's narrow host specificity. One option is the use of human liver chimeric mice which are susceptible to HBV infection (Dandri and Petersen, 2012). These mice are generated by transgenic expression of the liver-toxic urokinase type plasmogen activator (uPA) under control of the albumin promotor. This results in subacute liver failure in newborn animals, which in turn enables efficient transplantation of hepatocytes (Rhim et al., 1994). The combination of uPA mice with severe combined immune deficient (SCID) mice allows the engraftment

of primary human hepatocytes that can be infected with wild-type HBV (Dandri et al., 2001). This model was already used to study the *in vivo* efficacy of adoptively transferred T cells engrafted with HBV-specific TCRs (Kah et al., 2017). To evaluate the bsAbs-mediated T-cell redirection in this model, mice will need to be injected with human effector cells (PBMC or isolated T-cells) and the bispecific antibodies. Another model combines the transplantation of human hepatocytes with the establishment of a human immune system by injection of human $CD34^{+}$ hematopoietic stem cells into $Rag2^{-/-}$ IL-$2R\gamma c^{-/-}$ NOD.sirpa $uPA^{tg/tg}$ mice. These mice demonstrate a robust engraftment of human myeloid and lymphoid cell subsets and are moreover susceptible to HBV infection (Strick-Marchand et al., 2015). The availability of human effector and target cells resembles the situation in patients closer than other models. Experiments in cooperation with Hélène Strick-Marchant at the Institute Pasteur were planned already, but due to a lack of available animals could not been conducted so far.

A different approach is the development of murine surrogate antibodies that specifically interact with murine CD3 and CD28, followed by evaluation in immunocompetent AAV-HBV infected animals (Yang et al., 2014). Suitable scFv were already successfully introduced into the BiMAb format and the redirection of murine splenocytes in the presence of HBsAg has been demonstrated in our facility (Eva Loffredo-Verde, unpublished). The infection of C57BL/6J mice with AAV-HBV is well established in our facility (Julia Festag, unpublished) and provides a feasible model for the *in vivo* evaluation of the murine surrogate constructs in the near future. All models in 3.10 focus on the assessment of antibody-mediated T-cell redirection towards HBV infected cells located in the liver. Since the liver has been described as an immune privileged site (Wohlleber and Knolle, 2012), the efficacy of antibody mediated T-cell redirection may differ from the one observed against subcutaneous tumors. Targeting of HBVenv on hepatocytes by BiMAbs has already been demonstrated by Shanshan Luo. In this experiment, 50 µg and 100 µg of BiMAbαCD3 or BiMAbαCD28 were i.v. injected into transgenic HBV1.3xfs or C57BL/6 control mice. Two hours post injection, mice were sacrificed and liver sections were stained with anti-human IgG antibodies, following examination by immunohistochemistry, to evaluate the binding of BiMAbs to HBVenv on the hepatocytes. Positive IgG staining was exclusively found in livers of BiMAb-treated HBV1.3xfs mice, while PBS-controls as well as C57BL/6 control animals were negative (Quitt, Luo et al., accepted at Journal of Hepatoloy). To demonstrate that the bi- and trispecific antibodies can moreover mount a potent T-cell response against HBV-infected hepatocytes or HBVenv-positive tumors in the liver should be a major goal of upcoming *in vivo* studies, since it clearly underlines the feasibility as treatment option for chronic hepatitis B and HBV-associated HCC.

3.11 Limitations of HBV immunotherapy with bispecific antibodies

3.11.1 Specificity of the bsAb-mediated T-cell redirection

Throughout the project, bsAb-mediated T-cell proliferation and cytokine secretion was always completely dependent on the presence of the HBV envelope protein, which was either provided as immobilized HBsAg or expressed by Huh7S and infected HepG2 NTCP cells. However, at antibody concentration of 100 nM (Fig. 10) or late time points in some xCELLigence cultures (Fig. 19a, b), HBVenv-negative Huh7 cells showed bsAb-dependent loss of viability that was not accompanied by the release of IFNγ, IL-2, TNFα or grzB (Fig. 10, Fig. 19c-f). This effect can be mediated by formation of aggregates or adherence of the constructs to the cell culture plate, which may both induce receptor cross-linking and CD3/CD28-triggering in the absence of HBVenv. Moreover, the Huh7 cells and PBMC are not HLA-matched in this setting, which might result in an increased cytotoxic activity, especially in combination with mild CD28 triggering. Studies to investigate the specificity of T-cell redirection in cultures with Huh7 cells in more detail were performed by Shanshan Luo. In these experiments, Huh7 cells were mixed with 25, 50, 75 or 100% of Huh7S cells, and cultured with PBMC and BiMAbs in combination. Here, the loss of cell viability correlated clearly with the percentage of HBVenv-positive cells in the culture (Quitt, Luo et al., manuscript accepted at Journal of Hepatoloy).

HepG2 NTCP cells did not show any loss of cell viability in the absence of HBV, even at FabMAb concentrations of 100 nM (Fig. 23c). Moreover, the percentage of eliminated HepG2 NTCP cells correlated closely with the amount of infected cells that were determined by intracellular HBc staining (Fig. 22a, Fig. 23a, b). Along this line, the level of secreted cytokines corresponded well with the MOI that was used for infection (Fig. 24b). In addition, no unspecific activation of T cells in the absence of HBVenv or the bi- and trispecific antibodies was observed in experiments with HepG2 NTCP cells (Fig. 24b, c, Fig. 34b).

Taken together, we could demonstrate that the presence of the HBV envelope protein is clearly required to induce a potent T-cell redirection in the presence of bi- and trispecific antibodies. The potential risk of a cytokine release syndrome upon bsAb treatment needs to be considered, but can be reduced by careful dose-escalation studies and treatment with IL-6-specific mAbs (see 1.3.2.3).

3.11.2 Sensitivity of bsAb-mediated T-cell redirection

Co-culture experiments in 2.3.3 showed a clear correlation between the anti-viral effect correlated and the viral input. At an MOI of 500 HBV virions/cell, treatment with FabMAbs led to a profound reduction of viral parameters that was accompanied by substantial levels of proinflammatory cytokines in the culture (Fig. 24b, e). In contrast the anti-viral effect was greatly reduced at an MOI of 25 HBV virions/cell, even though cytokine

secretion was still measurable (Fig. 24b, e). The infection experiments in 2.3.1 suggest that the use of a high MOI will not only increase the overall percentage of infected cells in the culture, but also the number of virions that infect a single cell resulting in a relative increase of viral protein expression per cell (Fig. 22). It is expected that the bsAb-meditated T-cell redirection requires a certain threshold of accessible target antigen to induce effector cell activation. This idea is supported by HBsAg-titration experiments in 2.4.3.4, which show a clear TriMAb-mediated effect at a concertation of 1 µg/ml, while 0.2 µg/ml do not result in T-cell activation (Fig. 33b). Similar observations have been made in studies with CAR engrafted T-cells, which required an MOI above 25 to elicit an antiviral effect in co-cultures with infected HepG2 NTCP cells (Karin Wisskirchen, personal communication). These findings suggest that the anti-viral effect might be limited by the number of infected cells as well as the amount of accessible HBVenv per cells. However, the question remains if the level of HBVenv on infected hepatocytes in CHB patients will be sufficient to trigger T-cell activation, and even more so if the response is strong enough to control the HBV infection. Answers to these questions might be obtained by use of HBV-infected human liver chimeric mice, as described in 3.10.

3.11.3 Influence and side effects of soluble HBsAg

A concern for the clinical use of T-cell engaging bsAbs is the effect of secreted HBsAg. The influence of soluble HBsAg on the redirection potential of bsAbs was studied by titration of subviral particles in 2.2.3.3. The administration of subviral particles did not impair the elimination of Huh7S target cells, yet a loss of cell viability of HBVenv-negative Huh7 cells was detected, when the amount of particle exceeded $1x10^7$/ml (Fig. 20b). In contrast to the cytokine-independent elimination discussed in 3.11.1, the effect was accompanied by substantial secretion of cytokines. The elimination of Huh7 cells and the level of cytokines in the culture correlated clearly with the amount of administered subviral particles. Since T-cell activation was still dependent on the presence of HBVenv, the observation cannot be declared as unspecific effect. We propose that the subviral particles adhere to the cell culture plate or to Huh7 cells through interaction with HSPGs, and thereby mimic immobilized HBVenv molecules, which in turn can allow efficient crosslinking similar to HBsAg-coated plates. However, it is unclear if this effect will play a major role *in vivo*.

In the tumor transplant model, high levels of HBsAg in the circulation did neither prevent targeting of HBVenv on the tumor cell membrane, nor induced a systemic cytokine release syndrome (Quitt, Luo et al., accepted at Journal of Hepatoloy). Severe adverse side effects induced by OKT3 and TGN1412 antibodies have been described in a humanized mouse model of human PBMC-reconstituted NOD-RAG1$^{-/-}$Aβ$^{-/-}$HLADQ$^{(tg+ \text{ or } tg-)}$IL-2Rγc$^{-/-}$ mice. These mice showed severe signs of illness like reduced motility and rapid decline of body temperature within 2-6 hours post antibody injection, which was accompanied by elevated levels of human IFNγ and TNFα in the circulation (Weissmuller et al., 2016). Such signs of illness were not observed upon administration of BiMAbs, yet

human cytokine levels in the serum of the mice were not determined. It needs to be emphasized that this work was performed in Rag2/IL2Ryc$^{-/-}$ mice, which do hardly allow the evaluation of safety issues. Independently, the risk of HBsAg-mediated side effects can be substantially decreased by administration of HBV-neutralizing monoclonal antibodies prior to treatment. In clinical trials, administration of such antibodies demonstrated a rapid and significant decrease in HBsAg to undetectable levels and was well tolerated by patients (Galun et al., 2002). If neutralizing antibodies will impair bsAb-mediated T-cell redirection through masking of HBVenv on the hepatocyte membrane remains to be investigated, yet this approach would provide an option for a safe evaluation of the bsAbs in the clinical setting.

3.12 Final evaluation and outlook

Up to date, there is no curative therapy for chronic hepatitis B available. Current treatment options efficiently suppress HBV-replication, but rarely eliminate the viral infection. Even though viral suppression improves the outcome of CHB, patients require life-long treatment and still carry the risk of developing HBV-driven HCC. (Vlachogiannakos and Papatheodoridis, 2013, Chayanupatkul et al., 2017, Bruix et al., 2017). Elimination of the cccDNA in HBV-infected hepatocytes remains a major therapeutic goal in CHB therapy and will be required to cure the disease (Wieland et al., 2004b, Lucifora and Protzer, 2016). Thus, immunotherapy with bispecific antibodies that mount an effective T-cell response against HBV-infected hepatocytes is a promising approach to achieve functional cure. The data presented here demonstrate that bi- and trispecific antibodies, which target HBVenv as well as CD3 or CD28, can successfully redirect T cells to establish and maintain a cytotoxic immune response towards HBV infected cells. This T-cell redirection resulted in the induction of polyfunctional effector cells, efficient elimination of target cells and reduction of viral parameters.

During the study it became evident that administration of CD3-specific antibodies alone is not sufficient to induce a cytotoxic immune response against HBVenv-expressing target cells, yet this limitation was overcome by co-stimulation with CD28-specific bsAbs. In consideration of a therapeutic approach, both immune stimulatory scFv were successfully combined in a trispecific antibody that showed comparable redirection efficacy as the bispecific antibodies in combination. However, the clinical applicability of the trispecific construct will depend strongly on its efficient production and its stability, which requires further investigation.

In the tumor transplant model, BiMAbs attracted T cells to HBVenv-expressing tumors, resulting in T-cell activation, tumor infiltration and elimination of tumor cells. Further studies need to determine, if the bispecific antibodies can facilitate efficient T-cell recruitment to the liver followed by the establishment of a cytotoxic immune response against HBV-infected hepatocytes. Therefore, I propose that further studies should concentrate on experiments in murine HBV-infection models. This will provide valuable information about the antibody-mediated antiviral effect *in vivo.*

Taken together, the administration of HBVenv-targeting bsAbs facilitates a robust T-cell redirection towards HBVenv-expressing target cells and provides a feasible and promising approach for the treatment of chronic hepatitis B and HBV-associated HCC.

4 Material and Methods

4.1 Materials

4.1.1 Devices and technical equipment

Product	Supplier
Açu-jet pro	Brand
ArchitectTM	Abbott
BEP III (HBeAg measurement)	Siemens
Centrifuge 5920R	Eppendorf
CytoFLEX S	Beckman Coulter
ELISA-Reader infinite F200	Tecan
Flow cytometer FACS Canto II™	BD Biosciences
Freezing device	Nalgene / biocision Coolcell
Fusion Fx7	Peqlab
Incubator Heracell 150	Heraeus Holding GmbH
LightCycler® 480 II	Roche Diagnostics
1 °C freezing container	Nalgene
NanoDrop One	Thermo Scientific
Nanophotometer OD600	IMPLEN GmbH
Neubauer improved hemocytometer	Brand
Pipettes	Eppendorf
Shaker and incubator for bacteria	INFORS AG; Heraeus Holding GmbH
Sterile hood HERA safe	Thermo Scientific
T professional Trio Thermocycler	Analytik jena
Table-top centrifuge 5417R	Eppendorf
Thermo Mixer F1.5	Eppendorf
xCELLigence RTCA Single Plate	ACEA Biosciences
ÄKTApurifier (Protein Expression and Purification facility, HMGU)	GE healthcare lifesciences
Water bath WNB 10	Memmert GmbH
Agarose Gel electrophoresis device Bio Rad power bank basic	PegLab
SDS-Page device 40-0911	Biometra
Western Blotting device Trans Plot SD	Bio-Rad
Power supply for SDS-Page and WB E835	Consort

4.1.2 Consumables

Product	Supplier
Cell culture flasks, dishes, plates	TPP
Cell strainer 100 mm	Falcon
Cover glass 24 x 50 mm	VWR international
Cryo vials, Greiner Bio One	Merck
Cuvettes	Implen
ELISA 96-well plates Nunc MaxiSorb	Thermo Scientific
E-Plate (VIEW) 96	ACEA Biosciences
FACS 96-well V-bottom plates	Roth
Falcon tubes 15 ml / 50 ml	Greiner Bio One
Filter tips	Greiner Bio One
Filters 0.45 µm/0.2 µm	Sarstedt
FrameStar® 96 Well Semi-Skirted PCR Plates	4titude
Microvette 500 LH-Gel	Sarstedt
Needles	Braun
PCR tubes	Thermo Scientific
Pipette tips 10 ml – 1 ml	Biozym / Greiner Bio One / Gilson
Pipettes (disposable) 2, 5, 10, 25, 50 ml	Greiner Bio One
Reaction tubes 1.5 ml, 2 ml	Greiner Bio One, Eppendorf
Reagent reservoirs, sterile	Corning
Surgical Disposable Scalpels	Braun
Syringes	Braun
Gravity Flow columns (15 ml)	Bio-Rad
Amersham Hybond-P	GE healthcare lifesciences
Hi-Prep Sephacryl S-200 column (Protein Expression and Purification facility, HMGU)	GE healthcare lifesciences
HistoBond® adhesive microscope slides 76 x 26 x 1 mm	Paul Marienfeld GmbH & Co.KG
Whatman paper	GE healthcare lifesciences
Amicon Ultra 2ml Centrifugal filters 50 K	Merck
Stericup vacuum driven 0.45 µM	Merck

4.1.3 Chemicals and reagents

Product	Supplier
Acetic acid	Roth
Agarose	PeqLab
Ammonium persulfade (APS)	Roth
Ampicillin	Roth
Antibiotics/Antimycotics, 100x	ThermoFisher scientific
Biocoll separating solution (density 1.077 g/ml)	Biochrom
Blasticidin	Gibco
Bovine serum albumin (BSA)	Roth
Brefeldin A	Sigma-Aldrich
Cytofix/Cytoperm	BD Biosciences
Sodium dihydrogenic phosphate (NaH_2PO_4)	Roth
Dimethyl sulfoxide (DMSO)	Sigma-Aldrich
DMEM	Gibco
DMEM/F12	Gibco
DNA ladder 1kb / 100bp	Eurogentec
EDTA	Roth
Sodium hydroxide (NaOH)	Roth
Ethanol	Roth
Methanol (MetOH)	Roth
Imidazole	Sigma-Aldrich
Fetal calf serum (FCS)	ThermoFisher scientific
Fixable Viability Dye eF780	eBioscience
Coomassie brilliant blue-R250	Roth
Glycerol	Roth
Heparin-Natrium 25000	Ratiopharm
Page RulerPlus Protein standart (SDS-PAGE)	ThermoFisher scientific
Zeocin	Invivogen
Isopropanol	Roth
L-Glutamine, 200 mM	Gibco
LDS sample Buffer non-reducing (4x)	ThermoFisher scientific
LightCycler 480 SYBR green master mix	Roche
near-infrared live/dead	ThermoFisher scientific

FuGene HD	Promega
Mounting solution	Southern Biotech
Lipofectamine 2000	Invitrogen
Tris(hydroxymethyl)-aminomethan (TRIS)	Roth
6-aminocaproic acid	Sigma-Aldrich
2-Mercaptoethanol	Roth
Sodium chloride (NaCl)	Roth
Glycine	Roth
Propidium iodid	BD bioscience
CellTiter-Blue® Cell Viability Assay	Promega
Polyethylenglycol 6000 (PEG)	Merck
Trypsine	ThermoFisher scientific
Versene	ThermoFisher scientific
Wheat germ agglutinin (Alexa Flour 488 coupled)	ThermoFisher scientific
Collagen R Solution 0,2%, (10x)	SERVA
Phosphate Buffered Saline pH 7,4 (PBS)	ThermoFisher scientific
Minimum Essential Medium Non-essential amino acids (MEM NEAA) 100x	ThermoFisher scientific
Sodiumpyruvate (NaP) 100x	ThermoFisher scientific
Amersham ECL Prime Western Blotting Detection Reagent	GE healthcare lifesciences
Magnesium chloride	Roth
Magnesium sulfade	Roth
OptiMEM	ThermoFisher scientific
Milk powder	Roth
Peptone	Roth
Yeast extract	Roth
Tween 20	Roth
Ultra Pureprotogel	National diagnostics
Tryphan blue 0.4%	Sigma-Aldrich
Temed	Roth
3,3′,5,5′-Tetramethylbenzidin (TMB)	Invitrogen
SDSultra pure	Roth
Sulfuric acid (2 N)	Roth

Potassium chloride (KCl)	Roth

4.1.4 Buffers and solutions

Buffer	Ingredients/source	
ELISA assay diluent	1% BSA in PBS	
FACS buffer	0.1% BSA in PBS	
PBS-T	0.05% Tween 20 in PBS	
NPI-10 Adjust pH to 8.0 using NaOH	NaH_2PO_4 NaCl Imidazole	50 mM 300 mM 10 mM
NPI-20 Adjust pH to 8.0 using NaOH	NaH_2PO_4 NaCl Imidazole	50 mM 300 mM 20 mM
NPI-250 Adjust pH to 8.0 using NaOH	NaH_2PO_4 NaCl Imidazole	50 mM 300 mM 250 mM
Tris-acetate-EDTA buffer (50x)	Tris Acetic acid EDTA pH 8.0 in H2O	2 M 2 M 50 mM
SDS-Page running buffer (10x)	Tris Glycin SDS	250 mM 2 M 1%
Stacking gel buffer (SDS-PAGE) pH 6.8	Tris SDS In H2O	0.5 M 0.4%
Separation gel buffer (SDS-PAGE) pH 8.8	Tris SDS In H2O	1.5 M 0.4%
WB buffer A1	Tris MetOH In H2O	0.3 M 2%
WB buffer A2	Tris MetOH In H2O	25 mM 2%
WB buffer cathode buffer	Tris 6-aminocaproic acid MetOH In H2O	25 mM 40 mM 2%

Immunofluorescence blocking buffer	BSA PBS	5%
3x reducing loading dye (SDS PAGE)	Tris-HCL pH 6.8 Glycerine 20% SDS 2-Mercaptoethanol H2O	2.5 ml 10 ml 10 ml 5 ml 2.5 ml
ELISA assay diluent Immunofluorescence washing buffer	BSA In PBS	1%
ELISA coating buffer	PBS	
SDS Page stacking gel (5 ml)	H_2O Lower buffer Acrylamide 30% Temed 10% APS	2.975 ml 1.3 ml 0.67 ml 0.005 ml 0.05 ml
SDS Page 12% separation gel (10 ml)	H_2O Lower buffer Acrylamide 30% Temed 10% APS	3.2 ml 2.7 ml 4 ml 0.01 ml 0.1 ml
SDS Page 8% separation gel (10 ml)	H_2O Lower buffer Acrylamide 30% Temed 10% APS	4.6 ml 2.7 ml 2.6 ml 0.01 ml 0.1 ml
10x FastDigest buffer	ThermoFisher scientific	
10x Shrimp alkaline phosphatase buffer	ThermoFisher scientific	
Coomassie staining solution	H_2O MetOH Acetic acid CBB-R250/G250	50% 40% 10% 0.1%
Coomassie de-staining solution	H_2O MetOH Acetic acid	50% 40% 10%
10x T4 ligase buffer	ThermoFisher scientific	
4x non-reducing loading dye (SDS-PAGE)	ThermoFisher scientific	

4.1.5 Enzymes

Product	Supplier
Shrimp alkaline phosphatase	ThermoFisher scientific
T4 Ligase	ThermoFisher scientific

AarI Fast Digest	ThermoFisher scientific
AflI Fast Digest	ThermoFisher scientific
XhoI Fast Digest	ThermoFisher scientific
BamHI Fast Digest	ThermoFisher scientific
RsrII Fast Digest	ThermoFisher scientific
ApaI Fast Digest	ThermoFisher scientific
HindIII Fast Digest	ThermoFisher scientific
Kpn2I	ThermoFisher scientific
PvuI	ThermoFisher scientific
T5 exonulcease	New England Biolabs
EcoRI	ThermoFisher scientific

4.1.6 Proteins and virus

Protein	Source
HBsAg, serotype adw from human serum	Roche
hIL-12	Peprotech
Hyper-IL6	Institut für molekulare Immunologie TUM
subviral particles	AG Protzer
HBV	AG Protzer

4.1.7 Kits

Product	Supplier
ARCHITECT anti-HBsAg Reagent Kit	Abbott
BD OptEIA TNF ELISA Set	BD Biosciences
Enzygnost HBe	Siemens
FoxP3 Staining Kit	eBioscience
GeneJet Gel Extraction Kit	ThermoFisher scientific
GeneJet Plasmid Miniprep Kit	ThermoFisher scientific
hIFNγ uncoated ELISA Kit	ThermoFisher scientific
hIL-2 uncoated ELISA Kit	ThermoFisher scientific
Murex ELISA Version 3	DiaSorin
Phusion Hot Start Flex 2x Master Mix	New England Biolabs

Plasmid Plus Midi Kit	Qiagen
Protino Ni NTA beads	Macherey-Nagel
NucleoSpin® Tissue Kit	Macherey-Nagel
LEGENDplex Mulite-Analyte Flow Assy Kit	BioLegend

4.1.8 Cell lines and bacteria

Cell line	Description	Source
CHO-K1	Chinese hamster ovary cells for recombinant protein expression, deficient for proline synthesis	AG Protzer
HEK 293	Human embryonic kidney cells for recombinant protein expression	AG Protzer
HepG2 NTCP K7	Human hepatoma cell line with transgenic expression of human NTCP	AG Protzer
Huh7	Human hepatoma cell line	AG Protzer
Huh7S	Huh7 cells expressing the small HBV envelope protein	AG Protzer
One Shot® Stbl3	Chemically competent *E. coli* for transformation	ThermoFisher scientific

4.1.9 Antibodies

Product	Dilution	Supplier
Anti-6x His Tag antibody (ab18184)	1:500/1:5000	Abcam
anti-6x His-Tag antibody HRP-conjugate	1:500	Invitrogen
Erbitux (Cetuximab)	-	Merck
Goat anti-human Ig (H+L), HRP conjugate	1:1000	Southern Biotech
Goat anti-mouse IgG, HRP conjugate	1:1000/1:10000	Sigma-Aldrich
hCCR7 BV650, clone G043H7	1:20	BioLegend
hCD25 PE, clone M-A251	1:20	BD Biosciences
hCD28 (for co-stimulation in culture)	-	eBiosciences
hCD3 AF700, clone UCHT1	1:50	BD Biosciences
hCD4 FITC, RPA-T4	1:5	BD Biosciences
hCD4 PE-eFlour 610, clone RPA-T4	1:20	ThermoFisher scientific
hCD45RA APC, clone HI100	1:20	BioLegend

hCD45RO PE, clone UCHL1	1:20	BioLegend
hCD62L PE-Cy7, clone DREG-56	1:20	BioLegend
hCD8 APC, clone SK1	1:20	BD Biosciences
hCD8 PB, clone SK1	1:50	BioLegend
hgrzB PE, clone GB11	1:40	ThermoFisher scientific
hIFNγ AF700, clone B27	1:40	BD Biosciences
hIL-2 FITC, clone MQ1-17H12	1:40	BD Biosciences
hLAMP1 Alexa Flour 488, clone H4A3	1:20	ThermoFisher scientific
hTNFα eFlour 450, clone Mab11	1:40	ThermoFisher scientific
StrepMAb classic, HRP conjugate	1:500/1:4000	IBA GmbH
Donkey anti-rabbit IgG PE	1:10	BD Biosciences
Rabbit anti-HBc serum	1:4000	Michael Nassal

4.1.10 Primers

Primers were purchased from Microsynth AG, Balgach, Switzerland.

Name of Primer	Sequence
C8_hinge_AflII_fwd	GATCCTTAAGATGGATTTTGAGGTGCAGATTTTC
C8_hinge_rev	TGGGCACGGTGGGCATGTGT
cccDNA_fwd	GCCTATTGATTGGAAAGTATGT
cccDNA_rev	AGCTGAGGCGGTATCTA
CD28 AarI fwd	GATCCACCTGCGATCACTAGTCAGGTC
CD28 AarI rev	GATCCACCTGCGATCGATGCCGTTTGATCTC
CD28_pA1_KC_L1_AarI_fwd	GATCCACCTGCGATCGGGGGAGGGGGCAGCACTAGTCAG
CD28_pA1_KC_L1_AarI_rev	GATCCACCTGCGATCGAGCTCACCGTTTGATCTCCAGCTTGG
CD3_AarI_fwd	GATCCACCTGCGATCGGCGGAGGGGGCTCTGGCGGCGGAGGGTCTGGGGGAGGGGGCAGCACTAGTCAGGTGC
CD3_AarI_rev	GATCCACCTGCGATCCTCAATTGATTTCCAG
CD3_pA1_HC_CH1_AarI_fwd	GATCCACCTGCGATCGGGGGAGGGGGCAGCACTAGTCAGGTGC
CD3_pA1_HC_CH1_AarI_rev	GATCCACCTGCGATCGAGCTCAATTGATTTCCAGCTTGGTGCCC
fusion_upstream_AflII_fwd	GATCCTTAAGGCCACCATGGACTTCGAG

HC_CH1_Kpn2I_fwd	GATCTCCGGAGGCGGAGGGTCTGAGGTGC AACTG
HC_CH1_XhoI_rev	GATCCTCGAGACAAGATTTGGGCTCCACTTT
HC_XhoI_rev	GATCCTCGAGTCAATGGTGGTGATGGTGGT GGTGATGGTGGTGGTTGAT
hinge_CD28_fwd	GAGCCCAAATCTTGTGACAAAACTCACACAT GCCCACCGTGCCCAGGAGGCGGAGGGTCT GGCGGAGGGGGGAGCACTAGTCAG
hinge_CD28_XhoI_rev	GATCCTCGAGCTACCGTTTGATCTCCAGCTT GGTC
KC_LC_Kpn2I_fwd	GATCTCCGGAGGCGGAGGGTCTGACATTGT GATGACCC
KC_LC_XhoI_rev	GATCACTCGAGCGCACTCGCCCCGGTTG
LC_AflII_fwd	GATCCTTAAGGCCACCATGGATTTTGAAGTG CAG
LC_XhoI_rev	GATCCTCGAGTCATTTCTCGAACTGGGGGT G
p84 AarI fwd	GATCCACCTGCGATCCATCACCACCAT
p84 AarI rev	GATCCACCTGCGATCTAGTGCTGCCCCCTC C
pA1_C8_HC_VD_CD3_AarI_fwd	GATCCACCTGCGATCGCTCGAGTCTAGAGG GCACG
pA1_C8_HC_VD_CD3_AarI_rev	GATCCACCTGCGATCCCCCAGAGCCCCCTC CGCCAACTTTCTTGTCCACCTTGG
pA1_C8_KC_LC_CD28_AarI_fwd	GATCCACCTGCGATCGCTCGAGTCTAGAGG GCACG
pA1_C8_KC_LC_CD28_AarI_rev	GATCCACCTGCGATCCCCCAGAGCCCCCTC CGCCGCACTCGCCCCGGTTGAAGCTCTTGG
pB_AarI_fwd	GATCCACCTGCGATCTGAGAATTCTAGCTCG AG
pB_AarI_rev	GATCCACCTGCGATCCGCCAGACCCTCCGC CGCCAGAGCCCCCTCCGCCGCACTCGCCC CGGTTGAAGCTCTTGG
Prp_fwd	TGCTGGGAAGTGCCATGAG
Prp_rev	CGGTGCATGTTTTCACGATAGTA
rcDNA_fwd	GTTGCCCGTTTGTCCTCTAATTC
rcDNA_rev	GGAGGGATACATAGAGGTTCCTTGA
TriMAb_hinge_AarI_fwd	GATCCACCTGCGATCTCCTGCGGAGGCGGC GGATCTGGTGGTGG
TriMAb_hinge_AarI_rev	GATCCACCTGCGATCAGGACTTGGGTTCCA CTTTCTTGTCCACCTTGGTATTGGAGGGC

WA468	CTCTCTGGCTAACTAGAGAACCCACTGC
WA469	GAAAGGACAGTGGGAGTGGCACCTTC
WA579	GGCTGCCTGGTGAAGGACTACTTC
WA580	GACAAGAGCAGCTCCACAGCCTATATG
WA609_5F9_LC_fwd	GTGCTCTGGATCCCTGGAGCCATTGGGGAC ATTGTGATGACCCAGTCGCACAAATTC
WA610_5F9_LC_rev	CAGCCACGGTCCGTTTTATTTCCAGCTTGGT CCCCCCTCCGAAC
WA613_5F9_HC_fwd	AAACTTAAGCTTCTCAACATGAACTTAGGGC TCAGCTTCATTTTCCTTG
WA614_5F9_HC_rev	ACGCTTGGGCCCTTGGTGCTGGCTGAGGAG ACTGTGAGAGTGGTGCCTTG

4.1.11 Plasmids

Name of plasmid	Number in plasmid bank	Source
p84 based on pcDNA3.1 (Invitrogen)	1142	provided by Sandra Lüttgau
pHBVenv_small (pSVBX24H)	1145	provided by Volker Bruß
pmCherry_HBVenv	523	provided by Volker Bruß
pA1_scFvC8	277	Master`s Thesis Francesca Pinci
pB1_scFvC8	279	Master`s Thesis Francesca Pinci
p84_FabMAbαCD3	1146	generated in thesis
p84_FabMAbαCD28	1147	generated in thesis
pA1_HC_5F9	1148	generated in thesis
pA1_HC_5F9_scFvCD28	1155	generated in thesis
pA1_C8_HC_CH1_scFvCD3 = pA1_TriMAb_HC	1150	generated in thesis
pA1_C8_KC_LC_scFvCD28 = pA1_TriMAb_LC	1151	generated in thesis
pA1_C8_CH1_hinge_scFvCD28 = pA1_OKTriMAb_HC	1152	generated in thesis
pB1_C8_LC_scFvCD3 = pA1_OKTriMAb_LC	1153	generated in thesis
pA1_scFv_CD28	1155	generated in thesis
p84_TriMAb_hinge	1157	generated in thesis

pA1_TriMAb_HC	1158	generated in thesis
pA1_Blasti_TriMAb_LC	1159	generated in thesis

4.1.12 Media

Medium	Ingredients	
DMEM full medium	DMEM	500 ml
	FCS	50 ml
	Pen/Strep, 10,000 IU/ml	5.5 ml
	L-Glutamine, 200 mM	5.5 ml
	NEAA, 100x	5.5 ml
	Sodium pyruvate, 100 mM	5.5 ml
DMEM/F12 full medium	DMEM/F12	500 ml
	FCS	50 ml
	Pen/Strep, 10,000 IU/ml	5.5 ml
	L-Glutamine, 200 mM	5.5 ml
	NEAA, 100x	5.5 ml
	Sodium pyruvate, 100 mM	5.5 ml
Freezing medium	FCS	90%
	DMSO	10%
HepG2 Diff. medium	DMEM	500 ml
	FCS	50 ml
	Pen/Strep, 10,000 IU/ml	5.5 ml
	L-Glutamine, 200 mM	5.5 ml
	NEAA, 100x	5.5 ml
	Sodium pyruvate, 100 mM	5.5 ml
	DMSO	10.5 ml
RPMI full medium	RPMI	500 ml
	FCS	50 ml
	Pen/Strep, 10,000 IU/ml	5.5 ml
	L-Glutamine, 200 mM	5.5 ml
	NEAA, 100x	5.5 ml
	Sodium pyruvate, 100 mM	5.5 ml
Lysogen Broth (LB)-Medium	NaCl	9 g/l
	Peptone	10 g/l
	Yeast extract	5 g/l
	Agar (optional)	14 g/l
	In H_20	
Super optimal broth (SOB) medium	LB medium with	
	Potassium chloride	2.5 mM
	Magnesium chloride	10 mM
	Magnesium sulfide	10 mM

4.1.13 Mouse strains

Mouse strain	Source
C57BL/6	AG Protzer

4.1.14 Software

Software	Application	Supplier
FlowJo, Version 10.4	Flow cytometry analysis	BD Biosciences
ImageJ	Purity calculation of Coomassie stains	National Institutes of Health
LightCycler 480 SW 1.5.1	qPCR analysis	Roche
Prism 5.01	Graph design, statistical calculation	Graphpad Software inc.
RTCA software 2.0	xCELLigence viability analysis	ACEA Biosciences
Serial cloner	DNA and protein analysis	SerialBasics

4.2 Methods

4.2.1 Cloning strategy for bi- and trispecific constructs

4.2.1.1 FabMAbαCD3 and FabMAbαCD3

FabMAbαCD3 was cloned by exchanging the heavy and light chain of the construct CD22xOKT3 (V_HCD22_huCH1γ_$(G_4S)_3$_V_HOKT3_$(G_4S)_3$_VκOKT3_10xHis_P2A_ V_LCD22_huCH1κ) provided by Gerhard Moldenhauer/Sandra Lüttgau, with the variable domains of the HBs-specific murine antibody 5F9. Therefore, variable domains were amplified from cDNA (provided by Forough Golsaz Shirazi) via PCR using the primers WA613_5F9_HC_fwd and WA614_5F9_HC_rev for the heavy chain as well as WA609_5F9_LC_fwd and WA610_5F9_LC_rev for the light chain. The PCR fragments were inserted into p84 (based on pcDNA3.1, Invitrogen) by usage of the unique restriction sites ApaI/HindIII in case of the heavy chain and BamHI/RsrII in case of the light chain. To exchange the scFvOKT3 for scFvCD28, the restriction site AarI was introduced via PCR using the primers CD28 AarI fwd, CD28 AarI rev, and the template pA1_CD28 as well as p84 AarI fwd, p84 AarI rev, and the template p84_FabMAbαCD3, resulting in the two fragments AarI_ scFvCD28_AarI and AarI_10xHis_P2A_V_L5F9_ huCH1κ_backbone_V_H5F9_huCH1γ_$(G_4S)_3$_AarI. The ligation of the two fragments resulted in the construct FabMAbαCD28. The correct sequence was verified by Sanger sequencing (Eurofins, GATC) using the primers WA468, WA469, WA597 and WA580.

4.2.1.2 TriMAb

The heavy chain was amplified by PCR employing the two primers HC_CH1_Kpn2I_fwd and HC_CH1_XhoI_rev on the template pA1_HC_5F9. The PCR fragment was inserted into the plasmid pA1_scFvC8 using the restriction sites Kpn2I and XhoI, resulting in the interim construct pA1_scFvC8_HC_CH1. To introduce the scFvOKT3, the restriction site AarI was introduced via PCR using the primers CD3_pA1_HC_CH1_AarI_fwd and CD3_pA1_HC_ CH1_AaeI_rev on the template p84_FabMAbαCD3 as well as pA1_C8_HC_CH1_CD3_AarI_fwd and pA1_C8_HC_CH1_CD3_AarI_rev on the template pA1_scFvC8_HC_CH1, resulting in the two fragments AarI_scFvCD3_AarI and AarI_BB_C8_HC_CH1_AarI. The ligation of the two fragments resulted in the construct C8_HC_CH1_scFvCD3. The same procedure was repeated for the light chain using the primers KC_LC_Kpn2I_fwd and KC_LC_XhoI_rev on pB_LC_5F9, following insertion into pA1_scFvC8 which resulted in the interim construct pA1_scFvC8_KC_LC. The scFvCD28 was introduced via PCR using the primers CD28_pA1_KC_L1_AarI_fwd and CD28_pA1_KC_L1_AarI_rev on the template p84_FabMAbαCD28 and pA1_C8_KC_LC_CD28_AarI_fwd and pA1_C8_ KC_LC_CD28_AarI_rev on the template pA1_scFvC8_KC_LC, resulting in the fragments Aar1_scFvCD28_Aar1 and AarI_BB_C8_KC_LC_AarI. The ligation of the two fragments generated the construct C8_KC_LC_scFvCD28.

4.2.1.3 Sequence optimization of TriMAb

Since TriMAb was chosen as lead candidate, the sequence was optimized for expression in CHO cells (GeneArt, Thermofisher Scientific). The heterodimeric construct was designed as one open reading frame with both chains being separated by a P2A site. Moreover, the heavy chain was equipped with a 6x His Tag and the light chain with a Strep Tag II. The sequence included the terminal restriction sites AflII and EcoRI, which allowed one-step sub-cloning into the vector p84. However, the GenaArt sequence lacked the amino acids EPKSC of the hinge domain and therefore disulfide bond formation between heavy and light chain could not occur. These AA were introduced via PCR with the primers TriMAb_hinge_AarI_fwd and TriMAb_hinge_AarI_rev, digestion with AarI, and self-ligation of generated fragment, which resulted in the constructs p84 TriMAb_hinge. Moreover, heavy and light chain were sub-cloned in two different expression plasmids, as this could provide a higher expression efficiency (see 2.4.3.1). The chains were amplified via PCR using the primers fusion_upstream_AflII_fwd and HC_XhoI_rev as well as LC_AflII_fwd and LC_XhoI_rev and inserted into the plasmids pA1 and pA1_Blasti, respectively. During amplification of the heavy chain, 4 further histidines were added to the n-terminus of the sequence, resulting in a 10x His Tag.

4.2.1.4 OKTriMAb

The heavy chain C8_CH1_hinge_scFv_CD28 was generated by insertion of the PCR fragment C8_hinge_CD28_fusion into the backbone pA1_scFv_C8 using the restriction sites AflII and XhoI. The PCR fragment was created through fusion PCR, combining the fragment C8_hinge amplified with the primers C8_hinge_AflII_fwd and C8_hinge_rev employing the template pA1scFvC8 and the fragment hinge_scFvCD28 was generated with the primers hinge_CD28_fwd and hinge_CD28_XhoI_rev using the template pA1_HC_5F9_CD28. The light chain C8_LC_scFv_CD3 was constructed through ligation of the PCR fragments AarI_scFvCD3_AarI generated with the primers CD3_AarI_fwd, CD3_AarI_rev, and the template p84_FabMAbαCD3, and the fragment AarI_BB_C8_LC_AarI amplified with the primers pB_AarI_fwd and pB_AarI_rev, using the template pB1_scFvC8.

4.2.2 Molecular cloning methods

4.2.2.1 Culturing and transformation of Escherichia coli (E. coli)

For transformation and cloning, One Shot® Stbl3™ chemically competent *E. coli* cells were used. For transformation, 90 µl of freshly thawed cell suspension were mixed with 10 µl ligation product and incubated for 15 min on ice. For re-transformation 1 µg plasmid DNA was used. After a heat shock at 42 °C for 90 seconds (sec), 400 µl of SOB medium were added and bacteria were incubated for 45 min at 37 °C and 230 rpm. Then, cells were centrifuged in a table-top centrifuge 5417R (5 min, 600 xg), 400 µl of supernatant were discarded, and the pellet was re-suspended. Finally, the suspension was plated on LB-agar plates containing the appropriate antibiotic for selection. The working concentration of Ampicillin and Kanamycin was 50 µg/ml. Clones were picked with 10 µl pipette tips and transferred to a 3 ml LB medium supplemented with the respective

antibiotic. Suspension cultures were placed in a shaker at 300 rounds per minute (rpm) and incubated at 37 °C over night.

4.2.2.2 Polymerase chain reaction (PCR)

PCR was performed using the Phusion Hot Start Flex 2 Master Mix (NEB) with 20 pmol/µl of each primer and 1-5 µg template DNA. Temperature and duration of the cycles were performed according to the provided protocol. The optimal annealing temperature was assessed by the TM-calculator software of New England Biolabs (https://tmcalculator.neb.com/#!/main). Amplification was performed in a T Professional Trio Thermocycler and efficiency was analyzed by agarose gel-electrophoresis (1% Agarose) and the Fusion Fx7 gel-documentation device (PeqLab). Upon successful amplification, the product was purified using the Gene Jet Plasmid Gel Extraction Kit (ThermoFisher scientific). Purified DNA was either directly digested or stored at -20 °C. All primers for cloning are listed in 4.1.4.

2.2.3.5 Digestion and Ligation

For cloning, FastDigest enzymes (ThermoFisher scientific) were used. Digestion was performed according to the manufacturers' protocol and results were analyzed by agarose gel electrophoresis. Upon successful digestion, the respective fragments were cut out from the gel and purified using Gene Jet Plasmid Gel Extraction Kit (ThermoFisher scientific). Backbones of vectors were dephosphorylated using shrimp alkaline phosphatase (ThermoFisher scientific) according to the manufacturers' protocol. Ligation was performed with T4 Ligase (ThermoFisher scientific) according to the following protocol. First 100 ng of vector were mixed with a 5-fold excess of insert (regarding molarity not weight) and combined with 1 µl of 10x T4 Ligase Buffer and T4 Ligase. A final volume of 10 µl was adjusted by addition of H_2O millipore. Incubation took place for 1 hour at room temperature (RT, 23 °C). To control for vector re-ligation, the reaction was also performed without insert. Subsequently samples were transferred into *E. coli.* After incubation for 12 hours, clones were picked from the plate and cultivated in 3 ml LB medium under antibiotic selection.

4.2.2.3 Preparation of Plasmid-DNA

For preparation of plasmid DNA, the Gene Jet Plasmid Miniprep Kit and 2 ml of bacterial suspension were used. For higher DNA amounts (required for transfection of mammalian cells), the Plasmid Plus Midi Kit (Qiagen) and 100 ml of bacterial suspension were employed. All steps were performed according to the provided manuals. Afterwards, an aliquot of purified DNA was checked by control digestion and gel-electrophoresis. The concentration and quality of the preparation were determined with Nano Drop One (ThermoFisher scientific). Clones that showed appropriate migration patterns upon control digestion were sent for sequencing. Finally, all DNA samples were stored at -20 °C.

4.2.2.4 Sequence analysis

To obtain the sequence of generated PCR products and constructs, DNA was sent to GATC Biotech (now Eurofins: https://www.eurofinsgenomics.eu/). Planning of cloning

procedures and alignments were performed using serial cloner software (serialbasics.free.fr/Serial_Cloner).

4.2.3 Culture and transfection of mammalian cells

4.2.3.1 Cell culture

Human cell lines (HEK 293, Huh7, HepG2 NTCP) were cultured in Dulbecoo`s Minimum essential medium (DMEM, supplemented with 10% fetal bovine serum, 50 U/ml penicillin/streptomycin, 2 mM L-glutamine, 1% sodium pyruvate and 1% non-essential amino acids (NEAA), all from Life Technologies, referred to as DMEM full medium) using T25 or T75 cell culture flasks (TPP) and split every 3 to 4 days depending on their confluency. CHO K1 cells were cultured in DMEM/F12 medium and PBMC were cultured in Roswell Park Memorial Institute medium (RPMI), both with the same supplements as DMEM. Media with corresponding supplements are listed in 4.1.6. All cell lines were analyzed by microscopy once per day and their condition was assessed based on growth and morphology.

4.2.3.2 Preparation of peripheral blood mononuclear cells (PBMC)

Fresh blood was mixed with heparin to avoid coagulation, and diluted 1:1 with pre-warmed RPMI wash medium (50 U/ml penicillin/streptomycin). All centrifugation steps were performed in a 5417R (Eppendorf) at RT. 25 ml of the mixture were layered onto 13 ml Biocoll Separating solution with a density of 1.077 g/ml (Millipore, Merck), without mixing the two phases. After centrifugation at 1200 xg for 25 min without break, the PBMC were isolated and transferred to a 50 ml falcon tube. Two lymphocyte rings were pooled and the volume was adjusted to 40 ml by adding RPMI wash medium. The isolated PBMC were centrifuged for 10 min at 700 xg at RT and the pellet was resuspended in 40 ml RPMI wash medium. Next, PBMC were centrifuged at 80 xg with break 5 for 20 min. Two pellets were pooled and the volume was adjusted to 40 ml using RPMI wash medium. After a final centrifugation for 5 min at 350 xg, the cell number was determined and the concentration was adjusted to $2x10^6$ cells/ml. Cells were either frozen at -80 °C or rested overnight at 37 °C. After resting, PBMC were employed in co-cultures and referred to as “freshly isolated PBMC”.

4.2.3.3 Freezing and thawing of mammalian cells

For freezing, ~1 x 10^7 cells were resuspended in 500 µl FCS containing 10% dimethyl sulfoxide (DMSO, Sigma), transferred to a Greiner Cryo.S vial (Merck), placed in a 1 °C freezing container (Nalgene) and stored at -80 °C. For thawing, 1 ml of pre-warmed medium was added “drop by drop” to the partially defrosted cell suspension. The vial was inverted 5 times and the cells suspension was carefully transferred into a 50 ml flacon tube containing 25 ml of pre-warmed medium. After centrifugation for 5 minutes at 350 xg, cells were resuspended in medium and either counted and rested overnight (PBMC) or seeded in cell culture flasks (human and hamster cell lines).

4.2.3.4 Cell counting

To determine the cell number, cells were trypzinized and 10 µl of single cell suspension were diluted 1:1 with trypan blue (Sigma-Aldrich) and counted employing a Neubauer counting chamber (Brand).

4.2.3.5 Transfection of mammalian cells

Huh7 and HEK 293 cells were transfected with Lipofectamine® 2000 Reagent (ThermoFisher scientific) and CHO-K1 with FuGene HD (Promega) according to the manufacturers' protocol. Transfection was performed in the 6-well format (TTP). Cells were analyzed for transgene expression 24-48 hours after transfection.

4.2.3.6 Generation of stable cell lines

To achieve stable cells lines, plasmids were linearized via PvuI digestion and transfection was performed according to the protocol in 4.2.3.3. Thereupon, cells were selected using 400-600 µg/ml of Zeocin or 4-6 µg/ml Blasticidine for several days, until single clones were detectable on the plate. TriMAb cell lines got co-transfected with two plasmids, and consequently, selected with both antibiotics at once. The clones were trypsinized and transferred to a 48-well plate, where they were cultivated further. After reaching 100% confluency under selection pressure, the supernatants of the clone were checked for presence of bispecific constructs via ELISA. Positive clones were subjected to a single cell dilution. The cell concentration was adjusted to 2.5 cells/ml and 200 µl/well of the cell suspension were transferred to a 96-well plate. Cells were cultured for 2-4 weeks until single clones reached a confluency of 100%. The different clones were compared for antibody secretion and high-producing clones were isolated and transferred to T25 cell culture flasks. Producer cell lines were finally used for the production of antibodies or stored at -80 °C.

4.2.4 Antibody production and purity analysis

4.2.4.1 Production of bsAbs

BiMAbs were ordered from Proteros Biostructures, Martinsried, Germany. After expression in HEK293 cells, the constructs were purified with a combination of ion-exchange chromatography (IEX) and size exclusion chromatography (SEC). FabMAbs were produced by InVivo Biotech Services, Henningsdorf/Berlin, Germany. Constructs were expressed in HEK293 cells and purified a combination of metal chelate affinity chromatography (IMAC) and SEC. The protein concertation of the samples was determined with Nano Drop 1 (Protein→A280→IgG).

To remove the FabMAbαCD3 aggregates, a second SEC was performed at the protein expression and purification facility (German Research Center for Environmental Health) under the direction of Dr. Arie Geerlof using a HiPrep Sephacryl S-200 column, an ÄKTA purifier and a flow rate of 1.3 ml/min. In total, two runs with a total volume of 5 ml were performed and 24 fractions were collected, respectively. Following Coomassie staining analysis, fractions D7 till E1 were pooled and stored at 4 °C.

4.2.4.2 Expression and purification of TriMAb

The TriMAb producer cell line used for the purification studies was generated on the basis of CHO cells and transfected with two separate plasmids encoding for the heavy and light chain, respectively (see 2.4.3). A clonal producer cell line was established via single cell dilution and antibody expression was performed in a hyperflask (Cornig®, Sigma-Aldrich, Merck) according to the following protocol. Producer cell lines from 3 confluent T150 flasks were pooled, seeded into the hyperflask und cultured with DMEM/F12 medium containing 10% FCS for 48 hours. After 48 hours, the medium was changed to DMEM/F12 without FCS. The supernatant was collected, filtered (0.2 µM, Sarstedt) and stored at 4 °C. Cells were cultured for 48 hours without FCS and the supernatant was collected and filtered. In the following, both supernatants were used for the purification procedure employing Protino® Ni-NTA beads (Macherey-Nagel). The puffers NPI-10, NPI-20, and NPI-250 were prepared according to the manufacturer's protocol. The experimental procedure was based on 4.3 of the manufacturer's protocol "Batch purification of polyhistidine-tagged proteins under native conditions", but was slightly modified. Equilibration was performed according to the provided protocol. For batch binding 2 ml of original 50% solution were used per 250 ml of supernatant. Batch binding took place at 4 °C either for 2 hours or overnight on a rolling incubator. After batch binding the beads were transferred to 20 ml gravity flow columns (BioRad) and washed by addition of 10 bed volumes (10 ml) of NPI-20. Finally, 5 ml of NPI-250 elution puffer were added to the column and 5 fraction of 1 ml each were collected and analyzed by HBsAg-ELISA. The first 2 fractions were pooled and concentrated to a total volume of 100 µl employing centrifugal filters with a 30 kD cut-off (Merck). Concentrated TriMAb samples were stored at 4 °C.

4.2.4.3 SDS-polyacrylamide gel electrophoresis and Western blot analysis

SDS-Page and Western Blot (WB) analysis were performed to analyze the purity and integrity of the bi- and trispecific antibodies. 2.5 µg of purified antibody (BiMAbs, FabMAbs) or 15 µl of sample (TriMAb) were separated on a 12.5% SDS-Page under reducing and non-reducing conditions and stained with Coomassie CCB R250 (Roth). For analysis of TriMAb samples 8% acrylamide were employed. Since the protein concentration varied greatly, 15 µl of the 0% FCS sample and 3.5 µl of the 10% FCS sample were loaded. WB analysis was performed with 100 ng of protein. Samples were separated by PAGE as described above and transferred to a polyvinylidene fluoride membrane (Millipore) at 20 V for 1 hour. After blocking with 5% dry skimmed milk (Roth) in phosphate-buffered saline (PBS, ThermoFisher scientific) containing 1% Tween-20 (PBST, Roth) for 1 hour at room temperature (RT), membranes were incubated with a goat anti human IgG HRP conjugate (Sigma) diluted 1:10000 in PBST containing 5% milk overnight at 4 °C. Following 3 washing steps with PBST for 10 minutes each, membranes were incubated with Amersham ECL Prime Western Blotting Detection Reagent (GE) and bands were visualized in an ECL chemocam (Intas). The TriMAb LC was detected with the StrepMAb classic (IBA Life sciences) 1:2000 in PBST containing 5% milk. The TriMAb heavy chain was detected with a

combination of an anti-6x His Tag antibody (ab18184, Abcam) 1:5000 and a goat anti-mouse IgG HRP conjugate 1:10000 (Sigma-Aldrich, Merck), both in PBST containing 5% milk. The primary antibody was incubated at 4 °C overnight. After three washing steps with PBST for 10 minutes the secondary antibody was incubated for 1 hour at RT. Visualization of bands was performed as mentioned above.

4.2.5 Antibody binding-studies

4.2.5.1 ELISA for analysis of HBsAg-binding

ELISAs were performed in 96-well MaxiSorp plates (ThermoFisher scientific). HBsAg from patient serum (kindly provided by Roche) was added in PBS (100 µl; 1 µg/ml) and incubated overnight at 4 °C. From now on, all incubation steps were performed on a thermomixer compact (Eppendorf) at 300 rounds per minute (rpm). After 4 washing steps with PBS 0.5% tween (PBST), plates were blocked with 200 µl assay diluent (PBS containing 1% bovine serum albumin BSA, Roth) for 1 hour at RT. The plates were washed 4 times with 200 µl PBST and supernatant of PCLs or a dilution series of purified antibodies (1000, 316.2, 100, 31.62, 10, 3.162, 1, 0.316, 0.1, 0.031, 0.01, 0.003 nM) was applied in 100 µl assay diluent, followed by incubation for 1.5 hours. After 4 washing steps with PBST, 100 µl of goat anti human IgG HRP conjugate diluted 1:1000 in assay diluent were added to the plates and incubated for 1 hour. For detection of individual TriMAb chains, a combination of mouse anti-His Tag 1:500 (Abcam) and goat anti-mouse 1:1000 (Sigma-Aldrich) or StrepMAb classic-HRP 1:500 and goat anti-mouse 1:1000 was employed. After 5 final washing steps with PBST, the ELISA was developed by addition of 100 µl stabilized chromogen TMB (Life technologies) and the reaction was stopped with 100 µl 2N sulfuric acid (Roth). The OD was determined at 450 nm and background subtraction 560 nm employing an infinite F200 reader (Tecan)

4.2.5.2 HBsAg-genotype ELISA

To analyze the binding capacity to several HBsAg genotypes, a modified protocol of the Murex HBsAg Version 3 (DiaSorin) was conducted using the provided stripes. 25 µl sample diluent (provided with the kit) were transferred to the stripes, followed by addition of 75 µl assay diluent (1% BSA in PBS) containing either 1 IU (for FabMAb) or 5 IU (for BiMAb) antigen from an HBsAg-genotype panel (Paul-Ehrlich-Institute). The stripes were incubated for 1 hour at 37 °C and 50 nM FabMAb or 100 nM BiMAb were added in 25 µl assay diluent. After incubation for 30 min at 37 °C, antibodies were detected with an anti-6x His-Tag antibody HRP-conjugate (Invitrogen) diluted 1:500 (FabMAbs) or a StrepMAb classic-HRP diluted 1:4000 (BiMAb). Detection antibodies were applied in 25 µl assay diluent and incubated for 30 min at 37 °C. The stripes were washed 4 times and developed as mentioned in 4.2.5.1.

4.2.5.3 Confocal microscopy to visualize binding of bsAbs to HBVenv on membranes

$0.7x10^6$ Huh7 cells were seeded in a 6-well plate (TPP) and cultured for 24 hours until they reach a confluency of ~ 80%. Next, the cells were transfected with 5 µg mCherry-HBVenv plasmid DNA (kindly provided by Volker Bruss, German Research Center for Environmental Health, Munich) using FuGene HD according to the manufacturer's protocol. The transfected cells were cultured and monitored for 48 hours at 37 °C and the immunofluorescence staining was performed as described in the following. The cells were treated with 500 µl trypsin for 10 min and resuspended extensively after adding of 1 ml DMEM full medium to generate single cell suspensions. Cells were centrifuged at 500 xg for 2 min at 4 °C in a centrifuge 5417R. From now on, all steps were performed on ice to prevent internalization of antibodies. The supernatant was decanted and the pellet was resuspended in 1 ml blocking buffer (5% BSA in PBS) following incubation for 1 hour. Subsequently, the cells were washed 3 times using assay diluent (1% BSA in PBS) and incubated with 50 nM of bsAbs in 200 µl assay diluent for 1.5 hours. Cells were washed 3 times following incubation with 200 µl of a 1:1 dilution of Alexa Fluor 647 goat anti-human IgG (ThermoFisher scientific), 1:500 in assay diluent, and an Alexa 488 coupled wheat germ agglutinin (ThermoFisher scientific), 1:400 in assay diluent for 45 min. After 3 washing steps, cells were incubated with 4% paraformaldehyde in PBS (ChemCruz) for 15 min. After 3 washing steps, cells were resuspended in 100 µl mounting solution (Southern Biotech), transferred to HistoBond® adhesive microscope slides (Paul Marienfeld) and covered with borosilicate glass (VWR international). After overnight storage in the dark at 4 °C, the slides were analyzed employing a Fluoview FV10i (Olympus).

4.2.5.4 Flow cytometry to study binding of bsAbs to T cells

$2.5x10^5$ PBMC were washed once with PBS 0.1% BSA (FACS buffer) and incubated in FACS buffer containing 1000 nM or a dilution series of bsAbs (1000, 316.2, 100, 31.62, 10, 3.162, 1, 0.316, 0.1, 0.031) for 30 min at 4 °C. After 3 washing steps with 200 µl FACS puffer, cells were stained with a cocktail containing an anti-CD8 PB (clone DK25, Dako) 1:50, anti-CD4 FITC 1:5 (clone RPA-T4, BD) and anti-human IgG PE (clone G18-145, BD) 1:25 in 50 µl FACS buffer for 30 min at 4 °C in the dark. PBMC were washed 3 times, stained with 10 µl propidium iodide (BD), and analyzed on a CytoFlexS (Beckmann Coulter).

4.2.6 Co-culture experiments and functional readouts

4.2.6.1 Co-culture of PBMC and HBsAg or Huh7S cells

Co-cultures were performed in 96-well cell culture plates (TPP). HBsAg from patient serum (kindly provided by Roche) was added in PBS (100 µl; 1 µg/ml) and incubated overnight at 4 °C. Huh7S cells, a cell line that is stably transfected with HBVenv, served as target cells. $4x10^4$ of Huh7S or parental Huh7 cells were seeded to the plates and cultured for 24 hours. The next day, plates were washed once with PBS and $1x10^5$ freshly

isolated PBMC in 100 µl RPMI1640 full medium were seeded in each well. BsAbs or tsAbs were diluted in DMEM full medium and subsequently added to the PBMC. The co-culture was maintained for the indicated amount of time, and supernatants as well as T cells were analyzed at respective time points. For target cell elimination assays, cells were seeded in 96-well E-plates (ACEA Biosciences) one day prior to the start of the co-culture. Cell viability was measured for the indicated amount of time employing an xCELLigence RTCA SP device (ACEA Biosciences).

4.2.6.2 ELISA for quantification of proinflammatory cytokines

To study the cytokine secretion profile of activated T cells, supernatants of co-cultures were analyzed by the human IFN gamma uncoated ELISA kit (ThermoFisher scientific), the human IL-2 uncoated ELISA kit (ThermoFisher scientific) and the BD OptEIA human TNF ELISA set (BD), according to the manufacture's protocol. ELISAs were performed on MaxiSorp plates.

4.2.6.3 Cytokine measurement with LEGENDplex

For simultaneous measurement of IFNγ, IL-2, TNFα and grzB, the LEGENDplex Multi-Analyte Flow Assay Kit (BioLegend) for CD8/NK cells was employed. The experimental procedure was performed according to the manufacturers' protocol and samples were analyzed on a CytoFlexS.

4.2.6.4 FACS to analyze activation marker and proliferation

Prior to start of co-culture PBMC were stained using the cell trace violet proliferation kit (ThermoFisher scientific) according to the manufacturer's protocol. After 72 hours of co-culture, cells were harvested and washed with 200 µl FACS buffer, followed by staining with a 50 µl mix containing 1:20 dilutions of anti-CD4 PE-eFlour 610 (clone RPA-T4, ThermoFisher scientific), anti-CD8 APC (clone SK1, BD), anti-LAMP1 Alexa Flour 488 (clone H4A3, ThermoFisher scientific), anti-CD25 PE (clone M-A251, BD), as well as near-infrared live/dead (ThermoFisher scientific) 1:1000 in FACS buffer for 30 min at 4 °C in the dark. Cells were washed 3 times with 200 µl FACS buffer and analyzed on a CytoFlexS.

4.2.6.5 Intracellular cytokine staining

4 hours prior to harvest, cells were treated with 0.2 µg/ml Brefeldin A (Sigma). Cells were harvested at respective time points and stored at 4 °C, followed by simultaneous staining. Cells were washed with 200 µl FACS buffer and stained with CD4 PE-eFlour 610 (clone RPA-T4, ThermoFisher scientific) 1:20, CD8 APC (clone SK1, BD) 1:20 and near-infrared live/dead (ThermoFisher scientific) 1:1000 in 50 µl FACS buffer for 30 min at 4 °C in the dark. After 3 washing steps with 200 µl FACS buffer, cells were incubated with 100 µl Cytofix/Cytoperm (BD) for 20 min in the dark. Cells were washed 3 times with 200 µl Perm/Wash (BD) and stained with a cocktail containing anti-TNFα eFlour 450 (clone Mab11, ThermoFisher scientific), anti-IL-2 FITC (clone MQ1-17H12, BD), anti-IFNγ AF700 (clone B27, BD) and anti-grzB PE (clone GB11, ThermoFisher scientific), all 1:40 in FACS buffer for 30 min at 4 °C in the dark. Finally, cells were washed 3 times with 200 µl FACS buffer and analyzed on a CytoFlexS.

4.2.6.6 Staining for T-cell subset analysis

The subsets of $CD8^+$ T cells were defined employing the markers CD45RO, CD45RA, CCR7 and CD62L according to Golubovskaya and Wu (Golubovskaya and Wu, 2016). Cells were cultured for 72 hours on HBsAg-coated plates in the presence of 3 nM FabMAb or BiMAb in combination. After harvest, cells were washed once with 200 µl FACS buffer and stained with CD3 AF700 (clone UCHT1, BD) 1:50, CD4 FITC (RPA-T4, BD) 1:5, CD8 PB (clone SK1, BioLegend) 1:50, CD45RA APC (clone HI100, BioLegend) 1:20, CD45RO PE (clone UCHL1, BioLegend) 1:20, CCR7 BV650 (clone G043H7, BioLegend) 1:20, CD62L PE-Cy7 (clone DREG-56, BioLegend) 1:20 and near-infrared live/dead (ThermoFisher scientific) 1:1000 in 50 µl FACS buffer for 30 min at 4 °C in the dark. After 3 washing steps with 200 µl FACS buffer, cells were analyzed on a CytoFlexS.

4.2.7 HBV-infection and quantification of viral replication

4.2.7.1 Intracellular HBc-staining for flow cytometry

$1{,}2x10^6$ HepG2 NTCP K7 cells (Burwitz et al., 2017) per well were seeded in 6-well cell culture plates (TPP) in a total volume of 2 ml. The next day, when cells reached a confluency of ~90%, the medium was replaced by differentiation medium (DMEM containing 2.5% DMSO). After differentiation for 2 days, medium was discarded and cells were infected by addition of HBV (MOI of 0, 25, 50, 100, 250 and 500 HBV virions/cell) mixed with differentiation medium supplied with 4% polyethylene glycol (PEG) in a total volume of 1 ml. 24 hours after infection, medium was discarded, followed by 2 washing steps with 2 ml PBS. Fresh differentiation medium was added and cells were cultured for 8 days. The cells were washed once with PBS and incubated with 1 ml of a 1:1 mixture of trypsin and Versene solution (0.02%, both ThermoFisher Scientific) for 30 min at 37 °C. After trypsin inactivation by addition of 2 ml DMEM full medium, cells were passed through a 100 µM cell strainer (Falcon) to generate a single cell suspension. The cells were transferred to a 96-well V-bottom plate (Böttger) and washed once with FACS buffer. From now on, all incubation steps were performed at 4 °C in the dark. Cells were stained with fixable viability dye eFlour 780 (ebioscience) diluted 1:5000 in 50 µl FACS buffer for 30 minutes. After 3 washing steps with FACS buffer, the permeabilization of cells was achieved by treatment with 100 µl permeabilization solution (FoxP3 Staining kit, eBioscience) for 1 hour. Next, the cells were washed twice with permeabilization buffer (FoxP3 Staining kit, eBioscience) and stained with a rabbit anti-HBc antibody diluted 1:2000 in 50 µl permeabilization buffer for 30 minutes. After three washing steps with permeabilization buffer, the cells were stained with a $F(ab')_2$ Donkey anti-rabbit IgG PE (555416, BD) diluted 1:10 in 50 µl permeabilization buffer for 30 min. Finally, cells were washed 3 times with permeabilization buffer and resuspended in 200 µl FACS buffer. Analysis was performed employing a CytoFlexS.

4.2.7.2 Co-culture with infected HepG2 NTCP cells

Co-cultures with infected hepG2 NTCP K7 cells were performed in 24-well cell culture plates (TPP). $2x10^5$ cells were seeded in in a total volume of 500 µl and cultured until they reached a confluency of ~90%. The medium was replaced by differentiation medium

and cells were cultured for 2 days. Cells were infected by addition of HBV (MOI of 0, 25, 50, 100, 250 and 500 HBV virions/cell) mixed with differentiation medium supplied with 4% PEG in a total volume of 250 µl. 24 hours after infection, cells were washed twice with 1 ml PBS and cultured for 8 days in differentiation medium. 2 days prior to the start of co-culture the medium was exchanged. The co-culture started 10 days after infection. The supernatant was collected and $5x10^5$ freshly isolated PBMC were added in 250 µl RPMI1640 full medium and mixed with 250 µl DMEM full medium containing 10, 1 or 0.1 nM of the bsAbs or tsAb. The co-culture was supplied with 1% DMSO to prevent the de-differentiation of HepG2 NTCP cells. Every 2 days, the culture was supplied with 1 ml fresh medium containing bsAbs or tsAb. The co-culture was maintained for 10 days and supernatants were stored at -20 °C for simultaneous analysis. To analyze the cell viability, a cell titer blue assay (Promega) was performed according to the manufacturer's protocol at the end of the experiment. To quantify viral DNAs, cellular DNA was extracted employing a NucleoSpin® tissue kit (Macherey-Nagel) according to the provided protocol. For viability measurements in the xCELLigence device cells were infected in the 6-well format as described in 4.2.7.1. The infected cells were trypsinized 7 days post infection and $4x10^5$ cells per well were seeded in a 96-well E-plate. After 24 hours, co-cultures were performed as described in 4.2.6.1. To prevent the de-differentiation of HepG2 NTCP cells, co-cultures were additionally supplied with 1% DMSO.

4.2.7.3 Quantification of viral replication

Quantification of the viral parameters HBsAg, HBeAg, intracellular HBV-DNA, and cccDNA allowed the assessment of the antibody-mediated antiviral effect of redirected T cells on the HBV-infected HepG2 NTCP K7 cells. HBeAg and HBsAg levels in the supernatant of co-cultures were determined using the HBeAg BEP III test (DiaSorin, Saluggia, Italy) and Architect® (Abbott Laboratories), respectively. Intracellular HBV- and cccDNA levels were analyzed by quantitative real time PCR. DNA from 24-well plates was extracted employing a NucleoSpin® tissue kit (Macherey-Nagel) according to manufacturer´s protocol. Specific detection of cccDNA was ensured by T5 exonuclease digestion (New England Biolabs) according to the manufacturers protocol prior to PCR (Xia et al., 2016). To ensure specific detection of cccDNA (Xia et al., 2016), isolated DNA was subjected to T5 exonuclease digestion (New England Biolabs). Therefore, 8.5 µl of extracted DNA were mixed with 0.5 µl T5 exonuclease and 1 µl of NEB buffer. The digestion was incubated for 30 minutes at 37 °C following heat inactivation for 5 minutes at 99 °C. Digested samples were diluted 1:4 with H_2O and employed in qPCRs (Xia et al., 2017). *PRNP* was used as reference gene. Reactions were performed in FrameStar® 96 Well Semi-Skirted PCR plates (4Titude). One reaction contained 4 µl extracted DNA or T5-digested DNA, 0.5 µl forward and reverse primer (20 µM) and 5 µl LightCycler 480 SYBR Green I Master mix (Roche). Used primers were cccDNA 92- and cccDNA 2251 for cccDNA, HBV1745 and HBV1844 for intracellular HBV-DNA, and PRNP fwd and PRNP rev for *PRNP*. For detailed information about primer sequences see 4.1.4. (Xia et al., 2017) Measurements were performed on a LightCycler 480 (Roche Diagnostics) with the following qPCR programs.

qPCR conditions of cccDNA

	T [°C]	t [sec]	Ramp [°C/sec]	Acquisition mode	Cycles
Denaturation	95	600	4.4		1
Amplification	95	15	4.4		50
	60	5	2.2		
	72	45	4.4		
	88	2	4.4	single	
Melting	95	1	4.4		1
	65	15	2.2		
	95		0.11	continuous: 5/°C	
Cooling	40	30	2.2		1

qPCR conditions of rcDNA and *PRNP*

	T [°C]	t [sec]	Ramp [°C/sec]	Acquisition mode	Cycles
Denaturation	95	300	4.4		1
Amplification	95	25	4.4		40
	60	10	2.2		
	72	30	4.4	single	
Melting	95	1	4.4		1
	65	60	2.2		
	95		0.11	continuous: 5/°C	
Cooling	40	30	2.2		1

4.2.8 Determination of half-life in C57BL/6J mice

The pharmacokinetics of bsAbs *in vivo* were analysed employing C57BL/6 mice. Animals were injected with 50 µg of BiMAbαCD3 and FabMAbαCD28 in 200 µl PBS. Control mice were injected with PBS only. 3 animals each were injected intravenously (i.v.), intraperitoneally (i.p.), or subcutaneously (s.c.) and serum was collected after 1, 6, 12, 24, 48 and 72 hours. For the quantification of FabMAbs, an HBsAg ELISA was performed as described in 4.2.5.1. Different serum dilutions (1:20-1:160) were added and incubated for 1.5 hours at RT. As standard, a dilution series of FabMAbs (10, 5, 2.5, 1.25, 0.625,

0.3125, 0.1 and 0.05 µg/ml) was employed. FabMAbs were detected by goat anti-human Fab HRP diluted 1:1000 (Sigma). BiMAb levels in the serum were quantified by Architect®.

4.2.9 Statistics

All statistical analysis was performed with Prism 5.01.336 (Graphpad). EC_{50} was calculated using non-linear regression log(agonist) vs. response variable slope with a robust fit. IC_{50} was calculated with non-linear regression log(inhibitor) vs. response variable slope with a robust fit.

5 Table of figures

6 Bibliography

His-tagged Proteins – Production and Purification [Online]. Available: https://www.thermofisher.com/sg/en/home/life-science/protein-biology/protein-biology-learning-center/protein-biology-resource-library/pierce-protein-methods/his-tagged-proteins-production-purification.html [Accessed 02.05.2019].

ALLEMANN, P., DEMARTINES, N., BOUZOURENE, H., TEMPIA, A. & HALKIC, N. 2013. Long-term outcome after liver resection for hepatocellular carcinoma larger than 10 cm. *World J Surg,* 37**,** 452-8.

AMANN, M., BRISCHWEIN, K., LUTTERBUESE, P., PARR, L., PETERSEN, L., LORENCZEWSKI, G., KRINNER, E., BRUCKMEIER, S., LIPPOLD, S., KISCHEL, R., LUTTERBUESE, R., KUFER, P., BAEUERLE, P. A. & SCHLERETH, B. 2008. Therapeutic window of MuS110, a single-chain antibody construct bispecific for murine EpCAM and murine CD3. *Cancer Res,* 68**,** 143-51.

APPAY, V., ZAUNDERS, J. J., PAPAGNO, L., SUTTON, J., JARAMILLO, A., WATERS, A., EASTERBROOK, P., GREY, P., SMITH, D., MCMICHAEL, A. J., COOPER, D. A., ROWLAND-JONES, S. L. & KELLEHER, A. D. 2002. Characterization of CD4(+) CTLs ex vivo. *J Immunol,* 168**,** 5954-8.

ARMOUR, K. L., CLARK, M. R., HADLEY, A. G. & WILLIAMSON, L. M. 1999. Recombinant human IgG molecules lacking Fcgamma receptor I binding and monocyte triggering activities. *Eur J Immunol,* 29**,** 2613-24.

ARNOLD, F. H. 1991. Metal-affinity separations: a new dimension in protein processing. *Biotechnology (N Y),* 9**,** 151-6.

ARUFFO, A. & SEED, B. 1987. Molecular cloning of a CD28 cDNA by a high-efficiency COS cell expression system. *Proceedings of the National Academy of Sciences of the United States of America,* 84**,** 8573-8577.

ASABE, S., WIELAND, S. F., CHATTOPADHYAY, P. K., ROEDERER, M., ENGLE, R. E., PURCELL, R. H. & CHISARI, F. V. 2009. The size of the viral inoculum contributes to the outcome of hepatitis B virus infection. *J Virol,* 83**,** 9652-62.

BAEUERLE, P. A. & REINHARDT, C. 2009. Bispecific T-cell engaging antibodies for cancer therapy. *Cancer Res,* 69**,** 4941-4.

BALOGH, J., VICTOR, D., 3RD, ASHAM, E. H., BURROUGHS, S. G., BOKTOUR, M., SAHARIA, A., LI, X., GHOBRIAL, R. M. & MONSOUR, H. P., JR. 2016. Hepatocellular carcinoma: a review. *J Hepatocell Carcinoma,* 3**,** 41-53.

BAROJA, M. L., LORRE, K., VAN VAECK, F. & CEUPPENS, J. L. 1989. The anti-T cell monoclonal antibody 9.3 (anti-CD28) provides a helper signal and bypasses the need for accessory cells in T cell activation with immobilized anti-CD3 and mitogens. *Cell Immunol,* 120**,** 205-17.

BASU, R., WHITLOCK, B. M., HUSSON, J., LE FLOC'H, A., JIN, W., OYLER-YANIV, A., DOTIWALA, F., GIANNONE, G., HIVROZ, C., BIAIS, N., LIEBERMAN, J., KAM, L. C. & HUSE, M. 2016. Cytotoxic T Cells Use Mechanical Force to Potentiate Target Cell Killing. *Cell,* 165**,** 100-110.

BELLONI, L., ALLWEISS, L., GUERRIERI, F., PEDICONI, N., VOLZ, T., POLLICINO, T., PETERSEN, J., RAIMONDO, G., DANDRI, M. & LEVRERO, M. 2012. IFN-alpha inhibits HBV transcription and replication in cell culture and in humanized mice by targeting the epigenetic regulation of the nuclear cccDNA minichromosome. *J Clin Invest,* 122**,** 529-37.

BENSELER, V., WARREN, A., VO, M., HOLZ, L. E., TAY, S. S., LE COUTEUR, D. G., BREEN, E., ALLISON, A. C., VAN ROOIJEN, N., MCGUFFOG, C., SCHLITT, H. J., BOWEN, D. G., MCCAUGHAN, G. W. & BERTOLINO, P. 2011. Hepatocyte entry leads to degradation of autoreactive CD8 T cells. *Proc Natl Acad Sci U S A,* 108**,** 16735-40.

BERTOLETTI, A. & BERT, N. L. 2018. Immunotherapy for Chronic Hepatitis B Virus Infection. *Gut Liver*.

BEVAN, M. J. 1976a. Cross-priming for a secondary cytotoxic response to minor H antigens with H-2 congenic cells which do not cross-react in the cytotoxic assay. *The Journal of experimental medicine,* 143**,** 1283-1288.

BEVAN, M. J. 1976b. Minor H antigens introduced on H-2 different stimulating cells cross-react at the cytotoxic T cell level during in vivo priming. *J Immunol,* 117**,** 2233-8.

BEYERSDORF, N., KERKAU, T. & HUNIG, T. 2015. CD28 co-stimulation in T-cell homeostasis: a recent perspective. *Immunotargets Ther,* 4**,** 111-22.

BIAZAR, T., YAHYAPOUR, Y., HASANJANI ROUSHAN, M. R., RAJABNIA, R., SADEGHI, M., TAHERI, H., RANAEI, M. & BAYANI, M. 2015. Relationship between hepatitis B DNA viral load in the liver and its histology in patients with chronic hepatitis B. *Caspian J Intern Med,* 6**,** 209-12.

BIKOFF, E. & BIRSHTEIN, B. K. 1986. T cell clones specific for IgG2a of the a allotype: direct evidence for presentation of endogenous antigen. *J Immunol,* 137**,** 28-34.

BIRNBAUM, F. & NASSAL, M. 1990. Hepatitis B virus nucleocapsid assembly: primary structure requirements in the core protein. *J Virol,* 64**,** 3319-30.

BLINCYTO (BLINATUMOMAB) [PACKAGE INSERT] THOUSAND OAKS, C. A.

BLOCK, T. M., GISH, R., GUO, H., MEHTA, A., CUCONATI, A., THOMAS LONDON, W. & GUO, J. T. 2013. Chronic hepatitis B: what should be the goal for new therapies? *Antiviral Res,* 98**,** 27-34.

BLUEMEL, C., HAUSMANN, S., FLUHR, P., SRISKANDARAJAH, M., STALLCUP, W. B., BAEUERLE, P. A. & KUFER, P. 2010. Epitope distance to the target cell membrane and antigen size determine the potency of T cell-mediated lysis by BiTE antibodies specific for a large melanoma surface antigen. *Cancer Immunol Immunother,* 59**,** 1197-209.

BOCK, C. T., SCHRANZ, P., SCHRODER, C. H. & ZENTGRAF, H. 1994. Hepatitis B virus genome is organized into nucleosomes in the nucleus of the infected cell. *Virus Genes,* 8**,** 215-29.

BOHNE, F., CHMIELEWSKI, M., EBERT, G., WIEGMANN, K., KURSCHNER, T., SCHULZE, A., URBAN, S., KRONKE, M., ABKEN, H. & PROTZER, U. 2008. T cells redirected against hepatitis B virus surface proteins eliminate infected hepatocytes. *Gastroenterology,* 134**,** 239-47.

BOISE, L. H., MINN, A. J., NOEL, P. J., JUNE, C. H., ACCAVITTI, M. A., LINDSTEN, T. & THOMPSON, C. B. 1995. CD28 costimulation can promote T cell survival by enhancing the expression of Bcl-XL. *Immunity,* 3**,** 87-98.

BOLE, D. G., HENDERSHOT, L. M. & KEARNEY, J. F. 1986. Posttranslational association of immunoglobulin heavy chain binding protein with nascent heavy chains in nonsecreting and secreting hybridomas. *J Cell Biol,* 102**,** 1558-66.

BORST, J., ALEXANDER, S., ELDER, J. & TERHORST, C. 1983. The T3 complex on human T lymphocytes involves four structurally distinct glycoproteins. *J Biol Chem,* 258**,** 5135-41.

BORTH, N., MATTANOVICH, D., KUNERT, R. & KATINGER, H. 2005. Effect of increased expression of protein disulfide isomerase and heavy chain binding protein on antibody secretion in a recombinant CHO cell line. *Biotechnol Prog,* 21**,** 106-11.

BOTTCHER, J. P., SCHANZ, O., GARBERS, C., ZAREMBA, A., HEGENBARTH, S., KURTS, C., BEYER, M., SCHULTZE, J. L., KASTENMULLER, W., ROSE-JOHN,

S. & KNOLLE, P. A. 2014. IL-6 trans-signaling-dependent rapid development of cytotoxic CD8+ T cell function. *Cell Rep,* 8**,** 1318-27.

BOUVIER, M. & WILEY, D. C. 1994. Importance of peptide amino and carboxyl termini to the stability of MHC class I molecules. *Science,* 265**,** 398.

BROWN, D. M. 2010. Cytolytic CD4 cells: Direct mediators in infectious disease and malignancy. *Cell Immunol,* 262**,** 89-95.

BRUIX, J., QIN, S., MERLE, P., GRANITO, A., HUANG, Y. H., BODOKY, G., PRACHT, M., YOKOSUKA, O., ROSMORDUC, O., BREDER, V., GEROLAMI, R., MASI, G., ROSS, P. J., SONG, T., BRONOWICKI, J. P., OLLIVIER-HOURMAND, I., KUDO, M., CHENG, A. L., LLOVET, J. M., FINN, R. S., LEBERRE, M. A., BAUMHAUER, A., MEINHARDT, G., HAN, G. & INVESTIGATORS, R. 2017. Regorafenib for patients with hepatocellular carcinoma who progressed on sorafenib treatment (RESORCE): a randomised, double-blind, placebo-controlled, phase 3 trial. *Lancet,* 389**,** 56-66.

BURWITZ, B. J., WETTENGEL, J. M., MUCK-HAUSL, M. A., RINGELHAN, M., KO, C., FESTAG, M. M., HAMMOND, K. B., NORTHRUP, M., BIMBER, B. N., JACOB, T., REED, J. S., NORRIS, R., PARK, B., MOLLER-TANK, S., ESSER, K., GREENE, J. M., WU, H. L., ABDULHAQQ, S., WEBB, G., SUTTON, W. F., KLUG, A., SWANSON, T., LEGASSE, A. W., VU, T. Q., ASOKAN, A., HAIGWOOD, N. L., PROTZER, U. & SACHA, J. B. 2017. Hepatocytic expression of human sodium-taurocholate cotransporting polypeptide enables hepatitis B virus infection of macaques. *Nat Commun,* 8**,** 2146.

BUTI, M., TSAI, N., PETERSEN, J., FLISIAK, R., GUREL, S., KRASTEV, Z., AGUILAR SCHALL, R., FLAHERTY, J. F., MARTINS, E. B., CHARUWORN, P., KITRINOS, K. M., SUBRAMANIAN, G. M., GANE, E. & MARCELLIN, P. 2015. Seven-year efficacy and safety of treatment with tenofovir disoproxil fumarate for chronic hepatitis B virus infection. *Dig Dis Sci,* 60**,** 1457-64.

CANTOR, H. & BOYSE, E. A. 1975. Functional subclasses of T-lymphocytes bearing different Ly antigens. I. The generation of functionally distinct T-cell subclasses is a differentiative process independent of antigen. *J Exp Med,* 141**,** 1376-89.

CHAN, A. C., IRVING, B. A., FRASER, J. D. & WEISS, A. 1991. The zeta chain is associated with a tyrosine kinase and upon T-cell antigen receptor stimulation associates with ZAP-70, a 70-kDa tyrosine phosphoprotein. *Proc Natl Acad Sci U S A,* 88**,** 9166-70.

CHANG, J. J., SIRIVICHAYAKUL, S., AVIHINGSANON, A., THOMPSON, A. J., REVILL, P., ISER, D., SLAVIN, J., BURANAPRADITKUN, S., MARKS, P., MATTHEWS, G., COOPER, D. A., KENT, S. J., CAMERON, P. U., SASADEUSZ, J., DESMOND, P., LOCARNINI, S., DORE, G. J., RUXRUNGTHAM, K. & LEWIN, S. R. 2009. Impaired quality of the hepatitis B virus (HBV)-specific T-cell response in human immunodeficiency virus type 1-HBV coinfection. *J Virol,* 83**,** 7649-58.

CHAYANUPATKUL, M., OMINO, R., MITTAL, S., KRAMER, J. R., RICHARDSON, P., THRIFT, A. P., EL-SERAG, H. B. & KANWAL, F. 2017. Hepatocellular carcinoma in the absence of cirrhosis in patients with chronic hepatitis B virus infection. *J Hepatol,* 66**,** 355-362.

CHEN, M. T., BILLAUD, J. N., SALLBERG, M., GUIDOTTI, L. G., CHISARI, F. V., JONES, J., HUGHES, J. & MILICH, D. R. 2004. A function of the hepatitis B virus precore protein is to regulate the immune response to the core antigen. *Proc Natl Acad Sci U S A,* 101**,** 14913-8.

CHISARI, F. V., ISOGAWA, M. & WIELAND, S. F. 2010. Pathogenesis of hepatitis B virus infection. *Pathol Biol (Paris),* 58**,** 258-66.

DAHLEN, E., VEITONMAKI, N. & NORLEN, P. 2018. Bispecific antibodies in cancer immunotherapy. *Ther Adv Vaccines Immunother,* 6**,** 3-17.

DANDRI, M., BURDA, M. R., TOROK, E., POLLOK, J. M., IWANSKA, A., SOMMER, G., ROGIERS, X., ROGLER, C. E., GUPTA, S., WILL, H., GRETEN, H. & PETERSEN, J. 2001. Repopulation of mouse liver with human hepatocytes and in vivo infection with hepatitis B virus. *Hepatology,* 33**,** 981-8.

DANDRI, M. & PETERSEN, J. 2012. Chimeric mouse model of hepatitis B virus infection. *J Hepatol,* 56**,** 493-5.

DANE, D. S., CAMERON, C. H. & BRIGGS, M. 1970. Virus-like particles in serum of patients with Australia-antigen-associated hepatitis. *Lancet,* 1**,** 695-8.

DANIEL, P. T., KROIDL, A., KOPP, J., STURM, I., MOLDENHAUER, G., DORKEN, B. & PEZZUTTO, A. 1998. Immunotherapy of B-cell lymphoma with CD3x19 bispecific antibodies: costimulation via CD28 prevents "veto" apoptosis of antibody-targeted cytotoxic T cells. *Blood,* 92**,** 4750-7.

DATTA-MANNAN, A., WITCHER, D. R., TANG, Y., WATKINS, J., JIANG, W. & WROBLEWSKI, V. J. 2007. Humanized IgG1 variants with differential binding properties to the neonatal Fc receptor: relationship to pharmacokinetics in mice and primates. *Drug Metab Dispos,* 35**,** 86-94.

DAVIS, S. J. & VAN DER MERWE, P. A. 2006. The kinetic-segregation model: TCR triggering and beyond. *Nat Immunol,* 7**,** 803-9.

DEL PRETE, G. F., DE CARLI, M., MASTROMAURO, C., BIAGIOTTI, R., MACCHIA, D., FALAGIANI, P., RICCI, M. & ROMAGNANI, S. 1991. Purified protein derivative of Mycobacterium tuberculosis and excretory-secretory antigen(s) of Toxocara canis expand in vitro human T cells with stable and opposite (type 1 T helper or type 2 T helper) profile of cytokine production. *J Clin Invest,* 88**,** 346-50.

DELON, J., BERCOVICI, N., LIBLAU, R. & TRAUTMANN, A. 1998. Imaging antigen recognition by naive CD4+ T cells: compulsory cytoskeletal alterations for the triggering of an intracellular calcium response. *Eur J Immunol,* 28**,** 716-29.

DRABEK, D., JANSSENS, R., DE BOER, E., RADEMAKER, R., KLOESS, J., SKEHEL, J. & GROSVELD, F. 2016. Expression Cloning and Production of Human Heavy-Chain-Only Antibodies from Murine Transgenic Plasma Cells. *Front Immunol,* 7**,** 619.

ECKHARDT, S. G., MILICH, D. R. & MCLACHLAN, A. 1991. Hepatitis B virus core antigen has two nuclear localization sequences in the arginine-rich carboxyl terminus. *J Virol,* 65**,** 575-82.

EISENLOHR, L. C. & HACKETT, C. J. 1989. Class II major histocompatibility complex-restricted T cells specific for a virion structural protein that do not recognize exogenous influenza virus. Evidence that presentation of labile T cell determinants is favored by endogenous antigen synthesis. *J Exp Med,* 169**,** 921-31.

EREN, R., ILAN, E., NUSSBAUM, O., LUBIN, I., TERKIELTAUB, D., ARAZI, Y., BEN-MOSHE, O., KITCHINZKY, A., BERR, S., GOPHER, J., ZAUBERMAN, A., GALUN, E., SHOUVAL, D., DAUDI, N., EID, A., JURIM, O., MAGNIUS, L. O., HAMMAS, B., REISNER, Y. & DAGAN, S. 2000. Preclinical evaluation of two human anti-hepatitis B virus (HBV) monoclonal antibodies in the HBV-trimera mouse model and in HBV chronic carrier chimpanzees. *Hepatology,* 32**,** 588-96.

FEIGE, M. J., GROSCURTH, S., MARCINOWSKI, M., SHIMIZU, Y., KESSLER, H., HENDERSHOT, L. M. & BUCHNER, J. 2009. An unfolded CH1 domain controls the assembly and secretion of IgG antibodies. *Mol Cell,* 34**,** 569-79.

FENG, Y., BRAZIN, K. N., KOBAYASHI, E., MALLIS, R. J., REINHERZ, E. L. & LANG, M. J. 2017. Mechanosensing drives acuity of alphabeta T-cell recognition. *Proc Natl Acad Sci U S A,* 114**,** E8204-E8213.

FIELDS, B. N. & KNIPE, D. M. 1990. *Fields virology,* New York, Raven Press.

FREEDMAN, A. S., FREEMAN, G., HOROWITZ, J. C., DALEY, J. & NADLER, L. M. 1987. B7, a B-cell-restricted antigen that identifies preactivated B cells. *J Immunol,* 139**,** 3260-7.

GALUN, E., EREN, R., SAFADI, R., ASHOUR, Y., TERRAULT, N., KEEFFE, E. B., MATOT, E., MIZRACHI, S., TERKIELTAUB, D., ZOHAR, M., LUBIN, I., GOPHER, J., SHOUVAL, D. & DAGAN, S. 2002. Clinical evaluation (phase I) of a combination of two human monoclonal antibodies to HBV: safety and antiviral properties. *Hepatology,* 35**,** 673-9.

GANEM, D. & PRINCE, A. M. 2004. Hepatitis B virus infection--natural history and clinical consequences. *N Engl J Med,* 350**,** 1118-29.

GAO, Y., ZHANG, T. Y., YUAN, Q. & XIA, N. S. 2017. Antibody-mediated immunotherapy against chronic hepatitis B virus infection. *Hum Vaccin Immunother,* 13**,** 1768-1773.

GAUTHIER, L., MOREL, A., ANCERIZ, N., ROSSI, B., BLANCHARD-ALVAREZ, A., GRONDIN, G., TRICHARD, S., CESARI, C., SAPET, M., BOSCO, F., RISPAUD-BLANC, H., GUILLOT, F., CORNEN, S., ROUSSEL, A., AMIGUES, B., HABIF, G., CARAGUEL, F., ARRUFAT, S., REMARK, R., ROMAGNÉ, F., MOREL, Y., NARNI-MANCINELLI, E. & VIVIER, E. 2019. Multifunctional Natural Killer Cell Engagers Targeting NKp46 Trigger Protective Tumor Immunity. *Cell,* 177**,** 1701-1713.e16.

GEGINAT, J., LANZAVECCHIA, A. & SALLUSTO, F. 2003. Proliferation and differentiation potential of human CD8+ memory T-cell subsets in response to antigen or homeostatic cytokines. *Blood,* 101**,** 4260-6.

GEPPERT, T. D. & LIPSKY, P. E. 1988. Activation of T lymphocytes by immobilized monoclonal antibodies to CD3. Regulatory influences of monoclonal antibodies to additional T cell surface determinants. *J Clin Invest,* 81**,** 1497-505.

GERSHON, R. K. & KONDO, K. 1970. Cell interactions in the induction of tolerance: the role of thymic lymphocytes. *Immunology,* 18**,** 723-37.

GILL, U. S., ZISSIMOPOULOS, A., AL-SHAMMA, S., BURKE, K., MCPHAIL, M. J., BARR, D. A., KALLIS, Y. N., MARLEY, R. T., KOONER, P., FOSTER, G. R. & KENNEDY, P. T. 2015. Assessment of bone mineral density in tenofovir-treated patients with chronic hepatitis B: can the fracture risk assessment tool identify those at greatest risk? *J Infect Dis,* 211**,** 374-82.

GINALDI, L., DE MARTINIS, M., MATUTES, E., FARAHAT, N., MORILLA, R. & CATOVSKY, D. 1998. Levels of expression of CD19 and CD20 in chronic B cell leukaemias. *J Clin Pathol,* 51**,** 364-9.

GMBH, N. B. 2017. *Neovii completes marketing authorisation withdrawal of Removab® in the European Union* [Online]. Available: https://neovii.com/neovii-completes-marketing-authorisation-withdrawal-of-removab-in-the-european-union/?cn-reloaded=1 [Accessed 20.03.2019 2019].

GOLSAZ-SHIRAZI, F., MOHAMMADI, H., AMIRI, M. M., KHOSHNOODI, J., KARDAR, G. A., JEDDI-TEHRANI, M. & SHOKRI, F. 2016. Localization of immunodominant epitopes within the "a" determinant of hepatitis B surface antigen using monoclonal antibodies. *Arch Virol,* 161**,** 2765-72.

GOLSAZ SHIRAZI, F., MOHAMMADI, H., AMIRI, M. M., SINGETHAN, K., XIA, Y., BAYAT, A. A., BAHADORI, M., RABBANI, H., JEDDI-TEHRANI, M., PROTZER, U. & SHOKRI, F. 2014. Monoclonal antibodies to various epitopes of hepatitis B surface antigen inhibit hepatitis B virus infection. *J Gastroenterol Hepatol,* 29**,** 1083-91.

GOLUBOVSKAYA, V. & WU, L. 2016. Different Subsets of T Cells, Memory, Effector Functions, and CAR-T Immunotherapy. *Cancers (Basel),* 8.

GOWANS, J. L. & KNIGHT, E. J. 1964. THE ROUTE OF RE-CIRCULATION OF LYMPHOCYTES IN THE RAT. *Proc R Soc Lond B Biol Sci,* 159**,** 257-82.

GRETEN, T. F., PAPENDORF, F., BLECK, J. S., KIRCHHOFF, T., WOHLBEREDT, T., KUBICKA, S., KLEMPNAUER, J., GALANSKI, M. & MANNS, M. P. 2005. Survival rate in patients with hepatocellular carcinoma: a retrospective analysis of 389 patients. *Br J Cancer,* 92**,** 1862-8.

GREWAL, I. S. & FLAVELL, R. A. 1998. CD40 and CD154 in cell-mediated immunity. *Annu Rev Immunol,* 16**,** 111-35.

GROSSE-HOVEST, L., HARTLAPP, I., MARWAN, W., BREM, G., RAMMENSEE, H. G. & JUNG, G. 2003. A recombinant bispecific single-chain antibody induces targeted, supra-agonistic CD28-stimulation and tumor cell killing. *Eur J Immunol,* 33**,** 1334-40.

GUIDOTTI, L. G. & CHISARI, F. V. 2001. Noncytolytic control of viral infections by the innate and adaptive immune response. *Annu Rev Immunol,* 19**,** 65-91.

GURBAXANI, B., DELA CRUZ, L. L., CHINTALACHARUVU, K. & MORRISON, S. L. 2006. Analysis of a family of antibodies with different half-lives in mice fails to find a correlation between affinity for FcRn and serum half-life. *Mol Immunol,* 43**,** 1462-73.

HAAGEN, I.-A., DE LAU, W. B. M., BAST, B. J. E. G., GEERARS, A. J. G., CLARK, M. R. & DE GAST, B. C. 1994. Unprimed CD4+ and CD8+ T cells can be rapidly activated by a CD3×CD19 bispecific antibody to proliferate and become cytotoxic. *Cancer Immunology, Immunotherapy,* 39**,** 391-396.

HAN, J. Y., JUNG, W. H., CHON, C. Y. & PARK, C. I. 1993. The Tissue Expression of HBsAg and HBcAg in Hepatocellular Carcinoma and Peritumoral Liver. *J Pathol Transl Med,* 27**,** 371-378.

HARDING, F. A., MCARTHUR, J. G., GROSS, J. A., RAULET, D. H. & ALLISON, J. P. 1992. CD28-mediated signalling co-stimulates murine T cells and prevents induction of anergy in T-cell clones. *Nature,* 356**,** 607-9.

HEISS, M. M., MURAWA, P., KORALEWSKI, P., KUTARSKA, E., KOLESNIK, O. O., IVANCHENKO, V. V., DUDNICHENKO, A. S., ALEKNAVICIENE, B., RAZBADAUSKAS, A., GORE, M., GANEA-MOTAN, E., CIULEANU, T., WIMBERGER, P., SCHMITTEL, A., SCHMALFELDT, B., BURGES, A., BOKEMEYER, C., LINDHOFER, H., LAHR, A. & PARSONS, S. L. 2010. The trifunctional antibody catumaxomab for the treatment of malignant ascites due to epithelial cancer: Results of a prospective randomized phase II/III trial. *Int J Cancer,* 127**,** 2209-21.

HENDERSHOT, L., BOLE, D., KOHLER, G. & KEARNEY, J. F. 1987. Assembly and secretion of heavy chains that do not associate posttranslationally with immunoglobulin heavy chain-binding protein. *J Cell Biol,* 104**,** 761-7.

HENDERSHOT, L. M. 1990. Immunoglobulin heavy chain and binding protein complexes are dissociated in vivo by light chain addition. *J Cell Biol,* 111**,** 829-37.

HEUSER, C., DIEHL, V., ABKEN, H. & HOMBACH, A. 2003. Anti-CD30-IL-12 antibody-cytokine fusion protein that induces IFN-gamma secretion of T cells and NK cell-mediated lysis of Hodgkin's lymphoma-derived tumor cells. *Int J Cancer,* 106**,** 545-52.

HOLZ, L. E., BENSELER, V., BOWEN, D. G., BOUILLET, P., STRASSER, A., O'REILLY, L., D'AVIGDOR, W. M., BISHOP, A. G., MCCAUGHAN, G. W. & BERTOLINO, P. 2008. Intrahepatic murine CD8 T-cell activation associates with a distinct phenotype leading to Bim-dependent death. *Gastroenterology,* 135**,** 989-97.

HOLZ, L. E., BENSELER, V., VO, M., MCGUFFOG, C., VAN ROOIJEN, N., MCCAUGHAN, G. W., BOWEN, D. G. & BERTOLINO, P. 2012. Naive CD8 T cell activation by liver bone marrow-derived cells leads to a "neglected" IL-2low Bimhigh phenotype, poor CTL function and cell death. *J Hepatol,* 57**,** 830-6.

HORNIG, N., KERMER, V., FREY, K., DIEBOLDER, P., KONTERMANN, R. E. & MULLER, D. 2012. Combination of a bispecific antibody and costimulatory

antibody-ligand fusion proteins for targeted cancer immunotherapy. *J Immunother,* 35**,** 418-29.

HU, J. & LIU, K. 2017. Complete and Incomplete Hepatitis B Virus Particles: Formation, Function, and Application. *Viruses,* 9.

HU, Z., ZHANG, Z., DOO, E., COUX, O., GOLDBERG, A. L. & LIANG, T. J. 1999. Hepatitis B virus X protein is both a substrate and a potential inhibitor of the proteasome complex. *J Virol,* 73**,** 7231-40.

HUANG, H. C., CHEN, C. C., CHANG, W. C., TAO, M. H. & HUANG, C. 2012. Entry of hepatitis B virus into immortalized human primary hepatocytes by clathrin-dependent endocytosis. *J Virol,* 86**,** 9443-53.

HUMAN GENOME VARIATION SOCIETY , N. B. J. T. D. D., WEBSITE CREATED BY WILLIAM HONG. *Sequence variant nomenclature, protein recommendations* [Online]. Available: http://varnomen.hgvs.org/recommendations/protein/ [Accessed 04.02.2019 2019].

HUOVILA, A. P., EDER, A. M. & FULLER, S. D. 1992. Hepatitis B surface antigen assembles in a post-ER, pre-Golgi compartment. *J Cell Biol,* 118**,** 1305-20.

HUPPA, J. B. & DAVIS, M. M. 2003. T-cell-antigen recognition and the immunological synapse. *Nat Rev Immunol,* 3**,** 973-83.

HUSSAIN, K., HARGREAVES, C. E., ROGHANIAN, A., OLDHAM, R. J., CHAN, H. T., MOCKRIDGE, C. I., CHOWDHURY, F., FRENDEUS, B., HARPER, K. S., STREFFORD, J. C., CRAGG, M. S., GLENNIE, M. J., WILLIAMS, A. P. & FRENCH, R. R. 2015. Upregulation of FcgammaRIIb on monocytes is necessary to promote the superagonist activity of TGN1412. *Blood,* 125**,** 102-10.

IAVARONE, M., CABIBBO, G., PISCAGLIA, F., ZAVAGLIA, C., GRIECO, A., VILLA, E., CAMMA, C., COLOMBO, M. & GROUP, S. S. 2011. Field-practice study of sorafenib therapy for hepatocellular carcinoma: a prospective multicenter study in Italy. *Hepatology,* 54**,** 2055-63.

IDUSOGIE, E. E., PRESTA, L. G., GAZZANO-SANTORO, H., TOTPAL, K., WONG, P. Y., ULTSCH, M., MENG, Y. G. & MULKERRIN, M. G. 2000. Mapping of the C1q binding site on rituxan, a chimeric antibody with a human IgG1 Fc. *J Immunol,* 164**,** 4178-84.

IWAI, Y., TERAWAKI, S., IKEGAWA, M., OKAZAKI, T. & HONJO, T. 2003. PD-1 inhibits antiviral immunity at the effector phase in the liver. *J Exp Med,* 198**,** 39-50.

JACKMAN, J. K., MOTTO, D. G., SUN, Q., TANEMOTO, M., TURCK, C. W., PELTZ, G. A., KORETZKY, G. A. & FINDELL, P. R. 1995. Molecular cloning of SLP-76, a 76-kDa tyrosine phosphoprotein associated with Grb2 in T cells. *J Biol Chem,* 270**,** 7029-32.

JAMES, J. R. & VALE, R. D. 2012. Biophysical mechanism of T-cell receptor triggering in a reconstituted system. *Nature,* 487**,** 64-9.

JENKINS, M. K., TAYLOR, P. S., NORTON, S. D. & URDAHL, K. B. 1991. CD28 delivers a costimulatory signal involved in antigen-specific IL-2 production by human T cells. *J Immunol,* 147**,** 2461-6.

JI, M. & HU, K. 2017. Recent advances in the study of hepatitis B virus covalently closed circular DNA. *Virol Sin,* 32**,** 454-464.

JIANG, B., HIMMELSBACH, K., REN, H., BOLLER, K. & HILDT, E. 2015. Subviral Hepatitis B Virus Filaments, like Infectious Viral Particles, Are Released via Multivesicular Bodies. *J Virol,* 90**,** 3330-41.

JUNE, C. H., LEDBETTER, J. A., GILLESPIE, M. M., LINDSTEN, T. & THOMPSON, C. B. 1987. T-cell proliferation involving the CD28 pathway is associated with cyclosporine-resistant interleukin 2 gene expression. *Mol Cell Biol,* 7**,** 4472-81.

JUNG, S., UNUTMAZ, D., WONG, P., SANO, G., DE LOS SANTOS, K., SPARWASSER, T., WU, S., VUTHOORI, S., KO, K., ZAVALA, F., PAMER, E. G., LITTMAN, D. R. & LANG, R. A. 2002. In vivo depletion of CD11c+ dendritic

cells abrogates priming of CD8+ T cells by exogenous cell-associated antigens. *Immunity,* 17**,** 211-20.

KAFROUNI, M. I., BROWN, G. R. & THIELE, D. L. 2001. Virally infected hepatocytes are resistant to perforin-dependent CTL effector mechanisms. *J Immunol,* 167**,** 1566-74.

KAH, J., KOH, S., VOLZ, T., CECCARELLO, E., ALLWEISS, L., LUTGEHETMANN, M., BERTOLETTI, A. & DANDRI, M. 2017. Lymphocytes transiently expressing virus-specific T cell receptors reduce hepatitis B virus infection. *J Clin Invest,* 127**,** 3177-3188.

KILLAR, L., MACDONALD, G., WEST, J., WOODS, A. & BOTTOMLY, K. 1987. Cloned, Ia-restricted T cells that do not produce interleukin 4(IL 4)/B cell stimulatory factor 1(BSF-1) fail to help antigen-specific B cells. *J Immunol,* 138**,** 1674-9.

KIM, S. T., TAKEUCHI, K., SUN, Z. Y., TOUMA, M., CASTRO, C. E., FAHMY, A., LANG, M. J., WAGNER, G. & REINHERZ, E. L. 2009. The alphabeta T cell receptor is an anisotropic mechanosensor. *J Biol Chem,* 284**,** 31028-37.

KITAZAWA, T., IGAWA, T., SAMPEI, Z., MUTO, A., KOJIMA, T., SOEDA, T., YOSHIHASHI, K., OKUYAMA-NISHIDA, Y., SAITO, H., TSUNODA, H., SUZUKI, T., ADACHI, H., MIYAZAKI, T., ISHII, S., KAMATA-SAKURAI, M., IIDA, T., HARADA, A., ESAKI, K., FUNAKI, M., MORIYAMA, C., TANAKA, E., KIKUCHI, Y., WAKABAYASHI, T., WADA, M., GOTO, M., TOYODA, T., UEYAMA, A., SUZUKI, S., HARAYA, K., TACHIBANA, T., KAWABE, Y., SHIMA, M., YOSHIOKA, A. & HATTORI, K. 2012. A bispecific antibody to factors IXa and X restores factor VIII hemostatic activity in a hemophilia A model. *Nat Med,* 18**,** 1570-4.

KJER-NIELSEN, L., DUNSTONE, M. A., KOSTENKO, L., ELY, L. K., BEDDOE, T., MIFSUD, N. A., PURCELL, A. W., BROOKS, A. G., MCCLUSKEY, J. & ROSSJOHN, J. 2004. Crystal structure of the human T cell receptor CD3 epsilon gamma heterodimer complexed to the therapeutic mAb OKT3. *Proc Natl Acad Sci U S A,* 101**,** 7675-80.

KLINGER, M., BRANDL, C., ZUGMAIER, G., HIJAZI, Y., BARGOU, R. C., TOPP, M. S., GOKBUGET, N., NEUMANN, S., GOEBELER, M., VIARDOT, A., STELLJES, M., BRUGGEMANN, M., HOELZER, D., DEGENHARD, E., NAGORSEN, D., BAEUERLE, P. A., WOLF, A. & KUFER, P. 2012. Immunopharmacologic response of patients with B-lineage acute lymphoblastic leukemia to continuous infusion of T cell-engaging CD19/CD3-bispecific BiTE antibody blinatumomab. *Blood,* 119**,** 6226-33.

KNOLLE, P. A. 2012. The liver's imprint on CD8(+) T cell priming. *J Hepatol,* 57**,** 718-9.

KO, C., CHAKRABORTY, A., CHOU, W. M., HASREITER, J., WETTENGEL, J. M., STADLER, D., BESTER, R., ASEN, T., ZHANG, K., WISSKIRCHEN, K., MCKEATING, J. A., RYU, W. S. & PROTZER, U. 2018. Hepatitis B virus genome recycling and de novo secondary infection events maintain stable cccDNA levels. *J Hepatol*.

KO, C., MICHLER, T. & PROTZER, U. 2017. Novel viral and host targets to cure hepatitis B. *Curr Opin Virol,* 24**,** 38-45.

KOH, S., KAH, J., THAM, C. Y. L., YANG, N., CECCARELLO, E., CHIA, A., CHEN, M., KHAKPOOR, A., PAVESI, A., TAN, A. T., DANDRI, M. & BERTOLETTI, A. 2018. Nonlytic Lymphocytes Engineered to Express Virus-Specific T-Cell Receptors Limit HBV Infection by Activating APOBEC3. *Gastroenterology,* 155**,** 180-193 e6.

KONKLE, B. A., HUSTON, H. & NAKAYA FLETCHER, S. 1993. Hemophilia A. *In:* ADAM, M. P., ARDINGER, H. H., PAGON, R. A., WALLACE, S. E., BEAN, L. J. H., STEPHENS, K. & AMEMIYA, A. (eds.) *GeneReviews((R)).* Seattle (WA).

KONTERMANN, R. E. & BRINKMANN, U. 2015. Bispecific antibodies. *Drug Discov Today,* 20**,** 838-47.

KRAMVIS, A. 2014. Genotypes and genetic variability of hepatitis B virus. *Intervirology,* 57**,** 141-50.

KUNG, P., GOLDSTEIN, G., REINHERZ, E. L. & SCHLOSSMAN, S. F. 1979. Monoclonal antibodies defining distinctive human T cell surface antigens. *Science,* 206**,** 347-9.

LABRIJN, A. F., JANMAAT, M. L., REICHERT, J. M. & PARREN, P. 2019. Bispecific antibodies: a mechanistic review of the pipeline. *Nat Rev Drug Discov,* 18**,** 585-608.

LASEK, W., ZAGOZDZON, R. & JAKOBISIAK, M. 2014. Interleukin 12: still a promising candidate for tumor immunotherapy? *Cancer Immunol Immunother,* 63**,** 419-35.

LEBIEN, T. W. & TEDDER, T. F. 2008. B lymphocytes: how they develop and function. *Blood,* 112**,** 1570-80.

LEE, K. J., CHOW, V., WEISSMAN, A., TULPULE, S., ALDOSS, I. & AKHTARI, M. 2016. Clinical use of blinatumomab for B-cell acute lymphoblastic leukemia in adults. *Ther Clin Risk Manag,* 12**,** 1301-10.

LEE, K. P., TAYLOR, C., PETRYNIAK, B., TURKA, L. A., JUNE, C. H. & THOMPSON, C. B. 1990. The genomic organization of the CD28 gene. Implications for the regulation of CD28 mRNA expression and heterogeneity. *J Immunol,* 145**,** 344-52.

LEVI, M. & TEN CATE, H. 1999. Disseminated intravascular coagulation. *N Engl J Med,* 341**,** 586-92.

LI, J., STAGG, N. J., JOHNSTON, J., HARRIS, M. J., MENZIES, S. A., DICARA, D., CLARK, V., HRISTOPOULOS, M., COOK, R., SLAGA, D., NAKAMURA, R., MCCARTY, L., SUKUMARAN, S., LUIS, E., YE, Z., WU, T. D., SUMIYOSHI, T., DANILENKO, D., LEE, G. Y., TOTPAL, K., ELLERMAN, D., HOTZEL, I., JAMES, J. R. & JUNTTILA, T. T. 2017. Membrane-Proximal Epitope Facilitates Efficient T Cell Synapse Formation by Anti-FcRH5/CD3 and Is a Requirement for Myeloma Cell Killing. *Cancer Cell,* 31**,** 383-395.

LI, Y. & KURLANDER, R. J. 2010. Comparison of anti-CD3 and anti-CD28-coated beads with soluble anti-CD3 for expanding human T cells: differing impact on CD8 T cell phenotype and responsiveness to restimulation. *J Transl Med,* 8**,** 104.

LI, Y., SEDWICK, C. E., HU, J. & ALTMAN, A. 2005. Role for protein kinase Ctheta (PKCtheta) in TCR/CD28-mediated signaling through the canonical but not the non-canonical pathway for NF-kappaB activation. *J Biol Chem,* 280**,** 1217-23.

LIESCHKE, G. J., RAO, P. K., GATELY, M. K. & MULLIGAN, R. C. 1997. Bioactive murine and human interleukin-12 fusion proteins which retain antitumor activity in vivo. *Nat Biotechnol,* 15**,** 35-40.

LIM, T. S., GOH, J. K. H., MORTELLARO, A., LIM, C. T., HÄMMERLING, G. J. & RICCIARDI-CASTAGNOLI, P. 2012. CD80 and CD86 differentially regulate mechanical interactions of T-cells with antigen-presenting dendritic cells and B-cells. *PloS one,* 7**,** e45185-e45185.

LIN, C. L., YANG, H. C. & KAO, J. H. 2016. Hepatitis B virus: new therapeutic perspectives. *Liver Int,* 36 Suppl 1**,** 85-92.

LINDEMANN, M., KOLDEHOFF, M., FIEDLER, M., SCHUMANN, A., OTTINGER, H. D., HEINEMANN, F. M., ROGGENDORF, M., HORN, P. A. & BEELEN, D. W. 2016. Control of hepatitis B virus infection in hematopoietic stem cell recipients after receiving grafts from vaccinated donors. *Bone Marrow Transplant,* 51**,** 428-31.

LINKE, R., KLEIN, A. & SEIMETZ, D. 2010. Catumaxomab: clinical development and future directions. *MAbs,* 2**,** 129-36.

LIU, L., LAM, C. K., LONG, V., WIDJAJA, L., YANG, Y., LI, H., JIN, L., BURKE, S., GORLATOV, S., BROWN, J., ALDERSON, R., LEWIS, M. D., NORDSTROM, J. L., KOENIG, S., MOORE, P. A., JOHNSON, S. & BONVINI, E. 2017. MGD011, A CD19 x CD3 Dual-Affinity Retargeting Bi-specific Molecule Incorporating

Extended Circulating Half-life for the Treatment of B-Cell Malignancies. *Clin Cancer Res,* 23**,** 1506-1518.

LIU, S., KOH, S. S. & LEE, C. G. 2016a. Hepatitis B Virus X Protein and Hepatocarcinogenesis. *Int J Mol Sci,* 17.

LIU, Y., GAO, L. F., LIANG, X. H. & MA, C. H. 2016b. Role of Tim-3 in hepatitis B virus infection: An overview. *World J Gastroenterol,* 22**,** 2294-303.

LLOVET, J. M., BURROUGHS, A. & BRUIX, J. 2003. Hepatocellular carcinoma. *Lancet,* 362**,** 1907-17.

LOFFLER, A., KUFER, P., LUTTERBUSE, R., ZETTL, F., DANIEL, P. T., SCHWENKENBECHER, J. M., RIETHMULLER, G., DORKEN, B. & BARGOU, R. C. 2000. A recombinant bispecific single-chain antibody, CD19 x CD3, induces rapid and high lymphoma-directed cytotoxicity by unstimulated T lymphocytes. *Blood,* 95**,** 2098-103.

LOOMBA, R. & LIANG, T. J. 2017. Hepatitis B Reactivation Associated With Immune Suppressive and Biological Modifier Therapies: Current Concepts, Management Strategies, and Future Directions. *Gastroenterology,* 152**,** 1297-1309.

LOPES, A. R., KELLAM, P., DAS, A., DUNN, C., KWAN, A., TURNER, J., PEPPA, D., GILSON, R. J., GEHRING, A., BERTOLETTI, A. & MAINI, M. K. 2008. Bim-mediated deletion of antigen-specific CD8 T cells in patients unable to control HBV infection. *J Clin Invest,* 118**,** 1835-45.

LUCIFORA, J., ARZBERGER, S., DURANTEL, D., BELLONI, L., STRUBIN, M., LEVRERO, M., ZOULIM, F., HANTZ, O. & PROTZER, U. 2011. Hepatitis B virus X protein is essential to initiate and maintain virus replication after infection. *J Hepatol,* 55**,** 996-1003.

LUCIFORA, J. & PROTZER, U. 2016. Attacking hepatitis B virus cccDNA--The holy grail to hepatitis B cure. *J Hepatol,* 64**,** S41-8.

LUCIFORA, J., XIA, Y., REISINGER, F., ZHANG, K., STADLER, D., CHENG, X., SPRINZL, M. F., KOPPENSTEINER, H., MAKOWSKA, Z., VOLZ, T., REMOUCHAMPS, C., CHOU, W. M., THASLER, W. E., HUSER, N., DURANTEL, D., LIANG, T. J., MUNK, C., HEIM, M. H., BROWNING, J. L., DEJARDIN, E., DANDRI, M., SCHINDLER, M., HEIKENWALDER, M. & PROTZER, U. 2014. Specific and nonhepatotoxic degradation of nuclear hepatitis B virus cccDNA. *Science,* 343**,** 1221-8.

LUHDER, F., HUANG, Y., DENNEHY, K. M., GUNTERMANN, C., MULLER, I., WINKLER, E., KERKAU, T., IKEMIZU, S., DAVIS, S. J., HANKE, T. & HUNIG, T. 2003. Topological requirements and signaling properties of T cell-activating, anti-CD28 antibody superagonists. *J Exp Med,* 197**,** 955-66.

MA, Z., DISCHER, D. E. & FINKEL, T. H. 2012. Mechanical force in T cell receptor signal initiation. *Front Immunol,* 3**,** 217.

MACOVEI, A., RADULESCU, C., LAZAR, C., PETRESCU, S., DURANTEL, D., DWEK, R. A., ZITZMANN, N. & NICHITA, N. B. 2010. Hepatitis B virus requires intact caveolin-1 function for productive infection in HepaRG cells. *J Virol,* 84**,** 243-53.

MAINS, P. E. & SIBLEY, C. H. 1983. The requirement of light chain for the surface deposition of the heavy chain of immunoglobulin M. *J Biol Chem,* 258**,** 5027-33.

MAKABE, K., ASANO, R., ITO, T., TSUMOTO, K., KUDO, T. & KUMAGAI, I. 2005. Tumor-directed lymphocyte-activating cytokines: refolding-based preparation of recombinant human interleukin-12 and an antibody variable domain-fused protein by additive-introduced stepwise dialysis. *Biochem Biophys Res Commun,* 328**,** 98-105.

MANKARIOUS, S., LEE, M., FISCHER, S., PYUN, K. H., OCHS, H. D., OXELIUS, V. A. & WEDGWOOD, R. J. 1988. The half-lives of IgG subclasses and specific antibodies in patients with primary immunodeficiency who are receiving intravenously administered immunoglobulin. *J Lab Clin Med,* 112**,** 634-40.

MARCHESI, V. T. & GOWANS, J. L. 1964. THE MIGRATION OF LYMPHOCYTES THROUGH THE ENDOTHELIUM OF VENULES IN LYMPH NODES: AN ELECTRON MICROSCOPE STUDY. *Proc R Soc Lond B Biol Sci,* 159**,** 283-90.

MEHROTRA, P. T., WU, D., CRIM, J. A., MOSTOWSKI, H. S. & SIEGEL, J. P. 1993. Effects of IL-12 on the generation of cytotoxic activity in human CD8+ T lymphocytes. *J Immunol,* 151**,** 2444-52.

MENG, W., TANG, A., YE, X., GUI, X., LI, L., FAN, X., SCHULTZ, R. D., FREED, D. C., HA, S., WANG, D., ZHANG, N., FU, T. M. & AN, Z. 2018. Targeting Human-Cytomegalovirus-Infected Cells by Redirecting T Cells Using an Anti-CD3/Anti-Glycoprotein B Bispecific Antibody. *Antimicrob Agents Chemother,* 62.

MERCHANT, A. M., ZHU, Z., YUAN, J. Q., GODDARD, A., ADAMS, C. W., PRESTA, L. G. & CARTER, P. 1998. An efficient route to human bispecific IgG. *Nat Biotechnol,* 16**,** 677-81.

MEUER, S. C., ACUTO, O., HUSSEY, R. E., HODGDON, J. C., FITZGERALD, K. A., SCHLOSSMAN, S. F. & REINHERZ, E. L. 1983a. Evidence for the T3-associated 90K heterodimer as the T-cell antigen receptor. *Nature,* 303**,** 808-10.

MEUER, S. C., FITZGERALD, K. A., HUSSEY, R. E., HODGDON, J. C., SCHLOSSMAN, S. F. & REINHERZ, E. L. 1983b. Clonotypic structures involved in antigen-specific human T cell function. Relationship to the T3 molecular complex. *J Exp Med,* 157**,** 705-19.

MEYER-BERG, H. 2016. *Inducible Interleukin-12 Expression and its Influence on the Activity of S-CAR Redirected T Cells.* Master's Thesis, Technische Universität München.

MICCO, L., PEPPA, D., LOGGI, E., SCHURICH, A., JEFFERSON, L., CURSARO, C., PANNO, A. M., BERNARDI, M., BRANDER, C., BIHL, F., ANDREONE, P. & MAINI, M. K. 2013. Differential boosting of innate and adaptive antiviral responses during pegylated-interferon-alpha therapy of chronic hepatitis B. *J Hepatol,* 58**,** 225-33.

MILLER, R. H. & ROBINSON, W. S. 1984. Hepatitis B virus DNA forms in nuclear and cytoplasmic fractions of infected human liver. *Virology,* 137**,** 390-9.

MILSTEIN, C. & CUELLO, A. C. 1983. Hybrid hybridomas and their use in immunohistochemistry. *Nature,* 305**,** 537-40.

MINGUET, S., SWAMY, M., ALARCON, B., LUESCHER, I. F. & SCHAMEL, W. W. 2007. Full activation of the T cell receptor requires both clustering and conformational changes at CD3. *Immunity,* 26**,** 43-54.

MOSMANN, T. R., CHERWINSKI, H., BOND, M. W., GIEDLIN, M. A. & COFFMAN, R. L. 1986. Two types of murine helper T cell clone. I. Definition according to profiles of lymphokine activities and secreted proteins. *J Immunol,* 136**,** 2348-57.

MULLARD, A. 2020. Trispecific antibodies take to the clinic. *Nat Rev Drug Discov,* 19**,** 657-658.

MURATA, Y., KAWASHIMA, K., SHEIKH, K., TANAKA, Y. & ISOGAWA, M. 2018. Intrahepatic Cross-Presentation and Hepatocellular Antigen Presentation Play Distinct Roles in the Induction of Hepatitis B Virus-Specific CD8⁺ T Cell Responses. *Journal of Virology,* 92**,** e00920-18.

MURPHY, K. & WEAVER, C. 2016. *Janeway's immunobiology,* New York, NY, Garland Science/Taylor & Francis Group, LLC.

NASSAL, M. 2015. HBV cccDNA: viral persistence reservoir and key obstacle for a cure of chronic hepatitis B. *Gut,* 64**,** 1972-84.

OLDENBURG, J., MAHLANGU, J. N., KIM, B., SCHMITT, C., CALLAGHAN, M. U., YOUNG, G., SANTAGOSTINO, E., KRUSE-JARRES, R., NEGRIER, C., KESSLER, C., VALENTE, N., ASIKANIUS, E., LEVY, G. G., WINDYGA, J. & SHIMA, M. 2017. Emicizumab Prophylaxis in Hemophilia A with Inhibitors. *N Engl J Med,* 377**,** 809-818.

ONO, A., SUZUKI, F., KAWAMURA, Y., SEZAKI, H., HOSAKA, T., AKUTA, N., KOBAYASHI, M., SUZUKI, Y., SAITOU, S., ARASE, Y., IKEDA, K., KOBAYASHI, M., WATAHIKI, S., MINETA, R. & KUMADA, H. 2012. Long-term continuous entecavir therapy in nucleos(t)ide-naive chronic hepatitis B patients. *J Hepatol,* 57**,** 508-14.

PARK, J. J., WONG, D. K., WAHED, A. S., LEE, W. M., FELD, J. J., TERRAULT, N., KHALILI, M., STERLING, R. K., KOWDLEY, K. V., BZOWEJ, N., LAU, D. T., KIM, W. R., SMITH, C., CARITHERS, R. L., TORREY, K. W., KEITH, J. W., LEVINE, D. L., TRAUM, D., HO, S., VALIGA, M. E., JOHNSON, G. S., DOO, E., LOK, A. S., CHANG, K. M. & HEPATITIS, B. R. N. 2016. Hepatitis B Virus--Specific and Global T-Cell Dysfunction in Chronic Hepatitis B. *Gastroenterology,* 150**,** 684-695 e5.

PATHAN, N., HEMINGWAY, C. A., ALIZADEH, A. A., STEPHENS, A. C., BOLDRICK, J. C., ORAGUI, E. E., MCCABE, C., WELCH, S. B., WHITNEY, A., O'GARA, P., NADEL, S., RELMAN, D. A., HARDING, S. E. & LEVIN, M. 2004. Role of interleukin 6 in myocardial dysfunction of meningococcal septic shock. *Lancet,* 363**,** 203-9.

PATIENT, R., HOURIOUX, C., SIZARET, P. Y., TRASSARD, S., SUREAU, C. & ROINGEARD, P. 2007. Hepatitis B virus subviral envelope particle morphogenesis and intracellular trafficking. *J Virol,* 81**,** 3842-51.

PAZGAN-SIMON, M., SIMON, K. A., JAROWICZ, E., ROTTER, K., SZYMANEK-PASTERNAK, A. & ZUWALA-JAGIELLO, J. 2018. Hepatitis B virus treatment in hepatocellular carcinoma patients prolongs survival and reduces the risk of cancer recurrence. *Clin Exp Hepatol,* 4**,** 210-216.

PEERIDOGAHEH, H., MESHKAT, Z., HABIBZADEH, S., ARZANLOU, M., SHAHI, J. M., ROSTAMI, S., GERAYLI, S. & TEIMOURPOUR, R. 2018. Current concepts on immunopathogenesis of hepatitis B virus infection. *Virus Res,* 245**,** 29-43.

PENG, L. S., PENICHET, M. L. & MORRISON, S. L. 1999. A single-chain IL-12 IgG3 antibody fusion protein retains antibody specificity and IL-12 bioactivity and demonstrates antitumor activity. *J Immunol,* 163**,** 250-8.

PETERS, P. J., BORST, J., OORSCHOT, V., FUKUDA, M., KRAHENBUHL, O., TSCHOPP, J., SLOT, J. W. & GEUZE, H. J. 1991. Cytotoxic T lymphocyte granules are secretory lysosomes, containing both perforin and granzymes. *J Exp Med,* 173**,** 1099-109.

POLLACK, J. R. & GANEM, D. 1994. Site-specific RNA binding by a hepatitis B virus reverse transcriptase initiates two distinct reactions: RNA packaging and DNA synthesis. *J Virol,* 68**,** 5579-87.

PORTELL, C. A., WENZELL, C. M. & ADVANI, A. S. 2013. Clinical and pharmacologic aspects of blinatumomab in the treatment of B-cell acute lymphoblastic leukemia. *Clin Pharmacol,* 5**,** 5-11.

PROTZER, U., BOHNE , F., QUITT, O., MOMBURG, F. & MOLDENHAUER, G. 2016. *Trispecific binding molecules for treating HBV infection and associated conditions*.

PROTZER, U., MAINI, M. K. & KNOLLE, P. A. 2012. Living in the liver: hepatic infections. *Nat Rev Immunol,* 12**,** 201-13.

QADRI, I., FATIMA, K. & ABDE, L. H. H. 2011. Hepatitis B virus X protein impedes the DNA repair via its association with transcription factor, TFIIH. *BMC Microbiol,* 11**,** 48.

QUEZADA, S. A., SIMPSON, T. R., PEGGS, K. S., MERGHOUB, T., VIDER, J., FAN, X., BLASBERG, R., YAGITA, H., MURANSKI, P., ANTONY, P. A., RESTIFO, N. P. & ALLISON, J. P. 2010. Tumor-reactive CD4(+) T cells develop cytotoxic activity and eradicate large established melanoma after transfer into lymphopenic hosts. *J Exp Med,* 207**,** 637-50.

QUINTERO-HERNANDEZ, V., JUAREZ-GONZALEZ, V. R., ORTIZ-LEON, M., SANCHEZ, R., POSSANI, L. D. & BECERRIL, B. 2007. The change of the scFv into the Fab format improves the stability and in vivo toxin neutralization capacity of recombinant antibodies. *Mol Immunol,* 44**,** 1307-15.

QUITT, O. 2013. *Generation and functional analysis of bispecific antibodies for immunotherapy of chronic hepatitis B virus infection.* Master`s Thesis, Technische Universität München.

RABE, B., VLACHOU, A., PANTE, N., HELENIUS, A. & KANN, M. 2003. Nuclear import of hepatitis B virus capsids and release of the viral genome. *Proc Natl Acad Sci U S A,* 100**,** 9849-54.

RAMMENSEE, H. G., FRIEDE, T. & STEVANOVIIC, S. 1995. MHC ligands and peptide motifs: first listing. *Immunogenetics,* 41**,** 178-228.

REHERMANN, B. & NASCIMBENI, M. 2005. Immunology of hepatitis B virus and hepatitis C virus infection. *Nat Rev Immunol,* 5**,** 215-29.

REINHERZ, E. L., KUNG, P. C., GOLDSTEIN, G. & SCHLOSSMAN, S. F. 1979. Separation of Functional Subsets of Human T Cells by a Monoclonal Antibody. *Proceedings of the National Academy of Sciences of the United States of America,* 76**,** 4061-4065.

REINHERZ, E. L., MEUER, S., FITZGERALD, K. A., HUSSEY, R. E., LEVINE, H. & SCHLOSSMAN, S. F. 1982. Antigen recognition by human T lymphocytes is linked to surface expression of the T3 molecular complex. *Cell,* 30**,** 735-743.

REITER, Y., BRINKMANN, U., KREITMAN, R. J., JUNG, S. H., LEE, B. & PASTAN, I. 1994. Stabilization of the Fv fragments in recombinant immunotoxins by disulfide bonds engineered into conserved framework regions. *Biochemistry,* 33**,** 5451-9.

RETH, M. 1989. Antigen receptor tail clue. *Nature,* 338**,** 383-4.

RHIM, J. A., SANDGREN, E. P., DEGEN, J. L., PALMITER, R. D. & BRINSTER, R. L. 1994. Replacement of diseased mouse liver by hepatic cell transplantation. *Science,* 263**,** 1149-52.

RIESENBERG, R., BUCHNER, A., POHLA, H. & LINDHOFER, H. 2001. Lysis of prostate carcinoma cells by trifunctional bispecific antibodies (alpha EpCAM x alpha CD3). *J Histochem Cytochem,* 49**,** 911-7.

RINCÓN, M. & FLAVELL, R. A. 1994. AP-1 transcriptional activity requires both T-cell receptor-mediated and co-stimulatory signals in primary T lymphocytes. *The EMBO journal,* 13**,** 4370-4381.

RIZZETTO, M. & CIANCIO, A. 2008. Chronic HBV-related liver disease. *Mol Aspects Med,* 29**,** 72-84.

ROOHI, A., KHOSHNOODI, J., ZARNANI, A. H. & SHOKRI, F. 2005. Epitope mapping of recombinant hepatitis B surface antigen by murine monoclonal antibodies. *Hybridoma (Larchmt),* 24**,** 71-7.

ROSSI, D. L., ROSSI, E. A., CARDILLO, T. M., GOLDENBERG, D. M. & CHANG, C. H. 2014. A new class of bispecific antibodies to redirect T cells for cancer immunotherapy. *MAbs,* 6**,** 381-91.

ROYER, H. D., ACUTO, O., FABBI, M., TIZARD, R., RAMACHANDRAN, K., SMART, J. E. & REINHERZ, E. L. 1984. Genes encoding the Ti beta subunit of the antigen/MHC receptor undergo rearrangement during intrathymic ontogeny prior to surface T3-Ti expression. *Cell,* 39**,** 261-6.

RUDD, C. E., TREVILLYAN, J. M., DASGUPTA, J. D., WONG, L. L. & SCHLOSSMAN, S. F. 1988. The CD4 receptor is complexed in detergent lysates to a protein-tyrosine kinase (pp58) from human T lymphocytes. *Proc Natl Acad Sci U S A,* 85**,** 5190-4.

SALLUSTO, F., GEGINAT, J. & LANZAVECCHIA, A. 2004. Central memory and effector memory T cell subsets: function, generation, and maintenance. *Annu Rev Immunol,* 22**,** 745-63.

SALLUSTO, F., LENIG, D., FÖRSTER, R., LIPP, M. & LANZAVECCHIA, A. 1999. Two subsets of memory T lymphocytes with distinct homing potentials and effector functions. *Nature,* 402**,** 34-38.

SAUNDERS, K. O. 2019. Conceptual Approaches to Modulating Antibody Effector Functions and Circulation Half-Life. *Frontiers in immunology,* 10**,** 1296-1296.

SCHAEFER, S. 2007. Hepatitis B virus taxonomy and hepatitis B virus genotypes. *World J Gastroenterol,* 13**,** 14-21.

SCHMITT, J., HESS, H. & STUNNENBERG, H. G. 1993. Affinity purification of histidine-tagged proteins. *Mol Biol Rep,* 18**,** 223-30.

SCHMITZ, A., SCHWARZ, A., FOSS, M., ZHOU, L., RABE, B., HOELLENRIEGEL, J., STOEBER, M., PANTE, N. & KANN, M. 2010. Nucleoporin 153 arrests the nuclear import of hepatitis B virus capsids in the nuclear basket. *PLoS Pathog,* 6**,** e1000741.

SCHROEDER, H. W., JR. & CAVACINI, L. 2010. Structure and function of immunoglobulins. *J Allergy Clin Immunol,* 125**,** S41-52.

SCHULZE, A., GRIPON, P. & URBAN, S. 2007. Hepatitis B virus infection initiates with a large surface protein-dependent binding to heparan sulfate proteoglycans. *Hepatology,* 46**,** 1759-68.

SCHURICH, A., KHANNA, P., LOPES, A. R., HAN, K. J., PEPPA, D., MICCO, L., NEBBIA, G., KENNEDY, P. T., GERETTI, A. M., DUSHEIKO, G. & MAINI, M. K. 2011. Role of the coinhibitory receptor cytotoxic T lymphocyte antigen-4 on apoptosis-Prone CD8 T cells in persistent hepatitis B virus infection. *Hepatology,* 53**,** 1494-503.

SEEGER, C. & MASON, W. S. 2015. Molecular biology of hepatitis B virus infection. *Virology,* 479-480**,** 672-86.

SHAW, J. P., UTZ, P. J., DURAND, D. B., TOOLE, J. J., EMMEL, E. A. & CRABTREE, G. R. 1988. Identification of a putative regulator of early T cell activation genes. *Science,* 241**,** 202-5.

SHEN, L., ZHANG, X., HU, D., FENG, T., LI, H., LU, Y. & HUANG, J. 2013. Hepatitis B virus X (HBx) play an anti-apoptosis role in hepatic progenitor cells by activating Wnt/beta-catenin pathway. *Mol Cell Biochem,* 383**,** 213-22.

SHEPHERD, J. C., SCHUMACHER, T. N., ASHTON-RICKARDT, P. G., IMAEDA, S., PLOEGH, H. L., JANEWAY, C. A., JR. & TONEGAWA, S. 1993. TAP1-dependent peptide translocation in vitro is ATP dependent and peptide selective. *Cell,* 74**,** 577-84.

SHI, Y., WU, W., WAN, T., LIU, Y., PENG, G., CHEN, Z. & ZHU, H. 2013. Impact of polyclonal anti-CD3/CD28-coated magnetic bead expansion methods on T cell proliferation, differentiation and function. *Int Immunopharmacol,* 15**,** 129-37.

SHIMABUKURO-VORNHAGEN, A., GODEL, P., SUBKLEWE, M., STEMMLER, H. J., SCHLOSSER, H. A., SCHLAAK, M., KOCHANEK, M., BOLL, B. & VON BERGWELT-BAILDON, M. S. 2018. Cytokine release syndrome. *J Immunother Cancer,* 6**,** 56.

SIEFKEN, R., KLEIN-HESSLING, S., SERFLING, E., KURRLE, R. & SCHWINZER, R. 1998. A CD28-associated signaling pathway leading to cytokine gene transcription and T cell proliferation without TCR engagement. *J Immunol,* 161**,** 1645-51.

SKOKOS, D., WAITE, J. C., HABER, L., CRAWFORD, A., HERMANN, A., ULLMAN, E., SLIM, R., GODIN, S., AJITHDOSS, D., YE, X., WANG, B., WU, Q., RAMOS, I., PAWASHE, A., CANOVA, L., VAZZANA, K., RAM, P., HERLIHY, E., AHMED, H., OSWALD, E., GOLUBOV, J., POON, P., HAVEL, L., CHIU, D., LAZO, M., PROVONCHA, K., YU, K., KIM, J., WARSAW, J. J., STOKES ORISTIAN, N., SIAO, C. J., DUDGEON, D., HUANG, T., POTOCKY, T., MARTIN, J., MACDONALD, D., OYEJIDE, A., RAFIQUE, A., POUEYMIROU, W., KIRSHNER, J. R., SMITH, E., OLSON, W., LIN, J., THURSTON, G., SLEEMAN,

M. A., MURPHY, A. J. & YANCOPOULOS, G. D. 2020. A class of costimulatory CD28-bispecific antibodies that enhance the antitumor activity of CD3-bispecific antibodies. *Sci Transl Med,* 12.

STAPLETON, N. M., ARMSTRONG-FISHER, S. S., ANDERSEN, J. T., VAN DER SCHOOT, C. E., PORTER, C., PAGE, K. R., FALCONER, D., DE HAAS, M., WILLIAMSON, L. M., CLARK, M. R., VIDARSSON, G. & ARMOUR, K. L. 2018. Human IgG lacking effector functions demonstrate lower FcRn-binding and reduced transplacental transport. *Mol Immunol,* 95**,** 1-9.

STOYLE, C. L., STEPHENS, P. E., HUMPHREYS, D. P., HEYWOOD, S., CAIN, K. & BULLEID, N. J. 2017. IgG light chain-independent secretion of heavy chain dimers: consequence for therapeutic antibody production and design. *Biochem J,* 474**,** 3179-3188.

STRICK-MARCHAND, H., DUSSEAUX, M., DARCHE, S., HUNTINGTON, N. D., LEGRAND, N., MASSE-RANSON, G., CORCUFF, E., AHODANTIN, J., WEIJER, K., SPITS, H., KREMSDORF, D. & DI SANTO, J. P. 2015. A novel mouse model for stable engraftment of a human immune system and human hepatocytes. *PLoS One,* 10**,** e0119820.

SU, T. H., HU, T. H., CHEN, C. Y., HUANG, Y. H., CHUANG, W. L., LIN, C. C., WANG, C. C., SU, W. W., CHEN, M. Y., PENG, C. Y., CHIEN, R. N., HUANG, Y. W., WANG, H. Y., LIN, C. L., YANG, S. S., CHEN, T. M., MO, L. R., HSU, S. J., TSENG, K. C., HSIEH, T. Y., SUK, F. M., HU, C. T., BAIR, M. J., LIANG, C. C., LEI, Y. C., TSENG, T. C., CHEN, C. L., KAO, J. H., GROUP, C. T. S. & THE TAIWAN LIVER DISEASES, C. 2016. Four-year entecavir therapy reduces hepatocellular carcinoma, cirrhotic events and mortality in chronic hepatitis B patients. *Liver Int,* 36**,** 1755-1764.

SUNG, J. A., PICKERAL, J., LIU, L., STANFIELD-OAKLEY, S. A., LAM, C. Y., GARRIDO, C., POLLARA, J., LABRANCHE, C., BONSIGNORI, M., MOODY, M. A., YANG, Y., PARKS, R., ARCHIN, N., ALLARD, B., KIRCHHERR, J., KURUC, J. D., GAY, C. L., COHEN, M. S., OCHSENBAUER, C., SODERBERG, K., LIAO, H. X., MONTEFIORI, D., MOORE, P., JOHNSON, S., KOENIG, S., HAYNES, B. F., NORDSTROM, J. L., MARGOLIS, D. M. & FERRARI, G. 2015. Dual-Affinity Re-Targeting proteins direct T cell-mediated cytolysis of latently HIV-infected cells. *J Clin Invest,* 125**,** 4077-90.

SUNTHARALINGAM, G., PERRY, M. R., WARD, S., BRETT, S. J., CASTELLO-CORTES, A., BRUNNER, M. D. & PANOSKALTSIS, N. 2006. Cytokine storm in a phase 1 trial of the anti-CD28 monoclonal antibody TGN1412. *N Engl J Med,* 355**,** 1018-28.

TAKAHASHI, K., MACHIDA, A., FUNATSU, G., NOMURA, M., USUDA, S., AOYAGI, S., TACHIBANA, K., MIYAMOTO, H., IMAI, M., NAKAMURA, T., MIYAKAWA, Y. & MAYUMI, M. 1983. Immunochemical structure of hepatitis B e antigen in the serum. *J Immunol,* 130**,** 2903-7.

TANTIWETRUEANGDET, A., PANVICHIAN, R., SORNMAYURA, P., SUEANGOEN, N. & LEELAUDOMLIPI, S. 2018. Reduced HBV cccDNA and HBsAg in HBV-associated hepatocellular carcinoma tissues. *Med Oncol,* 35**,** 127.

TEACHEY, D. T., RHEINGOLD, S. R., MAUDE, S. L., ZUGMAIER, G., BARRETT, D. M., SEIF, A. E., NICHOLS, K. E., SUPPA, E. K., KALOS, M., BERG, R. A., FITZGERALD, J. C., APLENC, R., GORE, L. & GRUPP, S. A. 2013. Cytokine release syndrome after blinatumomab treatment related to abnormal macrophage activation and ameliorated with cytokine-directed therapy. *Blood,* 121**,** 5154-7.

TERRAULT, N. A., BZOWEJ, N. H., CHANG, K. M., HWANG, J. P., JONAS, M. M., MURAD, M. H. & AMERICAN ASSOCIATION FOR THE STUDY OF LIVER, D. 2016. AASLD guidelines for treatment of chronic hepatitis B. *Hepatology,* 63**,** 261-83.

THIMME, R., WIELAND, S., STEIGER, C., GHRAYEB, J., REIMANN, K. A., PURCELL, R. H. & CHISARI, F. V. 2003. CD8(+) T cells mediate viral clearance and disease pathogenesis during acute hepatitis B virus infection. *J Virol,* 77**,** 68-76.

THOMSON, A. W. & KNOLLE, P. A. 2010. Antigen-presenting cell function in the tolerogenic liver environment. *Nat Rev Immunol,* 10**,** 753-66.

TILLMANN, H. L. & PATEL, K. 2014. Therapy of acute and fulminant hepatitis B. *Intervirology,* 57**,** 181-8.

TINOCO, R., ALCALDE, V., YANG, Y., SAUER, K. & ZUNIGA, E. I. 2009. Cell-intrinsic transforming growth factor-beta signaling mediates virus-specific CD8+ T cell deletion and viral persistence in vivo. *Immunity,* 31**,** 145-57.

TRIVEDI, A., STIENEN, S., ZHU, M., LI, H., YURASZECK, T., GIBBS, J., HEATH, T., LOBERG, R. & KASICHAYANULA, S. 2017. Clinical Pharmacology and Translational Aspects of Bispecific Antibodies. *Clin Transl Sci,* 10**,** 147-162.

TUTTLEMAN, J. S., POURCEL, C. & SUMMERS, J. 1986. Formation of the pool of covalently closed circular viral DNA in hepadnavirus-infected cells. *Cell,* 47**,** 451-60.

UNVERDORBEN, F., RICHTER, F., HUTT, M., SEIFERT, O., MALINGE, P., FISCHER, N. & KONTERMANN, R. E. 2016. Pharmacokinetic properties of IgG and various Fc fusion proteins in mice. *MAbs,* 8**,** 120-8.

VALLE, A., BARBAGIOVANNI, G., JOFRA, T., STABILINI, A., PEROL, L., BAEYENS, A., ANAND, S., CAGNARD, N., GAGLIANI, N., PIAGGIO, E. & BATTAGLIA, M. 2015. Heterogeneous CD3 expression levels in differing T cell subsets correlate with the in vivo anti-CD3-mediated T cell modulation. *J Immunol,* 194**,** 2117-27.

VAN OERS, N. S., KILLEEN, N. & WEISS, A. 1996. Lck regulates the tyrosine phosphorylation of the T cell receptor subunits and ZAP-70 in murine thymocytes. *The Journal of experimental medicine,* 183**,** 1053-1062.

VAN SPRIEL, A. B., VAN OJIK, H. H. & VAN DE WINKEL, J. G. 2000. Immunotherapeutic perspective for bispecific antibodies. *Immunol Today,* 21**,** 391-7.

VEILLETTE, A., BOOKMAN, M. A., HORAK, E. M. & BOLEN, J. B. 1988. The CD4 and CD8 T cell surface antigens are associated with the internal membrane tyrosine-protein kinase p56lck. *Cell,* 55**,** 301-8.

VICTORA, G. D. & NUSSENZWEIG, M. C. 2012. Germinal Centers. *Annual Review of Immunology,* 30**,** 429-457.

VLACHOGIANNAKOS, J. & PAPATHEODORIDIS, G. 2013. Hepatocellular carcinoma in chronic hepatitis B patients under antiviral therapy. *World J Gastroenterol,* 19**,** 8822-30.

WANG, Y., WU, M. C., SHAM, J. S., TAI, L. S., FANG, Y., WU, W. Q., XIE, D. & GUAN, X. Y. 2002. Different expression of hepatitis B surface antigen between hepatocellular carcinoma and its surrounding liver tissue, studied using a tissue microarray. *J Pathol,* 197**,** 610-6.

WATANABE, T., SORENSEN, E. M., NAITO, A., SCHOTT, M., KIM, S. & AHLQUIST, P. 2007. Involvement of host cellular multivesicular body functions in hepatitis B virus budding. *Proc Natl Acad Sci U S A,* 104**,** 10205-10.

WEBSTER, G. J., REIGNAT, S., BROWN, D., OGG, G. S., JONES, L., SENEVIRATNE, S. L., WILLIAMS, R., DUSHEIKO, G. & BERTOLETTI, A. 2004. Longitudinal analysis of CD8+ T cells specific for structural and nonstructural hepatitis B virus proteins in patients with chronic hepatitis B: implications for immunotherapy. *J Virol,* 78**,** 5707-19.

WEI, L. H., CHOU, C. H., CHEN, M. W., ROSE-JOHN, S., KUO, M. L., CHEN, S. U. & YANG, Y. S. 2013. The role of IL-6 trans-signaling in vascular leakage: implications for ovarian hyperstimulation syndrome in a murine model. *J Clin Endocrinol Metab,* 98**,** E472-84.

WEISSMULLER, S., KRONHART, S., KREUZ, D., SCHNIERLE, B., KALINKE, U., KIRBERG, J., HANSCHMANN, K. M. & WAIBLER, Z. 2016. TGN1412 Induces Lymphopenia and Human Cytokine Release in a Humanized Mouse Model. *PLoS One,* 11**,** e0149093.

WHO 2017. Hepatitis B vaccines WHO position paper. *Weekly Epidemiological Record,* 92 (27)**,** 369-392.

WHO. 2019. *Hepatitis B, Fact sheet* [Online]. Available: https://www.who.int/news-room/fact-sheets/detail/hepatitis-b [Accessed].

WIELAND, S., THIMME, R., PURCELL, R. H. & CHISARI, F. V. 2004a. Genomic analysis of the host response to hepatitis B virus infection. *Proc Natl Acad Sci U S A,* 101**,** 6669-74.

WIELAND, S. F., SPANGENBERG, H. C., THIMME, R., PURCELL, R. H. & CHISARI, F. V. 2004b. Expansion and contraction of the hepatitis B virus transcriptional template in infected chimpanzees. *Proc Natl Acad Sci U S A,* 101**,** 2129-34.

WILL, H., REISER, W., WEIMER, T., PFAFF, E., BUSCHER, M., SPRENGEL, R., CATTANEO, R. & SCHALLER, H. 1987. Replication strategy of human hepatitis B virus. *J Virol,* 61**,** 904-11.

WILLBERG, C. B., WARD, S. M., CLAYTON, R. F., NAOUMOV, N. V., MCCORMICK, C., PROTO, S., HARRIS, M., PATEL, A. H. & KLENERMAN, P. 2007. Protection of hepatocytes from cytotoxic T cell mediated killing by interferon-alpha. *PLoS One,* 2**,** e791.

WILLUDA, J., HONEGGER, A., WAIBEL, R., SCHUBIGER, P. A., STAHEL, R., ZANGEMEISTER-WITTKE, U. & PLUCKTHUN, A. 1999. High thermal stability is essential for tumor targeting of antibody fragments: engineering of a humanized anti-epithelial glycoprotein-2 (epithelial cell adhesion molecule) single-chain Fv fragment. *Cancer Res,* 59**,** 5758-67.

WISSKIRCHEN, K., METZGER, K., SCHREIBER, S., ASEN, T., WEIGAND, L., DARGEL, C., WITTER, K., KIEBACK, E., SPRINZL, M. F., UCKERT, W., SCHIEMANN, M., BUSCH, D. H., KRACKHARDT, A. M. & PROTZER, U. 2017. Isolation and functional characterization of hepatitis B virus-specific T-cell receptors as new tools for experimental and clinical use. *PLoS One,* 12**,** e0182936.

WOHLLEBER, D. & KNOLLE, P. A. 2012. The Liver as an Immune-Privileged Site. *In:* STEIN-STREILEIN, J. (ed.) *Infection, Immune Homeostasis and Immune Privilege.* Basel: Springer Basel.

WU, L., SEUNG, E., XU, L., RAO, E., LORD, D. M., WEI, R. R., CORTEZ-RETAMOZO, V., OSPINA, B., POSTERNAK, V., ULINSKI, G., PIEPENHAGEN, P., FRANCESCONI, E., EL-MURR, N., BEIL, C., KIRBY, P., LI, A., FRETLAND, J., VICENTE, R., DENG, G., DABDOUBI, T., CAMERON, B., BERTRAND, T., FERRARI, P., POUZIEUX, S., LEMOINE, C., PRADES, C., PARK, A., QIU, H., SONG, Z., ZHANG, B., SUN, F., CHIRON, M., RAO, S., RADOŠEVIĆ, K., YANG, Z.-Y. & NABEL, G. J. 2020. Trispecific antibodies enhance the therapeutic efficacy of tumor-directed T cells through T cell receptor co-stimulation. *Nature Cancer,* 1**,** 86-98.

WURSTHORN, K., LUTGEHETMANN, M., DANDRI, M., VOLZ, T., BUGGISCH, P., ZOLLNER, B., LONGERICH, T., SCHIRMACHER, P., METZLER, F., ZANKEL, M., FISCHER, C., CURRIE, G., BROSGART, C. & PETERSEN, J. 2006. Peginterferon alpha-2b plus adefovir induce strong cccDNA decline and HBsAg reduction in patients with chronic hepatitis B. *Hepatology,* 44**,** 675-84.

XIA, Y., STADLER, D., KO, C. & PROTZER, U. 2017. Analyses of HBV cccDNA Quantification and Modification. *Methods Mol Biol,* 1540**,** 59-72.

XIA, Y., STADLER, D., LUCIFORA, J., REISINGER, F., WEBB, D., HOSEL, M., MICHLER, T., WISSKIRCHEN, K., CHENG, X., ZHANG, K., CHOU, W. M., WETTENGEL, J. M., MALO, A., BOHNE, F., HOFFMANN, D., EYER, F.,

THIMME, R., FALK, C. S., THASLER, W. E., HEIKENWALDER, M. & PROTZER, U. 2016. Interferon-gamma and Tumor Necrosis Factor-alpha Produced by T Cells Reduce the HBV Persistence Form, cccDNA, Without Cytolysis. *Gastroenterology,* 150**,** 194-205.

XU, C., GAGNON, E., CALL, M. E., SCHNELL, J. R., SCHWIETERS, C. D., CARMAN, C. V., CHOU, J. J. & WUCHERPFENNIG, K. W. 2008. Regulation of T cell receptor activation by dynamic membrane binding of the CD3epsilon cytoplasmic tyrosine-based motif. *Cell,* 135**,** 702-13.

XU, D., ALEGRE, M. L., VARGA, S. S., ROTHERMEL, A. L., COLLINS, A. M., PULITO, V. L., HANNA, L. S., DOLAN, K. P., PARREN, P. W., BLUESTONE, J. A., JOLLIFFE, L. K. & ZIVIN, R. A. 2000. In vitro characterization of five humanized OKT3 effector function variant antibodies. *Cell Immunol,* 200**,** 16-26.

YAN, H., ZHONG, G., XU, G., HE, W., JING, Z., GAO, Z., HUANG, Y., QI, Y., PENG, B., WANG, H., FU, L., SONG, M., CHEN, P., GAO, W., REN, B., SUN, Y., CAI, T., FENG, X., SUI, J. & LI, W. 2012. Sodium taurocholate cotransporting polypeptide is a functional receptor for human hepatitis B and D virus. *Elife,* 1**,** e00049.

YANG, D., LIU, L., ZHU, D., PENG, H., SU, L., FU, Y. X. & ZHANG, L. 2014. A mouse model for HBV immunotolerance and immunotherapy. *Cell Mol Immunol,* 11**,** 71-8.

YU, J., WANG, W. & HUANG, H. 2019. Efficacy and safety of bispecific T-cell engager (BiTE) antibody blinatumomab for the treatment of relapsed/refractory acute lymphoblastic leukemia and non-Hodgkin's lymphoma: a systemic review and meta-analysis. *Hematology,* 24**,** 199-207.

YUEN, M. F., SETO, W. K., CHOW, D. H., TSUI, K., WONG, D. K., NGAI, V. W., WONG, B. C., FUNG, J., YUEN, J. C. & LAI, C. L. 2007. Long-term lamivudine therapy reduces the risk of long-term complications of chronic hepatitis B infection even in patients without advanced disease. *Antivir Ther,* 12**,** 1295-303.

ZHANG, L., KERKAR, S. P., YU, Z., ZHENG, Z., YANG, S., RESTIFO, N. P., ROSENBERG, S. A. & MORGAN, R. A. 2011. Improving adoptive T cell therapy by targeting and controlling IL-12 expression to the tumor environment. *Mol Ther,* 19**,** 751-9.

ZHANG, S., ZHAO, J. & ZHANG, Z. 2018. Humoral immunity, the underestimated player in hepatitis B. *Cell Mol Immunol,* 15**,** 645-648.

ZHANG, W., SLOAN-LANCASTER, J., KITCHEN, J., TRIBLE, R. P. & SAMELSON, L. E. 1998. LAT: the ZAP-70 tyrosine kinase substrate that links T cell receptor to cellular activation. *Cell,* 92**,** 83-92.

ZHAO, L. H., LIU, X., YAN, H. X., LI, W. Y., ZENG, X., YANG, Y., ZHAO, J., LIU, S. P., ZHUANG, X. H., LIN, C., QIN, C. J., ZHAO, Y., PAN, Z. Y., HUANG, G., LIU, H., ZHANG, J., WANG, R. Y., YANG, Y., WEN, W., LV, G. S., ZHANG, H. L., WU, H., HUANG, S., WANG, M. D., TANG, L., CAO, H. Z., WANG, L., LEE, T. L., JIANG, H., TAN, Y. X., YUAN, S. X., HOU, G. J., TAO, Q. F., XU, Q. G., ZHANG, X. Q., WU, M. C., XU, X., WANG, J., YANG, H. M., ZHOU, W. P. & WANG, H. Y. 2016. Genomic and oncogenic preference of HBV integration in hepatocellular carcinoma. *Nat Commun,* 7**,** 12992.

ZINKERNAGEL, R. M. & DOHERTY, P. C. 1974. Immunological surveillance against altered self components by sensitised T lymphocytes in lymphocytic choriomeningitis. *Nature,* 251**,** 547-8.

ZOULIM, F., LEBOSSE, F. & LEVRERO, M. 2016. Current treatments for chronic hepatitis B virus infections. *Curr Opin Virol,* 18**,** 109-16.

Acknowledgments

First, I thank my first supervisor Prof. Ulrike Protzer for her guidance throughout my PhD study. She supported me continuously during all these years and gave valuable input for my project, but also room for my own ideas and development.

Moreover, I thank my second supervisor Prof. Percy Knolle for his time and the interesting ideas on my project during the thesis committee meetings and the shared retreats.

I also thank Prof. Dietmar Zehn for giving very detailed feedback on the written thesis and support during my thesis defense.

Special thanks go to my mentor Felix Bohne, who took me in as a Master student and taught me so much about being a scientist. We shared interesting ideas and fruitful discussions on a professional as well as a private level and I will always be grateful for your patience, your happiness and our friendship.

Next, I thank our collaborators Sandra Lüttgau and Frank Momburg, who gave scientific input on the development of the bi- and trispecific antibodies as well as valuable feedback on experimental setups and data. Frank also took over the position as my mentor in the graduate school, when Felix left the institute. Thank you very much.

I also thank Shanshan Luo, Eva Loffredo-Verde and Lili Zhao, who worked with me on the project. We had interesting discussions and generated valuable data, which are also included in the manuscript.

Thanks to Forough Shirazi and Fazel Shokri for sharing the cDNA of the hybridoma 5F9, which made it possible to clone the FabMAbs in the first place.

Moreover, I want to thank Francesca and Aida, who did their thesis and internship under my supervision. You taught me how to teach and thereby contributed a lot to my personal development.

Thanks to Arie Geerlof for helping me with the size exclusion chromatography by providing the technical equipment as well as scientific advice.

In addition, I thank my colleagues at the Institute of Virology for the scientific and emotional support every day, especially Theresa, Julia, Marvin, Sophia, Basti, Flo, Lisa, Fenna, Martin, Philipp, Romina and Maarten. I could easily write down the name of every single colleague in this Institute, because all of you made your contribution to the success of my thesis in some way and I am deeply grateful for your help and the time we shared. I will never forget you.

I also thank my family and friends outside the lab for their continuous support, good thoughts and positive energy, which was always a great motivation for me.

Very special thanks go to Lena, who supported me unconditionally through all these years. You gave me scientific advice as well as emotional support in countless hours and therefore I am more grateful than I can ever tell.

Publications and meetings

a) International conferences

Oliver Quitt, Sandra Lüttgau, Gerhard Moldenhauer, Forough Golsaz Shirazi, Felix Bohne and Ulrike Protzer. 2015 International Meeting - The Molecular Biology of Hepatitis B viruses. October 4-8, Bad Nauheim, Germany.

Poster presentation: Generation and functional analysis of bi- and trispecific antibodies for immunotherapy of chronic hepatitis B virus infection.

Oliver Quitt, Sandra Lüttgau, Gerhard Moldenhauer, Forough Golsaz Shirazi, Felix Bohne and Ulrike Protzer. 2016 International Meeting - The Molecular Biology of Hepatitis B viruses. September 21-24, Seoul, South Korea.

Oral presentation: Generation and functional analysis of bi- and trispecific antibodies for immunotherapy of chronic hepatitis B virus infection.

Travel Grand award.

b) Patents

Ulrike Protzer, Felix Bohne, **Oliver Quitt**, Frank Momburg and Gerhard Moldenhauer. Trispecific binding molecules for treating HBV infection and associated conditions.

International publication number: WO2016146702A1
International publication date: 22.09.2016

c) Articles in peer-reviewed journals

Suliman Qadir Afridi, Hassan Moeini, Behnam Kalali, Jochen Martin Wettengel, **Oliver Quitt**, Raphaela Semper, Markus Gerhard, Ulrike Protzer and Dieter Hoffmann. Quantitation of norovirus-specific IgG before and after infection in immunocompromised patients. 2019. Brazilian Journal of Microbiology.

Oliver Quitt, Shanshan Luo, Marten Meyer, Zhe Xie, Forough Golsaz-Shirazi, Eva Loffredo-Verde, Julia Festag, Jan Hendrik Bockmann, Lili Zhao, Daniela Stadler, Wen-Min Chou, Raindy Tedjokusumo, Jochen Martin Wettengel, Chunkyu Ko1, Elfriede Noeßner, Nadja Bulbuc, Fazel Shokri, Sandra Lüttgau, Mathias Heikenwälder1, Felix Bohne, Gerhard Moldenhauer, Frank Momburg, Ulrike Protzer. T-cell engager antibodies enable T cells to control hepatitis B virus infection and to target HBsAg-positive hepatoma in mice. Manuscript accepted at Journal of Hepatology.